

OCRWM

MODEL COVER SHEET

1. QA: QA
Page 1 of 144

2. Type of Mathematical Model

 Process Model Abstraction Model System Model

Describe Intended Use of Model

The intended use of this model is to estimate, within an appropriate level of confidence, the effects of evaporation on the chemical evolution of water and precipitated minerals within the proposed repository during the post-closure period.

3. Title

In-Drift Precipitates/Salts Model

4. DI (including Rev. No. and Change No., if applicable):

ANL-EBS-MD-000045 REV 01

5. Total Attachments

Four (4)

6. Attachment Numbers - No. of Pages in Each

I-91, II-7, III-6, IV-5

	Printed Name	Signature	Date
7. Originator	Paul Mariner	SIGNATURE ON FILE	10/21/03
8. CSO	Bruce Kirstein	SIGNATURE ON FILE	10/21/03
9. Checker	Charles Bryan	SIGNATURE ON FILE	10/21/03
10. QER	Darrell Svalstad	SIGNATURE ON FILE	10/21/03
11. Responsible Manager/Lead	Cliff Howard	SIGNATURE ON FILE	10/21/03
12. Responsible Manager	Paul Dixon	SIGNATURE ON FILE	10/21/03

13. Remarks

Contributing authors include Darren Jolley for Section 6.6.2.6 and Carlos Love-Colon, Russell Jarek, Ananda Wijesinghe, Joseph Rard, and Thomas Wolery for Attachment I.

Charles Bryan replaced Dennis Newell as Lead Checker. Dennis Newell performed the initial check.

**OFFICE OF CIVILIAN RADIOACTIVE WASTE MANAGEMENT
MODEL REVISION RECORD**

1. Page: 2 of 144

2. Model Title:
In-Drift Precipitates/Salts Model

3. DI (including Rev. No. and Change No., if applicable):
ANL-EBS-MD-000045 REV 01

4. Revision/Change No.	5. Description of Revision/Change
00	Initial Issue.
00/01	ICN to incorporate discussion affirming the application of this AMR and its calculations to backfill and no backfill scenarios. This ICN includes modifications resulting from changes in AP-3.10Q procedures and data qualification status.
00/02	ICN to qualify previously unqualified technical products.
00/03	ICN to improve transparency, incorporate model enhancements, document newly discovered model limitations, and qualify model enhancements used in calculations performed for the SSPA. This ICN affects Sections 1 through 8. Affected pages (except those for table of contents, table of figures, and table of tables) are identified by vertical change bars in the margin indicating the locations of the changes. Changes can be found on pages 1-15, 19-23, 25-27, 29, 31-38, 41, 42, 44, 45, 47-50, 52, 54, 56, 58, 62, 66, 69, 70, 72-74, 82, 93-100, and 102-106.
01	Revision to qualify and document major improvements to the In-Drift Precipitates/Salts model. These improvements include the use of a new software version of EQ3/6 (version 8.0) and a new Pitzer database, which together are designed to predict aqueous chemical reactions in highly concentrated brines. Additional model validation simulations are included for deliquescence points and the evaporation of seawater. Overall model uncertainties are estimated for output parameters used in TSPA-LA. These changes were extensive and required a full revision of the document.

ACKNOWLEDGMENTS

Two key contributions to this document must be acknowledged. One is the Pitzer thermodynamic database developed and documented in Attachment I. Carlos Jove-Colon with the assistance of Tom Wolery, Joseph Rard, Ananda Wijesinghe, and Russell Jarek developed the Pitzer database and provided the documentation included in Table 3, Table 4, and Attachment I. The other key contribution is the mineral suppression methodology presented in Section 6.6.2.6. This methodology was developed by Darren Jolley with the assistance of Richard Metcalf.

The work presented in this document was supported by the Office of Repository Design as part of the Civilian Radioactive Waste Management Program, managed by the U.S. Department of Energy.

INTENTIONALLY LEFT BLANK

CONTENTS

	Page
1. PURPOSE.....	13
2. QUALITY ASSURANCE	14
3. USE OF SOFTWARE.....	14
3.1 QUALIFIED SOFTWARE.....	14
3.1.1 EQ3/6 Version 8.0	14
3.1.2 GETEQDATA Version 1.0.1.....	15
3.1.3 SUPCRT92 Version 1.0.....	15
3.2 EXEMPT SOFTWARE.....	16
4. INPUTS	17
4.1 DIRECT INPUT	17
4.1.1 Data.....	17
4.1.2 Parameters.....	25
4.2 CRITERIA.....	27
4.2.1 Degradation of Engineered Barriers Acceptance Criteria	27
4.2.2 Quantity and Chemistry of Water Contacting Waste Packages and Waste Forms Acceptance Criteria	30
4.3 CODES AND STANDARDS.....	33
4.4 VALIDATION AND DEMONSTRATION DATA	33
5. ASSUMPTIONS	39
5.1 STANDARD STATE OF WATER.....	39
5.2 EQUILIBRIUM CONDITIONS.....	39
6. MODEL DISCUSSION	40
6.1 MODELING OBJECTIVES.....	40
6.2 FEATURES, EVENTS, AND PROCESSES INCLUDED IN MODEL	40
6.3 SALTS/PRECIPITATES PROCESSES.....	42
6.3.1 Evaporation, Relative Humidity, and Salt Precipitation.....	42
6.3.2 Formation and Chemistry of Brines and Salt Precipitates	43
6.3.3 Potential Brines and Salt Precipitates at Yucca Mountain.....	46
6.3.4 Simplified Binary Salts Model.....	48
6.4 BASE CASE CONCEPTUAL MODEL	50
6.5 CONSIDERATION OF ALTERNATIVE CONCEPTUAL MODELS	51
6.6 MODEL FORMULATION FOR BASE CASE MODEL.....	53
6.6.1 Mathematical Description of Base Case Model.....	53
6.6.2 Base Case Model Inputs and Boundary Conditions	57
6.6.3 Summary of Computational Model	66
6.7 DEMONSTRATION OF BASE CASE MODEL	71
6.7.1 Evaporation of Average In Situ J-13 Well Water.....	71
6.7.2 Dilution of Average In Situ J-13 Well Water	75
6.7.3 Resulting Model Lookup Tables.....	78

7.	VALIDATION	78
7.1	VALIDATION USING EVAPORATION DATA	81
7.1.1	Evaporation of Average J-13 Well Water at 85°C	81
7.1.2	Evaporation of 100x Average J-13 Well Water at 90°C and 85 Percent Relative Humidity	86
7.1.3	Evaporation of Topopah Spring Tuff Pore Water at 75°C	89
7.1.4	Seawater Evaporation	93
7.2	EVAPORATION OF DILUTE SALT SOLUTIONS	98
7.2.1	Aqueous Solubilities of Simple Salts	98
7.2.2	Deliquescence Relative Humidity Values of Simple Salts	102
7.3	COMPARISON OF PITZER AND YMP.R2 DATABASE PREDICTIONS	103
7.4	VALIDATION FOR MINERAL OUTPUTS	106
7.5	VALIDATION SUMMARY AND ESTIMATED UNCERTAINTIES	107
7.5.1	pH	108
7.5.2	Ionic Strength	108
7.5.3	Deliquescence Relative Humidity	108
7.5.4	Al, Br, CO ₃ , Cl, F, K, Na, NO ₃ , and SO ₄	108
7.5.5	Ca, Mg, and SiO ₂	109
7.5.6	Minerals	110
7.5.7	Cl:NO ₃ Ratio	110
8.	CONCLUSIONS	111
8.1	MODEL DESCRIPTION	111
8.2	DEVELOPED OUTPUTS	111
8.3	MODEL ABSTRACTION	113
8.4	UNCERTAINTY AND LIMITATIONS	113
8.5	YUCCA MOUNTAIN REVIEW PLAN CRITERIA ASSESSMENT	115
8.5.1	Degradation of Engineered Barriers Acceptance Criteria	115
8.5.2	Quantity and Chemistry of Water Contacting Waste Packages and Waste Forms Acceptance Criteria	120
9.	INPUTS AND REFERENCES	126
9.1	DOCUMENTS	126
9.2	DATA, LISTED BY TRACKING NUMBER	140
9.2.1	Input Data	140
9.2.2	Developed Data	141
9.3	CODES, STANDARDS, REGULATIONS, PROCEDURES, AND SOFTWARE ...	142
10.	ATTACHMENTS	143

FIGURES

	Page
Figure 1. Processes Simulated by the In-Drift Precipitates/Salts Model.....	51
Figure 2. The General Process Required to Give a Valid Technical Basis for Mineral Suppression or Inclusion in Geochemical Equilibrium Modeling.....	60
Figure 3. Representation of Steady-State Flow-Through for the In-Drift Precipitates/Salts Model.....	69
Figure 4. Example Aqueous Composition Evaporation Predictions vs. <i>RH</i>	72
Figure 5. Example Aqueous Composition Evaporation Predictions vs. <i>CF</i>	73
Figure 6. Example Acid-Neutralizing Capacity Species Concentration Evaporation Predictions vs. <i>RH</i>	73
Figure 7. Example Acid-Neutralizing Capacity Species Concentration Evaporation Predictions vs. <i>CF</i>	74
Figure 8. Example Mineral Precipitation Evaporation Predictions vs. <i>RH</i>	74
Figure 9. Example Mineral Precipitation Evaporation Predictions vs. <i>CF</i>	75
Figure 10. Example Aqueous Composition Condensation Predictions vs. <i>RH</i>	76
Figure 11. Example Aqueous Composition Condensation Predictions vs. <i>DF</i>	76
Figure 12. Example Acid-Neutralizing Capacity Species Concentration Condensation Predictions vs. <i>RH</i>	77
Figure 13. Example Acid-Neutralizing Capacity Species Concentration Condensation Predictions vs. <i>DF</i>	77
Figure 14. Predicted Aqueous Evolution of Synthetic J-13 Water for Evaporation Experiments of Rosenberg et al. (1999 [125338]).....	84
Figure 15. Predicted Mineral Evolution of Synthetic J-13 Water for Evaporation Experiments of Rosenberg et al. (1999 [125338]).....	84
Figure 16. Predicted vs. Measured Concentrations for Synthetic J-13 Water Evaporation Experiments of Rosenberg et al. (1999 [125338]).....	85
Figure 17. Predicted vs. Measured pH Values for Synthetic J-13 Water Evaporation Experiments of Rosenberg et al. (1999 [125338]).....	85
Figure 18. Predicted Aqueous Evolution of 100x Synthetic J-13 Water for Evaporation Experiments of CRWMS M&O (2000 [146460]).....	88
Figure 19. Predicted Mineral Evolution of 100x Synthetic J-13 Water for Evaporation Experiments of CRWMS M&O (2000 [146460]).....	88
Figure 20. Predicted vs. Measured Concentrations for 100x Synthetic J-13 Water Evaporation Experiments of CRWMS M&O (2000 [146460]).....	89
Figure 21. Predicted Aqueous Evolution of Synthetic Topopah Spring Tuff Pore Water for Evaporation Experiments of Rosenberg et al. (1999 [125339]).....	91
Figure 22. Predicted Mineral Evolution of Synthetic Topopah Spring Tuff Pore Water for Evaporation Experiments of Rosenberg et al. (1999 [125339]).....	92
Figure 23. Predicted vs. Measured Concentrations for Synthetic Topopah Spring Tuff Pore Water from Evaporation Experiments of Rosenberg et al. (1999 [125339]).....	92
Figure 24. Predicted vs. Measured pH Values for Synthetic Topopah Spring Tuff Pore Water from Evaporation Experiments of Rosenberg et al. (1999 [125339]).....	93

Figure 25. Predicted vs. Measured Ca, K, Mg, and Na Concentrations from Evaporation of Inagua Seawater 96

Figure 26. Predicted vs. Measured Br, Cl, and SO₄ Concentrations from Evaporation of Inagua Seawater 96

Figure 27. Predicted vs. Measured pH and Ionic Strength from Evaporation of Inagua Seawater 97

Figure 28. Predicted Mineral Precipitation from Evaporation of Inagua Seawater..... 97

Figure 29. Predicted vs. CRC Handbook Mineral Solubilities at 25°C..... 101

Figure 30. Predicted vs. CRC Handbook Mineral Solubilities at 100°C..... 101

Figure 31. Pitzer vs. Set 1 data0.ymp.R2 (YMP.R2) Aqueous Predictions for Average In Situ J-13 Well Water at 70°C and CO₂(g) Fugacity of 10⁻³ Bars 104

Figure 32. Pitzer vs. Set 1 data0.ymp.R2 (YMP.R2) pH and Ionic Strength Predictions for Average In Situ J-13 Well Water at 70°C and CO₂(g) Fugacity of 10⁻³ Bars..... 104

Figure 33. Pitzer vs. Set 2 data0.ymp.R2 (YMP.R2) Aqueous Predictions for Average In Situ J-13 Well Water at 70°C and CO₂(g) Fugacity of 10⁻³ Bars 105

Figure 34. Pitzer vs. Set 2 data0.ymp.R2 (YMP.R2) pH and Ionic Strength Predictions for Average In Situ J-13 Well Water at 70°C and CO₂(g) Fugacity of 10⁻³ Bars..... 105

TABLES

	Page
Table 1. Comparison of log K Values for the Dissolution Reactions of CaCl ₂ , NaNO ₃ , and Na ₂ CO ₃ :H ₂ O Obtained Using SUPCRT92 (Version 1.0) on Windows NT and Windows 2000 Operating Systems	16
Table 2. Input Sources for Pitzer Database.....	18
Table 3. Binary Pitzer Ion Interaction Coefficients.....	19
Table 4. Ternary Pitzer Ion Interaction Coefficients	21
Table 5. In-Drift Precipitates/Salts Model Input Parameters.....	26
Table 6. Input Sources for Mineral Suppression Determinations.....	26
Table 7. Water Chemistry Data From Experimental J-13 Well Water Evaporation of Rosenberg et al. (1999 [125338]).....	34
Table 8. pH Data From Experimental J-13 Well Water Evaporation of Rosenberg et al. (1999 [125338])	34
Table 9. Water Chemistry Data From Experimental 100x J-13 Well Water (CRWMS M&O 2000 [146460]).....	35
Table 10. Water Chemistry Data From Topopah Spring Pore Water Evaporation Experiment of Rosenberg et al. (1999 [125339])	35
Table 11. Sample Data for Evaporated Seawater	36
Table 12. Aqueous Solubilities of Na, K, Ca, and Mg Salts.....	37
Table 13. Equilibrium Relative Humidity for Saturated Aqueous Solutions in Contact With an Excess of Solid-Phase Salts	38
Table 14. Average In Situ Composition of Water from Well J-13	38
Table 15. TSPA-LA FEPs Included in Model.....	41
Table 16. Alternative Conceptual Models Considered.....	52
Table 17. MineralSuppressions Included in the IDPS Model.....	64
Table 18. Minerals Allowed to Precipitate in the IDPS Model	65
Table 19. Model Validation Objectives	80
Table 20. Estimated Model Uncertainty in Selected Output Parameters.....	80
Table 21. Calculation of "Measured" Ionic Strength in Average J-13 Well Water Evaporation Experiment	83
Table 22. Calculation of "Measured" Ionic Strength in Topopah Spring Tuff Pore Water Evaporation Experiment.....	91
Table 23. Unit Conversion of Aqueous Solubilities of Na, K, Ca, and Mg Salts.....	99
Table 24. Model Predictions of Aqueous Solubilities of Na, K, Ca, and Mg Salts.....	100
Table 25. Model Predictions of Equilibrium Relative Humidity for Saturated Aqueous Solutions in Contact With an Excess of Solid-Phase Salts.....	102
Table 26. Maximum Differences Between Predictions and Measurements for pH, Ionic Strength, Cl, NO ₃ , and the Cl:NO ₃ Ratio.....	107
Table 27. Developed Output.....	112

INTENTIONALLY LEFT BLANK

ACRONYMS AND ABBREVIATIONS

100x	concentration factor of 100
C_i	concentration of component i
CF	concentration factor
DF	dilution factor
DIRS	Document Input Reference System
DTN	Data Tracking Number
EBS	Engineered Barrier System
f_{CO_2}	carbon dioxide fugacity
f_{O_2}	oxygen fugacity
FEPs	features, events, and processes
gm	gram
IS	ionic strength
IDPS	In-Drift Precipitates/Salts
kg	kilogram
L	liter
mg	milligram
mL	milliliter
molal	moles per kilogram of water
Q^d	discharge rate (rate of flow out of cell)
Q^e	net evaporation rate (net of evaporation [positive] and condensation [negative])
Q^s	incoming seepage rate
R^{es}	relative evaporation rate (Q^e/Q^s)
RH	relative humidity
RH_d	deliquescence point or deliquescence relative humidity of a solution or mineral assemblage in RH units
S_m	Suppression flag for mineral m
T	temperature
TSPA	Total System Performance Assessment
TSPA-LA	Total System Performance Assessment - License Application
TSPA-SR	Total System Performance Assessment - Site Recommendation
TWP	Technical Work Plan
YMP	Yucca Mountain Project
YPF	data0.ypf Pitzer thermodynamic database

INTENTIONALLY LEFT BLANK

1. PURPOSE

As directed by *Technical Work Plan For: Engineered Barrier System Department Modeling and Testing FY03 Work Activities* (BSC 2003 [165601]), the In-Drift Precipitates/Salts (IDPS) model is developed and refined to predict the aqueous geochemical effects of evaporation in the proposed repository. The purpose of this work is to provide a model for describing and predicting the postclosure effects of evaporation and deliquescence on the chemical composition of water within the proposed Engineered Barrier System (EBS). Application of this model is to be documented elsewhere for the Total System Performance Assessment License Application (TSPA-LA). The principal application of this model is to be documented in REV 02 of *Engineered Barrier System: Physical and Chemical Environment Model* (BSC 2003 [165601]).

The scope of this document is to develop, describe, and validate the IDPS model. This model is a quasi-equilibrium model. All reactions proceed to equilibrium except for several suppressed minerals in the thermodynamic database not expected to form under the proposed repository conditions within the modeling timeframe. In this revision, upgrades to the EQ3/6 code (Version 8.0) and Pitzer thermodynamic database improve the applicable range of the model. These new additions allow equilibrium and reaction-path modeling of evaporation to highly concentrated brines for potential water compositions of the system Na-K-H-Mg-Ca-Al-Cl-F-NO₃-SO₄-Br-CO₃-SiO₂-CO₂-O₂-H₂O at temperatures in the range of 0°C to 125°C, pressures in the atmospheric range, and relative humidity in the range of 0 to 100 percent. This system applies to oxidizing conditions only, and therefore limits the model to applications involving oxidizing conditions.

A number of thermodynamic parameters in the Pitzer database have values that have not been determined or verified for the entire temperature range. In these cases, the known values are used to approximate the values for the rest of the temperature range. Although such treatment contributes to uncertainty in model outputs, the model validation test cases indicate that the model, with its associated uncertainty, is valid for its intended use.

The intended use of this model is to estimate and tabulate, within an appropriate level of confidence, the effects of evaporation, deliquescence, and potential environmental conditions on the pH, ionic strength, and chemical compositions of water and minerals on the drip shield or other location within the drift during the postclosure period. Specifically, the intended use is as follows:

- To estimate, within an appropriate level of confidence, the effects of evaporation and deliquescence on the presence and composition of water occurring within the proposed repository during the postclosure period (i.e., effects on pH, ionic strength, deliquescence relative humidity, total concentrations of dissolved components in the system Na-K-H-Mg-Ca-Al-Cl-F-NO₃-SO₄-Br-CO₃-SiO₂-CO₂-O₂-H₂O, and concentrations of the following aqueous species that potentially affect acid neutralizing capacity: HCO₃⁻, CO₃²⁻, OH⁻, H⁺, HSO₄⁻, Ca²⁺, Mg²⁺, CaHCO₃⁺, MgHCO₃⁺, HSiO₃⁻, and MgOH⁺),

- To estimate, within an appropriate level of confidence, mineral precipitation resulting from the evaporation of water occurring within the proposed repository during the postclosure period (specifically, minerals of the system Na-K-H-Mg-Ca-Al-Cl-F-NO₃-SO₄-Br-CO₃-SiO₂-CO₂-O₂-H₂O), and
- To provide a means for abstracting these effects into a set of lookup tables that provide input to downstream models used for performance assessment.

The presence and composition of liquid water in the drift depend upon relative humidity, temperature, incoming water composition, in-drift gas composition, and relative rates of evaporation and seepage. Intended input values for these parameters are abstracted results from thermal-hydrological-chemical models, water sample measurements, dust leachate samples, and values used in sensitivity and uncertainty analyses that encompass the expected ranges of these parameters.

2. QUALITY ASSURANCE

The Quality Assurance program has been determined to apply to the development of this document, as discussed in the technical work plan (TWP) *Technical Work Plan for Engineered Barrier System Department Modeling and Testing FY03 Work Activities* (BSC 2003 [165601]) because it involves activities that provide data used to assess the potential dispersion of radioactive materials from the proposed facility. This model feeds subsequent models that assess the potential for drip shield and waste package corrosion and invert chemistry which control, in part, radionuclide migration. This document does not investigate items in the *Q-list* (BSC 2003 [165179]). This document was developed as directed in the TWP, which directs all work identified in work package AEBM02. The TWP was prepared in accordance with AP-2.27Q, *Planning for Science Activities*. The methods used to control the electronic management of data as required by AP-SV.1Q, *Control of the Electronic Management of Information*, are identified in the TWP. As directed in the TWP, this document was prepared in accordance with AP-SIII.10Q, *Models* and reviewed in accordance with AP-2.14Q, *Document Review*.

3. USE OF SOFTWARE

3.1 QUALIFIED SOFTWARE

All qualified software discussed in this document was obtained from Software Configuration Management in accordance with AP-SI.1Q, *Software Management*. This software was used in the operating environments for which they were baselined. One of the software, SUPCRT92 Version 1.0, was also used in a non-baselined operating environment, as explained in Section 3.1.3.

3.1.1 EQ3/6 Version 8.0

EQ3/6 Version 8.0 (STN: 10813-8.0-00, BSC 2003 [162228]) was installed and used on IBM-compatible computers using the Microsoft Windows 2000 operating system. This software is appropriate for the application and was used only within the range of validation in accordance

with AP-SI.1Q, *Software Management*. No macros or software routines were developed for, or used by, this software.

3.1.2 GETEQDATA Version 1.0.1

GETEQDATA Version 1.0.1 (STN: 10809-1.0.1-00, BSC 2003 [161900]) was installed and used on IBM-compatible computers using the Microsoft Windows 2000 operating system. This software is appropriate for the application and was used only within the range of validation in accordance with AP-SI.1Q, *Software Management*. No other macros or software routines were developed for, or used by, this software.

3.1.3 SUPCRT92 Version 1.0

SUPCRT92 Version 1.0 (STN: 10058-1.0-00, LBNL 1999 [153218]) was first installed and used on an IBM-compatible computer using the Microsoft Windows 2000 operating system. Because the software was not qualified for this operating system, it was later installed and used on an IBM-compatible computer using the Microsoft Windows NT operating system to verify and justify use of the original calculations. Microsoft Windows NT is a qualified operating system for this code. All of the calculations performed on the Microsoft Windows 2000 operating system were rerun on the Microsoft Windows NT system. The results on the two platforms are identical, and both sets of calculations are documented in DTN: SN0306T0510102.007. These results are summarized in Table 1 and in file 'comparison_SUPCRT92_salts_Carlos_Yueting.xls' in DTN: SN0306T0510102.007. Details on how these calculations were used in this report are provided in Sections I-5, I-5.1, I-5.2, and I-5.3 of Attachment I. This software is appropriate for the Windows NT application and was used only within the range of validation in accordance with AP-SI.1Q, *Software Management*. No macros or software routines were developed for, or used by, this software.

Table 1. Comparison of log K Values for the Dissolution Reactions of CaCl₂, NaNO₃, and Na₂CO₃:H₂O Obtained Using SUPCRT92 (Version 1.0) on Windows NT and Windows 2000 Operating Systems

Temperature (°C)	Log K Calculated with SUPCRT92 (Windows NT)	Log K Calculated with SUPCRT92 (Windows 2000)	Salt Phase
0.1	13.177	13.177	CaCl ₂
25	11.942	11.942	CaCl ₂
60	10.325	10.325	CaCl ₂
100	8.649	8.649	CaCl ₂
150	6.738	6.738	CaCl ₂
200	4.935	4.935	CaCl ₂
250	3.124	3.124	CaCl ₂
300	1.126	1.126	CaCl ₂
0.1	0.679	0.679	NaNO ₃
25	1.039	1.039	NaNO ₃
60	1.386	1.386	NaNO ₃
100	1.644	1.644	NaNO ₃
150	1.819	1.819	NaNO ₃
200	1.861	1.861	NaNO ₃
250	1.769	1.769	NaNO ₃
300	1.496	1.496	NaNO ₃
0.1	11.404	11.404	Na ₂ CO ₃ :H ₂ O
25	10.974	10.974	Na ₂ CO ₃ :H ₂ O
60	10.46	10.46	Na ₂ CO ₃ :H ₂ O
100	9.985	9.985	Na ₂ CO ₃ :H ₂ O
150	9.499	9.499	Na ₂ CO ₃ :H ₂ O

DTN: SN0306T0510102.007

3.2 EXEMPT SOFTWARE

Microsoft Excel 2000

Microsoft Excel 2000, a commercially available spreadsheet software package, was installed and used on IBM-compatible computers using the Microsoft Windows 2000 operating system. This software was used to tabulate results, visually display results, and perform the algebraic equations documented in Section 6.6.3.5 and Attachment I. Hand calculations and visual inspection of these tabulations, charts, and equations confirm that the spreadsheet applications provided correct results. Except for GETEQDATA listed above, no macros or software routines were developed for, or used by, this software, and consequently it is an exempt software application in accordance with Section 2.1 of AP-SI.1Q, *Software Management*.

Output DTNs containing Excel spreadsheets include:

- DTN: MO0303MWDINJ13.000
- DTN: MO0303MWDJ13GD.000
- DTN: MO0303MWDJ13RB.000
- DTN: MO0303MWDSEDSS.000
- DTN: MO0303MWDTSWRB.000
- DTN: MO0304SPAJ13IS.001
- DTN: MO0307MWDSEAEV.000
- DTN: MO0307MWDUNEVP.000
- DTN: MO0308SPAESMUN.000
- DTN: MO0308SPAUCIMV.000
- DTN: SN0306T0510102.007.

4. INPUTS

4.1 DIRECT INPUT

This model report is a revision of a previously developed and validated in-drift precipitates/salts model (BSC 2001 [156065]). The current model and document completely replace the earlier versions. Consequently, the DTNs associated with the previous version are not used as input.

Data inputs used to develop the revised IDPS model and associated Pitzer thermodynamic database are presented in Sections 4.1.1 and 4.1.2. After reviewing a wide range of data, these data were found to be the most reliable and appropriate sources of technical information and data available for developing the model. Section 4.1.1 focuses on data constants in the model, and Section 4.1.2 focuses on variable model parameters and values for these parameters used in model validation. The Data Input Reference System (DIRS) is used to track the quality of these data. Independent data used to validate and demonstrate the IDPS model are presented in Section 4.4.

4.1.1 Data

A Pitzer thermodynamic database is developed in this report for use in the IDPS model. The IDPS model is designed to predict the evolution of water in the drift as it evaporates to a brine and, eventually, to the point at which there is no free water remaining. To predict aqueous concentrations and salt precipitation in brines, a Pitzer database is needed. This database is developed for the system Na-K-H-Mg-Ca-Al-Cl-F-NO₃-SO₄-Br-CO₃-SiO₂-CO₂-O₂-H₂O, which generally encompasses the most abundant ions in natural ground waters. It is designed for temperatures ranging from 0°C to 200°C, a broader range than that of the IDPS model (0°C to 125°C). The smaller range for the IDPS model is due to the smaller temperature range of the independent set of model validation data (25°C to 100°C). The model validation range (0°C to 125°C) is justified by the larger temperature range of the Pitzer database (0°C to 200°C) and the small chance for large errors in the IDPS model resulting from extrapolating its application to temperatures 25°C beyond the temperature range of the independent set of model validation data.

The development of the Pitzer database is discussed in Attachment I. The sources of technical information used in the development of the Pitzer database are listed in Table 2. Uncertainty associated with these data is also addressed in Attachment I.

Binary and ternary Pitzer temperature-dependent interaction coefficients are presented in Table 3 and Table 4. Uncertainty in the values of the coefficients is difficult to assess given the multiple sources of data and the series of refitting and conversions conducted in the retrieval of coefficient data. For practical purposes, the retrieved coefficients were tested upon refitting/conversion for the prediction of coefficients such as osmotic coefficients from their sources. When alternate data were available for the system in question, then a simple check comparison between coefficient values was also made. The error analyses and comparisons of these predictions are reported in the spreadsheets referenced in Attachment I and pertain only to the original sources where the fitted coefficients were derived.

Table 2. Input Sources for Pitzer Database

Type of Input	Source
Thermodynamic and/or solubility data	Barin and Platzki 1995 [157865]; Harvie et al. 1984 [118163]; Linke 1965 [162114]; Meisingset and Grønvold 1986 [162094]; Pitzer and Oakes 1994 [163583]; Pitzer and Shi 1993 [163582]; Robie and Hemingway 1995 [153683]; DTN: MO0302SPATHDYN.000, and DTN: MO0302SPATHDYN.001
Pitzer ion interaction coefficients and/or osmotic coefficient data	Archer 2000 [162065]; Clegg and Brimblecombe 1990 [162089]; Clegg and Brimblecombe 1990 [162067]; Clegg et al. 1996 [162068]; Felmy et al. 1994 [162112]; Felmy et al. 1994 [162111]; Greenberg and Moller 1989 [152684]; He and Morse 1993 [162090]; Holmes and Mesmer 1992 [162076]; Holmes and Mesmer 1983 [162073]; Holmes and Mesmer 1994 [162078]; Holmes and Mesmer 1998 [162083]; Holmes et al. 1987 [162075]; Moller 1988 [152695]; Oakes et al. 2000 [162102]; Pabalan and Pitzer 1987 [162096]; Pabalan and Pitzer 1987 [162147]; Pitzer 1991 [152709]; Sterner et al. 1998 [162116]; and Thiessen and Simonson 1990 [162108]
Equations and conversions	Garrels and Christ 1990 [144877]; Moller 1988 [152695]; Pitzer 1991 [152709]; Pitzer 1973 [152738]; and Rard and Wijesinghe 2003 [162327]

Table 3. Binary Pitzer Ion Interaction Coefficients

Ions	Coefficient Name	Coefficient Type	Coefficient Units	Coefficient Source	Coefficient Sources DIRS #	Coefficient Use in this Report
$\text{Na}^+ - \text{Cl}^-$	$\beta^{(0)}$, $\beta^{(1)}$, and $C^{(\phi)}$	Binary	kg/mol, kg/mol, and $(\text{kg/mol})^2$ respectively	Greenberg and Møller (1989)	152684	Attachment I
$\text{Na}^+ - \text{SO}_4^{2-}$	$\beta^{(0)}$, $\beta^{(1)}$, and $C^{(\phi)}$	Binary	kg/mol, kg/mol, and $(\text{kg/mol})^2$ respectively	Greenberg and Møller (1989)	152684	Attachment I
$\text{Na}^+ - \text{HSO}_4^-$	$\beta^{(0)}$, $\beta^{(1)}$, and $C^{(\phi)}$	Binary	kg/mol, kg/mol, and $(\text{kg/mol})^2$ respectively	Holmes and Mesmer (1994)	162078	Attachment I
$\text{Na}^+ - \text{OH}^-$	$\beta^{(0)}$, $\beta^{(1)}$, and $C^{(\phi)}$	Binary	kg/mol, kg/mol, and $(\text{kg/mol})^2$ respectively	Pabalan and Pitzer (1987)	162147	Attachment I
$\text{Na}^+ - \text{NO}_3^-$	$\beta^{(0)}$, $\beta^{(1)}$, and $C^{(\phi)}$	Binary	kg/mol, kg/mol, and $(\text{kg/mol})^2$ respectively	Archer (2000)	162065	Attachment I
$\text{Na}^+ - \text{CO}_3^{--}$	$\beta^{(0)}$, $\beta^{(1)}$, and $C^{(\phi)}$	Binary	kg/mol, kg/mol, and $(\text{kg/mol})^2$ respectively	He and Morse (1993)	162090	Attachment I
$\text{Na}^+ - \text{HCO}_3^-$	$\beta^{(0)}$, $\beta^{(1)}$, and $C^{(\phi)}$	Binary	kg/mol, kg/mol, and $(\text{kg/mol})^2$ respectively	He and Morse (1993)	162090	Attachment I
$\text{Na}^+ - \text{Br}^-$	$\beta^{(0)}$, $\beta^{(1)}$, and $C^{(\phi)}$	Binary	kg/mol, kg/mol, and $(\text{kg/mol})^2$ respectively	Holmes and Mesmer (1998)	162083	Attachment I
$\text{Na}^+ - \text{AlO}_2^-$	$\beta^{(0)}$, $\beta^{(1)}$, and $C^{(\phi)}$	Binary	kg/mol, kg/mol, and $(\text{kg/mol})^2$ respectively	Felmy et al. (1994)	162112	Attachment I
$\text{H}^+ - \text{Cl}^-$	$\beta^{(0)}$, $\beta^{(1)}$, and $C^{(\phi)}$	Binary	kg/mol, kg/mol, and $(\text{kg/mol})^2$ respectively	Holmes et al. (1987)	162075	Attachment I
$\text{H}^+ - \text{NO}_3^-$	$\beta^{(0)}$, $\beta^{(1)}$, and $C^{(\phi)}$	Binary	kg/mol, kg/mol, and $(\text{kg/mol})^2$ respectively	Felmy et al. (1994); Clegg and Brimblecombe (1990)	162111 162067	Attachment I
$\text{H}^+ - \text{SO}_4^{2-}$	$\beta^{(0)}$, $\beta^{(1)}$, and $C^{(\phi)}$	Binary	kg/mol, kg/mol, and $(\text{kg/mol})^2$ respectively	Holmes and Mesmer (1992)	162076	Attachment I
$\text{H}^+ - \text{HSO}_4^-$	$\beta^{(0)}$, $\beta^{(1)}$, and $C^{(\phi)}$	Binary	kg/mol, kg/mol, and $(\text{kg/mol})^2$ respectively	Holmes and Mesmer (1992)	162076	Attachment I
$\text{K}^+ - \text{Cl}^-$	$\beta^{(0)}$, $\beta^{(1)}$, and $C^{(\phi)}$	Binary	kg/mol, kg/mol, and $(\text{kg/mol})^2$ respectively	Greenberg and Møller (1989)	152684	Attachment I
$\text{K}^+ - \text{SO}_4^{2-}$	$\beta^{(0)}$, $\beta^{(1)}$, and $C^{(\phi)}$	Binary	kg/mol, kg/mol, and $(\text{kg/mol})^2$ respectively	Greenberg and Møller (1989)	152684	Attachment I
$\text{K}^+ - \text{Br}^-$	$\beta^{(0)}$, $\beta^{(1)}$, and $C^{(\phi)}$	Binary	kg/mol, kg/mol, and $(\text{kg/mol})^2$ respectively	Holmes and Mesmer (1998)	162083	Attachment I
$\text{Ca}^{++} - \text{Cl}^-$	$\beta^{(0)}$, $\beta^{(1)}$, and $C^{(\phi)}$	Binary	kg/mol, kg/mol, and $(\text{kg/mol})^2$ respectively	Sternner et al. (1998)	162116	Attachment I

Table 3. Binary Pitzer Ion Interaction Coefficients (Continued)

Ions	Coefficient Name	Coefficient Type	Coefficient Units	Coefficient Source	Coefficient Sources DIRS #	Coefficient Use in this Report
$\text{Ca}^{++} - \text{SO}_4^{2-}$	$\beta^{(0)}$, $\beta^{(1)}$, and $C^{(\phi)}$	Binary	kg/mol, kg/mol, and $(\text{kg/mol})^2$ respectively	Greenberg and Møller (1989)	152684	Attachment I
$\text{Ca}^{++} - \text{NO}_3^-$	$\beta^{(0)}$, $\beta^{(1)}$, and $C^{(\phi)}$	Binary	kg/mol, kg/mol, and $(\text{kg/mol})^2$ respectively	Oakes et al. (2000)	162102	Attachment I
$\text{Li}^+ - \text{Cl}^-$	$\beta^{(0)}$, $\beta^{(1)}$, and $C^{(\phi)}$	Binary	kg/mol, kg/mol, and $(\text{kg/mol})^2$ respectively	Holmes and Mesmer (1998)	162082	Attachment I
$\text{Li}^+ - \text{Br}^-$	$\beta^{(0)}$, $\beta^{(1)}$, and $C^{(\phi)}$	Binary	kg/mol, kg/mol, and $(\text{kg/mol})^2$ respectively	Holmes and Mesmer (1998)	162083	Attachment I
$\text{Mg}^{++} - \text{SO}_4^{2-}$	$\beta^{(0)}$, $\beta^{(1)}$, and $C^{(\phi)}$	Binary	kg/mol, kg/mol, and $(\text{kg/mol})^2$ respectively	Pabalan and Pitzer (1987)	162096	Attachment I
$\text{Mg}^{++} - \text{Cl}^-$	$\beta^{(0)}$, $\beta^{(1)}$, and $C^{(\phi)}$	Binary	kg/mol, kg/mol, and $(\text{kg/mol})^2$ respectively	Pabalan and Pitzer (1987)	162096	Attachment I
$\text{Cs}^+ - \text{Br}^-$	$\beta^{(0)}$, $\beta^{(1)}$, and $C^{(\phi)}$	Binary	kg/mol, kg/mol, and $(\text{kg/mol})^2$ respectively	Holmes and Mesmer (1998)	162083	Attachment I
$\text{Cs}^+ - \text{Cl}^-$	$\beta^{(0)}$, $\beta^{(1)}$, and $C^{(\phi)}$	Binary	kg/mol, kg/mol, and $(\text{kg/mol})^2$ respectively	Holmes and Mesmer (1983)	162073	Attachment I
$\text{NH}_4^+ - \text{SO}_4^{2-}$	$\beta^{(0)}$, $\beta^{(1)}$, and $C^{(\phi)}$	Binary	kg/mol, kg/mol, and $(\text{kg/mol})^2$ respectively	Clegg et al. (1996)	162068	Attachment I
$\text{NH}_4^+ - \text{Cl}^-$	$\beta^{(0)}$, $\beta^{(1)}$, and $C^{(\phi)}$	Binary	kg/mol, kg/mol, and $(\text{kg/mol})^2$ respectively	Thiessen and Simonson (1990)	162108	Attachment I

Table 4. Ternary Pitzer Ion Interaction Coefficients

Ions	Coefficient Name	Coefficient Type	Coefficient Units	Coefficient Source	Coefficient Sources DIRS #	Coefficient Use in this Report
$\text{Na}^+ - \text{K}^+$	θ	Ternary	kg/mol	Greenberg and Møller (1989)	152684	Attachment I
$\text{Na}^+ - \text{Ca}^{++}$	θ	Ternary	kg/mol	Greenberg and Møller (1989)	152684	Attachment I
$\text{K}^+ - \text{Ca}^{++}$	θ	Ternary	kg/mol	Greenberg and Møller (1989)	152684	Attachment I
$\text{Na}^+ - \text{Mg}^{++}$	θ	Ternary	kg/mol	Pabalan and Pitzer (1987)	162096	Attachment I
$\text{K}^+ - \text{Mg}^{++}$	θ	Ternary	kg/mol	Pabalan and Pitzer (1987)	162096	Attachment I
$\text{NO}_3^- - \text{AlO}_2^-$	θ	Ternary	kg/mol	Felmy et al. (1994)	162112	Attachment I
$\text{OH}^- - \text{AlO}_2^-$	θ	Ternary	kg/mol	Felmy et al. (1994)	162112	Attachment I
$\text{Cl}^- - \text{OH}^-$	θ	Ternary	kg/mol	Pabalan and Pitzer (1987)	162096	Attachment I
$\text{Cl}^- - \text{SO}_4^{2-}$	θ	Ternary	kg/mol	Greenberg and Møller (1989)	152684	Attachment I
$\text{HSO}_4^- - \text{SO}_4^{2-}$	θ	Ternary	kg/mol	Holmes and Mesmer (1992)	162076	Attachment I
$\text{SO}_4^{2-} - \text{OH}^-$	θ	Ternary	kg/mol	Pabalan and Pitzer (1987)	162096	Attachment I
$\text{Ca}^{++} - \text{Mg}^{++}$	θ	Ternary	kg/mol	Pitzer (1991)	152709	Attachment I
$\text{Cs}^+ - \text{H}^+$	θ	Ternary	kg/mol	Pitzer (1991)	152709	Attachment I
$\text{Cs}^+ - \text{K}^+$	θ	Ternary	kg/mol	Pitzer (1991)	152709	Attachment I
$\text{Cs}^+ - \text{Li}^+$	θ	Ternary	kg/mol	Pitzer (1991)	152709	Attachment I
$\text{Cs}^+ - \text{Na}^+$	θ	Ternary	kg/mol	Pitzer (1991)	152709	Attachment I
$\text{H}^+ - \text{K}^+$	θ	Ternary	kg/mol	Pitzer (1991)	152709	Attachment I
$\text{H}^+ - \text{Li}^+$	θ	Ternary	kg/mol	Pitzer (1991)	152709	Attachment I
$\text{H}^+ - \text{Mg}^{++}$	θ	Ternary	kg/mol	Pitzer (1991)	152709	Attachment I
$\text{H}^+ - \text{Na}^+$	θ	Ternary	kg/mol	Pitzer (1991)	152709	Attachment I
$\text{H}^+ - \text{NH}_4^+$	θ	Ternary	kg/mol	Pitzer (1991)	152709	Attachment I
$\text{H}^+ - \text{Sr}^{++}$	θ	Ternary	kg/mol	Pitzer (1991)	152709	Attachment I
$\text{K}^+ - \text{Li}^+$	θ	Ternary	kg/mol	Pitzer (1991)	152709	Attachment I
$\text{K}^+ - \text{Mg}^{++}$	θ	Ternary	kg/mol	Pitzer (1991)	152709	Attachment I
$\text{K}^+ - \text{Li}^+$	θ	Ternary	kg/mol	Pitzer (1991)	152709	Attachment I
$\text{Li}^+ - \text{Na}^+$	θ	Ternary	kg/mol	Pitzer (1991)	152709	Attachment I

Table 4. Ternary Pitzer Ion Interaction Coefficients (Continued)

Ions	Coefficient Name	Coefficient Type	Coefficient Units	Coefficient Source	Coefficient Sources DIRS #	Coefficient Use in this Report
SiO ₂ – NO ₃ ⁻	λ	Ternary	kg/mol	Felmy et al. (1994)	162111	Attachment I
SiO ₂ – Na ⁺	λ	Ternary	kg/mol	Felmy et al. (1994)	162111	Attachment I
SiO ₂ – Cl ⁻	λ	Ternary	kg/mol	Felmy et al. (1994)	162111	Attachment I
SiO ₂ – SO ₄ ²⁻	λ	Ternary	kg/mol	Felmy et al. (1994)	162111	Attachment I
SiO ₂ – Mg ⁺⁺	λ	Ternary	kg/mol	Felmy et al. (1994)	162111	Attachment I
O ₂ (aq) – Na ⁺	λ	Ternary	kg/mol	Clegg and Brimblecombe (1990)	162089	Attachment I
O ₂ (aq) – K ⁺	λ	Ternary	kg/mol	Clegg and Brimblecombe (1990)	162089	Attachment I
O ₂ (aq) – Mg ⁺⁺	λ	Ternary	kg/mol	Clegg and Brimblecombe (1990)	162089	Attachment I
O ₂ (aq) – Ca ⁺⁺	λ	Ternary	kg/mol	Clegg and Brimblecombe (1990)	162089	Attachment I
O ₂ (aq) – Al ⁺⁺⁺	λ	Ternary	kg/mol	Clegg and Brimblecombe (1990)	162089	Attachment I
O ₂ (aq) – Cl ⁻	λ	Ternary	kg/mol	Clegg and Brimblecombe (1990)	162089	Attachment I
O ₂ (aq) – Br ⁻	λ	Ternary	kg/mol	Clegg and Brimblecombe (1990)	162089	Attachment I
O ₂ (aq) – OH ⁻	λ	Ternary	kg/mol	Clegg and Brimblecombe (1990)	162089	Attachment I
O ₂ (aq) – SO ₄ ²⁻	λ	Ternary	kg/mol	Clegg and Brimblecombe (1990)	162089	Attachment I
O ₂ (aq) – H ⁺	λ	Ternary	kg/mol	Clegg and Brimblecombe (1990)	162089	Attachment I
O ₂ (aq) – Li ⁺	λ	Ternary	kg/mol	Clegg and Brimblecombe (1990)	162089	Attachment I
O ₂ (aq) – NH ₄ ⁺	λ	Ternary	kg/mol	Clegg and Brimblecombe (1990)	162089	Attachment I
O ₂ (aq) – Ba ⁺⁺	λ	Ternary	kg/mol	Clegg and Brimblecombe (1990)	162089	Attachment I
O ₂ (aq) – I ⁻	λ	Ternary	kg/mol	Clegg and Brimblecombe (1990)	162089	Attachment I
O ₂ (aq) – HCO ₃ ⁻	λ	Ternary	kg/mol	Clegg and Brimblecombe (1990)	162089	Attachment I
O ₂ (aq) – CO ₃ ²⁻	λ	Ternary	kg/mol	Clegg and Brimblecombe (1990)	162089	Attachment I
CO ₂ (aq) – Ca ⁺⁺	λ	Ternary	kg/mol	He and Morse (1993)	162090	Attachment I
CO ₂ (aq) – K ⁺	λ	Ternary	kg/mol	He and Morse (1993)	162090	Attachment I
CO ₂ (aq) – Mg ⁺⁺	λ	Ternary	kg/mol	He and Morse (1993)	162090	Attachment I
CO ₂ (aq) – Na ⁺	λ	Ternary	kg/mol	He and Morse (1993)	162090	Attachment I
CO ₂ (aq) – H ⁺	λ	Ternary	kg/mol	He and Morse (1993)	162090	Attachment I
CO ₂ (aq) – Cl ⁻	λ	Ternary	kg/mol	He and Morse (1993)	162090	Attachment I
CO ₂ (aq) – HSO ₄ ⁻	λ	Ternary	kg/mol	He and Morse (1993)	162090	Attachment I

Table 4. Ternary Pitzer Ion Interaction Coefficients (Continued)

Ions	Coefficient Name	Coefficient Type	Coefficient Units	Coefficient Source	Coefficient Sources DIRS #	Coefficient Use in this Report
CO ₂ (aq) – SO ₄ ²⁻	λ	Ternary	kg/mol	He and Morse (1993)	162090	Attachment I
CO ₂ (aq) – H ⁺ – Cl ⁻	ζ	Ternary	kg/mol	He and Morse (1993)	162090	Attachment I
CO ₂ (aq) – Na ⁺ – Cl ⁻	ζ	Ternary	kg/mol	He and Morse (1993)	162090	Attachment I
CO ₂ (aq) – K ⁺ – Cl ⁻	ζ	Ternary	kg/mol	He and Morse (1993)	162090	Attachment I
CO ₂ (aq) – Ca ⁺⁺ – Cl ⁻	ζ	Ternary	kg/mol	He and Morse (1993)	162090	Attachment I
CO ₂ (aq) – Mg ⁺⁺ – Cl ⁻	ζ	Ternary	kg/mol	He and Morse (1993)	162090	Attachment I
CO ₂ (aq) – H ⁺ – SO ₄ ²⁻	ζ	Ternary	kg/mol	He and Morse (1993)	162090	Attachment I
CO ₂ (aq) – Na ⁺ – SO ₄ ²⁻	ζ	Ternary	kg/mol	He and Morse (1993)	162090	Attachment I
CO ₂ (aq) – K ⁺ – SO ₄ ²⁻	ζ	Ternary	kg/mol	He and Morse (1993)	162090	Attachment I
CO ₂ (aq) – Mg ⁺⁺ – SO ₄ ²⁻	ζ	Ternary	kg/mol	He and Morse (1993)	162090	Attachment I
SiO ₂ – H ⁺ – NO ₃ ⁻	ζ	Ternary	kg/mol	Felmy et al. (1994)	162111	Attachment I
SiO ₂ – Na ⁺ – Cl ⁻	ζ	Ternary	kg/mol	Felmy et al. (1994)	162111	Attachment I
SiO ₂ – Mg ⁺⁺ – Cl ⁻	ζ	Ternary	kg/mol	Felmy et al. (1994)	162111	Attachment I
O ₂ (aq) – Na ⁺ – Cl ⁻	ζ	Ternary	kg/mol	Clegg and Brimblecombe (1990)	162089	Attachment I
O ₂ (aq) – Na ⁺ – Br ⁻	ζ	Ternary	kg/mol	Clegg and Brimblecombe (1990)	162089	Attachment I
O ₂ (aq) – Na ⁺ – OH ⁻	ζ	Ternary	kg/mol	Clegg and Brimblecombe (1990)	162089	Attachment I
O ₂ (aq) – Na ⁺ – NO ₃ ⁻	ζ	Ternary	kg/mol	Clegg and Brimblecombe (1990)	162089	Attachment I
O ₂ (aq) – Na ⁺ – SO ₄ ²⁻	ζ	Ternary	kg/mol	Clegg and Brimblecombe (1990)	162089	Attachment I
O ₂ (aq) – K ⁺ – Cl ⁻	ζ	Ternary	kg/mol	Clegg and Brimblecombe (1990)	162089	Attachment I
O ₂ (aq) – K ⁺ – Br ⁻	ζ	Ternary	kg/mol	Clegg and Brimblecombe (1990)	162089	Attachment I
O ₂ (aq) – K ⁺ – OH ⁻	ζ	Ternary	kg/mol	Clegg and Brimblecombe (1990)	162089	Attachment I
O ₂ (aq) – K ⁺ – NO ₃ ⁻	ζ	Ternary	kg/mol	Clegg and Brimblecombe (1990)	162089	Attachment I
O ₂ (aq) – K ⁺ – SO ₄ ²⁻	ζ	Ternary	kg/mol	Clegg and Brimblecombe (1990)	162089	Attachment I
O ₂ (aq) – H ⁺ – Cl ⁻	ζ	Ternary	kg/mol	Clegg and Brimblecombe (1990)	162089	Attachment I
O ₂ (aq) – Li ⁺ – Cl ⁻	ζ	Ternary	kg/mol	Clegg and Brimblecombe (1990)	162089	Attachment I
O ₂ (aq) – Ca ⁺⁺ – Cl ⁻	ζ	Ternary	kg/mol	Clegg and Brimblecombe (1990)	162089	Attachment I
O ₂ (aq) – Ca ⁺⁺ – NO ₃ ⁻	ζ	Ternary	kg/mol	Clegg and Brimblecombe (1990)	162089	Attachment I
O ₂ (aq) – Na ⁺ – HCO ₃ ⁻	ζ	Ternary	kg/mol	Clegg and Brimblecombe (1990)	162089	Attachment I

Table 4. Ternary Pitzer Ion Interaction Coefficients (Continued)

Ions	Coefficient Name	Coefficient Type	Coefficient Units	Coefficient Source	Coefficient Sources DIRS #	Coefficient Use in this Report
$O_2(aq) - Na^+ - CO_3^{2-}$	ζ	Ternary	kg/mol	Clegg and Brimblecombe (1990)	162089	Attachment I
$Na^+ - K^+ - Cl^-$	ψ	Ternary	kg/mol	Greenberg and Møller (1989)	152684	Attachment I
$Na^+ - K^+ - SO_4^{2-}$	ψ	Ternary	kg/mol	Greenberg and Møller (1989)	152684	Attachment I
$Na^+ - Ca^{++} - Cl^-$	ψ	Ternary	kg/mol	Greenberg and Møller (1989)	152684	Attachment I
$Na^+ - Ca^{++} - SO_4^{2-}$	ψ	Ternary	kg/mol	Greenberg and Møller (1989)	152684	Attachment I
$Na^+ - Mg^{++} - Cl^-$	ψ	Ternary	kg/mol	Pabalan and Pitzer (1987)	162096	Attachment I
$Na^+ - Cl^- - OH^-$	ψ	Ternary	kg/mol	Pabalan and Pitzer (1987)	162096	Attachment I
$Na^+ - Cl^- - SO_4^{2-}$	ψ	Ternary	kg/mol	Greenberg and Møller (1989)	152684	Attachment I
$Na^+ - NO_3^- - AlO_2^-$	ψ	Ternary	kg/mol	Felmy et al. (1994)	162112	Attachment I
$Na^+ - OH^- - SO_4^{2-}$	ψ	Ternary	kg/mol	Pabalan and Pitzer (1987)	162096	Attachment I
$Na^+ - OH^- - AlO_2^-$	ψ	Ternary	kg/mol	Pabalan and Pitzer (1987)	162096	Attachment I
$K^+ - Ca^{++} - Cl^-$	ψ	Ternary	kg/mol	Greenberg and Møller (1989)	152684	Attachment I
$K^+ - Mg^{++} - Cl^-$	ψ	Ternary	kg/mol	Pabalan and Pitzer (1987)	162096	Attachment I
$K^+ - Cl^- - SO_4^{2-}$	ψ	Ternary	kg/mol	Greenberg and Møller (1989)	152684	Attachment I
$Ca^{++} - Cl^- - SO_4^{2-}$	ψ	Ternary	kg/mol	Greenberg and Møller (1989)	152684	Attachment I
$Mg^{++} - Cl^- - SO_4^{2-}$	ψ	Ternary	kg/mol	Pabalan and Pitzer (1987)	162096	Attachment I

4.1.2 Parameters

The variable input parameters important to the IDPS model are summarized in Table 5. The modeled incoming seepage includes the following components: Na, K, Ca, Mg, Cl, F, CO₃, SO₄, NO₃, SiO₂, Al, H, H₂O, and potentially Br. The input for hydrogen (H) is the pH of the incoming water. pH is the negative logarithm of the activity of the hydrogen ion. Input values for the aqueous component concentrations are acquired directly from water sample analyses or qualified technical product output from geochemical model simulations. Values for T , RH , f_{CO_2} , and f_{O_2} are selected by the user of the IDPS model to cover the expected ranges of these parameters for the systems being modeled (Section 6.6.2.4). The approximate atmospheric value for f_{O_2} ($10^{-0.7}$ bars) limits the model to oxidizing conditions and inhibits the components from reducing to lower oxidation states. The actual value of f_{O_2} has very little effect on the model results when it is above $10^{-9.0}$ bars, as can be demonstrated by running the model at a f_{O_2} value of $10^{-9.0}$ bars. Though f_{O_2} in the drift could decrease markedly during the thermal period when much of the air is replaced with water vapor, f_{O_2} is not expected to fall below $10^{-9.0}$ bars. Consequently, f_{O_2} is set at approximately atmospheric for all runs. Sources used to assign mineral suppressions in this model report are listed in Table 6.

Use of the IDPS model is demonstrated in an example in Section 6.7. This example demonstrates how the IDPS model is used to produce technical product output. The input data for this example are introduced in Section 4.4. They are not introduced here because the example inputs are not used to develop the IDPS model and the results from this example are not directly used in performance assessment. Model calculations used as input to the TSPA are to be documented elsewhere, such as in REV 02 of *Engineered Barrier System: Physical and Chemical Environment Model* (BSC 2003 [165601]).

Table 5. In-Drift Precipitates/Salts Model Input Parameters

Parameter Name	Parameter Description	Parameter Units	Parameter Source Range	Parameter Use in this Report
C_i^s	Concentration or activity of each modeled component i in the incoming seepage	mass/volume, moles/mass, or moles/volume (or pH for the hydrogen ion activity)	Predicted or measured major ion composition of a starting water of the system Na-K-H-Mg-Ca-Al-Cl-F-Br-NO ₃ -SO ₄ -CO ₃ -SiO ₂ -CO ₂ -O ₂ -H ₂ O	Section 4.4, Section 6.6.2.1, Section 6.7, Sections 7.1 to 7.3
T	Temperature	degrees Celsius	0 to 125	Section 4.4, Section 6.6.2.4, Section 6.7, Sections 7.1 to 7.3
RH	Relative humidity	Non-dimensional or percentage	0% to 100%	Section 4.4, Section 6.6.2.4, Section 6.7, Sections 7.1 to 7.3
f_{CO_2}	Fugacity of carbon dioxide	bars	0 to 1	Section 4.4, Section 6.6.2.4, Section 6.7, Sections 7.1 to 7.3
f_{O_2}	Fugacity of oxygen	bars	$10^{-0.7}$ (This value is chosen to represent a range of oxidizing conditions from $10^{-9.0}$ to $10^{-0.0}$, as explained in Section 4.1.2.)	Section 4.4, Section 6.6.2.4, Section 6.7, Sections 7.1 to 7.3
R^{es} (or Q^e/Q^s)	Relative evaporation rate	Non-dimensional	-99 to 1	Section 6.6.2.5, Section 6.7, Sections 7.1 to 7.3
S_m	Suppression flag for mineral m	Boolean	True or False	Section 6.6.2.6, Section 6.7, Sections 7.1 to 7.3

Table 6. Input Sources for Mineral Suppression Determinations

Mineral Classification	Source
Suppressed Minerals ($S_m = \text{True}$)	Borchardt 1995 [156639]; Carlos et al. 1995 [105213]; Deer et al 1966 [102773]; Eugster and Hardie 1978 [100743]; Kerr 1977 [161606]; Krauskopf 1979 [105909]; Langmuir 1997 [100051]; Vaniman et al. 1992 [107066]
Unsuppressed Minerals ($S_m = \text{False}$)	Carlos et al. 1995 [105213]; Eugster and Hardie 1978 [100743]; Faust 1953 [162282]; Fleischer and Efremov 1954 [162312]; Fleischer and Pabst 1983 [162284]; Hay 1966 [105965]; Hay and Wiggins 1980 [162281]; Jones 1983 [162331]; Kent and Kastner 1985 [162345]; Kerr 1977 [161606]; Langmuir 1997 [100051]; Li et al. 1997 [159034]; Palache et al. 1951 [162280]; Papke 1976 [162274]; Vaniman et al. 1992 [107066]; Walling et al. 1995 [162283]; Wollast et al. 1968 [162340]

4.2 CRITERIA

Project Requirements Document (Canori and Leitner 2003 [161770]) contains three criteria that are relevant to the work documented in this report. They are:

- PRD-002/T-014 Performance Objectives for the Geologic Repository After Permanent Closure; see 10 CFR 63.113 for complete requirement text.
- PRD-002/T-015 Requirements for Performance Assessment; see 10 CFR 63.114 for complete requirement text.
- PRD-002/T-016 Requirements for Multiple Barriers; see 10 CFR 63.115 for complete requirement text.

Work described in this model report support these requirements, but more specific criteria exist in *Yucca Mountain Review Plan, Final Report* (NRC 2003 [163274]). Selected Yucca Mountain Review Plan acceptance criteria are presented in order to supplement or clarify the Project Requirements Document.

Yucca Mountain Review Plan, Final Report (NRC 2003 [163274]) acceptance criteria, identified as applicable to this model report, are presented in the following subsections.

4.2.1 Degradation of Engineered Barriers Acceptance Criteria

The degradation of engineered barriers acceptance criteria are referenced from Section 2.2.1.3.1.3 of NRC (2003 [163274]). These criteria originate from 10 CFR 63.114(a)-(c) and (e)-(g).

4.2.1.1 Acceptance Criterion 1 – System Description and Model Integration Are Adequate

- (1) The total system performance assessment adequately incorporates important design features, physical phenomena, and couplings, and uses consistent and appropriate assumptions throughout the degradation of engineered barriers abstraction process.
- (2) Assessment abstraction of the degradation of engineered barriers uses assumptions, technical bases, data, and models that are appropriate and consistent with other related U.S. Department of Energy abstractions. For example, the assumptions used for degradation of engineered barriers should be consistent with the abstractions of the quantity and chemistry of water contacting waste packages and waste forms (Section 2.2.1.3.3); climate and infiltration (Section 2.2.1.3.5); and mechanical disruption of waste packages (Section 2.2.1.3.2). The descriptions and technical bases provide transparent and traceable support for the abstraction of the degradation of engineered barriers.
- (3) The descriptions of engineered barriers, design features, degradation processes, physical phenomena, and couplings that may affect the degradation of the

engineered barriers are adequate. For example, materials and methods used to construct the engineered barriers are included, and degradation processes, such as uniform corrosion, pitting corrosion, crevice corrosion, stress corrosion cracking, inter-granular corrosion, microbially influenced corrosion, dry-air oxidation, hydrogen embrittlement, and the effects of wet and dry cycles, material aging and phase stability, welding, and initial defects on the degradation modes for the engineered barriers are considered.

- (4) Boundary and initial conditions used in the total system performance assessment abstractions are propagated consistently throughout the abstraction approaches. For example, the conditions and assumptions used in the degradation of engineered barriers abstraction are consistent with those used to model the quantity and chemistry of water contacting waste packages and waste forms (Section 2.2.1.3.3); climate and infiltration (Section 2.2.1.3.5); and mechanical disruption of waste packages (Section 2.2.1.3.2).
- (5) Sufficient technical bases for the inclusion of features, events, and processes related to degradation of engineered barriers in the total system performance assessment abstractions are provided.
- (7) Guidance in NUREG–1297 (Altman et al. 1988 [103597]) and NUREG–1298 (Altman et al. 1988 [103750]), or other acceptable approaches, is followed.

4.2.1.2 Acceptance Criterion 2 – Data Are Sufficient for Model Justification

- (1) Parameters used to evaluate the degradation of engineered barriers in the license application are adequately justified (e.g., laboratory corrosion tests, site-specific data such as data from drift-scale tests, in-service experience in pertinent industrial applications, and test results not specifically performed for the Yucca Mountain site, etc.). The U.S. Department of Energy describes how the data were used, interpreted, and appropriately synthesized into the parameters.
- (2) Sufficient data have been collected on the characteristics of the engineered components, design features, and the natural system to establish initial and boundary conditions for abstraction of degradation of engineered barriers.

4.2.1.3 Acceptance Criterion 3 – Data Uncertainty Is Characterized and Propagated Through the Model Abstraction

- (1) Models use parameter values, assumed ranges, probability distributions, and/or bounding assumptions that are technically defensible, reasonably account for uncertainties and variabilities, and do not result in an under-representation of the risk estimate.
- (2) For those degradation processes that are significant to the performance of the engineered barriers, the U.S. Department of Energy provides appropriate parameters, based on techniques that may include laboratory experiments, field measurements, industrial analogs, and process-level modeling studies conducted

under conditions relevant to the range of environmental conditions within the waste package emplacement drifts. The U.S. Department of Energy also demonstrates the capability to predict the degradation of the engineered barriers in laboratory and field tests.

- (3) For the selection of parameters used in conceptual and process-level models of engineered barrier degradation that can be expected under repository conditions, assumed range of values and probability distributions are not likely to underestimate the actual degradation and failure of engineered barriers as a result of corrosion.

4.2.1.4 Acceptance Criterion 4 – Model Uncertainty Is Characterized and Propagated Through the Model Abstraction

- (1) Alternative modeling approaches of features, events, and processes are considered and are consistent with available data and current scientific understanding, and the results and limitations are appropriately considered in the abstraction.
- (2) Consideration of conceptual model uncertainty is consistent with available site characterization data, laboratory experiments, field measurements, natural analog information and process-level modeling studies; and the treatment of conceptual model uncertainty does not result in an under-representation of the risk estimate.
- (3) The U.S. Department of Energy uses alternative modeling approaches, consistent with available data and current scientific understanding, and evaluates the model results and limitations, using tests and analyses that are sensitive to the processes modeled. For example, for processes such as uniform corrosion, localized corrosion, and stress corrosion cracking of the engineered barriers, the U.S. Department of Energy considers alternative modeling approaches, to develop its understanding of Review Plan for Safety Analysis Report environmental conditions and material factors significant to these degradation processes.

4.2.1.5 Acceptance Criterion 5 – Model Abstraction Output Is Supported by Objective Comparisons

- (1) Models implemented in this total system performance assessment abstraction provide results consistent with output from detailed process-level models and/or empirical observations (laboratory and field testings and/or natural analogs).
- (5) Accepted and well-documented procedures are used to construct and test the numerical models that simulate the engineered barrier chemical environment and degradation of engineered barriers.

4.2.2 Quantity and Chemistry of Water Contacting Waste Packages and Waste Forms Acceptance Criteria

The acceptance criteria for the quantity and chemistry of water contacting waste packages and waste forms are referenced from Section 2.2.1.3.3.3 of NRC (2003 [163274]) and 10 CFR 63.114(a)-(c) and (e)-(g).

4.2.2.1 Acceptance Criterion 1 – System Description and Model Integration are Adequate

- (1) Total system performance assessment adequately incorporates important design features, physical phenomena, and couplings, and uses consistent and appropriate assumptions throughout the quantity and chemistry of water contacting waste packages and waste forms abstraction process.
- (2) The abstraction of the quantity and chemistry of water contacting waste packages and waste forms uses assumptions, technical bases, data, and models, that are appropriate and consistent with other related U.S. Department of Energy abstractions. For example, the assumptions used for the quantity and chemistry of water contacting waste packages and waste forms are consistent with the abstractions of “Degradation of Engineered Barriers” (Section 2.2.1.3.1); “Mechanical Disruption of Waste Packages” (Section 2.2.1.3.2); “Radionuclide Release Rates and Solubility Limits” (Section 2.2.1.3.4); “Climate and Infiltration” (Section 2.2.1.3.5); and “Flow Paths in the Unsaturated Zone” (Section 2.2.1.3.6). The descriptions and technical bases provide transparent and traceable support for the abstraction of quantity and chemistry of water contacting waste packages and waste forms.
- (3) Important design features, such as waste package design and material selection, backfill, drip shield, ground support, thermal loading strategy, and degradation processes, are adequate to determine the initial and boundary conditions for calculations of the quantity and chemistry of water contacting waste packages and waste forms.
- (5) Sufficient technical bases and justification are provided for total system performance assessment assumptions and approximations for modeling coupled thermal-hydrologic-mechanical-chemical effects on seepage and flow, the waste package chemical environment, and the chemical environment for radionuclide release. The effects of distribution of flow on the amount of water contacting the waste packages and waste forms are consistently addressed, in all relevant abstractions.
- (6) The expected ranges of environmental conditions within the waste package emplacement drifts, inside of breached waste packages, and contacting the waste forms and their evolution with time are identified. These ranges may be developed to include: (i) the effects of the drip shield and backfill on the quantity and chemistry of water (e.g., the potential for condensate formation and dripping

from the underside of the shield); (ii) conditions that promote corrosion of engineered barriers and degradation of waste forms; (iii) irregular wet and dry cycles; (iv) gamma-radiolysis; and (v) size and distribution of penetrations of waste packages.

- (7) The model abstraction for quantity and chemistry of water contacting waste packages and waste forms is consistent with the detailed information on waste package design and other engineered features. For example, consistency is demonstrated for: (i) dimensionality of the abstractions; (ii) various design features and site characteristics; and (iii) alternative conceptual approaches. Analyses are adequate to demonstrate that no deleterious effects are caused by design or site features that the U.S. Department of Energy does not take into account in this abstraction.
- (12) Guidance in NUREG-1297 (Altman et al. 1988 [103597]) and NUREG-1298 (Altman et al. 1988 [103750]), or other acceptable approaches, is followed.

4.2.2.2 Acceptance Criterion 2 – Data are Sufficient for Model Justification

- (1) Geological, hydrological, and geochemical values used in the license application are adequately justified. Adequate description of how the data were used, interpreted, and appropriately synthesized into the parameters is provided.
- (2) Sufficient data were collected on the characteristics of the natural system and engineered materials to establish initial and boundary conditions for conceptual models of thermal-hydrologic-mechanical-chemical coupled processes, that affect seepage and flow and the waste package chemical environment.

4.2.2.3 Acceptance Criterion 3 – Data Uncertainty Is Characterized and Propagated Through the Model Abstraction

- (1) Models use parameter values, assumed ranges, probability distributions, and bounding assumptions that are technically defensible, reasonably account for uncertainties and variabilities, and do not result in an under-representation of the risk estimate.
- (2) Parameter values, assumed ranges, probability distributions, and bounding assumptions used in the total system performance assessment calculations of quantity and chemistry of water contacting waste packages and waste forms are technically defensible and reasonable, based on data from the Yucca Mountain region (e.g., results from large block and drift-scale heater and niche tests), and a combination of techniques that may include laboratory experiments, field measurements, natural analog research, and process-level modeling studies.
- (3) Input values used in the total system performance assessment calculations of quantity and chemistry of water contacting engineered barriers (e.g., drip shield and waste package) are consistent with the initial and boundary conditions and the assumptions of the conceptual models and design concepts for the Yucca

Mountain site. Correlations between input values are appropriately established in the U.S. Department of Energy total system performance assessment. Parameters used to define initial conditions, boundary conditions, and computational domain in sensitivity analyses involving coupled thermal-hydrologic-mechanical-chemical effects on seepage and flow, the waste package chemical environment, and the chemical environment for radionuclide release, are consistent with available data. Reasonable or conservative ranges of parameters or functional relations are established.

- (4) Adequate representation of uncertainties in the characteristics of the natural system and engineered materials is provided in parameter development for conceptual models, process-level models, and alternative conceptual models. The U.S. Department of Energy may constrain these uncertainties using sensitivity analyses or conservative limits. For example, the U.S. Department of Energy demonstrates how parameters used to describe flow through the engineered barrier system bound the effects of backfill and excavation-induced changes.

4.2.2.4 Acceptance Criterion 4 – Model Uncertainty Is Characterized and Propagated Through the Model Abstraction

- (1) Alternative modeling approaches of features, events, and processes are considered and are consistent with available data and current scientific understanding, and the results and limitations are appropriately considered in the abstraction.
- (2) Alternative modeling approaches are considered and the selected modeling approach is consistent with available data and current scientific understanding. A description that includes a discussion of alternative modeling approaches not considered in the final analysis and the limitations and uncertainties of the chosen model is provided.
- (3) Consideration of conceptual model uncertainty is consistent with available site characterization data, laboratory experiments, field measurements, natural analog information and process-level modeling studies; and the treatment of conceptual model uncertainty does not result in an under-representation of the risk estimate.
- (4) Adequate consideration is given to effects of thermal-hydrologic-mechanical-chemical coupled processes in the assessment of alternative conceptual models. These effects may include: (i) thermal-hydrologic effects on gas, water, and mineral chemistry; (ii) effects of microbial processes on the waste package chemical environment and the chemical environment for radionuclide release; (iii) changes in water chemistry that may result from the release of corrosion products from the waste package and interactions between engineered materials and ground water; and (iv) changes in boundary conditions (e.g., drift shape and size) and hydrologic properties, relating to the response of the geomechanical system to thermal loading.

4.2.2.5 Acceptance Criterion 5 – Model Abstraction Output is Supported by Objective Comparisons

- (1) The models implemented in this total system performance assessment abstraction provide results consistent with output from detailed process-level models and/or empirical observations (laboratory and field testings and/or natural analogs).
- (2) Abstracted models for coupled thermal-hydrologic-mechanical-chemical effects on seepage and flow and the waste package chemical environment, as well as on the chemical environment for radionuclide release, are based on the same assumptions and approximations demonstrated to be appropriate for process-level models or closely Review Plan for Safety Analysis Report analogous natural or experimental systems. For example, abstractions of processes, such as thermally induced changes in hydrological properties, or estimated diversion of percolation away from the drifts, are adequately justified by comparison to results of process-level modeling, that are consistent with direct observations and field studies.
- (3) Accepted and well-documented procedures are used to construct and test the numerical models that simulate coupled thermal-hydrologic-mechanical-chemical effects on seepage and flow, waste package chemical environment, and the chemical environment for radionuclide release. Analytical and numerical models are appropriately supported. Abstracted model results are compared with different mathematical models, to judge robustness of results.

4.3 CODES AND STANDARDS

10 CFR 63. Energy: Disposal of High-Level Radioactive Wastes in a Geologic Repository at Yucca Mountain, Nevada.

4.4 VALIDATION AND DEMONSTRATION DATA

Data used to validate and demonstrate the IDPS model are presented in Table 7 through Table 14. These data are independent of IDPS model development and therefore are not presented in Sections 4.1.1 or 4.1.2. The model is validated and demonstrated using these data in Sections 7 and 6.7, respectively. The data include laboratory evaporation data (Table 7 through Table 10), seawater evaporation data (Table 11), properties of salts and salt solutions (Table 12 and Table 13), and the composition of average J-13 well water (Table 14). The evaporation data are used and discussed in Section 7.1, the properties of salts and salt solutions in Section 7.2, and the average J-13 well water composition in Sections 6.7 and 7.3.

In-Drift Precipitates/Salts Model

Table 7. Water Chemistry Data From Experimental J-13 Well Water Evaporation of Rosenberg et al. (1999 [125338])

Constituent	Units	Synthetic J-13 Well Water for evap1	Evaporated Synthetic J-13 Well Water for evap1 (Concentration Factor: 956)	Synthetic J-13 Well Water for evap4	Evaporated Synthetic J-13 Well Water for evap4 (Concentration Factor: 157)
Ca	mg/kg	6.4	29.86	5.3	1.2
Mg	mg/kg	2.2	0.14	2.1	0.05
Na	mg/kg	46	44082	45.4	5298
K	mg/kg	5.3	4792	4.9	560
SiO ₂	mg/kg	11.3	18008	10	999
NO ₃	mg/kg	8.0	5532	8.0	1050
HCO ₃	mg/kg	108	24878	103	4295
Cl	mg/kg	6.9	4835	7.5	849
F	mg/kg	2.2	1550	2.4	247
SO ₄	mg/kg	18.1	12926	19	2162
pH	pH	7.84	nr ^a	8.33	10.18

DTN: LL991008104241.042 (Tables S00004_001 and S00004_004)

^a not reported

Table 8. pH Data From Experimental J-13 Well Water Evaporation of Rosenberg et al. (1999 [125338])

Concentration Factor	pH
1	8.46
1	8.65
1.05	9.04
1.29	9.43
1.6	9.58
2.41	9.67
6.08	9.67
6.37	9.77
7.59	9.79
11.6	9.95
12.6	10
15.3	10.03
20.9	10.08
25.2	10.09
34.4	10.12
52.1	10.18
104	10.18
157	10.18

DTN: LL991008104241.042 (Table S00004_003)

Table 9. Water Chemistry Data From Experimental 100x J-13 Well Water (CRWMS M&O 2000 [146460])

Constituent	Units	Synthetic 100x J-13 Well Water	Evaporated Synthetic 100x J-13 Well Water
Ca	mg/L	5	36
Mg	mg/L	2	0
Na	mg/L	4032	76314
K	mg/L	513	10832
NO ₃	mg/L	732	14085
CO ₃ (as HCO ₃)	mg/L	4142	54614
Cl	mg/L	730	14419
F	mg/L	208	3630
SO ₄	mg/L	1632	29783
pH	pH	nr ^a	nr

DTN: LL000202905924.117 (Table S00134_002)

^a not reported

Table 10. Water Chemistry Data From Topopah Spring Pore Water Evaporation Experiment of Rosenberg et al. (1999 [125339])

Constituent	Units	Synthetic Pore Water	Evaporated Synthetic Pore Water (Concentration Factor: 1243x)
Ca	mg/kg	57.2	15629
Mg	mg/kg	11.7	5478
Na	mg/kg	8.2	5961
K	mg/kg	4.2	2779
SiO ₂	mg/kg	9.8	513
NO ₃	mg/kg	11.0	nm ^a
HCO ₃	mg/kg	16.2	< 35
Cl	mg/kg	78.0	53084
F	mg/kg	2.3	< 577
SO ₄	mg/kg	81.7	2077
pH	pH	7.68	6-6.5 ^b

DTN: LL991008004241.041 (Table S00002_002)

^a not reported

^b estimation from pH paper

Table 11. Sample Data for Evaporated Seawater

Brine	T (°C)	Den. ^a (mg/ cm ³)	pH	IS	Deg. of Ev. ^b	Total Concentration (molal)						
						Cl	Br	SO ₄	Mg	Ca	K	Na
w63	28.4	1024	8.19	0.72	0.95	0.579	0.000883	0.0294	0.0520	0.00987	0.0107	0.497
w64	—	1024	-	0.73	0.98	0.585	0.000917	0.0303	0.0541	0.00985	0.0111	0.497
w49	28.6	1028	8.12	0.75	1.10	0.594	0.000931	0.0305	0.0604	0.0108	0.0120	0.506
w53	29.9	1028	8.15	0.83	1.17	0.649	0.00099	0.0339	0.0642	0.0118	0.0132	0.582
w57	30.0	1040	8.33	1.21	1.75	0.947	0.00149	0.0518	0.0965	0.0192	0.0179	0.839
w54	32.6	1050	8.43	1.5	2.26	1.21	0.00177	0.0615	0.124	0.0210	0.0219	1.01
w55	29.6	1060	8.53	1.79	2.68	1.44	0.00224	0.0781	0.147	0.0247	0.0266	1.22
w52	30.4	1075	8.35	2.23	3.16	1.79	0.00285	0.0956	0.174	0.0316	0.0348	1.60
w56	31.4	1088	8.11	2.48	3.53	2.03	0.00305	0.110	0.194	0.0401	0.0392	1.71
w51	30.2	1103	8.14	2.98	4.36	2.49	0.00375	0.123	0.240	0.0325	0.0468	2.16
w50	29.8	1141	7.85	3.95	6.07	3.50	0.00536	0.138	0.334	0.0171	0.0623	2.93
w58	32.3	1151	7.70	4.41	6.91	3.87	0.00584	0.156	0.381	0.0185	0.0723	3.36
w48	28.8	1181	7.60	5.37	8.45	4.90	0.00733	0.184	0.466	0.0123	0.0905	4.17
w59	32.6	1181	7.56	5.39	8.62	4.90	0.00722	0.175	0.475	0.0121	0.0877	4.21
w61	32.1	1187	7.53	5.46	9.03	4.90	0.00757	0.190	0.498	0.0107	0.0914	4.22
w46	33.2	1215	7.42	6.25	10.5	5.67	0.00880	0.205	0.579	0.00610	0.112	5.00
w62	34.1	1215	7.43	6.34	11.0	5.88	0.00938	0.232	0.604	0.00581	0.109	4.83
w37	29.5	1220	7.41	6.49	12.6	5.91	0.0108	0.254	0.691	0.00433	0.115	4.70
w43	32.5	1220	7.45	6.68	13.2	5.75	0.0119	0.274	0.728	0.00352	0.152	5.02
w35	28.9	1224	7.44	6.88	15.1	6.04	0.0127	0.287	0.830		0.157	4.74
w42	32.8	1224	7.34	6.94	16.4	5.82	0.0138	0.314	0.904		0.180	4.67
w44	31.9	1225	7.40	6.96	17.6	5.72	0.0146	0.328	0.968		0.190	4.48
w34	31.8	1231	7.25	7.27	20.1	5.98	0.0167	0.381	1.11		0.208	4.14
w32	32.0	1231	7.28	7.34	20.4	6.01	0.0174	0.399	1.13		0.212	4.13
w33	30.7	1236	7.22	7.75	23.4	6.08	0.0195	0.446	1.29		0.249	4.11
w30	31.4	1239	7.28	7.61	23.6	5.98	0.0208	0.417	1.30		0.242	3.96
w28	32.4	1239	7.13	7.87	25.4	6.08	0.0195	0.478	1.40		0.253	3.81
w41	32.7	1242	7.22	7.84	26.8	5.85	0.0230	0.450	1.48		0.278	3.72
w45	35.1	1249	7.06	8.42	31.4	5.92	0.0264	0.600	1.73		0.33	3.32
w38	29.6	1254	7.12	8.65	32.8	5.96	0.0287	0.678	1.81		0.339	3.17
w36	29.9	1254	7.03	8.64	34.0	5.83	0.0282	0.632	1.87		0.342	3.19
w40	32.1	1260	7.00	9.01	36.8	5.89	0.0299	0.694	2.03		0.379	3.06
w39	32.6	1260	6.99	9.33	39.4	5.93	0.0331	0.776	2.17		0.402	2.83
36#1				9.29	40.4	5.86	0.0343	0.753	2.23		0.417	2.63
40#1				9.47	43.5	5.74	0.0356	0.796	2.39		0.443	2.31
36#2				9.81	44.8	6.03	0.0384	0.849	2.47		0.449	2.27
40#2				10.1	48.9	5.80	0.0401	0.895	2.70		0.495	1.96
36#3				11.3	58.1	6.10	0.0482	1.11	3.20		0.591	1.37
40#3				11.4	58.6	6.26	0.0481	1.09	3.23		0.588	1.50
40#4				11.9	63.6	6.23	0.0518	1.19	3.50		0.637	1.16
39#1				12.7	66.2	6.62	0.0590	1.21	3.91		0.632	0.842
36#4				13.0	69.2	6.47	0.0598	1.35	3.99		0.754	0.712
40#5				12.3	72.9	7.13	0.0661	0.966	3.76		0.782	0.825
40#6				12.3	78.8	7.38	0.0716	0.763	3.98		0.712	0.545
39#6				12.2	87.9	7.50	0.0777	0.679	4.03		0.565	0.413
39#2				11.8	87.9	6.89	0.0748	0.703	3.96		0.348	0.553
39#3				12.4	93.3	7.50	0.0773	0.664	4.20		0.311	0.500
36#5				12.8	97.1	7.80	0.0828	0.713	4.27		0.597	0.428
39#4				9.53	98.1	5.99	0.0774	0.366	3.35		0.125	0.169

Source: (McCaffrey et al. 1987 [164481] Tables 1 through 3)

^a density of sample^b degree of evaporation (equivalent to concentration factor, relative to seawater)

Table 12. Aqueous Solubilities of Na, K, Ca, and Mg Salts

Salt	Aqueous Solubility at 25°C (mass percent of solute)	Aqueous Solubility at 100°C (mass percent of solute)
NaCl	26.45%	28.05%
KCl	26.22%	36.05%
CaCl ₂	44.83%	59.94%
MgCl ₂	35.90%	42.15%
NaHCO ₃	9.32%	19.10%
KHCO ₃	26.6%	40.45% at 70°C
Na ₂ CO ₃	23.5%	30.09%
K ₂ CO ₃	52.7%	61.0%
NaF	3.97%	4.82%
KF	50.4%	60.0% at 80°C
CaF ₂	0.0016%	not reported above 25°C
MgF ₂	0.013%	not reported above 25°C
Na ₂ SO ₄	21.94%	29.67%
K ₂ SO ₄	10.7%	19.3%
CaSO ₄	0.205%	0.163%
MgSO ₄	26.3%	33.3%
NaBr	48.6%	54.9%
KBr	40.4%	50.8%
CaBr ₂	61.0%	73.0% at 60°C
MgBr ₂	50.6%	55.7%
NaNO ₃	47.7%	63.8%
KNO ₃	27.7%	70.8%
Ca(NO ₃) ₂	59.0%	78.5%
Mg(NO ₃) ₂	41.6%	72.0%

Source: (Lide 2000 [162229] pp. 8-102 to 8-110)

Table 13. Equilibrium Relative Humidity for Saturated Aqueous Solutions in Contact With an Excess of Solid-Phase Salts

Salt	Equilibrium Relative Humidity (%)	Temperature of Measurement (°C)
NaCl	76.4	80
KCl	79.5	80
MgCl ₂ · 6H ₂ O	33.0	25
Na ₂ CO ₃ · 10H ₂ O	87 ^a	24.5
K ₂ CO ₃ · 2H ₂ O	42	40
NaF	96.6 ^a	100
KF	22.9 ^a	100
Na ₂ SO ₄ · 10H ₂ O	93 ^a	20
K ₂ SO ₄	96	60
NaNO ₃	65.5	80
KNO ₃	82	60
KNO ₃ , NaNO ₃ , and NaCl	30.49 ^a	16.39

Source: (Dean 1992 [100722] p. 11.6)

^a Weast and Astle 1981 [100833] p. E-44

Table 14. Average In Situ Composition of Water from Well J-13

Constituent	Units	Average J-13 Well Water Concentration
Al	mg/L	0.028 ^a
Ca	mg/L	13
Mg	mg/L	2.01
Na	mg/L	45.8
K	mg/L	5.04
Si	mg/L	28.5
NO ₃	mg/L	8.78
Alkalinity (as HCO ₃)	mg/L	128.9
Cl	mg/L	7.1
F	mg/L	2.2
SO ₄	mg/L	18.4
Lab pH	standard units	7.41
Field pH	standard units	6.9 and 7.1 ^b
Temperature	Celsius	31 ^b
O ₂ (aq)	mg/L	5.5 to 5.7 ^b

DTN: MO0006J13WTRCM.000

^a mean detected value in Table 4.2 (Harrar et al. 1990 [100814] p 4.3)

^b Harrar et al. 1990 [100814] p 4.9

5. ASSUMPTIONS

This section addresses the assumptions built into the IDPS model. There are no upstream assumptions relevant to the IDPS model.

5.1 STANDARD STATE OF WATER

Assumption: Water is at standard state.

Basis: As discussed in Section 6.3.1, an aqueous solution at standard state has an equilibrium relative humidity that is equivalent to the activity of water in the aqueous solution. Standard state in this sense implies that the water-air interface is flat (i.e, that the boundary between water and air is a plane) and that the behavior of the water molecule (H₂O) is not influenced by solid surfaces in contact with the water. Adsorption and air-water interface curvature, such as the curvature of menisci caused by capillary forces, create non-standard state conditions with respect to vapor pressure and equilibrium relative humidity near the air-water interface (Walton 1994 [127454]; Koorevaar et al. 1983 [125329] pp. 67-68).

For the IDPS model, non-standard state water is not considered. Only dissolved salts and temperature are considered to affect liquid-vapor equilibrium. The small amounts of water held in double layers and adsorbed to solid surfaces have negligible roles in radionuclide transport and waste package corrosion due to their near immobility. Water held by the surface tension effects of capillary binding are more mobile than water in double layers or adsorbed to solids; however, even capillary forces under very dry conditions (in the range of negative 500 meters water pressure head) have a limited effect on H₂O activity in solution (Walton 1994 [127454] pp. 3480-3481). Because of this limited effect, the assumption that water in the IDPS model is at standard state is negligible compared to the more sizable uncertainties in the IDPS model and model inputs (Section 8.4).

Confirmation Status: No further confirmation is required.

Use in the Model: This assumption is used throughout.

5.2 EQUILIBRIUM CONDITIONS

Assumption: The system is in a state of local metastable equilibrium. All aqueous and gas constituents in the model achieve and maintain local equilibrium, and most mineral phases achieve and maintain local equilibrium upon saturation. Several slow-forming and unlikely minerals identified in Section 6.6.2.6 will not precipitate upon saturation or super saturation. The model can be used, however, to make steady-state non-equilibrium predictions with respect to relative humidity, provided the appropriate inputs are used (Section 6.6.3.3).

Basis: Most chemical reactions included in the model occur rapidly compared to the modeling timeframe. Redox reactions, which generally are not rapid, are not included in the model. Similarly, certain mineral precipitation reactions are not expected to be rapid enough to occur to a considerable degree for the anticipated applications of the model. Mineral precipitation reactions that fall into this category are suppressed, as explained in Section 6.6.2.6, permitting the formation of metastable mineral phases in the model.

Confirmation Status: No further confirmation is required.

Use in the Model: This assumption is used throughout.

6. MODEL DISCUSSION

6.1 MODELING OBJECTIVES

The objective of the IDPS model is to predict the effects of evaporation and deliquescence on the chemical evolution of potential aqueous solutions and mineral deposition within the proposed repository. Specific details of these objectives are described in Section 1. The data used to develop the model are identified in Section 4.1. Data used to demonstrate the model (Section 6.7) are presented in Table 14 of Section 4.4. Data used in validation are addressed in Section 7.

6.2 FEATURES, EVENTS, AND PROCESSES INCLUDED IN MODEL

The development of a comprehensive list of features, events, and processes (FEPs) potentially relevant to postclosure performance of the potential Yucca Mountain repository is an ongoing, iterative process based on site-specific information, design, and regulations. The approach for developing an initial list of FEPs, in support of Total System Performance Assessment - Site Recommendation (TSPA-SR) (CRWMS M&O 2000 [153246]), was documented in Freeze et al. (2001 [154365]). The initial FEP list contained 328 FEPs, of which 176 were included in TSPA-SR models (CRWMS M&O 2000 [153246] Tables B-9 through B-17). To support TSPA-LA, the FEP list was re-evaluated in accordance with the Enhanced FEP Plan (BSC 2002 [158966] Section 3.2). Table 15 provides a list of FEPs that are included in TSPA-LA models described in this model document.

Table 15 includes all FEPs identified in the EBS TWP (BSC 2003 [165601] Table 6) as included in the IDPS model. For each of these FEPs, the implementation in TSPA-LA is described in this model document. Details of the implementations are summarized here in the table, including specific references to sections within this document.

Table 15. TSPA-LA FEPs Included in Model

FEP Number	FEPs Subject	Section Where Disposition is Described	Summary of Disposition in TSPA-LA
2.1.09.01.0A	Chemical characteristics of water in drifts	Section 6.6.3.5	<p>This model document provides a partial treatment of this FEP. The relevant parameters and ranges for this model are listed in Table 5. The IDPS model is designed to perform in-drift water chemistry calculations that provide detail required for predicting interactions of water chemistry with in-drift materials. Further disposition of this FEP is to be addressed in REV 02 of <i>Engineered Barrier System: Physical and Chemical Environment Model</i> (BSC 2003 [165601]).</p> <p>The IDPS model lookup table output includes boundary values, abstraction output, and supplemental calculations, as defined in Section 6.6.3.5. Boundary values include temperature, the fugacities of carbon dioxide and oxygen, and the reaction progress. Abstraction output includes pH, activity of water, ionic strength, mass of solvent water remaining, total concentrations of each element, concentrations of select aqueous species that potentially contribute to acid-neutralizing capacity, and amounts of solids precipitating in a given EQ6 run. Supplemental calculations include relative humidity, concentration factor, relative evaporation rate, and dilution factor.</p>
2.1.09.28.0A, 2.1.09.28.0B	Deliquescence on waste package outer surface and deliquescence on drip shield outer surface	Section 6.4	<p>This model document provides a partial treatment of these FEPs. The IDPS model is intended to be used in REV 02 of <i>Engineered Barrier System: Physical and Chemical Environment Model</i> to predict the composition of water on the waste package and/or drip shield resulting from the deliquescence of salts and dust deposited on these surfaces (BSC 2003 [165601]).</p> <p>The IDPS model lookup table output includes boundary values, abstraction output, and supplemental calculations, as defined in Section 6.6.3.5. Boundary values include temperature, the fugacities of carbon dioxide and oxygen, and the reaction progress. Abstraction output includes pH, activity of water, ionic strength, mass of solvent water remaining, total concentrations of each element, concentrations of select aqueous species that potentially contribute to acid-neutralizing capacity, and amounts of solids precipitating in a given EQ6 run. Supplemental calculations include relative humidity, concentration factor, relative evaporation rate, and dilution factor.</p>
2.1.09.06.0A	Reduction-oxidation potential in EBS	Section 4.1.2	<p>This model document provides a partial treatment of this FEP. The IDPS model is only validated for oxidizing conditions. Oxidizing conditions prevail as long as the equilibrium fugacity of oxygen does not fall far below 10^{-9} bars.</p> <p>The IDPS model lookup table output includes boundary values, abstraction output, and supplemental calculations, as defined in Section 6.6.3.5. Boundary values include temperature, the fugacities of carbon dioxide and oxygen, and the reaction progress. Abstraction output includes pH, activity of water, ionic strength, mass of solvent water remaining, total concentrations of each element, concentrations of select aqueous species that potentially contribute to acid-neutralizing capacity, and amounts of solids precipitating in a given EQ6 run. Supplemental calculations include relative humidity, concentration factor, relative evaporation rate, and dilution factor.</p>

Table 15. TSPA-LA FEPs Included in Model (Continued)

FEP Number	FEPs Subject	Section Where Disposition is Described	Summary of Disposition in TSPA-LA
2.1.09.07.0A	Reaction kinetics in EBS	Section 5.2	This model document provides a partial treatment of this FEP. In the IDPS model, all aqueous and gas constituents achieve and maintain local equilibrium, and most mineral phases achieve and maintain local equilibrium upon saturation. Most chemical reactions included in the model occur rapidly compared to the modeling timeframe. Redox reactions, which generally are not rapid, are not included in the model. Similarly, certain mineral precipitation reactions are not expected to be rapid enough to occur to a considerable degree for the anticipated applications of the model. Mineral precipitation reactions that fall into this category are suppressed, as explained in Section 6.6.2.6, permitting the formation of metastable mineral phases in the model. Reaction rates themselves are not included in the model because the model is used to develop lookup tables that provide water compositions that are independent of time, i.e., at metastable equilibrium.
2.1.11.01.0A	Heat generation in EBS	Section 6.6.2.4	This model document provides a partial treatment of this FEP because the IDPS model is designed to cover temperatures ranging up to 125°C (Table 5), which can result from heat generation. Processes in the model that could cause heat generation (e.g., condensation) are likely negligible compared to other sources. Thus, actual generation of heat by the processes in the model is not considered.
2.1.11.08.0A	Thermal effects on chemistry and microbial activity in the EBS	Section 6.6.3.5	This model document provides a partial treatment of this FEP. The IDPS model performs in-drift water chemistry calculations that provide detail required for predicting interactions of water chemistry with microbes. Disposition of this FEP is to be addressed in detail in REV 02 of <i>Engineered Barrier System: Physical and Chemical Environment Model</i> (BSC 2003 [165601]). The IDPS model lookup table output includes boundary values, abstraction output, and supplemental calculations, as defined in Section 6.6.3.5. Boundary values include temperature, the fugacities of carbon dioxide and oxygen, and the reaction progress. Abstraction output includes pH, activity of water, ionic strength, mass of solvent water remaining, total concentrations of each element, concentrations of select aqueous species that potentially contribute to acid-neutralizing capacity, and amounts of solids precipitating in a given EQ6 run. Supplemental calculations include relative humidity, concentration factor, relative evaporation rate, and dilution factor.

6.3 SALTS/PRECIPITATES PROCESSES

6.3.1 Evaporation, Relative Humidity, and Salt Precipitation

Within a drift environment, water exists in two phases, liquid and vapor. Because these two phases are in contact with one another throughout time (except in the event that all liquid water vaporizes), Brownian motion causes water molecules to exchange constantly between the two phases. According to the Maxwell-Boltzmann law, a fraction of the molecules in one phase has the energy required to make the transformation to the other phase, and vice versa, for as long as both phases exist (Mahan 1975 [125331] pp. 131-139).

Under equilibrium conditions, there is no net movement of water molecules from one phase to the other, i.e., the non-zero evaporation rate equals the non-zero condensation rate. For liquid water to be in equilibrium with the vapor phase, the partial pressure of water vapor must equal the saturation vapor pressure of the liquid water.

RH , is the ratio, expressed in percent, of the measured water vapor pressure and the saturated water vapor pressure at the same temperature and total pressure. This definition applies to water in its standard state. In porous media or on solid surfaces, there are other mechanisms that decrease the saturation water vapor pressure of the liquid, such as capillary binding of water by surface tension, osmotic binding of water in double layers, and direct adhesion of water molecules to solid surfaces by London-van der Waals forces (Koorevaar et al. 1983, p. 63 [125329]). For the IDPS model, these effects are assumed negligible (Assumption 5.1).

Dissolved salts in water also decrease the saturation water vapor pressure because they reduce the chemical activity of water in the solution. The chemical activity of the water molecule, $a(w)$, is a function of the mole fraction of water in the aqueous solution and is equivalent to the equilibrium relative humidity of the solution (Kinsman 1976, p. 274 [100769]). As a result, brines reach liquid-vapor equilibrium, and thus stability, at relative humidity values below 100 percent. This effect on brine stability is included in the IDPS model.

Based on relative humidity measurements from the single heater test (Tsang 1999, Section 2.2.2 [124334]), the relative humidity within the potential drift is expected to fall below 99 percent for many years during the pre- and postclosure periods. As a result, dilute ground water in the unsaturated zone, having an activity of water greater than 0.99, is not expected to be at liquid-vapor equilibrium within the drift during this time. For any dilute ground water that resides or flows into the drift during this period, there is a net transfer of liquid water to the vapor phase that results in increasing concentrations of dissolved salts in the remaining liquid water. If the vaporization rate is rapid compared to the flux of liquid water flowing into the drift, brines will develop within the drift. In addition, if the relative humidity is sufficiently low, dissolved salts will precipitate until either a more stable brine develops or all free liquid water evaporates, adsorbs, and/or is incorporated in hydrated salts.

6.3.2 Formation and Chemistry of Brines and Salt Precipitates

As water evaporates from solution, dissolved solids concentrate until they become supersaturated with respect to a solid phase whereupon, assuming conditions are favorable and precipitation is sufficiently rapid, the solid phase will precipitate. If the solid phase is a binary salt and the normalities of the two reactants are not equal, the reactant having the lower normality will become depleted in solution while the reactant with higher normality will continue to concentrate (Eugster and Hardie 1978, pp. 243-7 [100743]; Eugster and Jones 1979, pp. 614-629 [123175]). This mechanism is known as a chemical divide (Drever 1988, p. 235-6 [118564]). A chemical divide determines which reactant concentrations are predominantly controlled by the solubility of a precipitating phase (i.e., those that become depleted in solution) and which reactant concentrations are only partially controlled by a precipitating phase (i.e., those that continue to concentrate in solution despite partial precipitation). It should be noted that the resulting evaporative evolution depends on how close the normalities of the reactants are. If they are very close, both reactants will maintain fairly constant concentrations as evaporation and precipitation

continue. Eventually, however, the normalities of the reactants will begin to diverge rapidly, with the predominant reactant concentrating and the lesser reactant depleting.

The chemical divide during evaporative precipitation is demonstrated by thermodynamic calculations and studies of saline lakes and sabkhas. Garrels and Mackenzie (1967 [123636]) thermodynamically simulated the evaporative evolution of Sierra Nevada spring water into a strongly alkaline sodium carbonate brine observed in natural saline lakes in the western United States. In these calculations, calcite precipitates first, depleting the aqueous calcium concentration. Calcite precipitation is an important evolutionary step because the chemical divide for calcium and carbonate determines whether the evaporating water becomes carbonate poor or carbonate rich (Eugster and Hardie 1978, pp. 244 [100743]). In this case, the water becomes carbonate rich. Next in the calculations, precipitation of sepiolite depletes the magnesium concentration. Continued evaporation results in a sodium carbonate brine with a pH near 10 (Garrels and Mackenzie 1967 [123636] p. 239).

Studies of saline lakes in the western United States show that alkaline sodium carbonate brines, such as the brine derived by Garrels and Mackenzie (1967 [123636]), are common (Eugster and Hardie 1978, p. 240 [100743]). Many of these same alkaline brines occur in volcanic terrain and have high silica content (Jones et al. 1967 [123170]). These waters are also enriched in chloride, sulfate, and to some extent potassium. Studies of naturally occurring brines indicate that potassium is largely removed during evaporative precipitation. The likely mechanisms for this removal are ion exchange reactions on clay minerals, silicate gels, and volcanic glass (Eugster and Hardie 1978, pp. 246 [100743]).

In the late stage of evaporation, the highly soluble components precipitate. In carbonate-rich brines, these salts include, but are not limited to, salts of Na, Cl, SO₄, CO₃, and SiO₂ (Eugster and Hardie 1978, p. 244 [100743]). The predominant dissolved components in carbonate-poor brines, such as brines resulting from the evaporation of seawater, are Na, Ca, Mg, Cl, and SO₄ (Eugster and Hardie 1978, p. 244 [100743]). Other dissolved components observed to become enriched in some brines include Ca, Mg, K, F, Br, Sr, PO₄, and B (Eugster and Hardie 1978, p. 239-241 [100743]). NO₃, although it is highly soluble, is not mentioned (and perhaps not investigated) in these studies.

The sequence of salt precipitation by evaporation depends on the chemistry of the solution and the environment. The relative and total activities of the dissolved salt species and the solubilities of the solid salt phases determine when a dissolved species becomes supersaturated, when it begins to precipitate, which other species precipitate with it, and which species continue to concentrate in the remaining solution.

The aqueous solubilities of various combinations of binary Na, K, Ca, and Mg salts at 25°C and 100°C are presented in Table 12 (Section 7.2). Each value represents the maximum amount of the specified salt that can be dissolved into pure water at the given temperature. These handbook values are useful in assessing semi-quantitatively the relative solubilities of different salts in an aqueous solution containing many different dissolved solids. For example, Table 12 indicates that sulfate salts and sodium fluoride are some of the least soluble of these salts.

In naturally occurring brines, high sulfate concentrations are attributed to the dissolution of gypsum in geologic strata or the oxidation of sulfides such as pyrite, which is widespread in the western United States (Eugster and Hardie 1978 [100743] pp. 243). In a carbonate-poor (calcium-rich) brine, such as a brine derived from the evaporation of seawater, sulfate precipitates as gypsum or anhydrite before halite precipitates (Kinsman 1976 [100769] p. 275). In carbonate-rich alkaline brines, sulfate precipitates as a sodium salt (Eugster and Hardie 1978 [100743] pp. 246). Based on the data in Table 12, sulfate salts would be expected to precipitate due to evaporation prior to halite or other more soluble salts, given approximately equal molar concentrations of sulfate and chloride in the solution.

Another indication of the likely sequence of salt precipitation is evident in the comparison of hygroscopic properties, i.e., the abilities of different brines or salts to absorb water from the air. Deliquescence is the process of dissolution of a solid by absorbing moisture from the air. This process is the reverse of evaporation to dryness and can be modeled as such. Table 13 lists literature values of the equilibrium relative humidity of aqueous solutions saturated with a given salt. Lower values in this table imply lower chemical activities of H₂O (see previous section) and therefore higher salt solubilities. This relationship is apparent when comparing the values in Table 12 and Table 13.

For evaporating seawater, when the chemical activity of H₂O falls below 0.93 due to net evaporation of water into air having a relative humidity less than 93 percent, calcium sulfate precipitates (Kinsman 1976 [100769] p. 273). In this same water, when the chemical activity of H₂O falls below 0.77 due to net evaporation of water into air having a relative humidity less than 77 percent, halite precipitates (Kinsman 1976 [100769] p. 274-5). Thus, as water evaporates, the chemical activity of water in the brine decreases, forcing less hygroscopic, less soluble salts to precipitate before more hygroscopic, more soluble salts. Based on the values in Table 12 and Table 13, it follows that the sequence of precipitation in a calcium-poor (carbonate-rich) brine is likely sodium sulfate followed by halite.

The most reliable method for determining the sequence of precipitation reactions is to track the aqueous activities of the dissolved components in a quantitative evaporation simulation. Such a simulation can be performed using a code like EQ3/6. An evaporation simulation is a series of incremental steps in which a small amount of water is removed (or evaporated) at the beginning of a step and the remaining solution is re-equilibrated at the end of the step. If the ion activity product of a salt exceeds the solubility equilibrium constant of the precipitation reaction at the beginning of the step, the salt will begin to precipitate, assuming the rate of the reaction is sufficiently rapid (Stumm and Morgan 1996 [125332] pp. 351-9). Precipitation will stop at the end of the step as soon as the ion activity product falls to the point where it is equal to the solubility equilibrium constant of the reaction.

Evaporative precipitation generally results in the precipitation of dissolved components from solution. One exception is carbonate because it can both precipitate and degas. Degassing of carbon dioxide in alkaline brines is represented by the reaction:



This reaction causes the pH to rise (Drever 1988 [118564] p. 244). The pH rise is enhanced by the decrease in carbon dioxide solubility as salinity increases (Eugster and Jones 1979 [123175] pp. 614). Carbonate precipitation includes calcite during the early stages of evaporation and various sodium carbonate salts at later stages (Jones et al. 1977 [123192] p. 64; Eugster and Hardie 1978 [100743] pp. 244-246).

For silica, wetting and drying cycles can be responsible for the silica precipitation observed in alkaline brines. At Lake Magadi in Kenya, complete evaporation causes the formation of silica crusts that do not easily dissolve during the following wetting cycle because of slow kinetics. As a result, only the most soluble salts; e.g., salts of Na, K, Cl, and SO₄, dissolve into the recharged interstitial waters (Eugster and Hardie 1978 [100743] pp. 245-6).

6.3.3 Potential Brines and Salt Precipitates at Yucca Mountain

A number of simulations and experimental studies have been performed to directly assess evaporative precipitation effects within and near the proposed repository in Yucca Mountain. In these studies, water entering the drift is predicted to have variable composition as a function of time as a result of the boiling/condensation and reaction of both heated and condensed waters with minerals and gases in the fractures of the host rocks (Arthur and Murphy 1989 [100699]; Glassley 1994 [100741]; Murphy 1993 [100804]; Wilder 1996 [100792]; Lichtner and Seth 1996 [100771]; Glassley 1997 [100742]; Hardin 1998 [100123] Section 6.2.2). These reacted, or thermally perturbed, fluid compositions could flow down fracture pathways and enter potential emplacement drifts where they could undergo reaction with introduced materials or be boiled again, depositing salts (Glassley 1994 [100741]; Murphy and Pabalan 1994 [100805]; Wilder 1996 [100792]; Lichtner and Seth 1996 [100771]). The salts deposited and brines that occur within the proposed drifts would depend on the volume, composition, and extent of evaporation of water seeping into the drift over time from the unsaturated zone.

As temperature increases, a number of changes could affect the geochemical behavior of the near-field environment. Mineral stabilities and phase equilibria are temperature dependent, and the rates at which reactions occur generally increase at higher temperatures. Both continuous reactions (such as the gradual dehydration or shift in cation composition of a solid phase) and discontinuous reactions (such as the disappearance of a phase outside of its stability range) occur as temperature increases (Glassley 1994 [100741]; Murphy 1993 [100804]; Hardin 1998 [100123] Sections 5 and 6).

The increased temperatures are predicted to vaporize much of the water in the near-field as an above-boiling zone forms within the drift and in the very near-field (Glassley 1994 [100741]). This transition would increase the capacity of the system to transport moisture as volatiles and would result in precipitation of dissolved solids from boiling fluids in the near-field. Condensation of water in cooler regions above the proposed repository horizon could dissolve new material, which could be transported through fractures back down into the boiling zone with subsequent boiling and phase precipitation.

Mineral precipitates including salts will form in the drift and near-field due to boiling and evaporation of water. Water undergoing boiling or evaporation or reacting with precipitated salts is predicted to become concentrated in a number of dissolved constituents either in close

proximity to, or within, potential emplacement drifts (Hardin 1998 [100123] Section 6.2.2). The evolving compositions of these fluids can be predicted by geochemical mass-transfer calculations for simplified systems designed to simulate the vaporization that would occur within a thermally perturbed repository environment. Results from two such calculations (Murphy and Pabalan 1994 [100805]; Wilder 1996 [100792]; Hardin 1998 [100123] Section 6.2.2) are discussed here.

In one calculation (Wilder 1996 [100792]; Hardin 1998 [100123] Section 6.2.2), J-13 water is predicted to evaporate/boil along a temperature rise from ambient to 95°C at equilibrium with atmospheric gases. This calculation represents 95 percent evaporation. The second set of calculations (Murphy and Pabalan 1994 [100805]) starts with model water evaporatively evolved at 75°C (heated J-13 water that has reacted with tuff) and heats it instantaneously to 100°C in equilibrium with atmospheric oxygen and the calculated CO₂ fugacity (this latter parameter value is higher than atmospheric values and was derived from a coupled reactive transport calculation in which both gas and fluid flow were calculated). The compositions resulting from this second set are reported to about 99.6 percent evaporation. Even though the results of these two calculations are not directly comparable because they represent different compositional systems and different controls on the gas phase, they appear to be roughly consistent. Relative to ambient compositions, these fluids, in general, have high ionic strength values (greater than 1 molal stoichiometric ionic strength for the 99.6 percent evaporated case); high concentrations of alkalis, chloride, sulfate, and other ligands (F⁻, and HCO₃⁻); and have high pH (around 9.5).

Because mineral precipitation occurs throughout these calculations (calcite, silica polymorphs, etc.), these compositions do not represent simply concentrated ambient values, but are selectively concentrated. In both sets of calculations, the dissolved Ca content is low (<50 mg/kg) because calcite precipitation removes Ca from the fluid. However, other elements that are conservative within the aqueous phase are orders of magnitude higher than at ambient conditions. For example, at the 99 and 99.6 percent evaporation points, chloride concentrations are about 100-times and about 250-times higher, respectively, than the average value for J-13 water (Murphy and Pabalan 1994 [100805]).

Modeling results of water evaporation indicate that resultant composition may be profoundly affected by the gas phase assumed to be in equilibrium with the evaporating water and by whether the system behaves as open to the atmosphere or in a closed manner (Wilder 1996 [100792]; Hardin 1998 [100123] Section 6.2.2). In an open system with a fixed partial pressure of carbon dioxide, J-13 well water evolves to pH above 9.5 at high degrees of evaporation. Alternatively, in a closed system, the pH falls below 6.8 after a similar extent of evaporation. The model results are very sensitive to the constraints on CO₂ fugacity (Murphy and Pabalan 1994 [100805]), with different solid phases precipitating for lower CO₂ fugacities. When refluxed water is nearly completely evaporated, more calcite precipitates in an open system compared to a closed system (Murphy and Pabalan 1994 [100805]). These results emphasize the need to have a model that incorporates consistently the evolution of near-field gas composition, and the need to have such constraints defined for each scenario.

In another modeling study, Lichtner and Seth (1996 [100771]) used a multiphase, multicomponent, non-isothermal reactive transport code to simulate the evolution, vaporization, and condensation of groundwater through the vertical centerline of the proposed repository

during the boiling period. This type of code does not fix local gas fugacities within the grid block, but evaluates them based on multiphase reactions. Their results predict that in the vicinity of the proposed repository, the pH will rise to about 10 and chloride concentration will increase to approximately 100 mg/L in the vicinity of the drift. This predicted pH rise suggests that the proposed repository will behave more like an open system than a closed system with respect to carbon dioxide. Lichtner and Seth (1996 [100771]) indicate that a 10-fold increase in J-13 fluid concentrations (for conservative elements) could be a reasonable water composition entering the drift through fractures during the boiling period. Quartz and calcite were predicted to dissolve where water was predicted to condense and to precipitate where water was predicted to evaporate (Lichtner and Seth 1996 [100771]).

6.3.4 Simplified Binary Salts Model

The conceptual IDPS model (Section 6.4) evolved from the simplified binary salts model (CRWMS M&O 1998 [100358]). The simplified binary salts model 1) defined the general processes that lead to salts accumulation, brine formation, and dry conditions in the proposed repository, 2) approximated the total accumulations of salts that might occur, and 3) predicted the effects of deliquescence and dissolution of precipitated salts as the relative humidity slowly increases during the cooling period. The results indicated that response surfaces, generated as a function of relative humidity or relative evaporation rate (instead of time), could be used to estimate water composition for the overall performance assessment model. The results of this model are presented below.

6.3.4.1 Salt Precipitation Results

The purpose of the simplified binary salts model was to derive a set of bounding analyses for the timing, accumulation, and total amount of salts that accumulate and dissolve in the drift and the effects of these salts and evaporative processes on the chemical composition of the water. The model considered the elements Al, C, Ca, Cl, F, Fe, H, K, Mg, N, Na, S, and Si. The incoming seepage water for these calculations was average J-13 well water.

To initialize the simplified binary salts model, separate EQ3/6 evaporation calculations using a non-Pitzer database were performed. These simulations predicted that Na, Si, S, Cl, K, N, and F, would increase in concentration in proportion to the amount of vaporization as the ionic strength increased to 1 molal. Changes in carbonate concentrations were similar, but some deviation from direct proportionality occurred. The fugacity of carbon dioxide for the periods modeled ranged from 10^{-10} to 10^{-4} bars. As the water became more saline and approached an ionic strength of 1 molal, the pH increased to values between 10.3 and 11.7 (CRWMS M&O 1998 [100358] Section 4.6.2.2.3.1).

Precipitation reactions in the thermodynamic database caused concentrations of Ca, Al, Mg, and Fe to decrease or remain essentially unchanged as water vaporized in the EQ3/6 calculations. As a result, approximately 98 percent or more of the dissolved components were precipitated as the seepage water became 98 percent vaporized. Ca concentrations were controlled primarily by calcite.

After evaporation of the average J-13 well water to 1 molal ionic strength using EQ3/6, Na and K accounted for more than 99.9 percent of the remaining positive charge. As a result, Na and K salts were responsible for the overwhelming majority of all salt precipitation in the late stage evaporation calculations of the simplified binary salts model, and the elements Si, Cl, S, C, F, and N and their stable hydrolyzed species were the primary sources of negative charge.

A spreadsheet was used to implement the simplified binary salts model for the late stage evaporation calculations. Normative binary salts were chosen to precipitate based on handbook solubilities, relative ion activity products, and conservation of mass and charge. All Ca precipitated as calcite due to its low solubility and an excess of carbonate. Next, sodium sulfate precipitated. The high concentration of sodium relative to sulfate caused the complete depletion of sulfate while depleting the sodium concentration by approximately 20 percent.

The simplified binary salts model was not capable of predicting the changes in pH. Because silica salt solubility is a function of pH at high pH, it was difficult to determine which salt would be the last to precipitate. Based on J-13 well water evaporation experiments, it was determined that nitrate would precipitate last along with potassium due to its high solubility (CRWMS M&O 2000 [146460] Section 6.4.2). Because there was slightly more nitrate than potassium in the reflux water, some nitrate was precipitated as sodium nitrate. Consistent with mass balance and charge balance constraints, the rest of the components, Na, Cl, C, F, and Si, precipitated as NaCl, Na₂CO₃, NaHCO₃, NaF, Na₂Si₂O₅, and Na₂SiO₃. The total accumulation of these normative salts on the waste package was directly proportional to the seepage rate.

6.3.4.2 Salt Dissolution Results

During the boiling period in the proposed repository, the simplified binary salts model analysis predicted that the high temperature and low relative humidity would cause all normative salts to precipitate and all seepage water to vaporize (CRWMS M&O 1998 [100358]). The dissolution of salt phases was essentially instantaneous once the relative humidity exceeded the maximum allowed for a stable solid phase. Such rapid dissolution is consistent with the observation that puddles of dissolved salt (primarily NaCl brine) occur overnight on salt flats of the Persian Gulf when the relative humidity rises above the maximum equilibrium relative humidity for solid-phase NaCl but remains far below the dew point (Kinsman 1976 [100769]). These same puddles then dry up during the day as soon as the relative humidity falls below the critical relative humidity.

In the simplified binary salts model analysis, the first critical value of relative humidity encountered as the potential drift cooled was determined to correspond to the nitrate phases. In this previous model, at about 160 years, the relative humidity was predicted to rise above 50 percent and the temperature to fall to about 117 °C (CRWMS M&O 1998 [100358]). This was taken to be the approximate relative humidity value that would cause NaNO₃ to dissolve. Also, the temperature at this time was below the boiling point of a concentrated solution of NaNO₃, which is around 120 °C (Saxton et al. 1928 [127320] V. 3, p. 326). Thus, all solid-phase NaNO₃, condensing water vapor from the in-drift air, deliquesced to a sodium nitrate brine. At the same time, KNO₃, which has hygroscopic properties similar to NaNO₃, was allowed to dissolve completely into the brine.

The next threshold in this earlier model was encountered at approximately 80 percent relative humidity around 105 °C, which corresponded to approximately 800 years (CRWMS M&O 1998 [100358]). NaCl, NaF, Na₂CO₃, NaHCO₃, Na₂Si₂O₅, and Na₂SiO₃ dissolved at this point based on their solubilities. The maximum relative humidity for NaCl is 76.4 percent at 80 °C in a pure NaCl aqueous solution (Table 13).

The final threshold in this earlier model was crossed at 1,250 years when the relative humidity exceeded approximately 90 percent and the temperature was around 100 °C (CRWMS M&O 1998 [100358]). Na₂SO₄ was no longer stable and was determined to dissolve completely, representing the last of the highly soluble salts precipitated throughout the boiling period. This left CaCO₃ as the only normative salt remaining and accumulating beyond 1,250 years.

6.4 BASE CASE CONCEPTUAL MODEL

The conceptual model for the IDPS model incorporates a set of processes that affect the chemical aqueous composition of water in the proposed repository. These processes, illustrated in Figure 1, include evaporation, condensation, deliquescence, exchange of gases with the atmosphere, and precipitation and dissolution of salts.

The conceptual model asserts that the starting water composition of the incoming seepage and drift conditions (specifically, relative humidity, temperature, and gas fugacities) are the controlling variables in the chemical evolution of water within the drift. Though interaction of this water with other solid materials within the drift could also control chemical evolution of seepage water, such interaction is accounted for in other models used in conjunction with the IDPS model. The base case conceptual model does not consider steady-state flow-through conditions. Consequently, the relative evaporation rate is not required as an input parameter. The steady-state equivalent of the IDPS model is discussed in Section 6.6.3.3.

The IDPS conceptual model is based on processes expected to occur within the proposed repository over its lifetime. In the early years, high temperatures and low values of relative humidity are expected to generate dry conditions as water boils away or evaporates completely. Seepage water that enters the drift during this period is expected to vaporize quickly, depositing its dissolved, nonvolatile constituents as salts and minerals.

Over time, temperature will fall and relative humidity will rise. At some point, the relative humidity will rise to a point at which the brine of a salt is more stable than the solid phase. For sodium nitrate at 100°C, the critical relative humidity that defines the cutoff between liquid and solid is around 65 percent for a pure aqueous solution of sodium nitrate (Table 13). Thus, if sodium nitrate is the most soluble and hygroscopic salt deposited from the evaporation of incoming seepage water, wet conditions will persist whenever the relative humidity exceeds about 65 percent. The critical relative humidity will vary depending on the concentrations of other ions in the mixed salts system. If a magnesium chloride salt is the most soluble and hygroscopic salt deposited, the critical relative humidity would be around 22 percent (BSC 2001 [155640] p. 29) or lower depending on the abundance of additional soluble components.

As the relative humidity continues to rise with time, the activity of water rises and precipitated salts either dissolve completely or to saturation. For example, halite will dissolve into an initial

sodium nitrate brine to maintain saturation with respect to halite. Because the sodium concentration is already extremely high in the sodium nitrate brine, very little halite will dissolve before halite saturation is reached. As the mole fraction of water rises due to increasing relative humidity, the sodium concentration effectively becomes more dilute allowing for additional halite dissolution. Eventually, this effective dilution process exhausts the halite in the system at a relative humidity near the critical relative humidity for halite, approximately 76 percent at 80°C (Table 13).

In the conceptual model, the effects of relative humidity and temperature on the evaporation and dilution processes are reversible. Because the conceptual model is an equilibrium model in which the relative humidity controls the extent of evaporation or dilution, the complete evaporative evolution of the aqueous solution to a final mineral assemblage describes in reverse the deliquescence and sequential dissolution of the mineral assemblage that produces the original incoming water composition. Thus, given the incoming seepage water composition, temperature, and the fugacities of O₂ (always set at atmospheric, as explained in Section 4.1.2) and CO₂, the conceptual model allows a single evaporation calculation to provide predictions of aqueous and mineral compositions for the full range of relative humidity potentially encountered under the specified conditions, regardless of whether relative humidity is rising or falling.

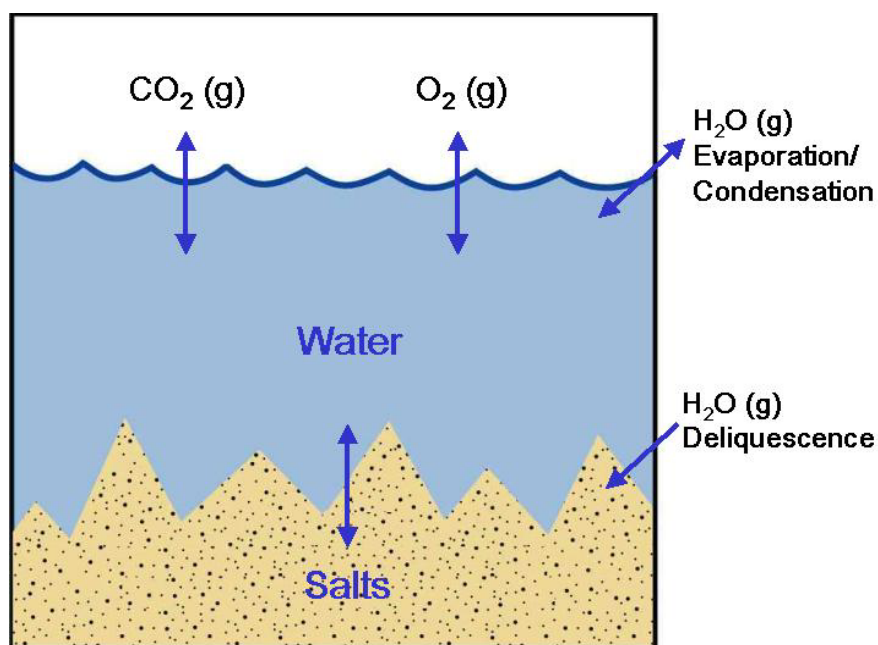


Figure 1. Processes Simulated by the In-Drift Precipitates/Salts Model

6.5 CONSIDERATION OF ALTERNATIVE CONCEPTUAL MODELS

Uncertainties in the conceptual model arise from an incomplete understanding of processes implemented in the model. This type of uncertainty is addressed in part by identifying, developing, and evaluating alternative conceptual models.

Table 16 lists six alternative conceptual models for the IDPS model. Five of the six are not utilized because they either are not as realistic as the IDPS model, do not provide the types of outputs requested of the IDPS model, or do not cover the necessary ranges of applicability. The one that is utilized, the steady-state model, is incorporated directly into the IDPS model lookup table output files. Details of the key assumptions of these alternative conceptual models and the associated screening assessments are presented in Table 16.

Table 16. Alternative Conceptual Models Considered

Alternative Conceptual Model	Key Assumptions	Screening Assessment and Basis
Ion Association Model	Non-ideal ion interaction can be adequately modeled using an ion association approach, such as the Davies equation or B-dot equation.	This model was not utilized because it cannot be used at the high ionic strengths of extensively evaporated natural waters. The IDPS model utilizes a Pitzer ion interaction model, which can be used at high ionic strength and low ionic strength. At low ionic strength, ion association and ion interaction models provide nearly identical results, as illustrated in Section 7.3.
Steady-State Model	The flow-through of incoming seepage water is too rapid to allow local equilibrium with respect to RH (Section 6.6.3.3, Figure 3).	This model is included in the current IDPS model (Section 6.6.3.3) and cross-referenced in the model lookup tables (Section 6.6.3.5). It can be implemented if two parameter values are determined prior to use: 1) the relative evaporation rate (R^{es}) at the location being modeled, and 2) the precise composition of the incoming water (or the approximate concentration factor of an abstracted incoming water).
Simplified Binary Salt Model	Evaporative evolution of a potential incoming ground water can be approximated by completely precipitating components of lowest normality upon chemical saturation with respect to binary salts as evaporation occurs.	This model is a predecessor to the IDPS model (Section 6.3.4). Unlike the IDPS model, it does not account for CO_2 dissolution or degassing or the effects of pH, ionic strength, and incomplete depletion of dissolved solids. Also, the simplified binary salt model cannot be used to predict all of the outputs required, such as pH and concentrations of aqueous species that potentially contribute to acid-neutralizing capacity.
SNORM (Bodine and Jones 1986 [162352])	An equilibrium normative salt assemblage at complete evaporation can be predicted from an aqueous solution composition without predicting the evaporative evolution of the aqueous solution.	This model was not utilized because predicting the evaporative evolution of the aqueous solution is the primary modeling objective. SNORM cannot predict the evaporative evolution of the aqueous solution. SNORM also is not capable of making predictions at temperatures other than $25^\circ C$ or making predictions involving silica or aluminum. The IDPS model can make these predictions.
Kinetic Model	Slow reactions are to be modeled using kinetic rate equations.	Kinetic rate equations are not utilized in the IDPS model because the IDPS model is designed to produce model abstractions that are necessarily independent of time. Slow redox reactions are excluded from the IDPS model and sufficiently slow mineral precipitation reactions are prevented by suppression (Section 6.6.2.6). Thus, the IDPS model is a quasi-equilibrium model.
Closed System Model with respect to CO_2	Carbonate exchange with the gas phase via CO_2 degassing or dissolution results in a corresponding increase or decrease of CO_2 in the gas phase.	A closed system with respect to CO_2 is not implemented in the IDPS model because the expected volume ratio of air to water in the drift is so large that CO_2 degassing from, or dissolution into, seepage water in the drift would negligibly affect the CO_2 fugacity compared to the uncertainty in the input value for CO_2 fugacity. To address this issue further, the IDPS model is to be used to quantify the output uncertainty resulting from the uncertainty in CO_2 fugacity in REV 02 of <i>Engineered Barrier System: Physical and Chemical Environment Model</i> (BSC 2003 [165601]).

6.6 MODEL FORMULATION FOR BASE CASE MODEL

The mathematical IDPS model is designed to simulate the conceptual model. As detailed in Section 1, the intended use of this model is to estimate and tabulate, within an appropriate level of confidence, the effects of evaporative processes and potential environmental conditions on the pH, ionic strength, deliquescence relative humidity, and chemical compositions of water and minerals on the drip shield or other location within the drift during the postclosure period. The appropriate level of confidence for the model is addressed in Section 7.

The current IDPS model covers two predominant regimes. The first regime occurs at low relative humidity ($RH < 98$ percent) where the solubilities of “soluble” salts begin to control the water chemistry. In this regime, incoming seepage water either evaporates completely (e.g., during the boiling period), thereby precipitating all dissolved solids of the seepage water, or it evaporates to a stable brine (e.g., during the early cool-down period). This regime also includes the realm of deliquescence, which occurs when RH rises to a level at which a hygroscopic salt is no longer stable in solid form. This first regime generally requires the use of Pitzer equations because the ionic strength of water in equilibrium with the relative humidity ($RH < 98$ percent) is generally around 1 molal or higher. This model regime is simulated using the geochemical code EQ3/6 Version 8.0 and the Pitzer database developed in Attachment I.

In the second regime, RH is 98 percent or higher. In this regime, the steady-state water composition can be more precisely controlled by the ratio of the rates of evaporation and seepage (Q^e/Q^s). This ratio is always less than one in this regime. If it were not, steady-state conditions would either be dry (if RH were sufficiently low) or consist of a steady-state brine, either of which is simulated in the first regime. This regime is also simulated using the geochemical code EQ3/6 Version 8.0. However, the thermodynamic database for this regime can either be the Pitzer database developed in Attachment I or the data0.ymp.R2 thermodynamic database (DTN: MO0302SPATHDYN.000). While the Pitzer equations are generally not required for this regime, it is accurate at low ionic strengths for major ion chemistry, as shown in Section 7.3.

6.6.1 Mathematical Description of Base Case Model

The IDPS model uses the code EQ3/6 Version 8.0 to execute the mathematical formulation of the conceptual model. A general description of the IDPS mathematical model is presented below. A full discussion of the relevant equations is presented in the appendices of the EQ3/6 user's manual (SNL 2003 [162494]).

EQ3/6 consists of two primary codes, EQ3NR and EQ6. EQ3NR is a speciation-solubility code designed to predict equilibrium aqueous species concentrations and to compute the degree of disequilibrium with respect to mineral phases, oxidation-reduction reactions, and various other phases and reactions. EQ6 is a companion code that takes the results of executed EQ3NR runs and performs reaction path calculations, such as evaporation, mineral precipitation, and mineral dissolution.

The governing equations consist primarily of mass balance and mass action equations. Mass balance equations ensure that the total mass of each chemical component (e.g., Na, K, Ca, Mg,

Cl, SO₄, etc.) is conserved, and mass action equations ensure that each chemical reaction involving these components achieves equilibrium, if equilibrium is desired.

The total mass of each component in solution is distributed among all aqueous species involving the component. The aqueous mass balance equation for each component is the cumulative mass of the component among all aqueous species involving the component multiplied by the appropriate stoichiometric coefficients. For example, the aqueous mass balance equation for F would be:

$$m_{T,F} = m_{F^-} + m_{HF(aq)} + 2m_{HF_2^-} + \dots \quad (\text{Eq. 6.6.1-1})$$

where $m_{T,F}$ is the total molality of F and m_i is the individual molality of each aqueous species i in the model. The set of species for a given component includes one basis species and a number of other species equal to the number of reactions in the database involving the component. For F, the basis species is F⁻. All other species involving F are determined from reactions involving the basis species F⁻.

The reactions of the basis species are represented by mass action equations. For the chemical reaction:



where “=” denotes a reversible reaction, the mass action equation is:

$$K_{HF_2^-} = \frac{a_{F^-}^2 a_{H^+}}{a_{HF_2^-}} \quad (\text{Eq. 6.6.1-3})$$

where K_i is the equilibrium constant of species i and a_i is the thermodynamic activity. The equilibrium constant for each species is provided by the thermodynamic database. At equilibrium, the value of the term on the right-hand side of this equation equals the equilibrium constant.

The thermodynamic activity a_i is related to the molal concentration m_i by the equation:

$$a_i = m_i \gamma_i \quad (\text{Eq. 6.6.1-4})$$

where γ_i is the activity coefficient. The activity coefficient is used to correct for non-ideal behavior that occurs when the aqueous solution is not highly dilute. Calculation of the activity coefficient depends on the model chosen. For the Pitzer ion interaction model, Pitzer equations are used, as described in Attachment I.

Substituting Equation 6.6.1-4 into Equation 6.6.1-3 gives:

$$K_{HF_2^-} = \frac{m_{F^-}^2 \gamma_{F^-}^2 m_{H^+} \gamma_{H^+}}{m_{HF_2^-} \gamma_{HF_2^-}} \quad (\text{Eq. 6.6.1-5})$$

which shows how the molalities of the reactants and products relate to the reaction equilibrium constant and the mass action equation.

Each mass action equation can be solved for the molality of the non-basis species (e.g., HF_2^-). The resulting functions can then be substituted into the mass balance equations to generate equations in which the only unknowns are the molalities of the basis species. Doing this for each component generates a set of n equations and n unknowns, which is solved in EQ3/6 using variations of the Newton-Raphson iteration method (SNL 2003 [162494]). The solution to these equations provides basis species concentrations that are then used to calculate the concentrations of each non-basis species via the mass action equations. By solving this set of equations simultaneously, the code can calculate equilibrium concentrations for each included chemical reaction while also maintaining mass balance for each component.

In some cases, the total component concentration is not an input. For example, the total hydrogen concentration is not a convenient measurement or bound for an aqueous model. Instead, another parameter, such as pH, is often used as the input value. The activity of the basis species H^+ can be directly computed from the pH using the equation:

$$a_{\text{H}^+} = 10^{-\text{pH}} \quad (\text{Eq. 6.6.1-6})$$

This value can then be converted to molality using the relation given in Equation 6.6.1-4. Thus, the molality of the basis species H^+ becomes a known value, and the total hydrogen mass balance equation is no longer needed to constrain the system.

In the case of a fixed fugacity of carbon dioxide, the activity of the carbonate basis species HCO_3^- can be determined explicitly from the pH and the equilibrium constant relating HCO_3^- to carbon dioxide. The relevant chemical reaction in the Pitzer database developed in Attachment I (DTN: SN0302T0510102.002) is:



which has an associated equilibrium constant $K_{\text{CO}_2(\text{g})}$. The mass action equation for this reaction is:

$$K_{\text{CO}_2(\text{g})} = \frac{a_{\text{HCO}_3^-} a_{\text{H}^+}}{a_{\text{CO}_2(\text{g})} a_{\text{H}_2\text{O}}} \quad (\text{Eq. 6.6.1-8})$$

When the pH is known, the activity of the hydrogen ion is determined directly from Equation 6.6.1-6. The activity of carbon dioxide is equivalent to the known fixed fugacity. Thus, the only two unknowns in Equation 6.6.1-8 are the activities of HCO_3^- and H_2O .

In dilute solutions (e.g., ionic strength less than 0.1 molal), the activity of H_2O is approximately one, and Equation 6.6.1-8 can be solved directly for the activity of HCO_3^- . Another way to solve for the activity of HCO_3^- is to allow equilibrium with a fixed relative humidity because at equilibrium the activity of H_2O is equivalent to the relative humidity. However, because relative humidity is an output of the titration and not an input, the activity of H_2O must be determined

based on the molalities of all other aqueous species in solution. For EQ3/6, the equation used to calculate the activity of H₂O and its derivation can be found in the EQ3/6 user's manual (SNL 2003 [162494] pp. B-28 to B-29). After estimating the activity of H₂O, solving Equation 6.6.1-8 for the activity of HCO₃⁻, and converting the HCO₃⁻ activity to molality using Equation 6.6.1-4, the molality of the carbonate basis species HCO₃⁻ is no longer an unknown. As a result, the total dissolved carbonate molality mass balance equation is no longer a constraint on the system, and the total molality of dissolved carbonate becomes an output of the model instead of an input.

In the IDPS model, the fugacity of carbon dioxide is fixed in the EQ6 input file. Because EQ6 is a reaction path code and the solution is previously equilibrated using EQ3NR, EQ6 effectively adds or subtracts dissolved carbon dioxide to bring the solution into equilibrium with the fixed fugacity. When CO₂(aq) is added to the solution, it acts like an acid according to the reaction in Equation 6.6.1-7. In accordance with Le Chatelier's principle, the increase in reactants results in an increase in products such that the overall effect on the system is minimized. Thus, addition of CO₂(aq) results in an increase in HCO₃⁻ and H⁺, implying a decrease in pH. Subtraction of CO₂(aq) has the opposite effect. In effect, EQ6 titrates (or “de-titrates”) the solution with dissolved carbon dioxide until the fixed fugacity of carbon dioxide is achieved.

Evaporation of water is also a process that is simulated using EQ6. For evaporation, H₂O is incrementally removed from solution. Each incremental removal of H₂O causes the total molalities of the aqueous components to change. As a result, the IDPS model system must be re-equilibrated after each incremental removal of H₂O (i.e., the set of *n* equations and *n* unknowns must be solved again using revised total molalities of components). In this way, the evolution of the solution can be predicted as evaporation occurs.

Mineral precipitation also affects the total molalities of aqueous components. Mineral precipitation occurs in EQ6 when the solution becomes supersaturated with respect to a mineral phase. As an example, the anhydrite mineral reaction is presented:



The corresponding mass action equation is:

$$K_{\text{CaSO}_4(\text{s})} = \frac{a_{\text{Ca}^{2+}} a_{\text{SO}_4^{2-}}}{a_{\text{CaSO}_4(\text{s})}} \quad (\text{Eq. 6.6.1-10})$$

The mass action equation for a mineral phase does not constrain the model unless the ion activity product (IAP) equals or potentially exceeds the equilibrium constant. The IAP is the term on the right-hand side of the mass action equation as presented in Equation 6.6.1-10. By convention, the activity of a pure solid phase is always one; thus, only the activities of aqueous basis species are important to the IAP.

If the solution to the set of *n* equations and *n* unknowns indicates that the IAP of a mineral exceeds the mineral's equilibrium constant, then either the solution will be supersaturated with respect to the mineral or the code will precipitate the mineral. In the IDPS model, suppressed

minerals are allowed to be supersaturated while unsuppressed minerals are required to precipitate to saturation. Thus, only unsuppressed mineral phases can constrain the IDPS model system.

Precipitation of a mineral phase moves a portion of the masses of the mineral components from the aqueous phase to the solid phase. This process requires adjustments to the total dissolved concentrations of the precipitating aqueous components and their corresponding mass balance equations. The exact amount of precipitation is determined by iteration. At equilibrium, the IAP for the precipitating mineral equals the mineral equilibrium constant, and the total masses of the mineral's components are conserved between the aqueous and solid phases.

6.6.2 Base Case Model Inputs and Boundary Conditions

6.6.2.1 Seepage Water Composition

The elements in the model include Na, K, Ca, Mg, Cl, F, C, S, N, Br, Si, Al, H, and O. Except for H and O, the incoming seepage water composition (C_i^s) for each element is defined by the total aqueous concentration of the corresponding basis species. For the Pitzer database, the corresponding basis species are Na^+ , K^+ , Ca^{2+} , Mg^{2+} , Cl^- , F^- , HCO_3^- , SO_4^{2-} , NO_3^- , Br^- , $\text{SiO}_2(\text{aq})$, and Al^{3+} . O and H are found in several of these basis species, but their elemental totals are almost entirely accounted for in the 1 kg of water solvent used to initialize each EQ3/6 run. Defining the mass of solvent is necessary for calculating the corresponding masses of the other components from their input concentrations. In addition, the negative log of the activity of the hydrogen ion is defined by entering the pH of the incoming seepage water.

6.6.2.2 Time Period Modeled

To capture the effects of time in the proposed repository, time is divided into discrete periods in which the incoming seepage water composition is fairly constant. Thus, for each time period, the incoming seepage water composition is constant while the relative humidity, temperature, and gas fugacities are varied over their potential ranges. Because chemical equilibrium conditions are assumed for each time period, time itself is not an input to the model.

6.6.2.3 Locations Modeled

The IDPS model can be used to describe evaporative processes at any location where evaporative or condensation processes occur. Possible locations are on the drip shield, on the waste package surface, and in the backfill if backfill is present.

6.6.2.4 Temperature, Gas Composition, and Relative Humidity

Temperature, gas composition, and relative humidity in the drift environment will change over time. The thermodynamic database is designed for a temperature range from 0 to 200 degrees Celsius, satisfying FEP 2.1.11.01.0A (Section 6.2). Discrete values are chosen for temperature and the fugacities of oxygen and carbon dioxide. The fugacity of oxygen is set at atmospheric for all applications. Relative humidity, however, is varied over the entire range from 100 percent to the critical relative humidity below which no water solvent remains. Because relative humidity is not an identified input or output parameter in EQ3/6, the activity of water is the

actual parameter that is allowed to vary over this range. The activity of water is equivalent to the relative humidity at equilibrium (Section 6.3.1). To evaporate a given water to the lowest relative humidity possible, an input value of 0 is entered for the final activity of water.

6.6.2.5 Relative Evaporation Rate

Relative evaporation rate can become important in the model after the relative humidity rises above 98 percent. The relative evaporation rate (R^{es}) [units: nondimensional] is defined by the equation:

$$R^{es} = \frac{Q^e}{Q^s} \quad (\text{Eq. 6.6.2.5-1})$$

where Q^e is the steady state net evaporation rate [units: volume/time] and Q^s is the incoming seepage rate [units: volume/time]. This parameter becomes important at RH greater than 98 percent because the extent of evaporation (or condensation) becomes highly sensitive to the precise value of RH in this range. At such high RH , the uncertainty in R^{es} is expected to propagate less uncertainty into the extent of evaporation (or condensation) than the uncertainty in RH would.

The model is designed for a range of R^{es} from -99 to 1. Negative values indicate condensation of water vapor. At steady state, the net evaporation rate cannot exceed the seepage rate (i.e., R^{es} cannot exceed 1) without achieving dry conditions.

R^{es} can be directly related to the concentration factor (CF) [units: nondimensional] of a conservative ion in the starting water. For example, if R^{es} is 0.9, then at steady state, the incoming water will evolve to a steady state in which the concentration of a conservative ion is 10 times the incoming concentration, i.e., a CF of 10. This relationship is described by the following equation:

$$CF = \frac{1}{1 - R^{es}} \quad (\text{Eq. 6.6.2.5-2})$$

Alternatively, a value of -99 for R^{es} is equivalent to CF of 0.01. Concentration factors less than one indicate condensation of water vapor. Defining a dilution factor (DF) [units: nondimensional] as the inverse of CF :

$$DF = \frac{1}{CF} \quad (\text{Eq. 6.6.2.5-3})$$

it would follow that the DF would be 100 for a R^{es} value of -99, implying that the original starting water is diluted 100-fold by the condensation of pure water vapor.

Version 8.0 of EQ3/6 does not provide for a solid-centered flow-through mode, which would be needed to directly simulate the relative rates of evaporation and seepage. However, because R^{es} is related to CF by Equation 6.6.2.5-2, all that is required in the calculations is that a sufficient amount of pure water be subtracted or added to the starting water to achieve the CF corresponding to the R^{es} desired. One additional equation is needed for this because CF must be

calculated from the EQ3/6 output, and there are no conservative ions that stay conservative for the entire range of concentration factors. Therefore, the best estimate of CF is provided by the relative amount of solvent water remaining (or accumulating) at each stage of evaporation (or condensation).

Each EQ3/6 run is designed to begin with 1 kg of water solvent. Dividing the original amount of water solvent (1 kg) by the amount of water solvent in the system at any point during evaporation or condensation defines the CF for the IDPS model. That is:

$$CF = \frac{M_{H_2O}^o}{M_{H_2O}} \quad (\text{Eq. 6.6.2.5-4})$$

where $M_{H_2O}^o$ is the original mass of water solvent in the system (1 kg) and M_{H_2O} is the mass of water solvent after evaporation or condensation.

6.6.2.6 MineralSuppressions

To understand the technical basis for why minerals are included in, or excluded from, applications of the IDPS model, such as applications to be documented in REV 02 of *Engineered Barrier System: Physical and Chemical Environment Model* (BSC 2003 [165601]), it is important to establish a framework for the selection of suppressed minerals. This framework is established in the subsections below for the anticipated geochemical boundary conditions at Yucca Mountain.

6.6.2.6.1 Geochemical Modeling Methodology

Generally, a reaction path geochemical equilibrium model is constructed using the steps outlined in Figure 2. First, a conceptual model is defined where the chemical system and state are defined. Constructing a first-order model tests this system and state. A first-order model generally simulates complete thermodynamic equilibrium. Results of the first-order model are compared with independent experimental, natural analog, or other modeling data to ensure that the model is reasonable for the system. If mineral phases are predicted to occur that are not appropriate for the system or timeframe being analyzed, then the precipitation/dissolution reactions involving these minerals should be suppressed.

Below is a brief summary of the importance of kinetics in determining whether a mineral phase should be suppressed. Detailed discussions of various aspects of this modeling methodology are documented elsewhere (Bethke 1996 [162270]; Smith and Missen 1991 [161602]; Van Zeggeren and Storey 1970 [161603]).

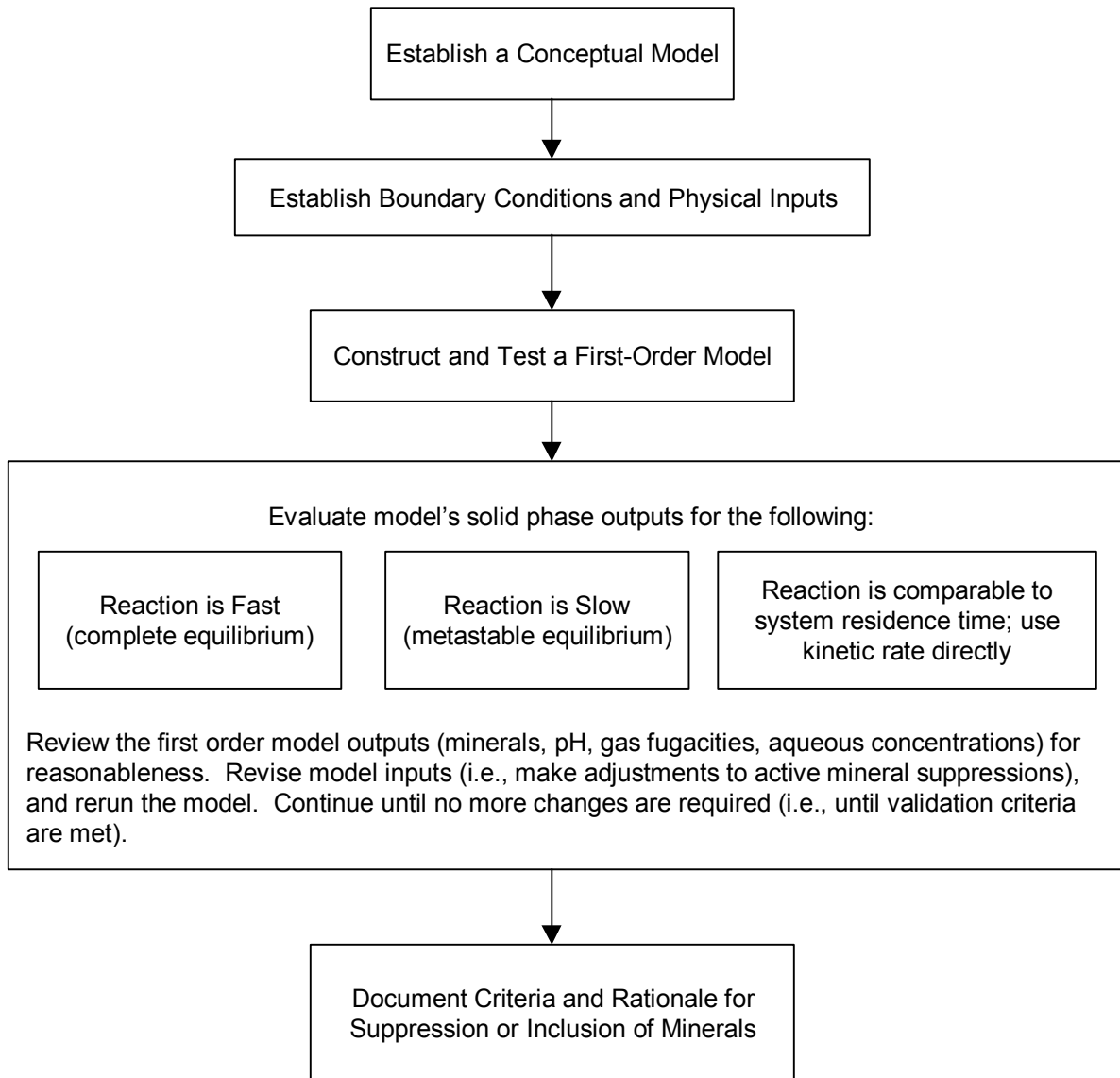


Figure 2. The General Process Required to Give a Valid Technical Basis for Mineral Suppression or Inclusion in Geochemical Equilibrium Modeling

6.6.2.6.2 Metastable Equilibrium

The IDPS model is designed to predict long-term chemical processes occurring within the proposed repository drift. “Long-term” for this model can vary from weeks to millennia, consistent with the abstracted time periods that the model is designed to simulate. While relatively short-term occurrences, such as a drop of water falling onto the drip shield, can cause sporadic divergence from equilibrium for a short period of time, a metastable local equilibrium approach is adopted for this model (Assumption 5.2). This approach generally represents the long-term processes that the model is designed to simulate.

An equilibrium reaction path model relies upon a thermodynamic database that contains the standard state and equation-of-state thermo-chemical properties of the different chemical species in a system to determine the chemical reaction equilibria as functions of the changing conditions. In addition to the homogeneous reactions that occur within each phase (e.g., water, gas, solid), there are heterogeneous reactions that involve more than one phase, such as mineral precipitation and degassing of volatile constituents from the aqueous phase.

Most of the reactions in the IDPS model are rapid relative to the timeframe of the modeling period; therefore, most reactions are allowed to reach local equilibrium. However, there are several minerals in the thermodynamic database that are not expected to form under the expected conditions of the repository. These minerals typically require high pressures or very high temperatures in order to achieve the kinetic rates of formation that would produce a considerable mass within the modeling timeframe. In this case, the system can be described by metastable equilibrium. Metastable equilibrium occurs when one or more chemical reactions proceed toward equilibrium at a rate that is so small on the time scale of interest that the system cannot produce a considerable quantity of the product (Bethke 1996 [162270] Chapter 2). The rates of nucleation or growth of some minerals frequently fall into this category. This state of metastable equilibrium can be simulated in the IDPS model by suppressing slow reactions.

The pressure in the proposed repository will remain near atmospheric, and the temperature at the drift wall will not likely rise above 200°C (BSC 2003 [162050]). These conditions would prevent many minerals in the database from forming at a rate that would produce a considerable mass. By suppressing a mineral that falls into this category, the IDPS model does not allow the mineral to precipitate, allowing for potential super saturation of that phase. The ability to suppress minerals, therefore, is necessary for equilibrium models that simulate systems in which metastable phases are more likely to occur. By suppressing unlikely minerals, slow kinetic processes can be qualitatively accounted for without knowing the precise kinetic rates of the dissolution or precipitation reactions.

6.6.2.6.3 Mineral Suppression Criteria

The Pitzer thermodynamic database developed in Attachment I contains more than 250 minerals, but only a small number of these are expected to require suppression. It is unnecessary to identify *a priori* every one of the 250-plus minerals that should be suppressed for the IDPS model. The limited range of chemical compositions of the waters likely to occur within the drift dictates that a large number of these minerals will never achieve a chemical potential favoring precipitation. Preliminary IDPS model runs for more than 40 different observed and predicted

water compositions at Yucca Mountain have been evaporated to dryness, yet fewer than 40 minerals have become saturated or supersaturated with respect to the aqueous composition. Of these, 12 are identified for suppression in the IDPS model (Section 6.6.2.6.4).

A methodology was developed to identify mineral phases to suppress in the IDPS model. Five criteria were developed to assist in determining the justification for suppression in the model in order to account for the kinetic or metastable equilibrium arguments stated above. An affirmative answer to any one of these criteria can be used to justify suppression of the mineral. This methodology was used to categorize the minerals in Table 17 and Table 18 is recommended for categorizing additional minerals when they are initially predicted to precipitate in IDPS model applications. These five criteria, which are not mutually exclusive, are presented below.

Criterion 1. Is the mineral of interest unreasonable for the defined chemical system of the model?

If the mineral lies outside or beyond the defined chemical system of the model, then there is no reason to allow the mineral to precipitate. For example, if the reactions between rainwater and a soil derived from the weathering of mafic minerals were being modeled, a clay mineral that is known to form exclusively from authigenic minerals that are felsic in composition would not be expected. For another example, minerals known only to form at high temperature or pressure would not be expected to form in a low temperature, low pressure system.

These determinations can be made using reference sources such as Klein and Hurlbut's *Manual of Mineralogy* (1999 [124293]), Kerr's *Optical Mineralogy* (1977 [161606]) or any reference source that discusses the petrology or mineralogy of a given system or analog system. One source that could be of use is a resource for the MINTQA2 software code (Wadley and Buckley 1997 [162329]). This source discusses the mineral forms at ambient temperature and pressure and gives comments on their occurrence or formation. The data from this online source has been condensed and summarized in a table in Attachment II. The table lists many of the minerals in the Pitzer (Attachment I) and data0.ymp.R2 (DTN: MO0302SPATHDYN.000) databases and provides information about whether a mineral would precipitate under the temperature and pressure boundary conditions of the proposed repository.

Criterion 2. Is the mineral precipitation or dissolution reaction so slow for the given system that the reaction hardly progresses at all during the timeframe of interest?

When a reaction is much slower than the residence time (for example, 100 times slower than the residence time), the reaction hardly progresses within the modeling timeframe. In this case, suppressing the mineral reaction provides results that would be nearly identical to the results of a kinetic model of the same system.

One of the most commonly suppressed minerals in EBS geochemical modeling is quartz. When precipitation initiates, amorphous phases will tend to form first, and then a process of mineral recrystallization will take place (Langmuir 1997 [100051] p. 55). Because precipitation of quartz and other crystalline silica phases is kinetically limited at low temperature and pressure, amorphous silica is generally the metastable phase allowed to precipitate in EBS models. If

instead the conceptual model were to account for a longer system residence time or higher temperatures, then the modeler would allow quartz or one of its polymorphs to precipitate.

Criterion 3. Is analytical or natural analog information available that warrants additional mineral suppressions?

A geochemical modeler can often find information or data from the relevant literature used to develop the conceptual model. This information often comes from analytical data or natural analog information and could warrant the suppression or inclusion of minerals that might otherwise be dispositioned differently based on an analysis using Criteria 1 and 2. In these instances, the analytical or analog data justify their use. This criterion allows for additional mineral suppressions that permit the formation of metastable phases observed to occur in the laboratory or natural analog.

Criterion 4. Do minerals need to be suppressed to test overall model uncertainty or sensitivity due to reported uncertainty in the supporting literature, database, or conceptual model?

For minerals whose potential occurrence is uncertain, runs can be performed with and without suppressing the minerals to evaluate the sensitivity of the output to these minerals.

Criterion 5. Does the suppression of a mineral whose occurrence is highly uncertain drive the resulting chemical output to a more or less conservative modeling result?

A sensitivity analysis could reveal whether suppression of an uncertain potential mineral results in a more conservative output than inclusion of the mineral, or *vice versa*. If so, the more conservative choice could potentially be justified.

6.6.2.6.4 Mineral Suppressions for the IDPS Model

Relevant natural analogs for mineral assemblages in the IDPS and Physical and Chemical Environment conceptual models are the evaporative mineral assemblages observed by Eugster and Hardie (1978 [100743]) and Papke (1976 [162274]) in the saline lakes and playa deposits of the western United States. The minerals from these types of evaporitic environments reflect the mineral assemblages that could form in a low-temperature, low-pressure, in-drift environment where the activity of water is below 0.99 and the solution compositions are comparable.

Table 17 provides a listing of the minerals that are suppressed in the IDPS and Physical and Chemical Environment models for the TSPA-LA. This list of minerals is documented in DTN: MO0303SPAMNSUP.000. Table 18 provides a listing of the minerals that have been allowed to precipitate.

Table 17. MineralSuppressions Included in the IDPS Model

Mineral	Formula	Criterion Selected	Rationale	References
Cristobalite (alpha)	SiO ₂	Criterion 2	Cristobalite forms at temperatures greater than 1470°C. At standard temperatures and pressures cristobalite will slowly convert to quartz.	Krauskopf 1979 [105909] Figure 14-1; Table A-1
Dolomite	CaMg(CO ₃) ₂	Criterion 2	Although dolomite is a common mineral in evaporite deposits from springs derived from carbonate and tuffaceous waters in southern Nevada at Yucca Mountain, its growth mechanism is slow when compared to the precipitation of calcite and Mg-bearing minerals.	Vaniman et al. 1992 [107066] Table A-1
Glaserite	NaK ₃ (SO ₄) ₂	Criterion 4	Although glaserite is a mineral that is expected to form in evaporitic type deposits, the thermodynamic data in the Pitzer database are questionable.	Suppressed, subject to sensitivity analysis.
Magnesite	MgCO ₃	Criterion 4	Magnesite is commonly associated with metamorphic mineral assemblages such as serpentine. There are instances where magnesite is associated with salt deposits, yet it is uncertain that it can form under standard temperatures and pressures as magnesite could be associated with the diagenesis of buried salt deposits.	Kerr 1977 [161606]; Eugster and Hardie 1978 [100743]; Suppressed, subject to sensitivity analysis.
Maximum Microcline	KAlSi ₃ O ₈	Criterion 1	Microcline is generally associated with the formation of granite, syenite and gneiss at high temperature and pressure. Although it is often found as a common mineral in sandstone or arkose, the occurrence in these instances is detrital and not authigenic.	Kerr 1977 [161606] p. 306; Table A-1
Quartz	SiO ₂	Criterion 2	Amorphous silica is at metastable equilibrium with respect to quartz at low temperatures and pressures. This is also evidenced by the precipitation of opal-CT (an amorphous silica phase) as opposed to quartz in evaporated carbonate and tuffaceous waters of southern Nevada.	Langmuir 1997 [100051]; Vaniman et al. 1992 [107066] Table A-1
Talc	Mg ₃ Si ₄ O ₁₀ (OH) ₂	Criterion 1	Talc is characteristically associated with low-grade metamorphic rock and hydrothermal alteration of ultrabasic rocks.	Kerr 1977 [161606]; Table A-1
Ca-saponite Mg-saponite Na-saponite H-saponite K-saponite	Ca _{0.165} Mg ₃ Al _{0.33} Si _{3.67} O ₁₀ (OH) ₂ Mg _{3.165} Al _{0.33} Si _{3.67} O ₁₀ (OH) ₂ Na _{0.33} Mg ₃ Al _{0.33} Si _{3.67} O ₁₀ (OH) ₂ H _{0.33} Mg ₃ Al _{0.33} Si _{3.67} O ₁₀ (OH) ₂ K _{0.33} Mg ₃ Al _{0.33} Si _{3.67} O ₁₀ (OH) ₂	Criterion 1	Saponite is a smectite clay. Smectite clays are commonly associated with fracture linings at Yucca Mountain. However, saponitic clays are associated with the weathering of basalt and not rhyolitic tuffs. Saponite also does not generally form independently from its associated parent material.	Krauskopf 1979 [105909]; Carlos et al. 1995 [105213]; Deer et al 1966 [102773]; Borchardt 1995 [156639]

Table 18. Minerals Allowed to Precipitate in the IDPS Model

Mineral	Formula	Rationale for Inclusion	References
Anhydrite	CaSO ₄	Anhydrite is associated with evaporite deposits in Nevada playas.	Papke 1976 [162274] Table 1; Kerr 1977 [161606] p. 221
Arcanite	K ₂ SO ₄	Arcanite is a very soluble mineral belonging to the Mascagnite group and can be precipitated in the laboratory from the slow evaporation of water solutions. This mineral is related to thenardite and should have similar properties.	Palache et al. 1951 [162280] pp. 398-400
Burkeite	Na ₆ CO ₃ (SO ₄) ₂	Burkeite is a saline mineral associated with Na-CO ₃ -SO ₄ -Cl brines.	Eugster and Hardie 1978 [100743], Table 3
Calcite	CaCO ₃	Calcite is a common evaporite mineral formed from evaporated waters of southern Nevada.	Vaniman et al. 1992 [107066]
Carnallite	KMgCl ₃ ·6H ₂ O	Carnallite is associated with evaporite deposits in Nevada playas.	Papke 1976 [162274] Table 1; Kerr 1977 [161606] p. 221
Celadonite	KMgAlSi ₄ O ₁₀ (OH) ₂	Although its occurrence is generally associated with hydrothermally altered mafic volcanic rocks and with illite-chlorite minerals, celadonite is also found as an authigenic silicate mineral in saline, alkaline, nonmarine environments such as playa deposits.	Li et al. 1997 [159034]; Hay 1966 [105965]
Fluorite	CaF ₂	Fluorite is associated with evaporite deposits in Nevada playas.	Papke 1976 [162274] Table 1; Table A-1
Glauberite	Na ₂ Ca(SO ₄) ₂	Glauberite is associated with evaporite deposits in Nevada playas.	Papke 1976 [162274] Table 1
Gypsum	CaSO ₄ ·2H ₂ O	Gypsum is associated with evaporite deposits in Nevada playas.	Papke 1976 [162274] Table 1; Kerr 1977 [161606] p. 221; Table A-1
Halite	NaCl	Halite is associated with evaporite deposits in Nevada playas.	Papke 1976 [162274] Table 1; Kerr 1977 [161606] p. 221; Table A-1
Huntite	CaMg ₃ (CO ₃) ₄	Huntite is a Mg carbonate mineral associated with cave and evaporite deposits as well as with meteoric (low-temperature) dissolution, and reprecipitation of calcite, dolomite or magnetite. Huntite will precipitate instead of calcite when Mg ²⁺ is concentrated in solutions with respect to Ca ²⁺ .	Faust 1953 [162282]; Walling et al. 1995 [162283] p. 360
Kieserite	MgSO ₄ ·H ₂ O	Kieserite is an evaporite mineral commonly found in salt deposits. Often it is associated with halite or carnallite.	Palache et al. 1951 [162280] pp. 477-479
Nahcolite	NaHCO ₃	Nahcolite is a saline mineral associated with Na-CO ₃ -Cl brines.	Eugster and Hardie 1978 [100743], Table 3
Natrite	Na ₂ CO ₃	Natrite is a highly soluble carbonate mineral associated with shortite, pirssonite, and gaylussite. These three minerals are also associated with the precipitation of trona, calcite and montmorillonite and are found in clay beds that have deposited in borax lakes.	Fleischer and Pabst 1983 [162284]; Palache et al. 1951 [162280]

In-Drift Precipitates/Salts Model

Table 18. Minerals Allowed to Precipitate in the IDPS Model (Continued)

Mineral	Formula	Rationale for Inclusion	References
Niter	KNO_3	Niter is associated with evaporite deposits in Nevada playas.	Papke 1976 [162274] Table 1
Pentasalt (Gorgeyite)	$\text{K}_2\text{Ca}_5(\text{SO}_4)_6 \cdot \text{H}_2\text{O}$	Gorgeyite occurs in association with glauberite, halite, and polyhalite in salt deposits.	Fleischer and Efremov 1954 [162312]
Phillipsite	$\text{K}_{0.7}\text{Na}_{0.7}\text{Ca}_{1.1}\text{Al}_{3.6}\text{Si}_{12.4}\text{O}_{32} \cdot 12.6\text{H}_2\text{O}$	Phillipsite is a zeolite mineral commonly associated with evaporite deposits.	Hay 1966 [105965]
Sellaite	MgF_2	Sellaite is the Mg analog to fluorite that forms in evaporite deposits.	Palache et al. 1951 [162280] pp. 37-39
Sepiolite	$\text{Mg}_4\text{Si}_6\text{O}_{15}(\text{OH})_2 \cdot 6\text{H}_2\text{O}$	Although the table in Attachment II indicates that sepiolite should not form at ambient temperatures and pressures, precipitation of sepiolite is common in conjunction with calcite precipitation in calcrete deposits. Sepiolite is a common fracture-lining mineral above the basal vitrophyre of the Topopah Spring Member at Yucca Mountain. Sepiolite is also known to commonly form on evaporation of either carbonate-source or tuff-source waters in southern Nevada. Poorly crystallized sepiolite precipitates readily at low temperature (~25°C) in alkaline solutions.	Hay and Wiggins 1980 [162281]; Carlos et al. 1995 [105213]; Vaniman et al. 1992 [107066]; Jones 1983 [162331]; Wollast et al. 1968 [162340]; Kent and Kastner 1985 [162345]
$\text{SiO}_2(\text{am})$	SiO_2	Literature evidence suggests that amorphous silica is at metastable equilibrium with respect to quartz at low temperatures and pressures. This is also evidenced by precipitation of opal-CT as opposed to quartz in evaporated carbonate and tuffaceous waters of southern Nevada.	Langmuir 1997 [100051]; Vaniman et al. 1992 [107066]
Soda Niter	NaNO_3	Soda Niter is associated with evaporite deposits in Nevada playas.	Papke 1976 [162274] Table 1
Stellerite	$\text{Ca}_2\text{Al}_4\text{Si}_{14}\text{O}_{36} \cdot 14\text{H}_2\text{O}$	Stellerite is a zeolite mineral commonly associated with fracture linings at Yucca Mountain.	Carlos et al. 1995 [105213]
Sylvite	KCl	Sylvite is associated with evaporite deposits in Nevada playas.	Papke 1976 [162274] Table 1; Kerr 1977 [161606] p. 221
Syngenite	$\text{K}_2\text{Ca}(\text{SO}_4)_2 \cdot \text{H}_2\text{O}$	Syngenite is associated with salt deposits (especially halite) and is known to be precipitated in cavities created by volcanic action. It precipitates at room temperatures from solutions that contain K_2SO_4 .	Palache et al. 1951 [162280] pp. 442-444
Thenardite	Na_2SO_4	Thenardite is associated with evaporite deposits in Nevada playas.	Papke 1976 [162274] Table 1
Trona	$\text{Na}_3\text{H}(\text{CO}_3)_2 \cdot 2\text{H}_2\text{O}$	Trona is associated with evaporite deposits in Nevada playas.	Papke 1976 [162274] Table 1

6.6.3 Summary of Computational Model

6.6.3.1 Preparation of Starting Water

The IDPS model starting water is the incoming seepage water or other aqueous solution subjected to evaporation by the IDPS model. For TSPA-LA, *Drift-Scale Coupled Processes (DST and THC Seepage) Models* (BSC 2003 [162050]) will be the primary provider of this water

and its composition. For validation or other analyses, starting waters can include synthesized starting waters used in laboratory evaporation experiments, hypothetical dilute binary solutions of soluble salts, and compositions of water samples collected from the site.

To prepare these starting waters for evaporation, it is important to charge balance them. The reason for this is that evaporation will result in precipitation of minerals and/or degassing of carbon dioxide. Because the precipitating minerals and carbon dioxide are neutrally charged, each of these processes removes an equivalent amount of positive and negative charge from the solution. Thus, if the starting water is not charge balanced prior to evaporation, the charge imbalance can increase to unacceptable levels after much of the dissolved solids have precipitated or degassed.

Although outputs from upstream models may be charge balanced in the upstream model, they are not necessarily charge balanced for the IDPS model. Small differences in the thermodynamic databases of models can generate small but considerable differences in charge balance calculations. Therefore, to ensure that the starting waters provided by upstream models are charge balanced for the IDPS model calculations, the EQ3NR is instructed to charge balance the starting waters.

Charge balance is achieved in the IDPS model by manually identifying the dissolved component in each starting water that has the largest normality and selecting the option to add or subtract this component to achieve charge balance. This method results in the smallest percentage adjustment of a starting component concentration.

For starting waters in which information is missing or measurements are known to be highly uncertain or below high detection limits, other approaches can be justified for charge balancing. These approaches might include fixing the fugacity of carbon dioxide to atmospheric values, or preventing super saturation of readily precipitated minerals, or other methods. Whatever the approach, it must be documented in the analysis.

6.6.3.2 Simple Evaporation

Evaporative concentration of dissolved solids in solution can be performed using EQ3/6. Water, the designated reactant, is incrementally removed from the solution while the remaining solution is maintained at equilibrium. Depending on mineral saturation indices and interaction with the gas phase, removal of water causes the dissolved ions to concentrate, precipitate, and/or degas.

A simple evaporation mode is used in the IDPS model to predict the evolution of a given water composition at a given temperature and carbon dioxide fugacity as it evaporates. For this mode, there is no solution flowing into the cell and no solution flowing out, as depicted in the conceptual model illustrated in Figure 1 (Section 6.4). The run begins with a given starting water composition, the solution is equilibrated with the fixed gas fugacities, all supersaturated unsuppressed minerals are allowed to precipitate, and water is incrementally removed from the system. In EQ3/6 Version 8.0, "H2O" is declared the aqueous species reactant, and the rate constant (rk1) is set at -1.0. The concentration factor of the evolving solution is calculated from Equation 6.6.2.5-4.

These reactions are simulated to an ionic strength of about 1 molal using traditional ion activity correction equations such as the B-dot equation (SNL 2003 [162494], p. B-32 of user's manual). However, with EQ3/6 Version 8.0 and the Pitzer database in Attachment I, evaporation for the system Na-K-H-Mg-Ca-Al-Cl-F-NO₃-SO₄-Br-CO₃-SiO₂-CO₂-O₂-H₂O can proceed until there is essentially no free water remaining.

In the simple evaporation mode, the activity of water decreases as water evaporates. Because this mode assumes equilibrium conditions at all times (Assumption 5.2), the resulting activity of water after each incremental decrease in solvent determines the equilibrium relative humidity. As evaporation proceeds to its extreme, the model produces a complete sweep of equilibrium results down to the relative humidity of the dry out point of the solution. In the opposite direction, the model predicts equilibrium results for condensation of water into an initial seepage water. Condensation predictions can be obtained for dilution factors of 100 or more. Together, the evaporation and condensation results can then be tabulated in a set of lookup tables so that the equilibrium composition can be identified or interpolated for any given equilibrium relative humidity (Section 6.6.3.5).

6.6.3.3 Representation of Steady-State Evaporation with Flow-Through

The IDPS model abstraction for TSPA-LA simulates discrete time intervals in which the seepage rate of water flowing into the drift can be modeled as a constant. If the relative humidity is high enough to permit the formation of a stable brine (usually around 65 percent or higher), then a steady-state condition can develop such that some of the water will remain in a pool and some will flow out of the assigned control volume. Such a steady state condition is represented in Figure 3. EQ3/6 Version 8.0 cannot directly model a flow-through system like this, but there is a way to represent this system using the simple evaporation mode presented in the previous section.

In the simple evaporation mode, the total volume (or mass) of water within the cell (or control volume) decreases with evaporation. This is not the case for the steady-state flow-through mode. In the steady-state flow-through mode, the total volume (or mass) of water in the cell is maintained. At steady state, the flux of water seeping into the cell (Q^s) is equivalent to the sum of the evaporation flux (Q^e) and the flux of water flowing out of the cell (Q^d) (Figure 3). As a result, the water composition within the cell will reach a steady-state concentration factor that depends only on the incoming water composition and the relative evaporation rate, R^{es} , as described by Equation 6.6.2.5-2.

For example, from Equation 6.6.2.5-2, a CF of 10 implies a R^{es} value of 0.9. This implies that if R^{es} equals 0.9, a conservative constituent in the incoming seepage water will reach a steady-state concentration in the cell that is a factor of 10 higher than the incoming seepage concentration. Thus, whether the incoming seepage undergoes simple evaporation or steady-state flow-through evaporation, a unique and identical resulting water composition can be determined from the incoming seepage composition and the CF .

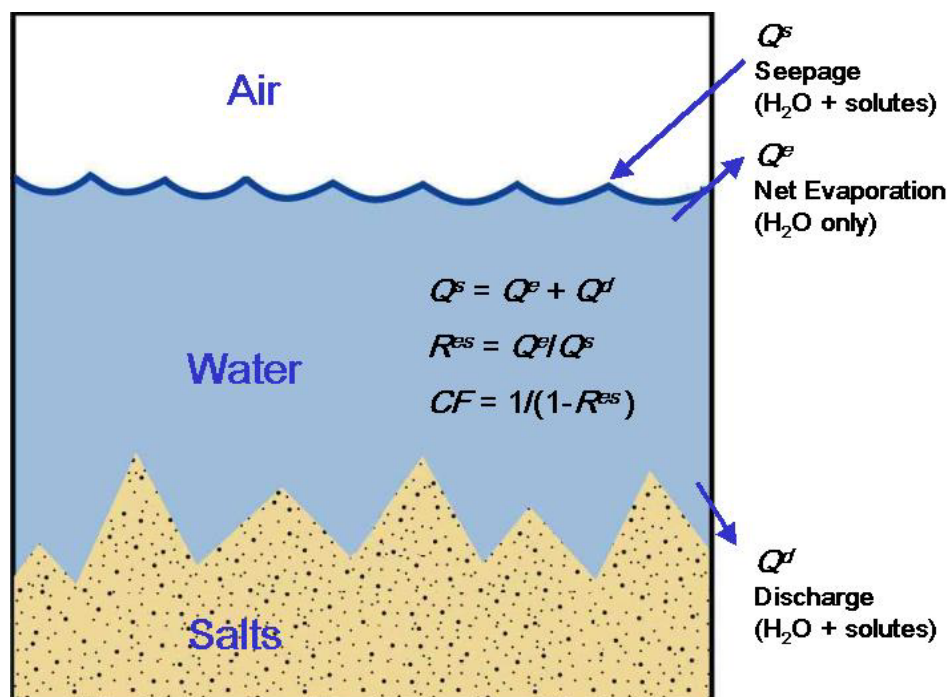


Figure 3. Representation of Steady-State Flow-Through for the In-Drift Precipitates/Salts Model

In the IDPS model abstractions for TSPA-LA, the time required to reach equilibrium or steady state is negligible compared to the abstraction timeframes to which a given incoming seepage is applied. For simple evaporation, water evaporates quickly when the relative humidity is considerably below 100 percent. For flow-through conditions, steady-state compositions are nearly achieved after as few as 10 cell flushes (i.e., after the total volume of incoming seepage exceeds 10 cell volumes). Because abstraction timeframes are long compared to the time required for equilibrium evaporation of static water or 10 cell flushes under flow-through conditions, equilibrium or steady-state assumptions provide reasonable evaporation predictions.

It is possible for steady-state conditions to develop such that equilibrium with respect to relative humidity will *not* occur. For example, if the evaporation rate is one half of the seepage rate (i.e., R^{es} equals 0.5), Equation 6.6.2.5-2 dictates that conservative ions will reach a steady state concentration that is twice the incoming concentration (CF equals 2). The importance of this is that if the incoming seepage water is dilute, the steady-state activity of water could be around 0.999 or higher. If this is the case and the relative humidity in the drift is much lower than 99.9 percent, then equilibrium with respect to RH would not be achieved at steady state.

6.6.3.4 Model Input Files

Three EQ3/6 input files are required to represent the IDPS model. The first is the EQ3NR input file used to define the starting water, as described in Section 6.6.3. The other two are the EQ6 input files used to either evaporate the starting water or dilute the starting water with condensed water vapor. The EQ3NR pickup files, produced by EQ3NR, must be appended to the

corresponding EQ6 input files to initialize the EQ6 runs. The general formats of these input files are documented in DTN: MO0303SPAMEQ36.000.

6.6.3.5 Model Output

Application of the IDPS model generates EQ3/6 output files that describe the boundary conditions, equilibrium calculations, and effects of evaporation and condensation on water composition and precipitation of solids. These output files contain much more information than is used in downstream modeling. Lookup tables are generated to summarize the outputs important to the TSPA-LA.

Three types of model output are tabulated in the lookup tables: boundary values, abstraction output, and supplemental calculations. The first two types of output are directly provided in the EQ6 output files. The third type, supplemental calculations, consists of simple algebraic manipulations of the EQ6 output.

Boundary values include temperature, the fugacities of carbon dioxide and oxygen, and the reaction progress. These values are, for all practical purposes, input values. The reaction progress is a measure of the extent of evaporation or condensation that has occurred for a set of equilibrium output values.

Abstraction output includes all EQ6 calculations for the aqueous output variables of interest in the TSPA-LA. It includes the pH, activity of water, ionic strength, mass of solvent water remaining, total concentrations of each element, concentrations of select aqueous species that potentially contribute to acid-neutralizing capacity, and amounts of solids precipitating in a given EQ6 run. This information is useful in understanding how a starting water chemically evolves for a given set of boundary conditions. It is also used to support downstream calculations that evaluate interaction of this water with potential cementitious materials, steel, and microbes (FEPs 2.1.09.01.0A and 2.1.11.08.0A in Section 6.2).

Supplemental calculations include lookup table calculations for relative humidity (RH), concentration factor (CF), relative evaporation rate (R^{es} or Q^e/Q^s), and dilution factor (DF or $1-Q^e/Q^s$). These calculations support the base case equilibrium model (Figure 1) and steady-state alternative conceptual model (Figure 3). RH is calculated by multiplying the activity of water by 100 percent. CF is calculated using Equation 6.6.2.5-2 above. R^{es} (or Q^e/Q^s) is calculated from an algebraic manipulation of Equation 6.6.2.5-2. Solving Equation 6.6.2.5-2 for R^{es} gives:

$$R^{es} = 1 - \frac{1}{CF} \quad (\text{Eq. 6.6.3.5-1})$$

Finally, the dilution factor (DF or $1-Q^e/Q^s$) is calculated by subtracting Q^e/Q^s from one. The value of $(1-Q^e/Q^s)$ is equivalent to the dilution factor (DF) defined in Equation 6.6.2.5-3. This calculation is useful for plotting and visually comparing the results of various EQ6 runs. In addition, plotting evaporative evolution as a function of $(1-Q^e/Q^s)$ generally linearizes the results. This is useful when interpolations must be made because linear interpolation of linearized data can increase the accuracy of interpolations. An example lookup table is presented in Section 6.7.3.

6.7 DEMONSTRATION OF BASE CASE MODEL

An example application of the IDPS model is presented in this section to demonstrate how the model is used to produce lookup tables for the TSPA-LA. For this demonstration, an average in situ J-13 well water is used as the incoming seepage composition.

The composition of in situ J-13 well water used in the demonstration is summarized in Table 14. This composition originates from the Harrar et al. (1990 [100814]) report, in which sample data for individual dissolved components in well J-13 water were compiled and averaged. These averages are documented in DTN: MO0006J13WTRCM.000. For this example, pH is set at 7.0, which is the average of the two field-measured pH values (6.9 and 7.1) reported in Harrar et al. (1990 [100814] p. 4.9). Similarly, for this example, dissolved oxygen is set at 5.6 mg/L, which is in the middle of the 5.5 to 5.7 mg/L range reported in Harrar et al. (1990 [100814] p. 4.9). The initial temperature is set at 31°C, corresponding to the approximate down-hole temperature reported in Harrar et al. (1990 [100814] p. 4.9). This demonstration is not directly used in performance assessment.

6.7.1 Evaporation of Average In Situ J-13 Well Water

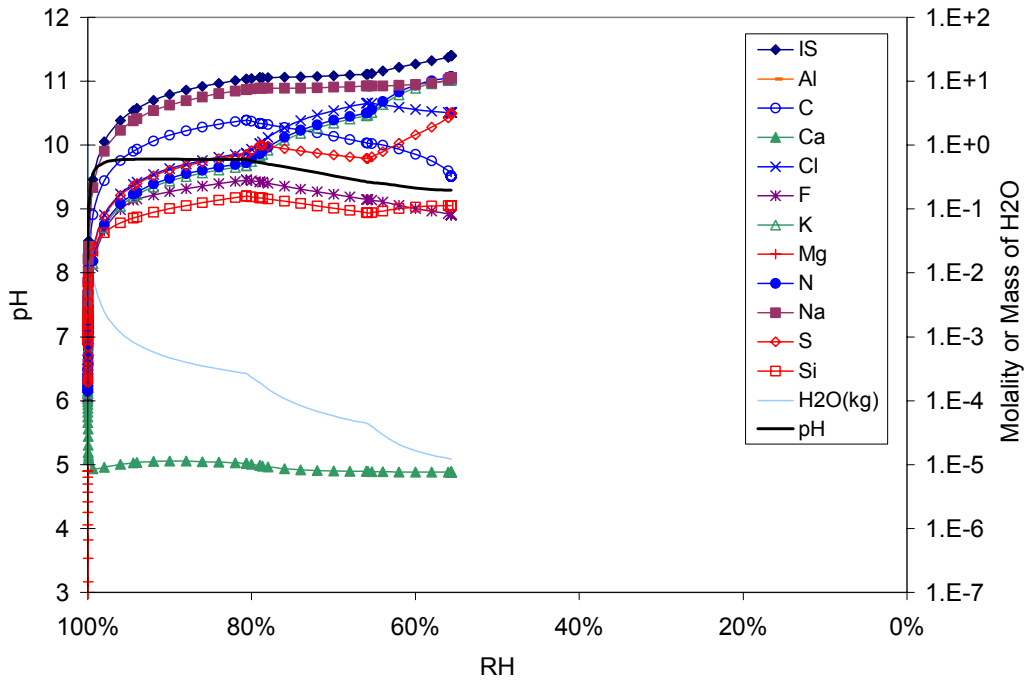
Average in situ J-13 water (summarized in Table 14 and described in Section 6.7 above) was evaporated using the IDPS model. For this simulation, EQ3/6 Version 8.0 and the Pitzer thermodynamic database (Attachment I) were the code and database used to run the IDPS model. The temperature for the evaporation was reset at 70°C and the carbon dioxide fugacity was fixed at 10^{-3} bars. The results are documented in DTN: MO0303MWDIOJ13.000 and MO0304SPAJ13IS.001.

Figure 4 and Figure 5 show the predicted evolution of pH, ionic strength (*IS*), and total concentrations of aqueous constituents as a function of equilibrium *RH* and concentration factor (*CF*). In the model, *RH* reflects the equilibrium activity of water, and *CF* reflects the ratio of the original and remaining masses of H₂O in solution (Equation 6.6.2.5-4). These results show that more than 99 percent of the H₂O is evaporated before the equilibrium *RH* falls below 99 percent.

As shown in Figure 5, in the early stages of evaporation, Cl, F, K, Na, N, and S concentrate in a linear manner such that the concentration at a given *CF* equals the starting equilibrium concentration multiplied by *CF*. This linear relationship implies conservative behavior (i.e., the total masses of these components are conserved within the evaporating solution). Departures from conservative behavior are caused by heterogeneous reactions such as precipitation or degassing. At a *CF* around 1,200, which corresponds to an equilibrium *RH* of about 94 percent, F begins to depart from the linear trend. Beyond this point, Cl, K, and N continue to concentrate in a conservative manner until Cl departs from this trend at a *CF* around 22,000. K and N continue to concentrate linearly until the run is complete at a *CF* around 82,400 (*RH* around 56 percent).

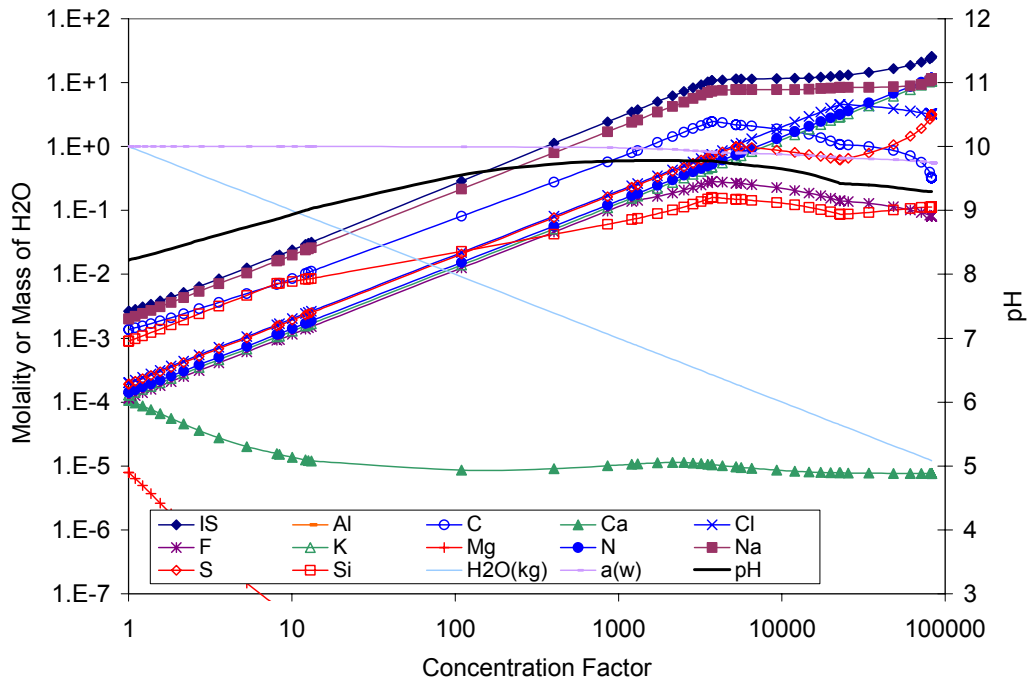
Aqueous species that potentially contribute to acid-neutralizing capacity are plotted in Figure 6 and Figure 7.

Figure 8 and Figure 9 show the predicted accumulations of precipitating minerals. At the start, calcite, sepiolite, and stellerite are predicted to precipitate. As the solution evaporatively concentrates by a factor of about 1,000, stellerite is replaced by celadonite and amorphous silica begins to precipitate. At a *CF* of about 1,200, fluorite begins to precipitate, which corresponds to the point at which F departs from the linear trend (Figure 4). Further evaporation results in precipitation of natrite, thenardite, and eventually halite.



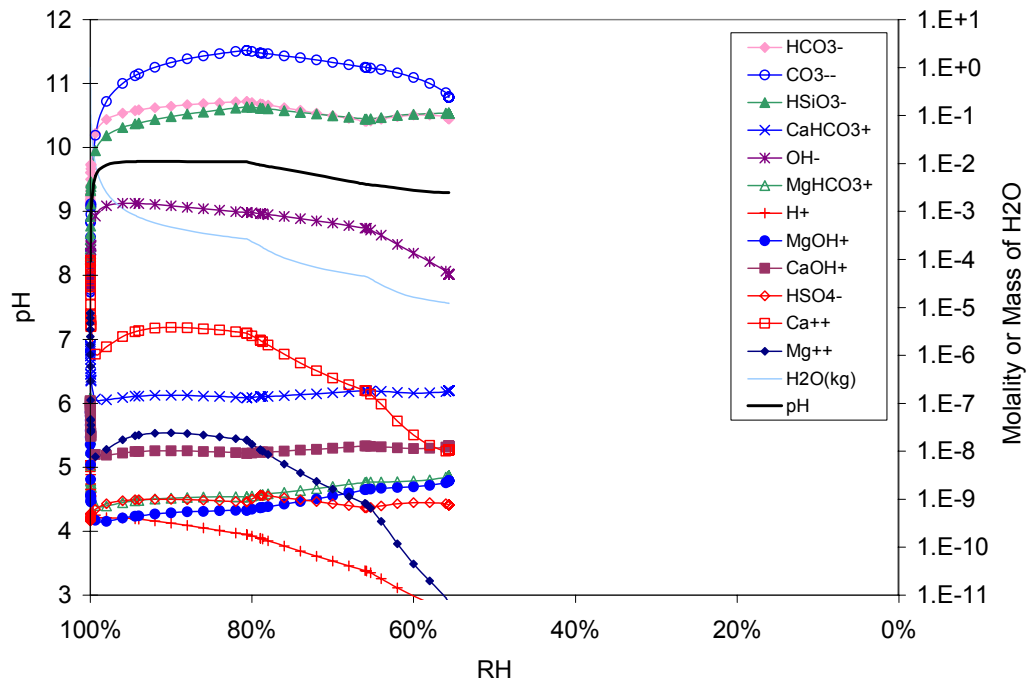
DTN: MO0304SPAJ13IS.001

Figure 4. Example Aqueous Composition Evaporation Predictions vs. *RH*



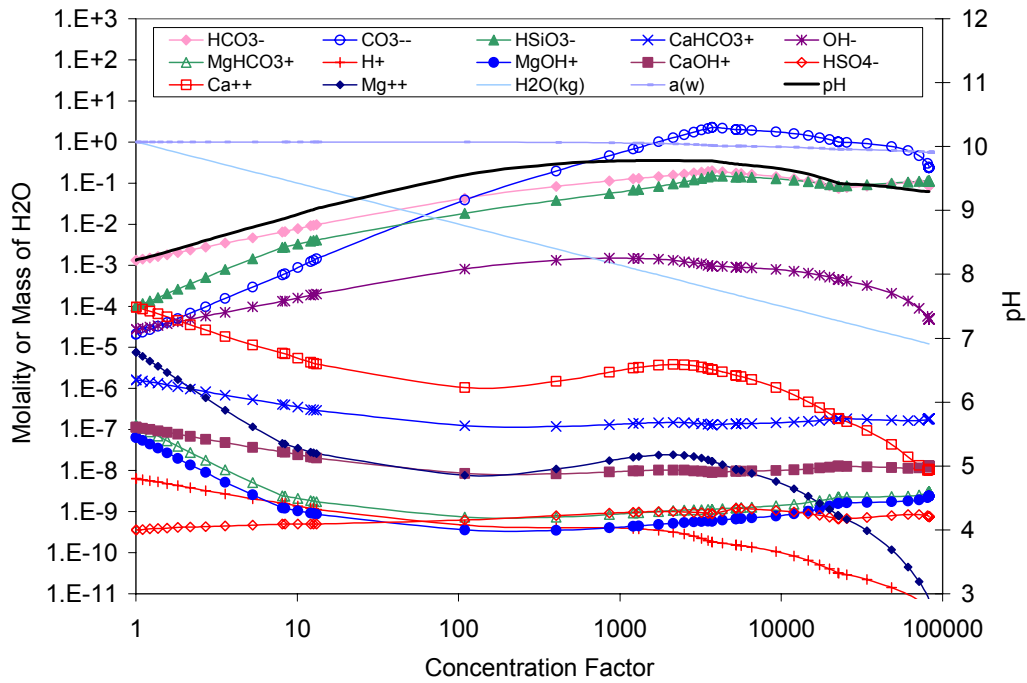
DTN: MO0304SPAJ13IS.001

Figure 5. Example Aqueous Composition Evaporation Predictions vs. *CF*



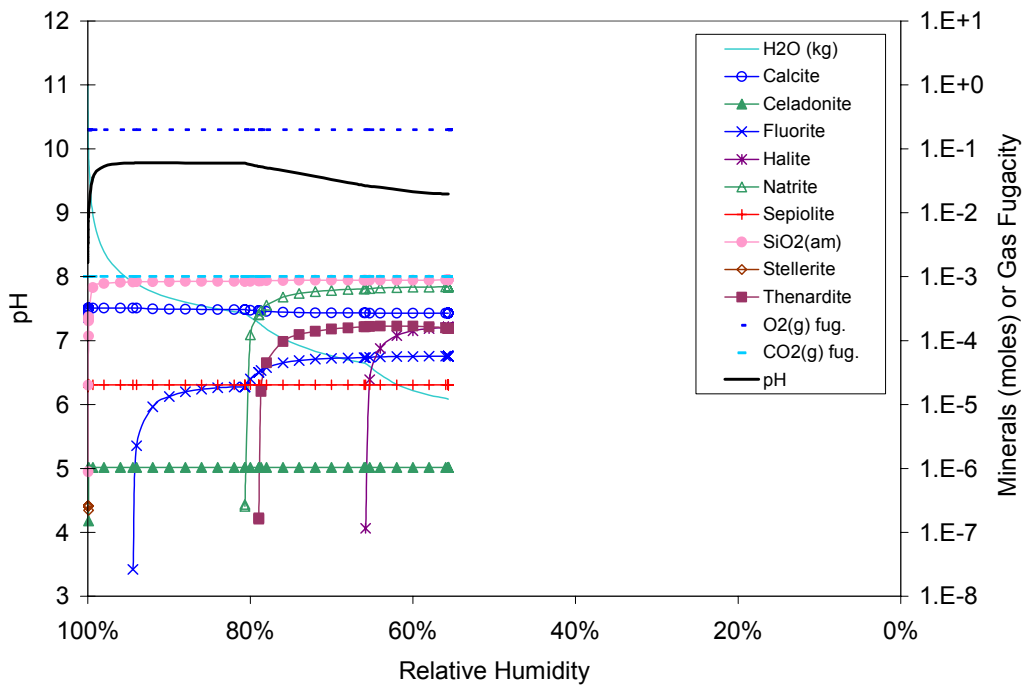
DTN: MO0304SPAJ13IS.001

Figure 6. Example Acid-Neutralizing Capacity Species Concentration Evaporation Predictions vs. *RH*



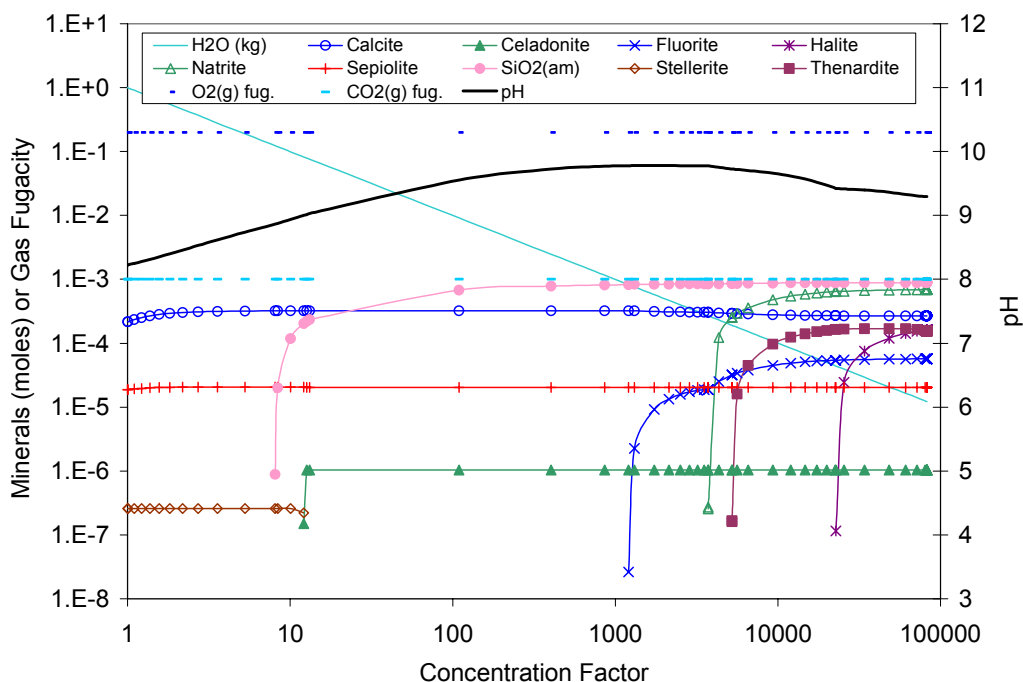
DTN: MO0304SPAJ13IS.001

Figure 7. Example Acid-Neutralizing Capacity Species Concentration Evaporation Predictions vs. *CF*



DTN: MO0304SPAJ13IS.001

Figure 8. Example Mineral Precipitation Evaporation Predictions vs. *RH*



DTN: MO0304SPAJ13IS.001

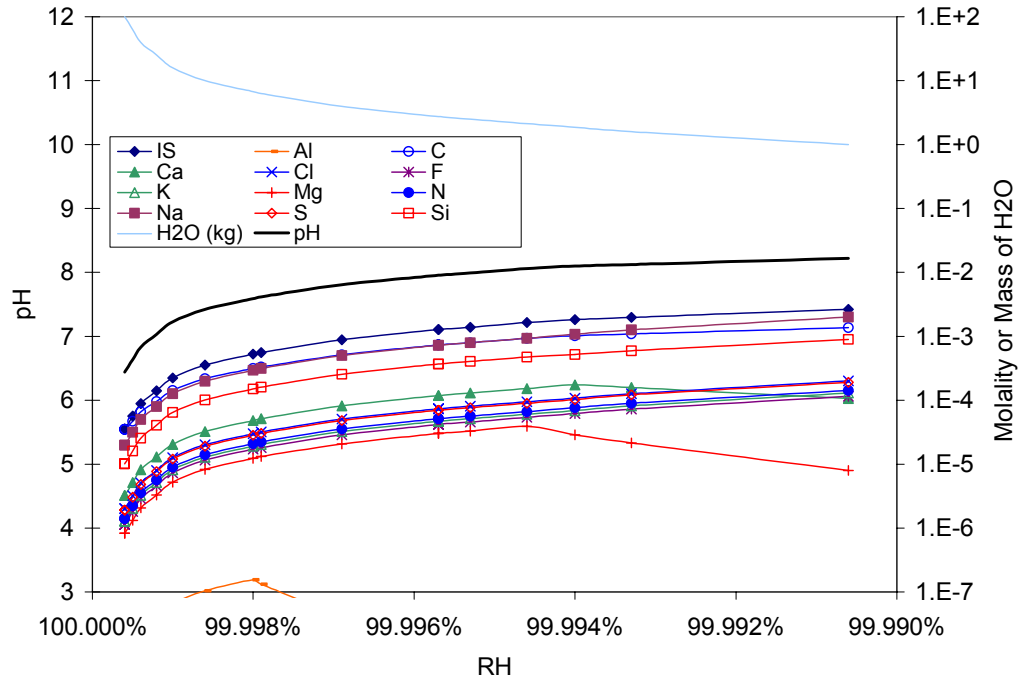
Figure 9. Example Mineral Precipitation Evaporation Predictions vs. *CF*

6.7.2 Dilution of Average In Situ J-13 Well Water

Dilution of equilibrated seepage water could also occur in the proposed repository. A brine that has equilibrated with the atmosphere will have a net influx of condensed water vapor if the *RH* increases. It is necessary to use the IDPS model to predict the effects of dilution for each incoming seepage water because the *RH* in the drift could potentially exceed the activity of water of the abstracted incoming seepage water.

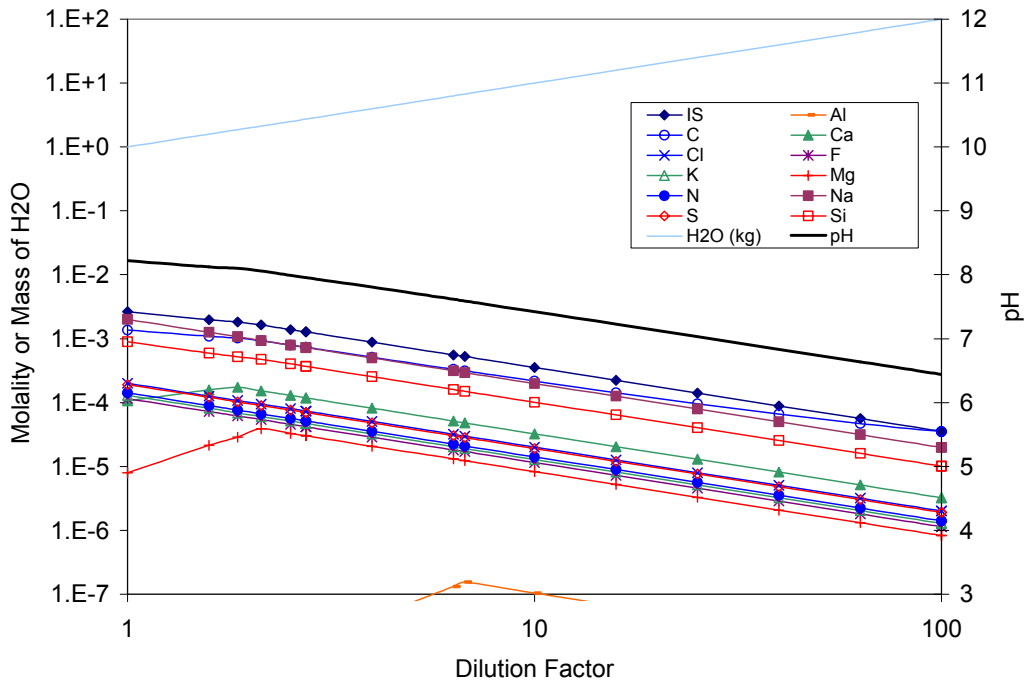
To ensure that the lookup tables provide outputs for potential dilution of incoming seepage for each TSPA-LA realization, each identified incoming seepage water must be diluted as needed using the IDPS model. For the example here, the starting average in situ J-13 well water is diluted by a factor of 100. This is done by incrementally adding water until the final mass of water equals the original mass multiplied by the dilution factor. The results for this example are documented in DTN: MO0303MWDIOJ13.000 and MO0304SPAJ13IS.001.

Figure 10 and Figure 11 show the results of diluting the example water by a factor of 100. In general, the aqueous concentrations behave conservatively, decreasing in proportion to the dilution factor. There are departures, however, resulting from heterogeneous reactions such as exchange of carbonate with the atmosphere and dissolution of minerals that precipitated upon initial equilibration of the starting composition. Aqueous species that potentially contribute to acid neutralizing capacity are plotted in Figure 12 and Figure 13.



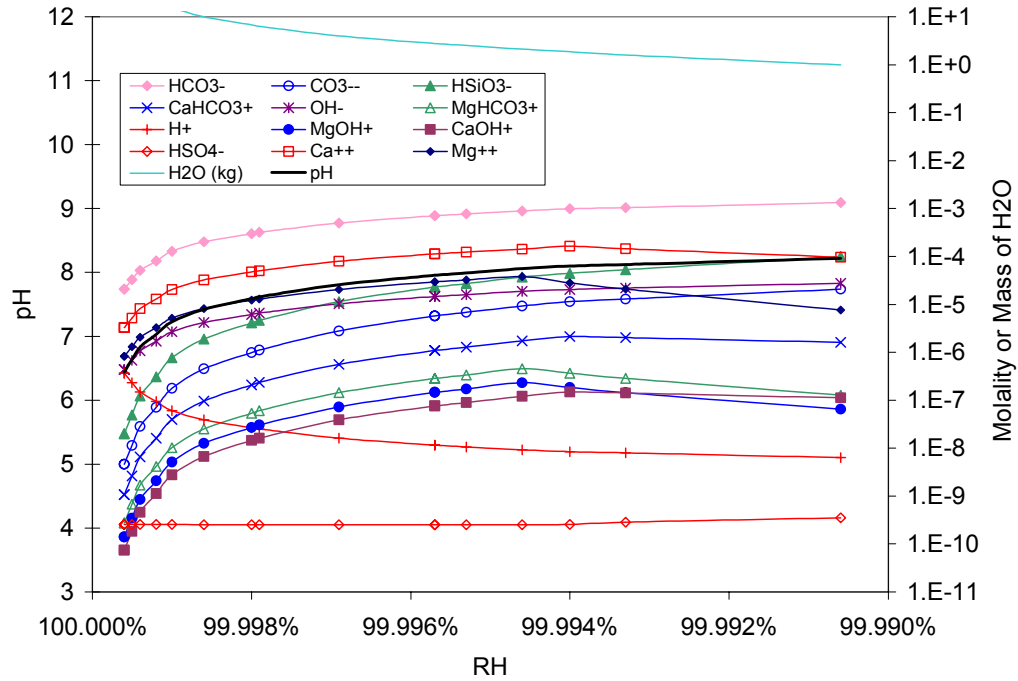
DTN: MO0304SPAJ13IS.001

Figure 10. Example Aqueous Composition Condensation Predictions vs. *RH*



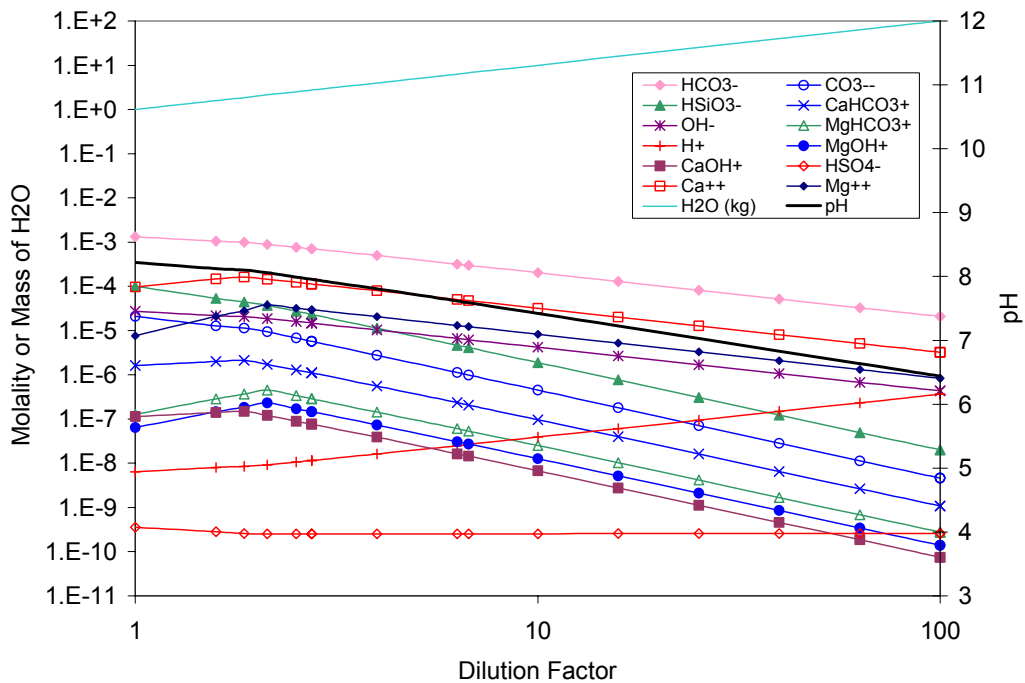
DTN: MO0304SPAJ13IS.001

Figure 11. Example Aqueous Composition Condensation Predictions vs. *DF*



DTN: MO0304SPAJ13IS.001

Figure 12. Example Acid-Neutralizing Capacity Species Concentration Condensation Predictions vs. *RH*



DTN: MO0304SPAJ13IS.001

Figure 13. Example Acid-Neutralizing Capacity Species Concentration Condensation Predictions vs. *DF*

6.7.3 Resulting Model Lookup Tables

As described in Section 6.6.3.5, the IDPS model outputs that are important to the TSPA-LA include boundary conditions, abstraction output, and supplemental calculations. Each evaporation or condensation lookup table is specific to a defined set of boundary conditions. These tables provide snapshots of the output parameter values as the water incrementally evolves due to evaporation or condensation given the defined boundary conditions. Each snapshot is defined by a unique equilibrium RH , CF (and/or DF), and Q^e/Q^s .

An example set of lookup tables is provided in Attachments III and IV. Attachment III is the lookup table associated with the evaporation of the average in situ J-13 well water presented in Section 6.7.1. Attachment IV is the corresponding lookup table for condensation (Section 6.7.2). These lookup tables are documented in DTN: MO0304SPAJ13IS.001.

The evaporation lookup tables are divided into sections by column. The first three columns are supplemental spreadsheet calculations for concentration factor (CF), relative evaporation rate (Q^e/Q^s), and dilution factor (DF). These calculations are described in Section 6.6.3.5. The next column is the equilibrium RH , calculated by multiplying the activity of water (in column K) by 100 percent. The rest of the columns are filled using GETEQDATA Version 1.0.1 (BSC 2003 [161900]). Columns 5 through 8 show reaction progress and the boundary conditions for the starting water, i.e., the temperature and the fugacities of oxygen and carbon dioxide. Columns 9 through 24 show reaction progress, pH, ionic strength, mass of H₂O in the reactor, and the total concentrations of the aqueous components. Columns 25 through 38 present reaction progress, mass of H₂O in the reactor, and the concentrations of potential acid-neutralizing species. Finally, columns 39 through 56 are reserved to show the amounts of minerals accumulated in the reactor. This last section is not included in the condensation lookup tables because mineral outputs from the IDPS model are only needed from evaporation runs. The top three rows in these spreadsheets provide a visual check that the correct type of information was entered into each column. The values in the lookup tables may be used to define response surfaces so that interpolations or extrapolations may be obtained for precise input values not provided in the tables.

7. VALIDATION

This section documents the validation of the IDPS model. As stated in AP-SIII.10Q, *Models*, model validation is a process used to establish confidence that a mathematical model and its underlying conceptual model adequately represent with sufficient accuracy the system, process, or phenomenon in question. Validation is designed to demonstrate that the model is appropriate and adequate for the intended use. The intended use is defined in Section 1. All data used in the validation are identified in Section 4.4.

As stated in Section 1.2.2.6 of the EBS TWP (BSC 2003 [165601]), the criterion for model validation is agreement of the following comparisons within the uncertainty range established with past and planned model uncertainty and sensitivity studies:

1. Comparing model results to the results of past and ongoing evaporation tests.
2. Comparing model results to published data.

Past uncertainty and sensitivity studies have shown a varying degree of model accuracy for the IDPS model output parameters. To articulate the validation criterion in the TWP, quantitative validation objectives were developed for specific IDPS model output parameters. These objectives, presented in Table 19, approximate the model accuracy called for by the EBS TWP (BSC 2003 [165601]).

The validation objectives were developed based on previous results obtained from modeling evaporation at Yucca Mountain (Sections 6.3.3 and 6.3.4). In general, these earlier models accurately predicted aqueous concentrations to within an order of magnitude (factor of 10). The exceptions included the prediction of aqueous Ca, Mg, and Si concentrations (BSC 2001 [156065]).

The IDPS model output parameters that will be directly used in the TSPA-LA are pH, ionic strength, concentrations of Cl and NO₃, the Cl:NO₃ ratio, and deliquescence relative humidity (*RH_d*). These outputs are important for predicting corrosion, colloid stability, and radionuclide mobility. The model uncertainties related to these output parameters are estimated in Table 20. These uncertainties represent the uncertainties in the output parameters due to uncertainties in the model. They do not include the uncertainties due to uncertainties in the model input values. These estimates are based on professional judgment. They are intended to represent reasonable uncertainty ranges bounded by values that would represent approximate 95 percent confidence intervals if the underlying distributions were normally distributed. Uniform probability distributions across these ranges are recommended because supporting data are sparse and uniform distributions are conservative relative to distributions that weigh the middle values more heavily (i.e., uniform distributions tend to err on the side of representing too much uncertainty). As summarized in Section 7.5, these estimates of uncertainty are supported and justified by the model validation comparisons in Sections 7.1 through 7.3.

Sections 7.1 through 7.3 respectively present model validation simulations to compare with the results of multi-component evaporation experiments, sample data for evaporated seawater, handbook aqueous solubilities and deliquescence relative humidity values of simple salts, and predictions using an independent database. These sections focus primarily on validating the aqueous outputs of the IDPS model. Section 7.4 draws upon these model validation simulations to document how the IDPS model is validated for mineral outputs. Section 7.5 summarizes the results of the simulations and their implications.

Table 19. Model Validation Objectives

Category of Model Output	Related Components	Related ANC Species	Related Minerals	Experimental Agreement for Aqueous Components and ANC Species	Experimental Agreement for Minerals
pH	H	H ⁺ , OH ⁻	not applicable	pH within 1 pH unit; Concentration within 1 order of magnitude (factor of 10)	not applicable
Ionic Strength	Al, Br, Ca, CO ₃ , Cl, F, K, Mg, Na, NO ₃ , SiO ₂ , SO ₄	not applicable	not applicable	Concentration within 1 order of magnitude (factor of 10)	not applicable
Deliquescence Relative Humidity (<i>RH_d</i>)	H ₂ O	not applicable	Highly soluble minerals in the system Al-Br-Ca-CO ₃ -Cl-F-K-Mg-Na-NO ₃ -SO ₄ -SiO ₂ -H-H ₂ O at potential repository temperatures and pressures	Activity of water within 0.1 of deliquescence relative humidity (<i>RH_d</i>)	Solubility within 1 order of magnitude (factor of 10)
Rapidly equilibrated components and their associated ANC species and minerals	Al, Br, CO ₃ , Cl, F, K, Na, NO ₃ , SO ₄	HCO ₃ ⁻ , CO ₃ ²⁻ , HSO ₄ ⁻	Unsuppressed potential minerals of the system Al-Br-CO ₃ -Cl-F-K-Na-NO ₃ -SO ₄ -H-H ₂ O at potential repository temperatures and pressures	Concentration within 1 order of magnitude (factor of 10)	Solubility within 1 order of magnitude (factor of 10)
Less rapidly equilibrated components and their associated ANC species and minerals	Ca, Mg, SiO ₂	Ca ²⁺ , Mg ²⁺ , CaHCO ₃ ⁺ , MgHCO ₃ ⁺ , MgOH ⁺ , HSiO ₃ ⁻	Unsuppressed potential Ca, Mg, and SiO ₂ minerals of the system Al-Br-Ca-CO ₃ -Cl-F-K-Mg-Na-NO ₃ -SO ₄ -SiO ₂ -H-H ₂ O at potential repository temperatures and pressures	Concentration within 2 orders of magnitude (factor of 100)	Equilibrium solubility within 1 order of magnitude (factor of 10)

NOTE: ANC = acid-neutralizing capability

Table 20. Estimated Model Uncertainty in Selected Output Parameters

IDPS Model Output Parameter	Uncertainty Range	Probability Distribution
pH	± 1 pH unit	Uniform
Ionic Strength	± 30% RPD ^a	Uniform
Cl	± 30% RPD	Uniform
NO ₃	± 30% RPD	Uniform
Cl:NO ₃ ratio	± 30% RPD	Uniform
<i>RH_d</i>	± 5% <i>RH</i> units	Uniform

DTN: MO0308SPAESMUN.000

^a relative percent difference

7.1 VALIDATION USING EVAPORATION DATA

Several sources of evaporation data are relevant to the validation of the model. They include Rosenberg et al. (1999 [125338]; 1999 [125339]), CRWMS M&O (2000 [146460]), and McCaffrey et al. (1987 [164481]). These data are presented in Table 7 through Table 11 in Section 4.4.

7.1.1 Evaporation of Average J-13 Well Water at 85°C

Rosenberg et al. (1999 [125338]) evaporated synthetic J-13 well water in a beaker that was open to the atmosphere and maintained at a constant elevated temperature of 85°C. In the experiment named evap1, synthetic average J-13 well water was evaporated without contact with tuff or other non-precipitated rock material. The experiment began with 30 liters of synthetic average J-13 well water with a measured composition as shown in Table 7. A peristaltic pump was used to pump this water into a 1-liter Pyrex beaker at a constant rate while a hot plate was used to maintain a water temperature of 85°C to evaporate the water. Water samples were collected after the 30 liters had been evaporated to approximately 30 mL. Results of this experiment are also included in Table 7. The solids that had accumulated at this stage were identified by x-ray diffraction to be amorphous silica, aragonite, and calcite. Analysis of solids after complete evaporation indicated the additional presence of halite, niter, thermonatrite, and possibly gypsum, anhydrite, and hectorite.

In a similar synthetic J-13 well water evaporation experiment (named evap4), the pH of the evaporating water was monitored (Rosenberg et al. 1999 [125338]). The experiment used approximately the same J-13 starting solution as evap1 (Table 7). The pH measurements are presented in Table 8 as a function of concentration factor. The concentration factor was measured as the ratio of the initial water mass divided by the measured water mass at the time of analysis.

The results of these evaporation experiments were modeled using the IDPS model and Pitzer database. Total aqueous concentrations, pH, ionic strength (*IS*), and mineral precipitation predictions are plotted in Figure 14 and Figure 15. Comparisons of measurements and predictions are plotted in Figure 16 and Figure 17. Modeling results are documented in DTN: MO0303MWDJ13RB.000.

One adjustment to the model was to augment the Pitzer database sepiolite ($\text{Mg}_4\text{Si}_6\text{O}_{15}(\text{OH})_2 \cdot 6\text{H}_2\text{O}$) log K by 6 log K units. This was done to represent an amorphous sepiolite because a crystalline sepiolite, like the sepiolite in the Pitzer database, requires up to 10 years to form at 25°C (Jones and Galan 1988 [162347] Chapter 16). Formation of an amorphous sepiolite in short timeframes like the evaporation experiment is more likely described by log K values closer to those provided by Wollast et al. (1968 [162340]). Augmenting the Pitzer database log K for sepiolite by 6 log K units is approximately equivalent (after stoichiometric normalization) to the difference between the amorphous phase log K value of Wollast et al. (1968 [162340]) and the crystalline phase log K value of Stoessel (1988 [127964]) (Jones and Galan 1988 [162347] Table 6, Chapter 16).

As shown in Figure 16, the modeled evaporation results approximate the Na, F, HCO₃, Cl, K, Mg, NO₃, SO₄, and SiO₂ concentrations within a factor of 10 or better when compared to the laboratory measurements. Ca predictions are within a factor of 100 of the measurements. The differences in the predicted and measured aqueous concentrations are within the acceptable range of the model validation objectives listed in Table 19.

Figure 17 shows general agreement between the laboratory measured pH and modeled pH in evap4. The predicted pH is largely controlled by the fugacity of carbon dioxide, which is fixed at 10^{-3.4} bars to approximate the laboratory condition of a beaker open to the atmosphere. Water in evap4 was concentrated to 157 times the original solution.

The discrepancies between the predicted and measured Si, Ca, and Mg concentrations and pH may be due to errors or uncertainty in the Pitzer thermodynamic database, kinetic limitations of precipitation reactions, and/or analytical errors such as incomplete removal of small particles of minerals containing these elements from the aqueous samples. If errors and uncertainty in the database and analytical measurements can be ruled out, the relatively short laboratory experiments could have produced sustained supersaturated conditions for calcite and sepiolite. Calcite, the more rapidly precipitated of the two minerals, is perpetually supersaturated in surface seawater where evaporation is an ongoing process (Drever 1988 [118564] pp. 71-72) and has been shown to be supersaturated in laboratory evaporation experiments (Krauskopf and Bird 1995 [101702] p. 72). Precipitation of calcite when the pH is below 10 results in the release of a proton from the bicarbonate ion:



Thus, slow precipitation of calcite could also explain why the model predicts lower pH than observed. These minerals precipitate in the model at a concentration factor of 157 as shown in Figure 15.

The fixed carbon dioxide fugacity is another possible explanation for the observed discrepancies in pH. In a solution that is boiling or evaporating from a beaker, it is possible that the atmospheric partial pressure of carbon dioxide is below atmospheric values because of an increased partial pressure of water vapor and a net flux of vapor flowing out of the beaker. If this was the case, the actual carbon dioxide fugacity would have been lower and pH predictions would have been higher.

At a concentration factor of 956 (*CF* 956) in evap1, precipitation of amorphous silica (SiO₂ (am)), aragonite (CaCO₃), and calcite (CaCO₃) was identified in the experiment. These minerals cannot account for the loss of Mg, whose concentration decreases by more than a factor of 10 rather than increases by a factor of 956. At this stage the model predicts precipitation of calcite and sepiolite. Actual precipitation of amorphous sepiolite (Mg₄Si₆O₁₅(OH)₂·6H₂O) would be consistent with the reported precipitation of amorphous silica, if the loss of Mg was accounted for in the observed mineral assemblage at *CF* 956.

Upon complete evaporation, the following minerals were observed: amorphous silica, aragonite, calcite, halite, niter, thermonatrite, gypsum, anhydrite, and hectorite. The last three minerals were not positive matches. These minerals do not account for the precipitation of Mg or F

(except for the possible occurrence of hectorite). In comparison, the following minerals were predicted by the IDPS model to precipitate: calcite, fluorite, halite, natrite, sepiolite, amorphous silica, and thenardite. Although the predicted phases may not perfectly match the actual phases that precipitate in the experiment, their predicted precipitation accurately accounts for mass balance and produces a scenario that is consistent with the observed evaporative evolution of the solution to *CF 956*.

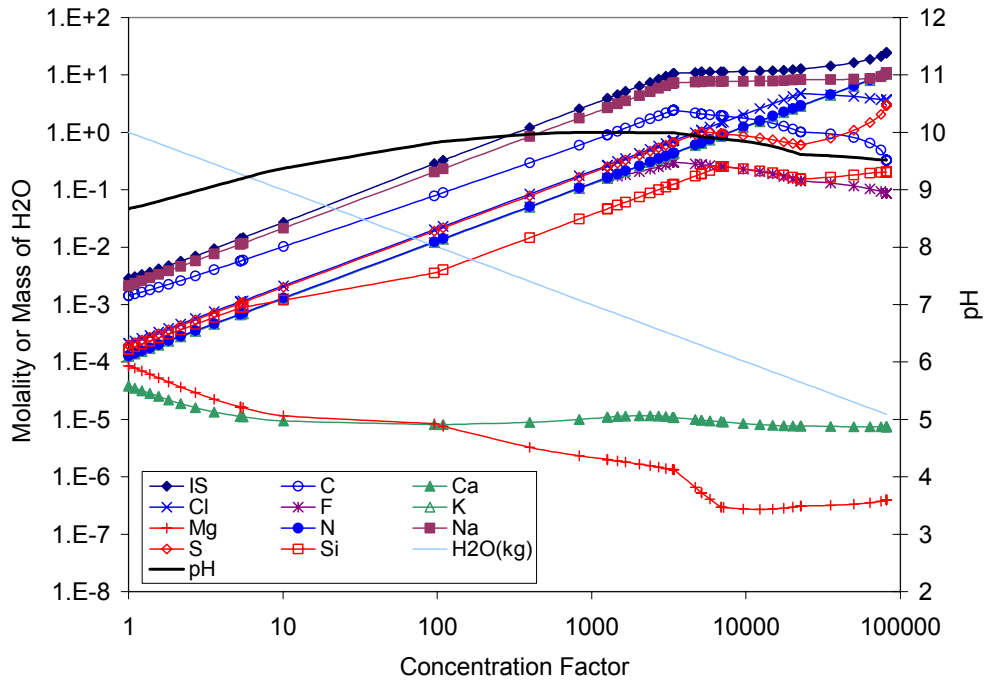
Ionic strength was not directly measured in these experiments. However, a "measured" ionic strength was estimated from the reported evaporated water compositions using EQ3NR. This was done by entering the reported water compositions and instructing the code to maintain any charge imbalances while it equilibrated the solutions. These EQ3NR calculations did not permit precipitation of potentially supersaturated minerals and did not equilibrate the solution with fixed partial pressures. Such heterogeneous reactions would alter the water compositions from the measured concentrations. Thus, the results provided estimated "measured" values of ionic strength, as the data0.ypf database would calculate them. These calculations are documented in DTN: MO0307MWDUNEVP.000 and are summarized in Table 21. "Measured" ionic strength was not estimated at a concentration factor of 956 because pH was not measured at this concentration factor. Ionic strength can be highly sensitive to pH.

It should be noted that the concentration factors reported in LL991008104241.042 are overestimated. Cl and NO₃ should have concentrated conservatively in this experiment. These components should not have precipitated at the concentration factors reported because the concentration factors were not nearly high enough for them to become saturated with respect to any minerals. In fact, no Cl and NO₃ minerals were identified by x-ray diffraction at these concentration factors. The overestimates in the reported concentration factors are substantiated by the measured concentrations of SO₄ and K, which also should not precipitate in this concentration factor range, as predicted in Figure 15. If the concentration of NO₃ or Cl had been used to determine the concentration factor in the experiment (instead of indirectly estimating the concentration factor from measurements of amounts of water evaporated), then the measured concentration factors would have been approximately 16% to 33% percent lower and the simulated evaporations would have been stopped much earlier. This would have considerably lowered the predicted concentrations and reduced the differences between predictions and measurements of Cl, NO₃, SO₄, and K. Thus, the majority of the differences observed in Figure 16 between the predicted and measured values for these components is due to errors in the estimation of the reported concentration factors. These errors also explain the considerable overestimate of ionic strength in the concentrated sample in Table 21.

Table 21. Calculation of "Measured" Ionic Strength in Average J-13 Well Water Evaporation Experiment

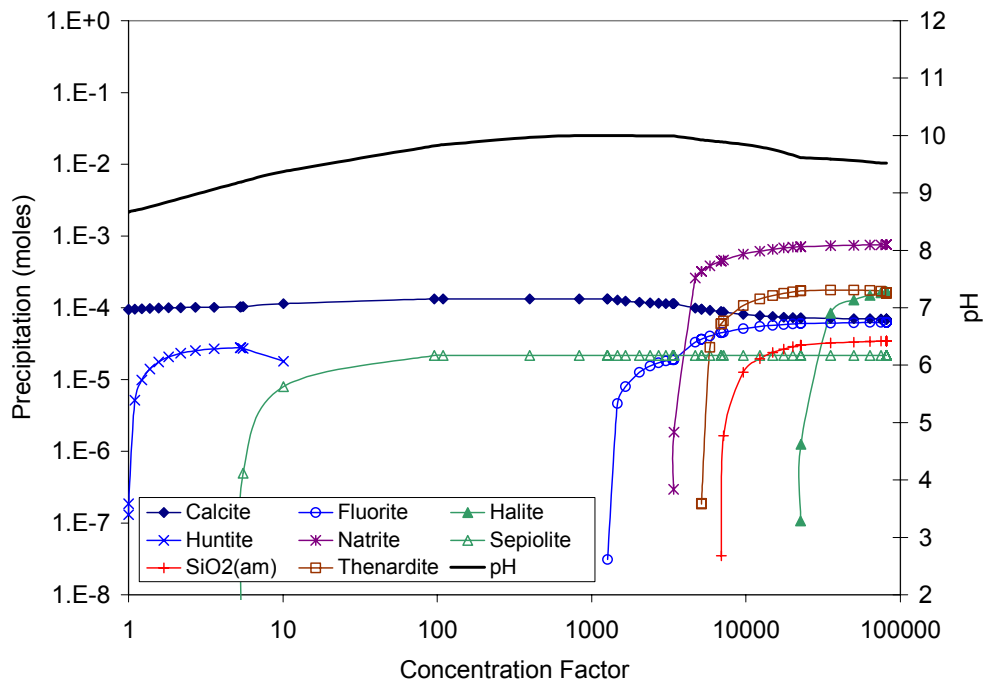
Concentration Factor	EQ3NR Input/Output Filenames	"Measured" Ionic Strength (molal)	Predicted Ionic Strength (molal)
1	j13n1is.3i, j13n1is.3o	2.97E-03	2.84E-03
157	j13n157i.3i, j13n157i.3o	3.27E-01	4.79E-01

DTN: MO0307MWDUNEVP.000, File: "Experimental Uncert.xls"



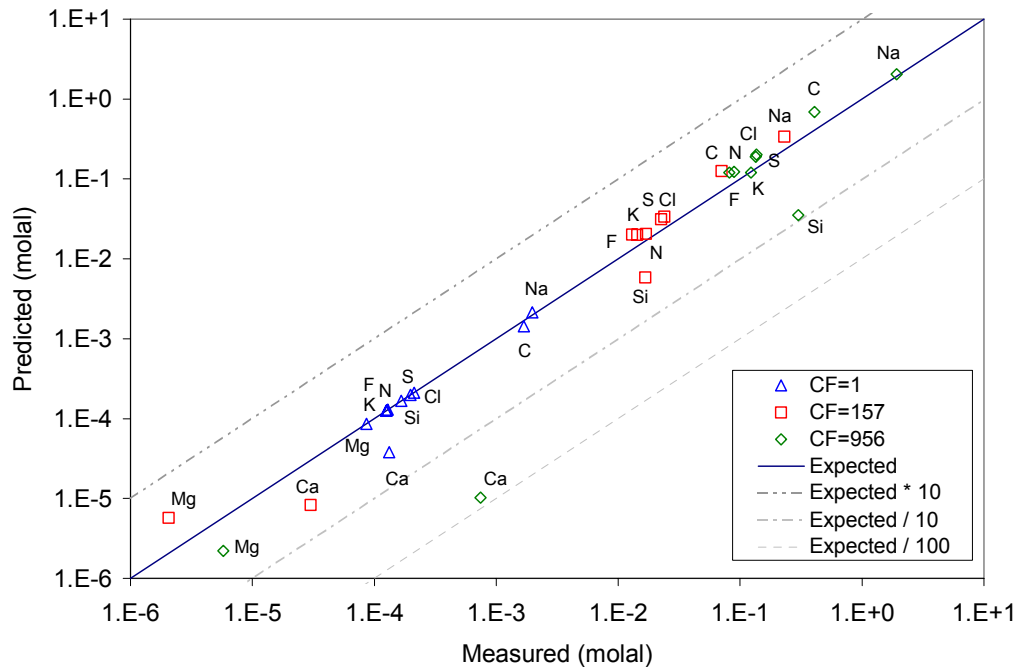
DTN: MO0303MWDJ13RB.000

Figure 14. Predicted Aqueous Evolution of Synthetic J-13 Water for Evaporation Experiments of Rosenberg et al. (1999 [125338])



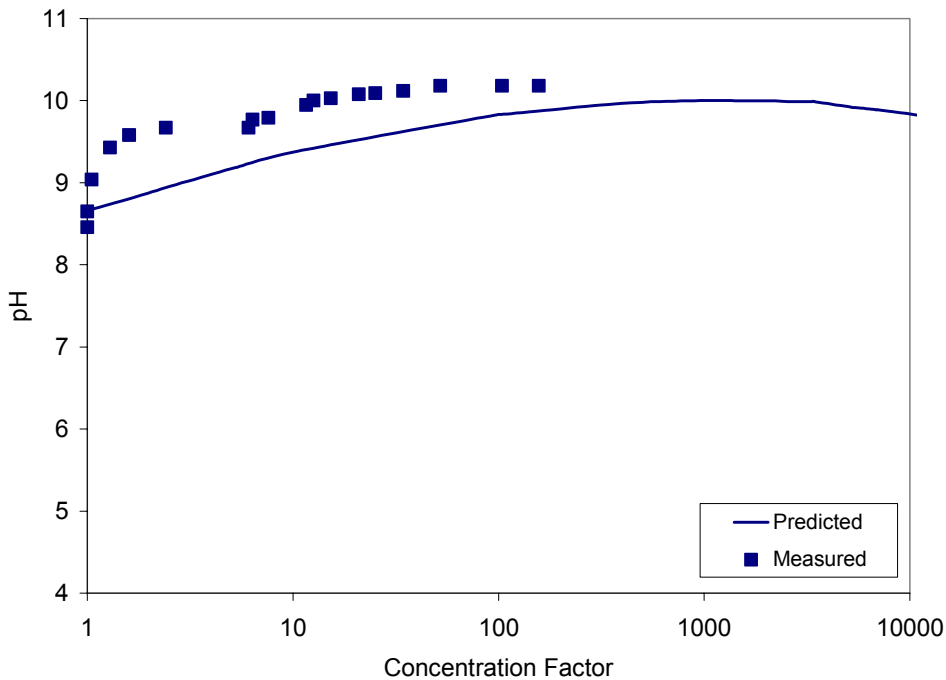
DTN: MO0303MWDJ13RB.000

Figure 15. Predicted Mineral Evolution of Synthetic J-13 Water for Evaporation Experiments of Rosenberg et al. (1999 [125338])



DTN: MO0303MWDJ13RB.000

Figure 16. Predicted vs. Measured Concentrations for Synthetic J-13 Water Evaporation Experiments of Rosenberg et al. (1999 [125338])



DTN: MO0303MWDJ13RB.000

Figure 17. Predicted vs. Measured pH Values for Synthetic J-13 Water Evaporation Experiments of Rosenberg et al. (1999 [125338])

7.1.2 Evaporation of 100x Average J-13 Well Water at 90°C and 85 Percent Relative Humidity

In another synthetic J-13 well water evaporation experiment, a synthetic 100-times concentrated (100x) average J-13 well water was dripped through a column of heated tuff into a Teflon beaker (CRWMS M&O 2000 [146460] p. 6-16). In this experiment (called Batch 1), the beaker was open to the atmosphere and maintained at a constant temperature of 90°C and relative humidity of 85 percent. The solution was then allowed to evaporate to a volume of approximately five percent of the original volume, based on the concentration factors reported (The actual volume or mass decrease in the solution was not reported.). The starting and final solution compositions are displayed in Table 9. The recipe for the synthetic 100x J-13 well water did not include Si, Al, or Fe, likely because these components have limited solubility or are minor constituents (Al and Fe). A 100x concentration of these components cannot be prepared without making adjustments, such as raising the pH to an unrealistic value. A true 100x J-13 water can only be realistically derived by evaporating unconcentrated J-13 in a container open to a fixed fugacity of carbon dioxide and allowing supersaturated minerals to precipitate from solution during the process (as was done in Rosenberg et al. (1999 [125338])).

The results of these evaporation experiments were modeled using the IDPS model and the Pitzer database. Predictions of total aqueous concentrations, pH, ionic strength, and mineral precipitation upon evaporation are documented in DTN: MO0303MWDJ13GD.000 and plotted in Figure 18 and Figure 19. Measurements and predictions are compared in Figure 20. No pH measurements were reported. In this simulation, the sepiolite log K was not augmented as was done when modeling the evaporation experiment in Section 7.1.1 because sepiolite did not precipitate. If the evaporating water never becomes saturated with respect to the crystalline form, it will never become saturated with respect to the amorphous form.

Figure 20 shows that the predictions closely approximate the Na, F, Cl, K, NO₃, HCO₃, and SO₄ concentrations when compared to the laboratory measurements. To compare the results to the data, the reported nitrate concentration factor of 20.7 is used to represent the concentration factor of the solution. However, because the original concentration factor of the synthesized 100x J-13 water is defined as 100, the final concentration factor is represented here as 2070 (100 x 20.7). As shown in the figures, the agreement between the Na, F, Cl, K, HCO₃, and SO₄ measurements and predictions indicate that the concentration factor of the solution is well represented by the nitrate concentration factor.

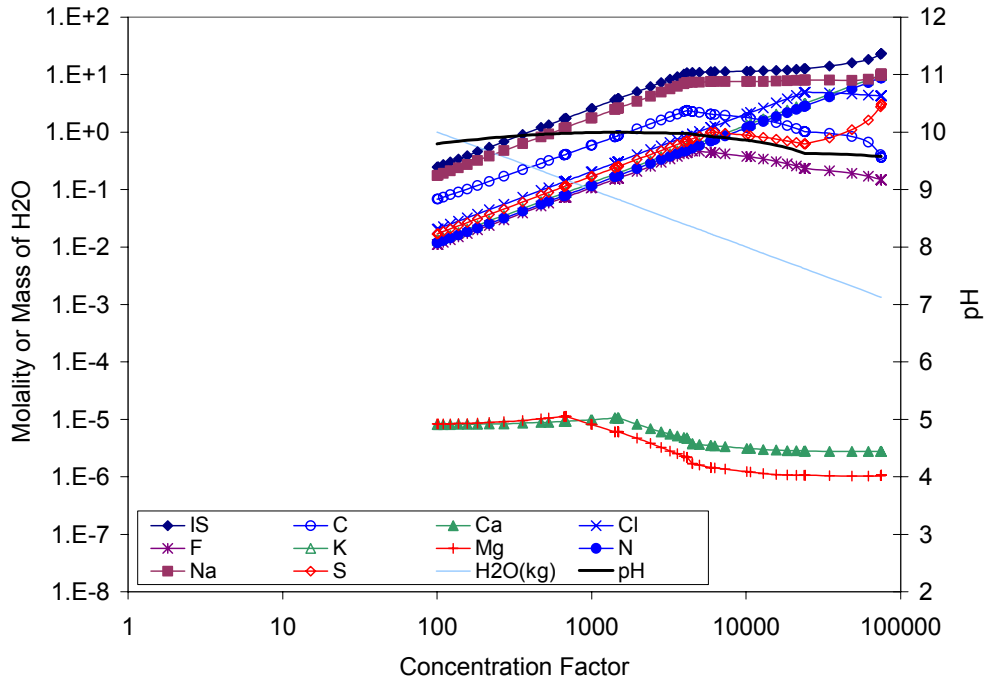
The model underestimates Ca and Mg by about 1 to 2 orders of magnitude when compared to the laboratory measurements. Two of several possible explanations for these underestimates are errors or uncertainties in the Pitzer database and/or analytical measurements. The concentration factor of 100 represents the starting water prior to the water flowing through the column of crushed tuff. According to the EQ3/6 calculations, this starting water is supersaturated with respect to calcite and huntite. No pH measurements were reported, so pH was predicted by EQ3/6 based on heterogeneous equilibrium with respect to an atmospheric carbon dioxide fugacity of 10^{-3.4} bars. Thus, other potential explanations for the underestimates of Ca and Mg are that predictions of pH might be higher than actual, the actual carbon dioxide fugacity might be considerably lower than atmospheric, and/or the precipitation of calcite and huntite is not rapid enough to achieve equilibrium in the laboratory experiment. At a concentration factor of

around 2070, the model predicts additional precipitation of Ca and Mg minerals fluorite and sellaite, as shown in Figure 19. Precipitation of these minerals could also be kinetically limited in the experiment. Laboratory analysis of the precipitates was not performed.

In a solution that is boiling or evaporating from a beaker, it is possible that the atmospheric partial pressure of carbon dioxide is below atmospheric values because of an increased partial pressure of water vapor and a net flux of vapor flowing out of the beaker. If this was the case, the actual carbon dioxide fugacity would have been lower and the pH predictions would have been higher.

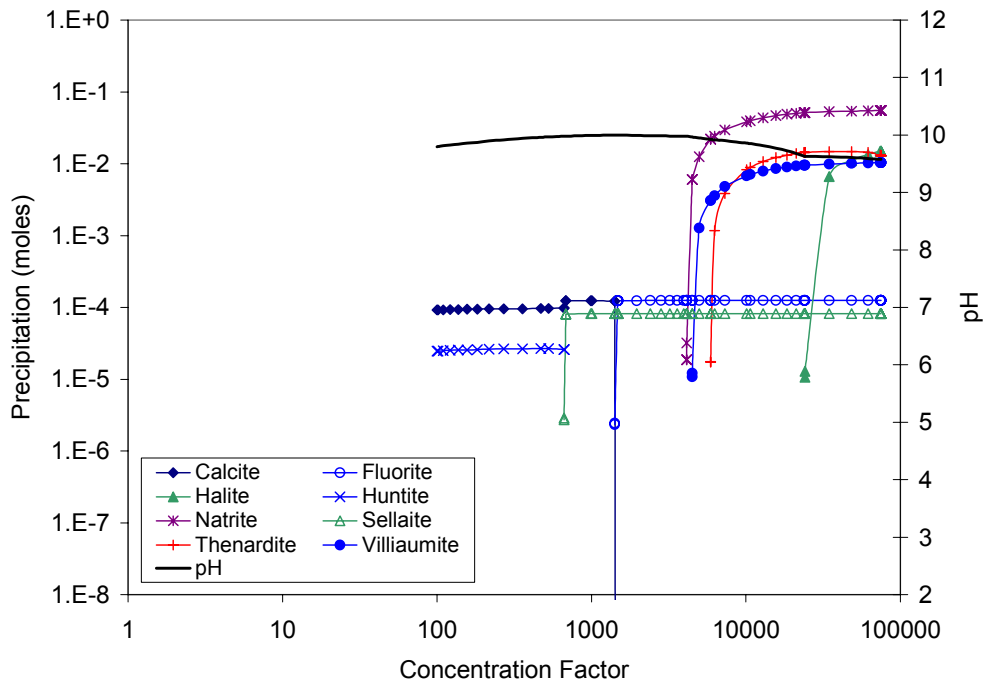
Calcite can be supersaturated by as much as a factor of two when calcium and carbonate concentrations are slowly increased in laboratory experiments (Krauskopf and Bird 1995 [101702] p. 72). This phenomenon may partly explain why measured Ca concentrations in this evaporation experiment (and the one in the previous section) are larger than the predicted values. Because the model assumes equilibrium for calcite due to the long periods of time that the model is designed to simulate for TSPA-LA, it is understandable that the model might under predict the Ca concentration in a short-term laboratory evaporation experiment. Regardless, the model cannot be invalidated for its intended use simply because the prediction of Ca in a short-term experiment falls slightly outside the validation objectives approximated in Table 19. If calcite were allowed to be supersaturated in the simulation due to the slow kinetics of calcite precipitation and the short-term experiment, Ca predictions would have fallen within the approximated validation objectives. Alternatively, if the evaporation experiment had been conducted over a longer period of time, on the scale of the time periods that the IDPS model is designed to simulate for TSPA-LA, calcite precipitation would have had time to progress towards equilibrium, resulting in a Ca concentration closer to the value predicted by the IDPS model.

Ionic strength was not directly measured in these experiments and cannot be accurately estimated without pH measurements. Thus, "measured" ionic strength was not estimated for this experiment using EQ3NR, as was done for the data in Sections 7.1.1 and 7.1.3.



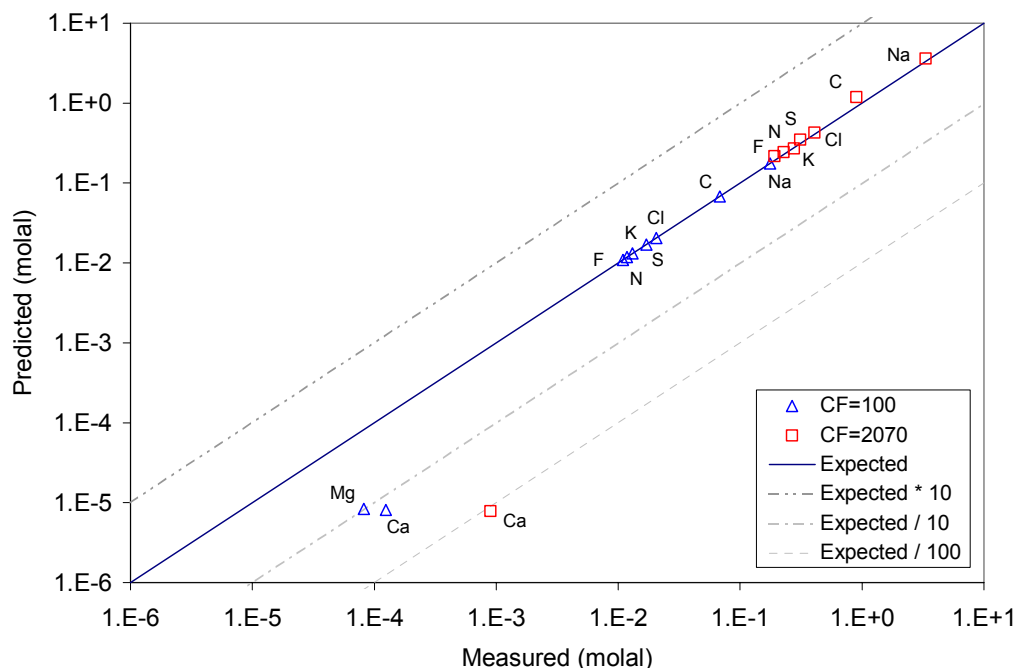
DTN: MO0303MWDJ13GD.000

Figure 18. Predicted Aqueous Evolution of 100x Synthetic J-13 Water for Evaporation Experiments of CRWMS M&O (2000 [146460])



DTN: MO0303MWDJ13GD.000

Figure 19. Predicted Mineral Evolution of 100x Synthetic J-13 Water for Evaporation Experiments of CRWMS M&O (2000 [146460])



DTN: MO0303MWDJ13GD.000

Figure 20. Predicted vs. Measured Concentrations for 100x Synthetic J-13 Water Evaporation Experiments of CRWMS M&O (2000 [146460])

7.1.3 Evaporation of Topopah Spring Tuff Pore Water at 75°C

Synthetic Topopah Spring tuff pore water was evaporated in an experiment reported in Rosenberg et al. (1999 [125339]). The experiment, named *evap3*, was performed following the same procedures as in Rosenberg et al. (1999 [125338]) presented in Section 7.1.1, except that the temperature was maintained at 75°C. Both the starting and final solutions are provided in Table 10. The final solution was reported to have an approximate concentration factor of 1243 ± 10 percent. An x-ray diffraction analysis at this concentration factor detected gypsum. After complete evaporation, tachyhydrite was also detected.

These evaporation experiments were simulated using the IDPS model and the Pitzer database. Predictions of total aqueous concentrations, pH, ionic strength, and mineral precipitation upon evaporation are documented in DTN: MO0303MWDTSWRB.000 and plotted in Figure 21 and Figure 22. These predictions are compared to the measurements in Figure 23 and Figure 24. As in the evaporation experiment in Section 7.1.1, the sepiolite log K was augmented by 6 log K units to represent an amorphous sepiolite (see Section 7.1.1).

Figure 23 shows that the modeled results closely approximate the measured Na, Mg, Ca, Cl, and K concentrations. At a concentration factor of 1243, modeled results underestimate the measured SO_4 and Si concentrations by approximately 0.5 and 2 orders of magnitude, respectively. Final NO_3 , HCO_3 , and F laboratory data are not reported (Rosenberg et al. 1999 [125339]).

Figure 24 shows close agreement between the laboratory measured pH and predicted pH. Unlike the observations in the J-13 evaporation experiments, the pH decreased with increasing evaporation, resulting in a value around 6.3 by the end of the experiment. The predicted pH is largely controlled by the fugacity of carbon dioxide, which is fixed at $10^{-3.4}$ bars to approximate the laboratory condition of a beaker open to the atmosphere.

Gypsum was identified by x-ray diffraction in the laboratory experiment at the 1243 concentration factor. In contrast, the model predicted calcite, sepiolite, and anhydrite precipitation at *CF* 1243. Anhydrite (CaSO_4) is predicted to be more stable than gypsum ($\text{CaSO}_4 \cdot 2\text{H}_2\text{O}$) at the 75°C temperature of the experiment. However, the short term of the experiment may have prevented a perceivable accumulation of anhydrite. Other potential explanations for the difference are potential inaccuracies in experimental measurements or the Pitzer database. Regardless of the difference, however, either mineral provides a good explanation why the aqueous Ca and SO_4 concentrations at *CF* 1243 are not nearly 1243 times their initial concentrations (Table 10).

Mass balance suggests that gypsum could not be the only mineral precipitating at *CF* 1243. As indicated in Table 10, the Si concentration did not nearly increase by a *CF* of 1243, nor did HCO_3 . Thus, some Si and C likely precipitated, which is consistent with the calcite and sepiolite precipitation that the IDPS model independently predicted based on aqueous solubilities.

Upon complete evaporation, the only other mineral identified to precipitate was tachyhydrite. The relative amounts of gypsum and tachyhydrite in the final mineral assemblage were not measured. The minerals predicted by the IDPS model to precipitate upon complete evaporation are displayed in Figure 22. No precipitation was identified in the experiment that contained Na, K, CO_3 , F, Si, or NO_3 . Mass balance indicates that these components should be there. Without quantitative and nearly complete information on the composition of precipitation in an experiment, experimental measurements and model predictions of mineral assemblages cannot be easily corroborated.

Ionic strength was not directly measured in these experiments. However, a "measured" ionic strength was estimated from the reported evaporated water compositions using EQ3NR, as described in Section 7.1.1. These calculations are documented in DTN: MO0307MWDUNEVP.000 and are summarized in Table 22.

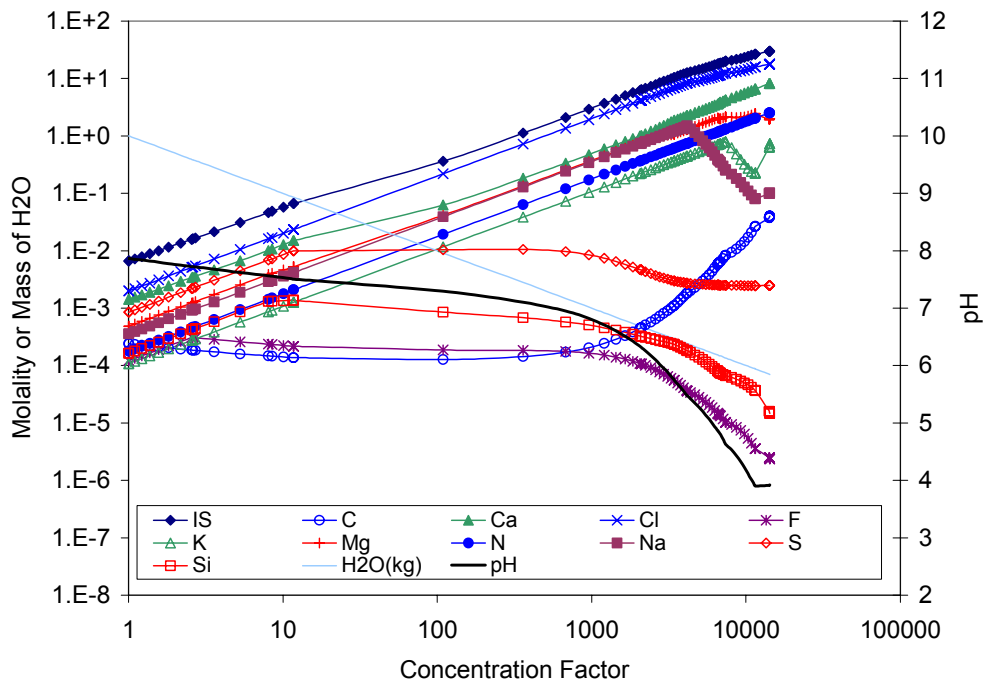
As in the average J-13 well water evaporation experiment simulated in Section 7.1.1, the reported concentration factor in the Topopah Spring tuff pore water evaporation experiment (Table 10) was overestimated. Cl and NO_3 should have concentrated conservatively. No Cl and NO_3 minerals were identified by x-ray diffraction at the reported 1243 concentration factor. The overestimate is substantiated by the measured concentrations of Na, K, Ca, and Mg, which also should have concentrated conservatively (or nearly conservatively in the case of Ca), as predicted in Figure 21. The NO_3 concentration was not measured in the evaporatively concentrated sample because the sample was mistakenly preserved with nitric acid. However, if the Cl concentration had been used to determine the concentration factor in the experiment (instead of indirectly estimating the concentration factor from measurements of amounts of water evaporated), then the measured concentration factor would have been around 680, not 1243. If this lower concentration factor had been reported, then the simulation would have been stopped

at *CF* 680 and the differences between predictions and measurements of Cl, Ca, Mg, Na, and K (Figure 23) would have been much lower. Thus, the majority of the differences observed between the predicted and measured values for these components is an artifact of errors in the estimation of the reported concentration factor. These errors also explain the considerable overestimate of ionic strength in the concentrated sample in Table 22.

Table 22. Calculation of "Measured" Ionic Strength in Topopah Spring Tuff Pore Water Evaporation Experiment

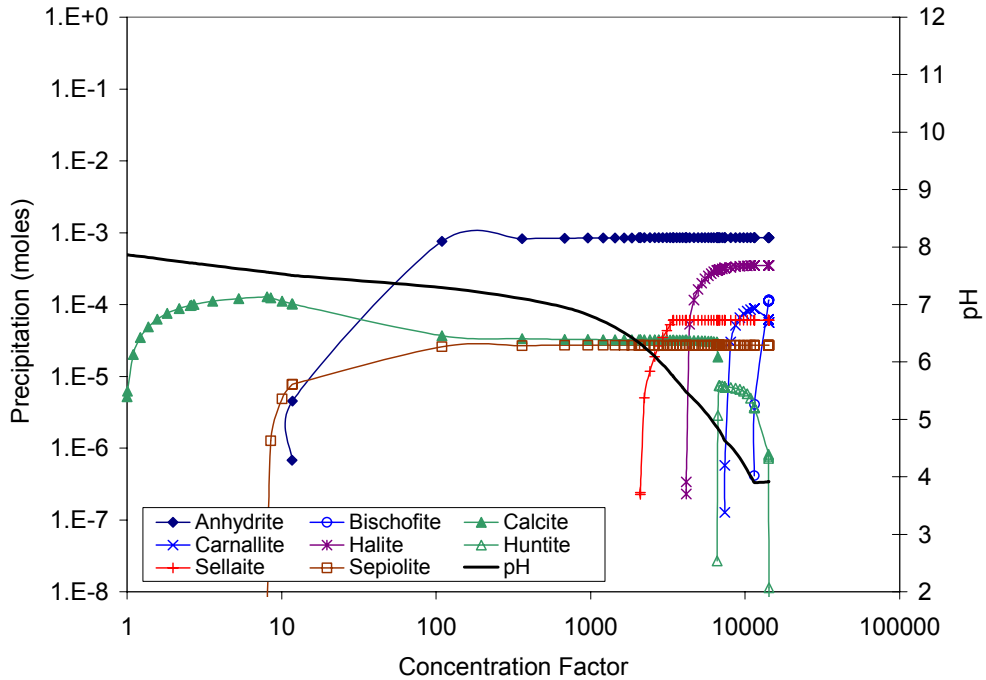
Concentration Factor	EQ3NR Input/Output Filenames	"Measured" Ionic Strength (molal)	Predicted Ionic Strength (molal)
1	tspw3is.3i, tspw3is.3o	6.73E-03	6.60E-03
1243	tsp1243i.3i, tsp1243i.3o	2.27E+00	3.79E+00

DTN: MO0307MWDUNEVP.000, File: "Experimental Uncert.xls"



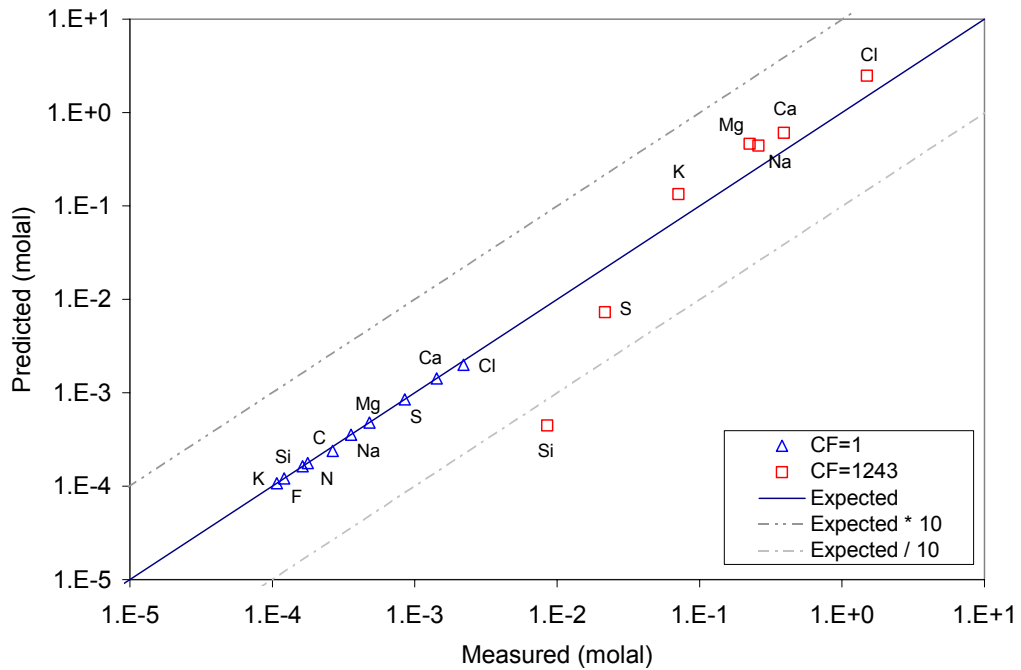
DTN: MO0303MWDTSWRB.000

Figure 21. Predicted Aqueous Evolution of Synthetic Topopah Spring Tuff Pore Water for Evaporation Experiments of Rosenberg et al. (1999 [125339])



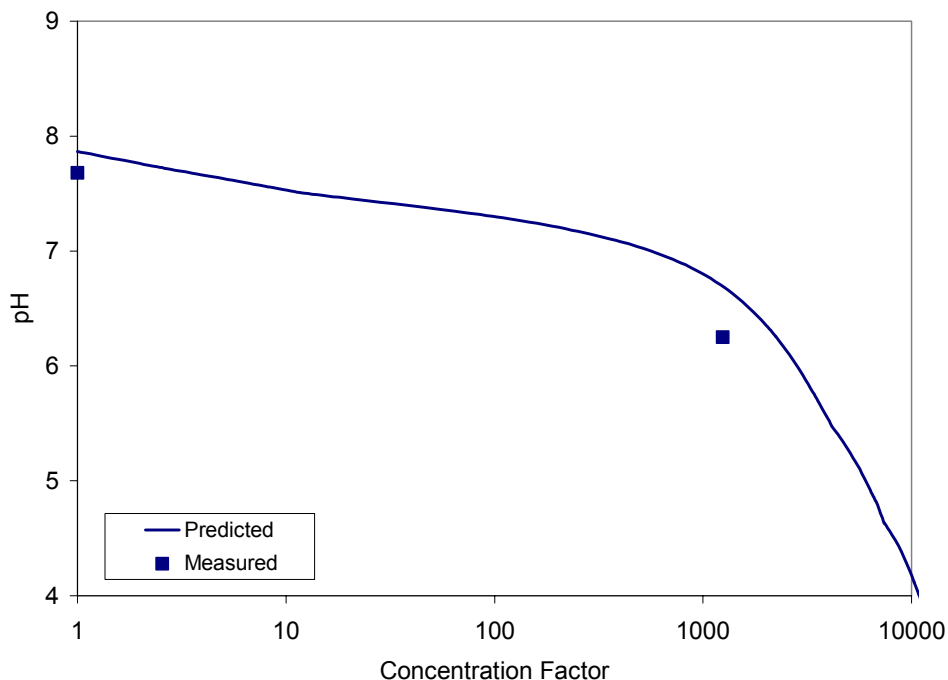
DTN: MO0303MWDTSWRB.000

Figure 22. Predicted Mineral Evolution of Synthetic Topopah Spring Tuff Pore Water for Evaporation Experiments of Rosenberg et al. (1999 [125339])



DTN: MO0303MWDTSWRB.000

Figure 23. Predicted vs. Measured Concentrations for Synthetic Topopah Spring Tuff Pore Water from Evaporation Experiments of Rosenberg et al. (1999 [125339])



DTN: MO0303MWDTSWRB.000

Figure 24. Predicted vs. Measured pH Values for Synthetic Topopah Spring Tuff Pore Water from Evaporation Experiments of Rosenberg et al. (1999 [125339])

7.1.4 Seawater Evaporation

The Morton Bahamas solar salt production facility on Great Inagua Island in the Bahamas provides an excellent example of the evaporative chemical evolution of a natural multicomponent water. At this plant, seawater is evaporatively concentrated in a sequence of reservoirs to precipitate table salt (halite). This production process results in a final brine with a concentration factor near 40 with respect to seawater. One of the primary advantages of this data set compared to samples taken from saline lakes is that these reservoirs are not subject to large mixing effects from streams and rivers. In addition, the reservoirs are shallow and open to the atmosphere, facilitating equilibrium conditions with respect to atmospheric partial pressures of carbon dioxide and oxygen. Thus, the major processes affecting the evolution of seawater at the plant are the same processes incorporated in the IDPS model.

McCaffrey et al. (1987 [164481]) sampled and analyzed the chemical compositions of the evolving seawater at the plant. Three of the most concentrated samples were evaporated even further in the laboratory. The data for both the reservoir samples and the laboratory evaporation experiments are presented in Table 11. The samples in the table that start with a "w" were collected directly from the plant reservoirs while the remainder were artificially evaporated from samples w36, w39, and w40. The reported degree of evaporation is equivalent to the concentration factors of conservative components. For degrees of evaporation up to 70, the concentration factor for Mg was used to determine degree of evaporation. Beyond 70, the concentration factor of lithium was used.

The IDPS model was used to simulate the seawater evaporation at the plant. The results are documented in DTN: MO0307MWDSEAEV.000. Sea intake water (sample w63) was used as the starting water. This sample, collected at the plant intake, had a degree of evaporation slightly less than seawater, perhaps because it was composed of seawater mixed with a small amount of fresh water from a nearby stream. In the simulation, the temperature was fixed at 31.25°C, the average value of the reservoir samples. To balance the charge, the model decreased the Cl concentration by about 1.5 percent. The partial pressures of carbon dioxide and oxygen were set approximately at atmospheric values, $10^{-3.5}$ and $10^{-0.7}$ bars, respectively. Because carbonate was not measured, the concentration of dissolved carbonate was set at heterogeneous equilibrium with the partial pressure of carbon dioxide. Finally, the minerals listed in Table 17 were suppressed.

It is important to note that the laboratory evaporation experiments were closed to the atmosphere. These experiments resulted in the samples in Table 11 that have degrees of evaporation greater than 40. These samples were derived by placing samples of w36, w39, and w40 in uncovered teflon vials and sealing them in desiccation chambers containing CaCl_2 crystals, a desiccant (McCaffrey et al. 1987 [164481] p. 931). Sealing the desiccation chambers does not allow for exchange of oxygen and carbon dioxide with the atmosphere. This could have caused partial pressure deviations from atmospheric values. Changes in carbon dioxide partial pressure affects pH, which in turn has the potential to affect which minerals precipitate. No pH values were measured for these samples. Thus, the composition of these concentrated samples could represent the effects of processes not considered by the IDPS model and not expected to occur in the evaporation of seawater in an open system. Therefore, differences between IDPS model predictions and measurements at these high concentrations do not necessarily reflect poorly on the accuracy of the IDPS model. To be conservative, however, these differences are nevertheless attributed to model uncertainty.

The IDPS model predictions are compared to sample measurements in Figure 25, Figure 26, and Figure 27. These figures show that the IDPS model predictions are highly accurate. Comparison of the predicted mineral precipitation in Figure 28 to the dissolved concentrations confirms that halite precipitation begins to control the concentrations of Na and Cl at a degree of evaporation around 10. Degree of evaporation relative to seawater was calculated from the IDPS model output by multiplying the IDPS concentration factor (CF) by 0.95, the degree of evaporation of the sea intake water used as the starting water for the evaporation. The CF calculated by the IDPS model reflects the degree of evaporation relative to the intake water.

Like halite, other minerals that control the evaporative concentration of the dissolved components are revealed by the trajectories of their concentrations in the figures. For example, McCaffrey et al. (1987 [164481] p. 935) found that gypsum ($\text{CaSO}_4 \cdot 2\text{H}_2\text{O}$) begins to precipitate at a degree of evaporation around 3.8. This explains the decrease in Ca concentrations at this degree of evaporation. The IDPS model predicts that gypsum starts precipitating at a degree of evaporation of around 7 and is immediately replaced by anhydrite (CaSO_4). From that point until the degree of evaporation reaches about 10, anhydrite is the predicted controlling phase for Ca. Above a degree of evaporation of 10 but below about 57, glauberite ($\text{Na}_2\text{Ca}(\text{SO}_4)_2$) replaces anhydrite as the controlling phase for Ca in the simulation. The differences between the minerals predicted to precipitate and those observed to precipitate may be due to several factors, such as errors in the equilibrium constants of the minerals, nonequilibrium conditions (e.g.,

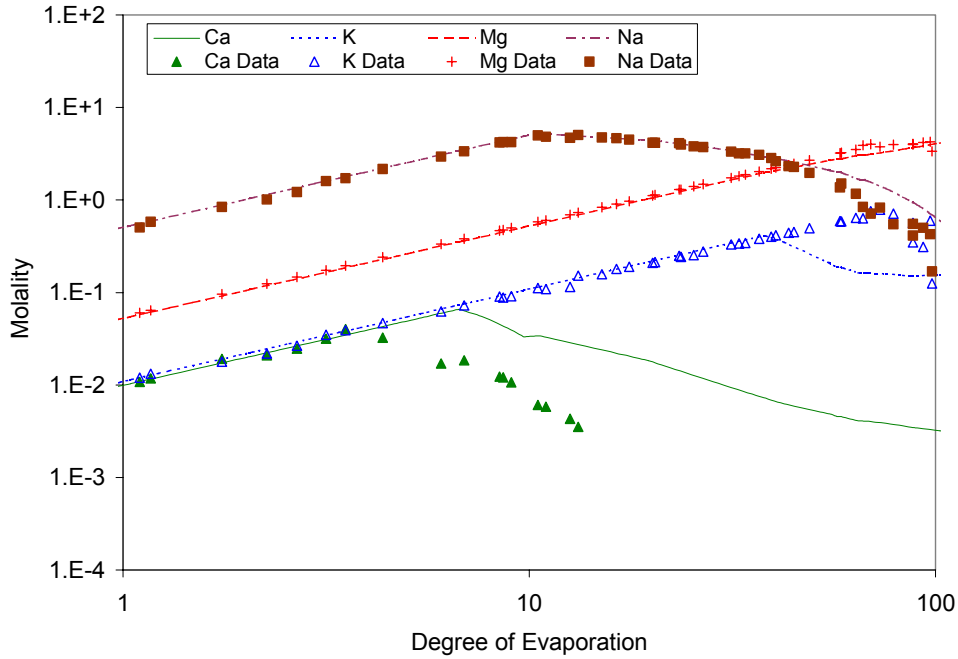
mineral super saturation), errors in boundary conditions (e.g., the partial pressure of carbon dioxide), and sampling error. The end result, however, is that above a degree of evaporation of 3.8 the model overestimates Ca concentrations by as much as a factor of six.

Figure 25 shows that measured K concentrations begin to decrease sharply after concentrations reach approximately 80 times that of seawater. McCaffrey et al. (1987 [164481] p. 935) did not determine the K-bearing phases precipitating at this degree of evaporation. In the IDPS model simulation, precipitation of polyhalite ($K_2MgCa_2(SO_4)_4 \cdot 2H_2O$) begins to control K concentrations starting around concentrations 45 times that of seawater. This difference results in a maximum overestimation of K by a factor of about five at a degree of evaporation around 73.

Model predictions of Na, Mg, Cl, Br, and SO_4 compare well with sample concentrations for the entire range of measurements. Ignoring the most concentrated sample, which appears to be an outlier, the largest overestimate is a factor of about 2.3 for Na at a degree of evaporation of 87.9. The largest underestimate is a factor of about 2.2 for SO_4 at a degree of evaporation of 69.2. The marked decrease in SO_4 measurements above this degree of evaporation is due to the precipitation of one or more magnesium sulfates (McCaffrey et al. 1987 [164481] p. 935). The largest differences between predictions and measurements for Mg, Cl, and Br are approximately -23%, 12%, and 12%, respectively, relative to the measurements. The 12% estimate for Cl does not consider the most concentrated sample because it appears to be an outlier based on Figure 27.

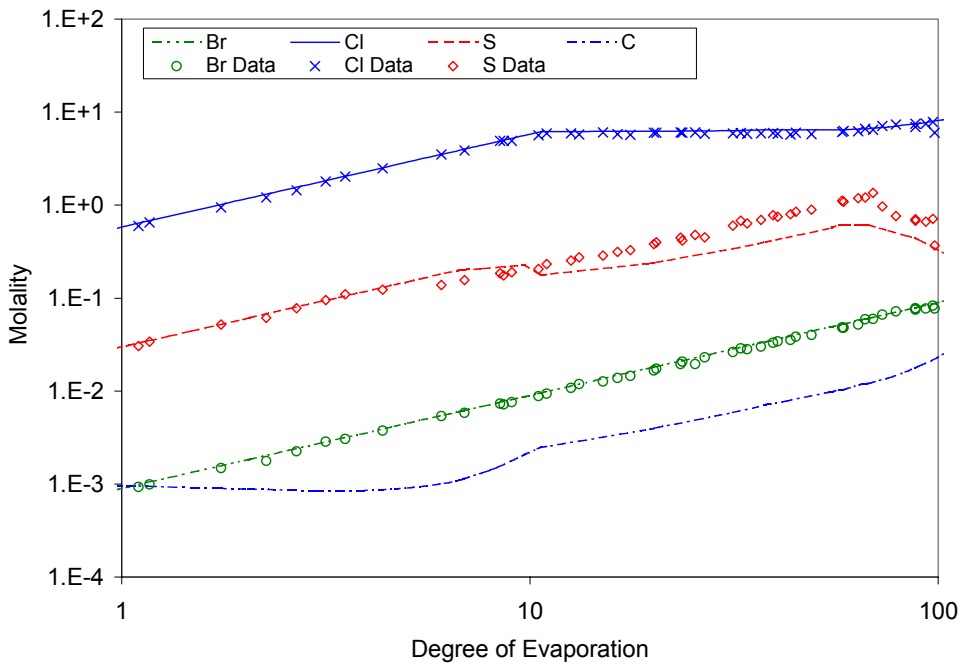
Figure 27 shows good agreement between measurements and predictions for pH and ionic strength. The largest difference observed for pH is approximately 0.76 pH units. For ionic strength, the largest difference is approximately 15 percent, except for the sample at the highest degree of evaporation, which is suspect because it is an outlier. The predicted activity of water is also plotted in this figure to show how it changes as a function of the degree of evaporation.

An additional simulation was performed in which huntite ($CaMg_3(CO_3)_4$) was added to the list of suppressed minerals. In the simulation, documented in DTN: MO0307MWDSEAEV.000, calcite precipitates instead of huntite. This difference has a negligible effect on aqueous Ca and Mg concentrations but a considerable effect on predicted values for aqueous CO_3 and pH. The predicted aqueous CO_3 concentration increases by a factor of around 1.5 to 3 while the pH predictions increase by about 0.2 pH units. Though the pH predictions continue to underestimate pH, the largest underestimate of pH in this sensitivity run is 0.56, which is 0.20 pH units less than the largest underestimate when huntite is allowed to precipitate. These results suggest that suppression of huntite in the IDPS model would slightly improve evaporation predictions for seawater and perhaps other natural waters under similar environmental conditions.



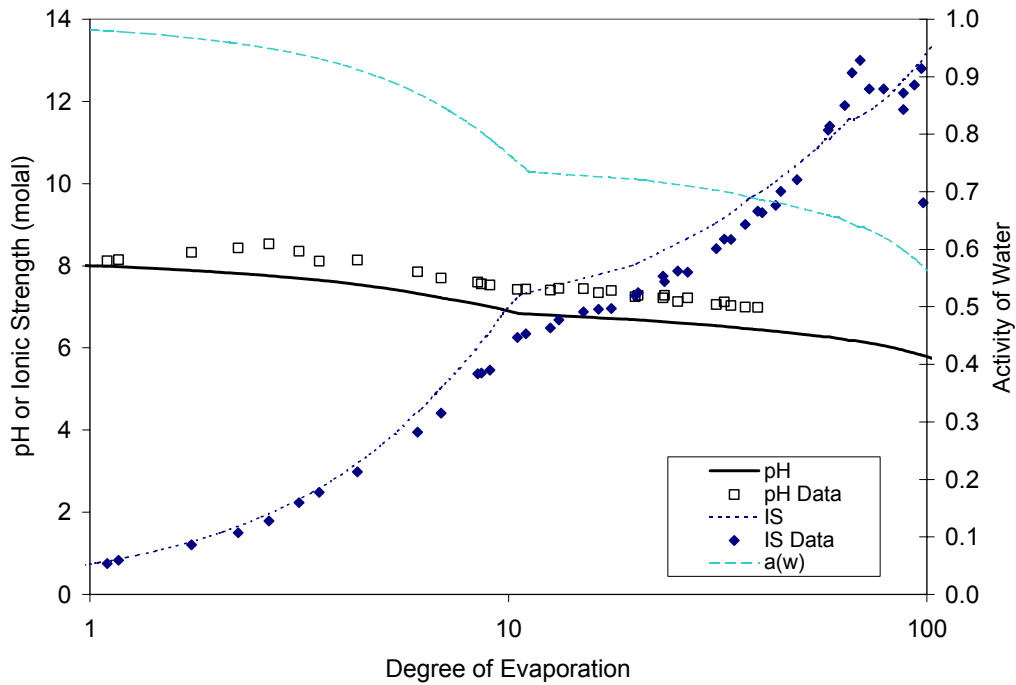
(McCaffrey et al. 1987 [164481])
DTN: MO0307MWDSEAEV.000

Figure 25. Predicted vs. Measured Ca, K, Mg, and Na Concentrations from Evaporation of Inagua Seawater



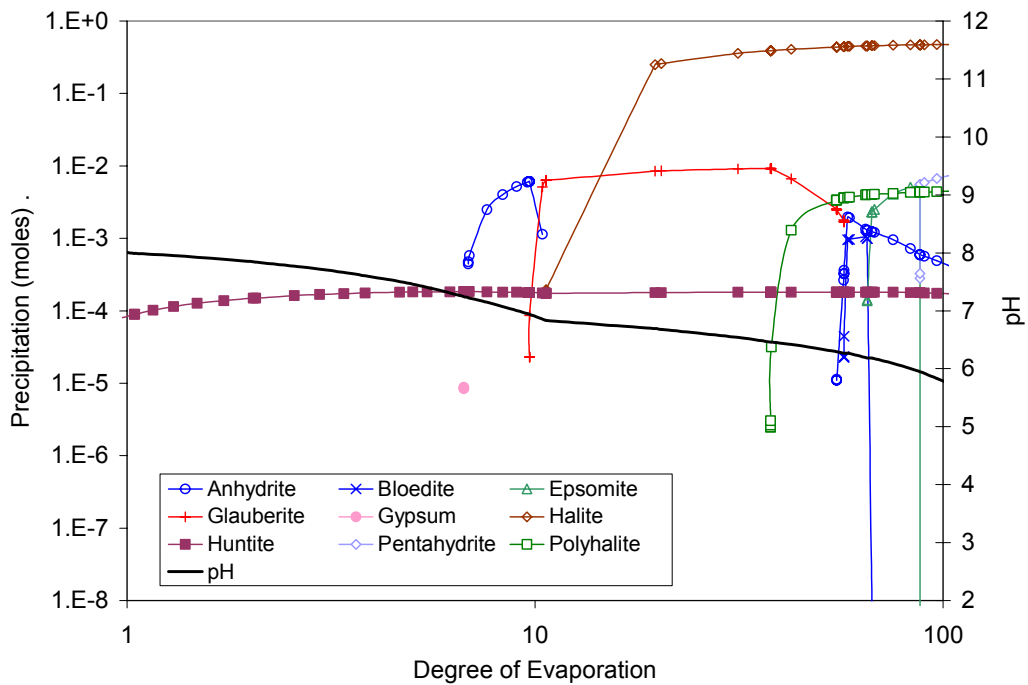
(McCaffrey et al. 1987 [164481])
DTN: MO0307MWDSEAEV.000

Figure 26. Predicted vs. Measured Br, Cl, and SO₄ Concentrations from Evaporation of Inagua Seawater



(McCaffrey et al. 1987 [164481])
DTN: MO0307MWDSEAEV.000

Figure 27. Predicted vs. Measured pH and Ionic Strength from Evaporation of Inagua Seawater



DTN: MO0307MWDSEAEV.000

Figure 28. Predicted Mineral Precipitation from Evaporation of Inagua Seawater

7.2 EVAPORATION OF DILUTE SALT SOLUTIONS

Dilute salt solutions were evaporated to assess whether the IDPS model can accurately predict the aqueous solubilities and deliquescence points of simple salts. Solubilities are predicted and compared to handbook values in Section 7.2.1, and deliquescence points are predicted and compared to handbook values in Section 7.2.2.

7.2.1 Aqueous Solubilities of Simple Salts

To demonstrate model validation for predicting aqueous solubilities of simple salts, the IDPS model and Pitzer database were used to evaporate dilute solutions (0.0001 molal) of simple Na, K, Ca, and Mg salts to mineral saturation at two different temperatures (typically 25°C and 100°C). The final aqueous compositions were then compared to salt solubilities reported in *CRC Handbook of Chemistry and Physics* (Lide 2000 [162229] pp. 8-102 to 8-110).

Table 12 lists the solubility of each of the salts studied in mass percent of solute (w_i) as provided in the reference. These solubilities are converted to molal concentrations (C_i) in Table 23 using the following equation:

$$C_i = \frac{1000 \frac{w_i}{100\%}}{MW_i \left(1 - \frac{w_i}{100\%} \right)} \quad (\text{Eq. 7.2-1})$$

where MW_i is the molecular weight (in grams per mole) of salt i (Lide 2000 [162229] p. 8-102).

The evaporations began with a 0.0001 molal solution of the particular salt whose solubility was to be estimated. Because the pH of pure water can be affected by the salt dissolved in it and by the temperature, the starting solution was charge balanced on the hydrogen ion. For evaporations involving carbonate, a closed system was prescribed.

The results of the simulations are documented in DTN: MO0303MWDSEDSS.000 and displayed in Table 24, Figure 29, and Figure 30. The table provides the predicted solubilities, relative error with respect to handbook values, and the specific mineral phase that reached saturation at the given temperature. The comparison shows that for every salt in the table, the IDPS model predicted solubility within a factor of 10 of handbook values. Most predictions are within 20 percent.

Three nitrate salts did not reach saturation in the calculations before their runs became unstable and terminated: $\text{Ca}(\text{NO}_3)_2$ (100°C), $\text{Mg}(\text{NO}_3)_2$ (25°C and 100°C), and KNO_3 (100°C). These highly soluble salts are essentially inconsequential when the IDPS model is invoked for its intended use because concentrated brines of these salts are not expected to occur. For these salts, the errors could only happen at low relative humidity (e.g., below 50 percent) and for those incoming waters whose chemical divides allow extensive concentration of the components of these salts. In the event that one or more of these salts does become concentrated in an application, using the end of the run as the maximum solubility is not expected to introduce unacceptable errors compared to the validation objectives. The absolute limit for the

In-Drift Precipitates/Salts Model

concentration of these salts is an ionic strength of 100 molal, which causes EQ6 to terminate the run. Thus, however the runs terminate, the predicted maximum concentrations of these salt components would remain well within one order of magnitude of the actual salt solubilities, meeting validation objectives. For example, for $\text{Mg}(\text{NO}_3)_2$ at 25°C, the EQ6 evaporation terminates at a Mg concentration of 13.4 molal (Table 24). This concentration is only 2.8 times the measured solubility at this temperature (Table 23).

Table 23. Unit Conversion of Aqueous Solubilities of Na, K, Ca, and Mg Salts

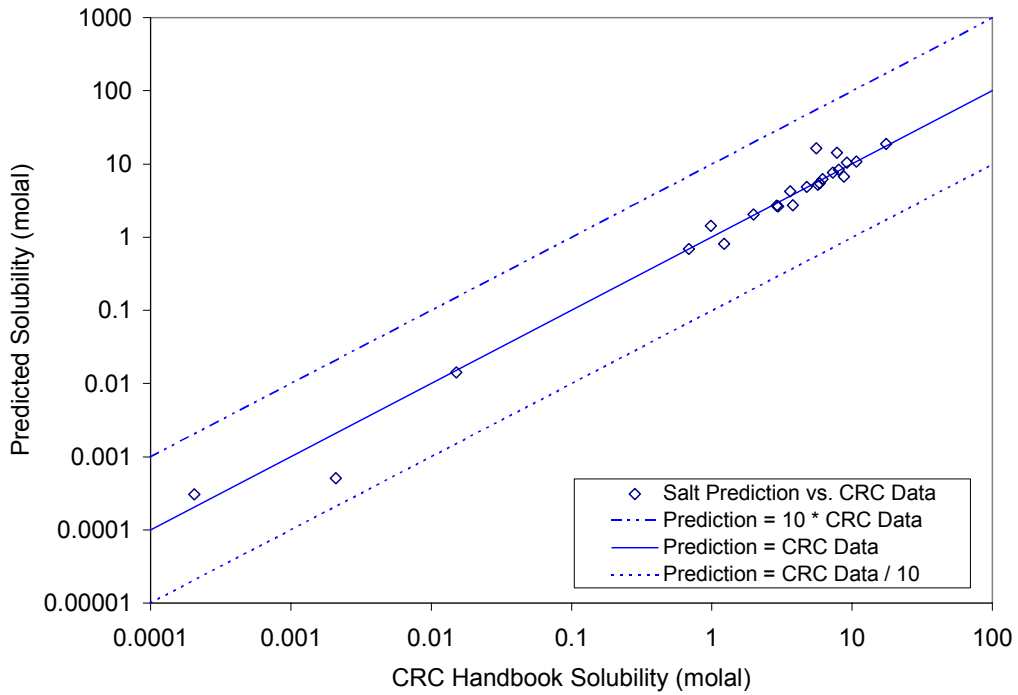
Salt	Molecular Weight (gram/mole)	Aqueous Solubility at 25°C		Aqueous Solubility at 100°C	
		Mass Percent of Solute (%)	(molal)	Mass Percent of Solute (%)	(molal)
NaCl	58.44	26.45%	6.153	28.05%	6.671
KCl	74.55	26.22%	4.767	36.05%	7.562
CaCl ₂	110.98	44.83%	7.322	59.94%	13.482
MgCl ₂	95.21	35.90%	5.882	42.15%	7.653
NaHCO ₃	84.01	9.32%	1.22	19.10%	2.81
KHCO ₃	100.12	26.6%	3.62	40.45% at 70°C	6.78 at 70°C
Na ₂ CO ₃	105.99	23.5%	2.90	30.09%	4.06
K ₂ CO ₃	138.21	52.7%	8.06	61.0%	11.32
NaF	41.99	3.97%	0.985	4.82%	1.206
KF	58.10	50.4%	17.5	60.0% at 80°C	25.8 at 80°C
CaF ₂	78.07	0.0016%	0.00020	not reported above 25°C	not reported above 25°C
MgF ₂	62.30	0.013%	0.0021	not reported above 25°C	not reported above 25°C
Na ₂ SO ₄	142.04	21.94%	1.979	29.67%	2.970
K ₂ SO ₄	174.26	10.7%	0.688	19.3%	1.372
CaSO ₄	136.14	0.205%	0.0151	0.163%	0.0120
MgSO ₄	120.37	26.3%	2.96	33.3%	4.15
NaBr	102.89	48.6%	9.19	54.9%	11.83
KBr	119.00	40.4%	5.70	50.8%	8.68
CaBr ₂	199.89	61.0%	7.82	73.0% at 60°C	13.53 at 60°C
MgBr ₂	184.11	50.6%	5.56	55.7%	6.83
NaNO ₃	84.99	47.7%	10.7	63.8%	20.7
KNO ₃	101.10	27.7%	3.79	70.8%	23.98
Ca(NO ₃) ₂	164.09	59.0%	8.77	78.5%	22.25
Mg(NO ₃) ₂	148.31	41.6%	4.80	72.0%	17.34

Source: (Lide 2000 [162229] pp. 8-102 to 8-110)

Table 24. Model Predictions of Aqueous Solubilities of Na, K, Ca, and Mg Salts

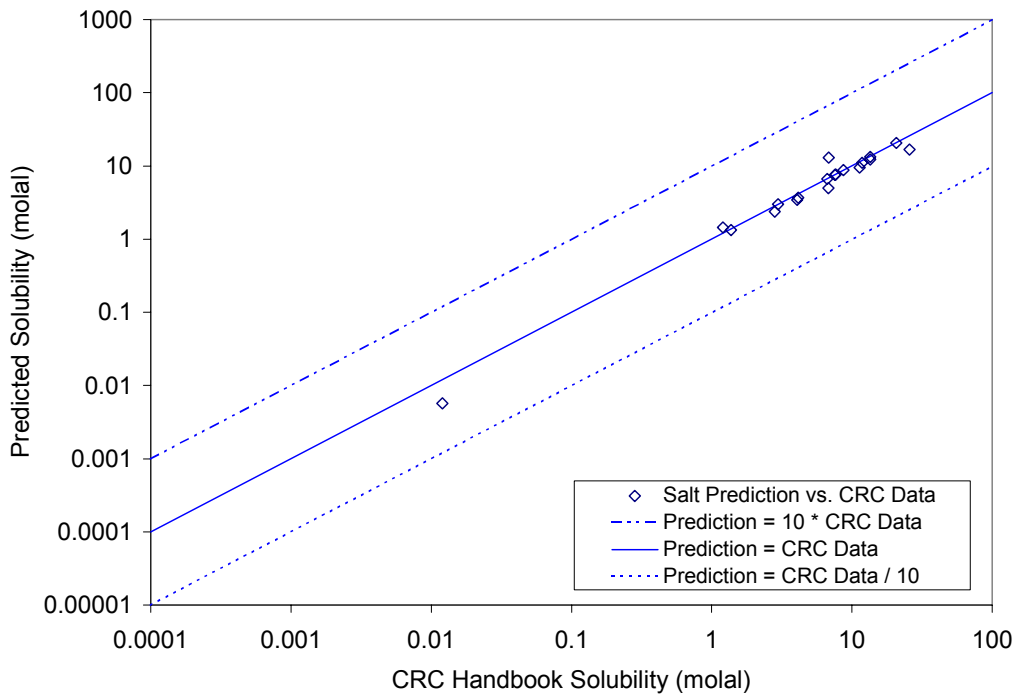
Salt	Aqueous Solubility at 25°C			Aqueous Solubility at 100°C		
	Predicted (molal)	Relative Error (%)	Mineral	Predicted (molal)	Relative Error (%)	Mineral
NaCl	6.170	0.3%	Halite	6.63	-0.6%	Halite
KCl	4.867	2.1%	Sylvite	7.52	-0.6%	Sylvite
CaCl ₂	7.603	3.8%	Antarcticite	13.28	-1.5%	CaCl ₂ ·2H ₂ O
MgCl ₂	5.455	-7.3%	Bischofite	7.62	-0.4%	Bischofite
NaHCO ₃	0.808	-34.0%	Nahcolite	2.38	-15.4%	Nahcolite
KHCO ₃	4.22	16.6%	Kalcanite	4.99 at 70°C	-26.5%	Kalcanite
Na ₂ CO ₃	2.68	-7.6%	Natron	3.43	-15.4%	Natrite
K ₂ CO ₃	8.36	3.7%	K ₂ CO ₃ ·1.5H ₂ O	9.54	-15.7%	K ₂ CO ₃
NaF	1.42	44.5%	Villiamite	1.44	19.2%	Villiamite
KF	18.77	7.3%	Carobbite	16.64 at 80°C	-35.6%	Carobbite
CaF ₂	0.00030	48.6%	Fluorite	0.00033 (100°C)	not applicable (100°C)	Fluorite
MgF ₂	0.00051	-75.6%	Sellaite	0.00028 (100°C)	not applicable (100°C)	Sellaite
Na ₂ SO ₄	2.049	3.5%	Mirabilite	2.98	0.5%	Thenardite
K ₂ SO ₄	0.689	0.3%	Arcanite	1.33	-3.0%	Arcanite
CaSO ₄	0.0141	-6.5%	Gypsum	0.00567	-52.7%	Anhydrite
MgSO ₄	2.65	-10.7%	Epsomite	3.70	-10.9%	Kieserite
NaBr	10.45	13.7%	NaBr	10.99	-7.1%	NaBr
KBr	5.23	-8.1%	KBr	8.77	1.1%	KBr
CaBr ₂	14.16	81.0%	CaBr ₂	12.27 at 60°C	-9.3%	CaBr ₂
MgBr ₂	16.27	192.5%	MgBr ₂	13.02	90.6%	MgBr ₂
NaNO ₃	10.84	1.0%	Soda Niter	20.70	-0.2%	Soda Niter
KNO ₃	2.74	-27.7%	Niter	> 18.6	> -22.4%	none
Ca(NO ₃) ₂	6.69	-23.7%	Ca(NO ₃) ₂ ·4H ₂ O	> 23.6	> 6.1%	none
Mg(NO ₃) ₂	> 13.4	> 179.0%	none	> 13.2	> -23.9%	none

DTN: MO0303MWDSEDSS.000



DTN: MO0303MWDESS.000

Figure 29. Predicted vs. CRC Handbook Mineral Solubilities at 25°C



DTN: MO0303MWDESS.000

Figure 30. Predicted vs. CRC Handbook Mineral Solubilities at 100°C

7.2.2 Deliquescence Relative Humidity Values of Simple Salts

To demonstrate model validation for predicting the deliquescence points (i.e., deliquescence relative humidity, RH_d) of simple salts, the same approach as in Section 7.2.1 was used. The IDPS model and Pitzer database were used to evaporate dilute solutions (0.0001 molal) of simple Na, K, Ca, and Mg salts from Table 13 to mineral saturation at the temperatures listed in the table. The predicted deliquescence relative humidity (RH_d) values were then compared to those reported in Table 13.

The evaporations began with a 0.0001 molal solution of the particular salt whose deliquescence relative humidity was to be estimated. Because the pH of pure water can be affected by the salt dissolved in it and by the temperature, the starting solution was charge balanced on the hydrogen ion. For evaporations involving carbonate, a closed system was prescribed.

The results of the simulations are documented in DTN: MO0307MWDUNEVP.000 and displayed in Table 25. This table lists the predicted deliquescence points (or equilibrium relative humidity values), the relative error with respect to handbook values, and the specific mineral phase that reached saturation in the evaporation. The comparison shows that the largest predicted difference in the value of the deliquescence relative humidity is 5.1 percent (in RH percentage units).

Table 25. Model Predictions of Equilibrium Relative Humidity for Saturated Aqueous Solutions in Contact With an Excess of Solid-Phase Salts

Salt	Predicted Equilibrium Relative Humidity (or Deliquescence Point) (%RH)	Temperature (°C)	Difference Compared to Handbook Values Listed in Table 13 (%RH)	Precipitating Mineral
NaCl	74.7%	80	-1.7%	Halite
KCl	77.0%	80	-2.5%	Sylvite
MgCl ₂ · 6H ₂ O	36.9%	25	3.9%	Bischofite
Na ₂ CO ₃ · 10H ₂ O	90.2%	24.5	3.2%	Natron
K ₂ CO ₃ · 2H ₂ O	37.8%	40	-4.2%	K ₂ CO ₃ · 1.5H ₂ O
NaF	95.9%	100	-0.7%	Villiumite
KF	28.0%	100	5.1%	Carobbite
Na ₂ SO ₄ · 10H ₂ O	95.6%	20	2.6%	Mirabilite
K ₂ SO ₄	96.4%	60	0.4%	Arcanite
NaNO ₃	62.2%	80	-3.3%	Soda Niter
KNO ₃	77.8%	60	-4.2%	Niter

DTN: MO0307MWDUNEVP.000

7.3 COMPARISON OF PITZER AND YMP.R2 DATABASE PREDICTIONS

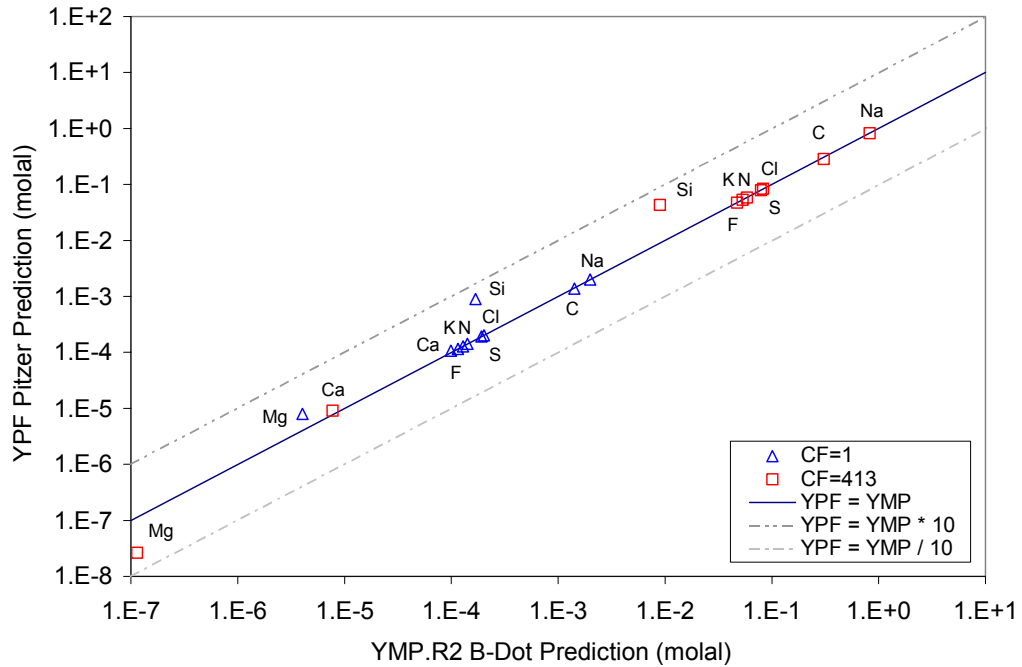
The model was further validated by comparing model predictions, using the Pitzer database, to those generated using the data0.ymp.R2 thermodynamic database (DTN: MO0302SPATHDYN.000). The J-13 example water in Section 6.7 was evaporated to an ionic strength of 1 molal using the data0.ymp.R2 database. The B-dot equation option was chosen for calculating the activity coefficients. This option is generally valid for solutions having ionic strength values as high as 1 molal (SNL 2003 [162494] Section B.2.1).

The results of this comparison are documented in DTN: MO0303MWDINJ13.000. Evaporating this J-13 water to an ionic strength of 1 molal using the data0.ymp.R2 database and B-dot equation results in a concentration factor of about 413.

Two sets of results were generated using the data0.ymp.R2 database. In the first set, only the minerals in Table 17 were suppressed from forming. The results for this set are compared to the Pitzer database predictions in Figure 31 and Figure 32. Because the data0.ymp.R2 database contains many more minerals than the Pitzer database, two minerals not included in the Pitzer database (tridymite and dolomite-ord) precipitated in this set of results. These minerals are not predicted to form under the conditions of the proposed repository. Tridymite is only stable at temperatures between 870°C and 1470°C at atmospheric pressure (Klein and Hurlbut 1999 [124293] p. 530), and dolomite formation is slow (Vaniman et al. 1992 [107066] Table A-1). Despite these differences in the predicted mineral precipitation, the comparisons in Figure 31 and Figure 32 show strong agreement between the two databases in the values of the aqueous output parameters.

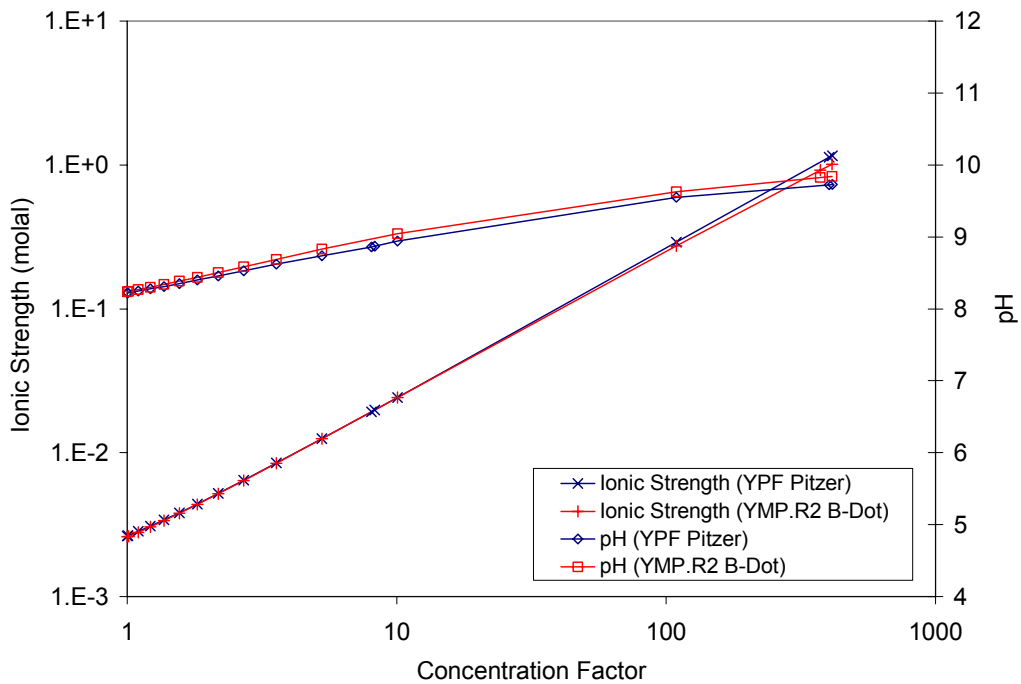
In the second set of data0.ymp.R2 results, only the minerals that precipitated in the Pitzer results (calcite, amorphous silica, and sepiolite) were allowed to precipitate. The results for this set are compared to the Pitzer database predictions in Figure 33 and Figure 34. Except for Si, these results are almost identical to the Pitzer results.

These simulations demonstrate that the IDPS model produces similar aqueous output (up to an ionic strength of 1 molal) regardless of whether the Pitzer database or the data0.ymp.R2 database is used. As a result, the calculations for each aqueous output parameter in this example fall within model validation specifications.



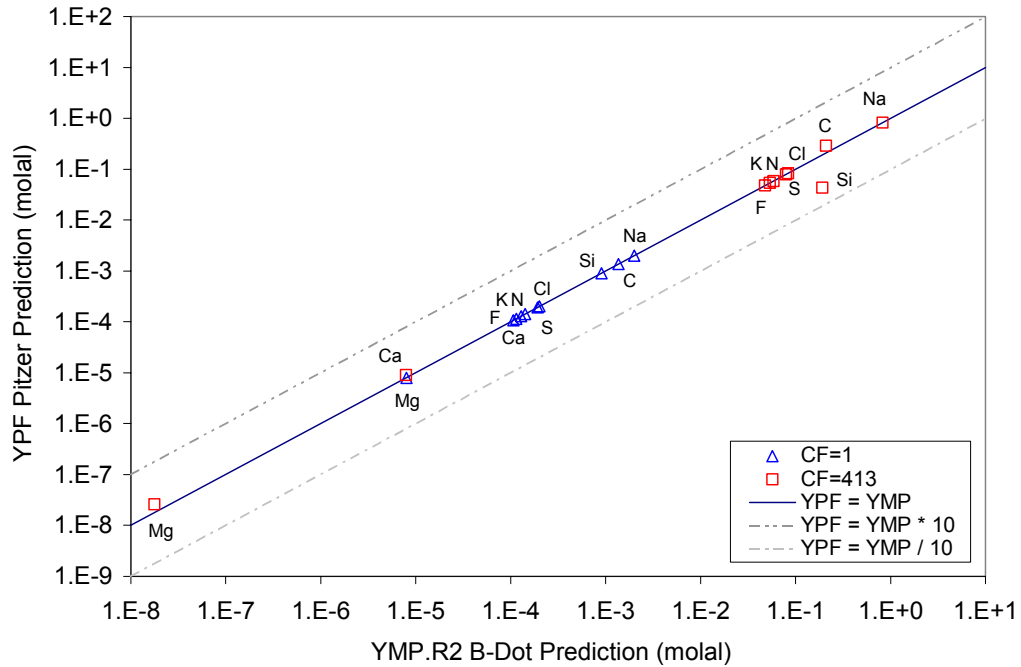
DTN: MO0303MWDINJ13.000

Figure 31. Pitzer vs. Set 1 data0.ymp.R2 (YMP.R2) Aqueous Predictions for Average In Situ J-13 Well Water at 70°C and CO₂(g) Fugacity of 10⁻³ Bars



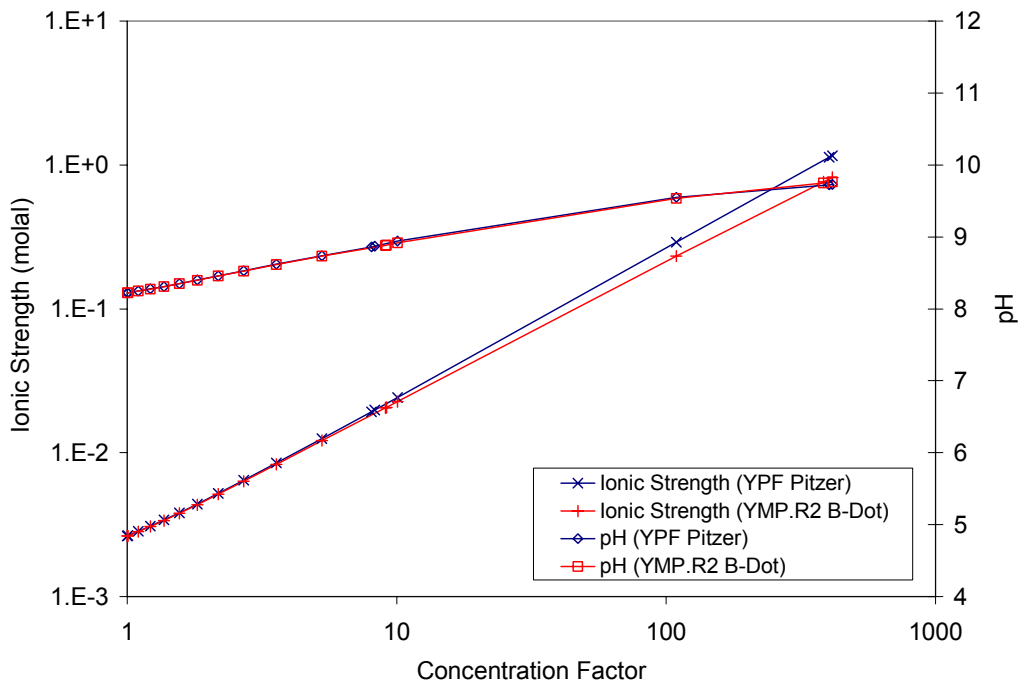
DTN: MO0303MWDINJ13.000

Figure 32. Pitzer vs. Set 1 data0.ymp.R2 (YMP.R2) pH and Ionic Strength Predictions for Average In Situ J-13 Well Water at 70°C and CO₂(g) Fugacity of 10⁻³ Bars



DTN: MO0303MWDINJ13.000

Figure 33. Pitzer vs. Set 2 data0.ymp.R2 (YMP.R2) Aqueous Predictions for Average In Situ J-13 Well Water at 70°C and CO₂(g) Fugacity of 10⁻³ Bars



DTN: MO0303MWDINJ13.000

Figure 34. Pitzer vs. Set 2 data0.ymp.R2 (YMP.R2) pH and Ionic Strength Predictions for Average In Situ J-13 Well Water at 70°C and CO₂(g) Fugacity of 10⁻³ Bars

7.4 VALIDATION FOR MINERAL OUTPUTS

A major feature of the IDPS model is the selection of minerals that are allowed (or not allowed) to precipitate upon saturation. Each mineral that precipitates creates a new chemical divide that has important consequences on the evolution of the aqueous phase (Section 6.3). Thus, mineral precipitation in the model determines the aqueous evolution of the evaporating solution. In the IDPS model, the minerals allowed to precipitate are those in the thermodynamic database that are not suppressed in the input file. The codependence of the evolving aqueous and mineral phases is imposed by the conservation of mass. At all times, the total mass of each component in the system is the sum of the masses of the component in the mineral and aqueous phases. Precipitation transfers a portion of the component mass from the aqueous to the mineral phase such that the total mass in the system remains constant. There are two components, however, whose masses do not remain constant in the system described by the IDPS model. They are water, which is incrementally removed by evaporation, and carbonate, which exchanges with the atmosphere via degassing and dissolution of carbon dioxide. Removal of water or carbonate (via carbon dioxide) does not affect the total mass of other components in the system.

Because the IDPS model imposes the principle of conservation of mass, the fact that the IDPS model predicts aqueous evolution within specified model validation objectives (Sections 7.1 through 7.3) validates the IDPS model for predicting bulk compositions of precipitated minerals. The bulk mineral composition is the set of the total masses of each elemental component in the total precipitation. While model validation for predicting the bulk mineral composition does not imply that the model accurately predicts exactly which minerals precipitate, at least this line of reasoning implies that the minerals predicted by the model to precipitate were adequate for predicting the evaporative evolution of the aqueous phase.

For TSPA-LA, it is the latter conclusion that is paramount - that the minerals predicted by the model to precipitate are adequate for predicting the composition of the aqueous phase. The minerals themselves do not threaten performance of the proposed repository. It is the potential aqueous solution that can be produced by deliquescence or dissolution of these minerals that is important to TSPA-LA in predicting corrosion rates and radionuclide mobility. Thus, predicting the specific mineral assemblage that would be generated by evaporation of a given water is not required. What is required, however, is predicting a mineral assemblage that will generate sufficiently accurate aqueous solutions upon deliquescence or dissolution. As Sections 7.1 through 7.3 show, the mineral assemblages predicted by the model accomplish this objective, thereby validating the mineral outputs for their intended use.

This model validation argument is not as easily applied to the carbonate minerals because total carbonate in the system is not constant. The fixed partial pressure of carbon dioxide largely controls the mass of dissolved carbonate. If the solution becomes momentarily supersaturated with a non-suppressed carbonate mineral, that mineral is allowed to precipitate, thereby quantitatively transferring carbonate from the aqueous phase to the mineral phase. This loss of carbonate from the aqueous phase in turn permits additional dissolution of carbon dioxide. The code iterates on these mass transfers until equilibrium is attained.

Validating the open system IDPS model for carbonate minerals requires that the model adequately predict not only the aqueous evolution of dissolved carbonate but also the evolution

of pH. Removal and addition of carbonate from the aqueous phase via precipitation, dissolution, and degassing of carbon dioxide have important consequences on the evolution of pH. The pH and carbonate concentrations are predicted within specifications in the open system laboratory evaporation tests in Section 7.1. In addition, calcite was observed as predicted in the synthesized J-13 evaporation tests (Section 7.1.1). Adequate mineral identification was not performed in the other two evaporation tests, as explained in Sections 7.1.2 and 7.1.3.

The evaporation simulations of dilute salt solutions in Section 7.2, which includes carbonate minerals, add to the validation of the IDPS model for mineral outputs. In essentially each of these evaporations, the solubility of the mineral phase was predicted within a factor of 10 and usually within 20 percent (Table 24, Figure 29, and Figure 30). In a few cases (KNO₃, Ca(NO₃)₂, and Mg(NO₃)₂), the solubility was never reached by the model; however, the potential impact of these salts on IDPS model results is negligible. These three salts are highly soluble salts and their precipitation in the IDPS model is not required to predict evaporative evolution within the uncertainty limitations prescribed by the model validation objectives. For additional verification of the accuracy of mineral solubility predictions, the reader is referred to the Pitzer database attachment.

7.5 VALIDATION SUMMARY AND ESTIMATED UNCERTAINTIES

According to the results of the validation simulations, the accuracy of the IDPS model satisfies the model validation objectives in Table 19. In the subsections that follow, each validation objective is compared to the results of the simulations, and the results are compared to the estimated model uncertainties listed in Table 20. Maximum differences for selected IDPS model output parameters are summarized in Table 26.

Table 26. Maximum Differences Between Predictions and Measurements for pH, Ionic Strength, Cl, NO₃, and the Cl:NO₃ Ratio

Evaporation Simulation	pH (pH units)	Ionic Strength (RPD ^a)	Cl (RPD)	NO ₃ (RPD)	Cl:NO ₃ Ratio (RPD)
J-13 Evaporation Experiment (Section 7.1.1)	0.78	47% ^b	48% ^b	38% ^b	16%
100x J-13 Evaporation Experiment (Section 7.1.2)	nm ^c	ne ^d	5%	7%	-3%
Topopah Spring Tuff Pore Water Evaporation Experiment (Section 7.1.3)	0.46	67% ^b	66% ^b	nm	nm
Seawater Evaporation (Section 7.1.4)	0.76	15% ^e	10% ^e	nm	nm

DTN: MO0308SPAUCIMV.000

^a RPD (relative percent difference) = 100% * ([predicted concentration] - [measured concentration]) / [measured concentration]

^b Most of the difference is due to overestimation in the concentration factor reported in the data source (see Section 7.1.1 or Section 7.1.3 for details).

^c nm = not measured

^d ne = not estimated, pH needed for estimate

^e This value ignores the sample with the highest degree of evaporation because it is an outlier (Figure 26 and Figure 27).

7.5.1 pH

The IDPS model validation objective for pH is to predict pH within one pH unit (Table 19). In each of the simulations, pH is predicted within 0.78 pH unit or less (Figure 17, Figure 24, and Figure 27). The maximum pH differences in each of the evaporation data sets are summarized in Table 26.

The estimated model uncertainty for pH is plus or minus one pH unit (Table 20). This estimate is justified and supported by the results.

7.5.2 Ionic Strength

The model validation objective for ionic strength is to predict ionic strength within a factor of 10 (Table 19). In each of the simulations, ionic strength is predicted within a factor of 2 or less (Table 21, Table 22, and Figure 27). As shown in Table 26, the maximum observed ionic strength difference is 67 percent. However, as discussed below, only a small part of this difference is due to uncertainties in the IDPS model.

The estimated model uncertainty for ionic strength is plus or minus 30 percent (Table 20). Most of the error reported in Table 26 for ionic strength is not due to model uncertainty. Rather, it is due to overestimates of the reported concentration factors. These overestimates are addressed and substantiated in Sections 7.1.1 and 7.1.3. Concentration factors were determined and reported more accurately in the seawater evaporation samples. Unlike the J-13 and Topopah Spring tuff pore water evaporation experiments, the reported concentration factors for the seawater samples were directly determined from the measured concentration factors of non-reacting dissolved components. The maximum difference between measured and predicted ionic strength in the seawater samples is approximately 15 percent, except for an outlier at the highest degree of evaporation (Figure 27). Considering the accuracy in the predicted seawater ionic strength and the effects of the overestimated concentration factors in the J-13 and Topopah Spring tuff pore water evaporation experiments, the estimated plus or minus 30 percent model uncertainty for ionic strength is supported and justified by the model validation analyses.

7.5.3 Deliquescence Relative Humidity

The model validation objective for deliquescence relative humidity (RH_d) is to predict RH_d within 5 percent in RH units (Table 19). In each of the deliquescence simulations, the RH_d was predicted within this range, rounding to one significant figure (Table 25).

The estimated model uncertainty for RH_d is also plus or minus 5 percent in RH units (Table 20). This estimate is justified and supported by the results (Table 25).

7.5.4 Al, Br, CO₃, Cl, F, K, Na, NO₃, and SO₄

The model validation objective for Al, Br, CO₃, Cl, F, K, Na, NO₃, and SO₄ is to predict the total concentrations of these components within a factor of 10 (Table 19). Except for Al and K, the total concentrations of each of these components were predicted within a factor of 3 or less (Figure 16, Figure 20, Figure 23, Figure 25, Figure 26, and Table 24). This factor is readily confirmed by the log-scale graphs because a line drawn at a factor of 3.16 would plot

equidistantly between lines drawn at factors of 1 and 10 (i.e., $10^{1/2} = 3.16$). Al was not involved in the model validation because of a lack of evaporation data involving Al. K was predicted within a factor of 3 or less in all cases except the later stages of the seawater evaporation, where K predictions differed from measurements by nearly a factor of 5 (Figure 25). In one case, the predicted Na concentration was not within a factor of 3; however, this case, the most concentrated sample in the seawater data set (Figure 25), appears to be an outlier (e.g., Figure 27). Thus, while the accuracy of the IDPS model prediction of Al could not be demonstrated to meet model validation objectives, model validation objectives of one order of magnitude (factor of 10) are met for Br, CO₃, Cl, F, K, Na, NO₃, and SO₄.

Model uncertainty in Cl and NO₃ predictions is estimated to be plus or minus 30 percent (Table 20). This estimated model uncertainty is larger than the errors observed for Cl and NO₃ salts in simple salt solubility model validation simulations (Table 24). As for the evaporation simulations, the maximum differences in predictions and measurements for Cl and NO₃ in each of the evaporation data sets are summarized in Table 26. Large differences are observed in the J-13 and Topopah Spring tuff pore water evaporation experiments; however, the majorities of these differences are not due to model uncertainty. Rather, these differences result primarily from overestimates of the reported concentration factors. These overestimates are evaluated and substantiated in Sections 7.1.1 and 7.1.3. Concentration factors were determined and reported more accurately in the seawater evaporation samples. Unlike the J-13 and Topopah Spring tuff pore water evaporation experiments, the reported concentration factors for the seawater samples were directly determined from the measured concentration factors of non-reacting dissolved components. The maximum difference between measured and predicted Cl in the seawater samples is approximately 10 percent, except for an outlier at the highest degree of evaporation (Figure 27). NO₃ was not measured in the seawater study. Considering 1) the model accuracy in the predicted solubilities of Cl and NO₃ salts, 2) the accuracy of predicted Cl concentrations in evaporated seawater samples, and 3) the effects of the overestimated concentration factors in the J-13 and Topopah Spring tuff pore water evaporation experiments, the estimated plus or minus 30 percent model uncertainty for predictions of Cl and NO₃ concentrations is supported and justified by the results of the model validation analyses.

7.5.5 Ca, Mg, and SiO₂

The model validation objective for Ca, Mg, and SiO₂ is to predict the total concentrations of these components within a factor of 100 (Table 19). The larger validation range for Ca, Mg, and SiO₂ recognizes the importance of kinetic limitations in the precipitation of Ca, Mg, and SiO₂ minerals. Equilibrium in the short timeframes of laboratory experiments may not be attained with respect to Ca, Mg, or SiO₂ species and minerals; however, they may be nearly or completely attained in the repository timeframes that the IDPS model is intended to simulate. Thus, the differences observed between IDPS model predictions and laboratory measurements may be due to slow formation of Ca, Mg, and SiO₂ minerals in short-term evaporation experiments. For Ca and Mg, whose solubilities are strongly affected by pH and total carbonate, differences may also be due to errors in the presumed values of carbon dioxide fugacity during the experiments and/or to errors in the predicted pH value. These effects are discussed in more detail in Section 7.1.2. As a result, the larger uncertainty in the predicted concentrations of Ca, Mg, and SiO₂ is reflected in the validation objectives for these outputs.

The model validation objective for Ca, Mg, and SiO₂ is met in nearly every validation simulation (Figure 16, Figure 20, Figure 23, Figure 25, and Table 24). The one exception is for Ca in the 100x J-13 evaporation experiment (Figure 20). The Ca concentration predicted by the IDPS model was slightly more than two orders of magnitude lower than the measured concentration. This exception can be explained by the importance of slow calcite precipitation in the short-term laboratory evaporation experiments (Section 7.1.2). Processes that are only important in the short term do not fall into the scope of the intended use of the IDPS model.

7.5.6 Minerals

Because the IDPS model imposes the principle of conservation of mass, the fact that the IDPS model predicts aqueous evolution within specified model validation objectives validates the IDPS model for predicting bulk compositions of precipitated minerals. While model validation for predicting the bulk mineral composition does not imply that the model accurately predicts the exact minerals observed to precipitate in laboratory evaporation experiments (and for various reasons, it often does not, as explained in Section 7.4), this line of reasoning implies that the minerals predicted by the model to precipitate are adequate for predicting the evaporative evolution of the aqueous phase. This is important because the minerals themselves do not affect the performance of the proposed repository. It is the potential aqueous solution produced by deliquescence or dissolution of these minerals that is important in predicting corrosion rates and radionuclide mobility.

7.5.7 Cl:NO₃ Ratio

Model validation objectives were not established for the Cl:NO₃ ratio because objectives were already established for Cl and NO₃ separately (Table 19). However, the uncertainty in the Cl:NO₃ ratio is an important consideration in corrosion calculations. Consequently, uncertainty in the Cl:NO₃ ratio due to IDPS model uncertainty was estimated for propagation in TSPA-LA (Table 20).

The model uncertainty in the Cl:NO₃ ratio is estimated to be plus or minus 30 percent (Table 20). The maximum differences in this ratio are summarized in Table 26 for each of the evaporation data sets that measured both Cl and NO₃. The largest difference between measurement and prediction is 16 percent. Because only two evaporation data sets provided measurements for the Cl:NO₃ ratio, the results justify and support the plus or minus 30 percent estimated model uncertainty in the Cl:NO₃ ratio.

8. CONCLUSIONS

Evaporation can have a profound effect on the chemical composition of water that could potentially seep into the proposed repository. It can turn dilute ground water into a corrosive brine, and complete evaporation can result in the precipitation of hygroscopic salts. The In-Drift Precipitates/Salts (IDPS) model is developed to predict the effects of evaporation on water composition and mineral precipitation in the proposed repository for TSPA-LA. This report documents the development, validation, use, limitations, and uncertainties of this model.

8.1 MODEL DESCRIPTION

In accordance with the purpose and scope of this modeling activity, a model is developed, validated, and documented to predict the effects of evaporation and deliquescence on the chemical evolution of potential aqueous solutions within the proposed repository. The resulting model, called the IDPS model, is designed for the system Na-K-H-Mg-Ca-Al-Cl-F-NO₃-SO₄-Br-CO₃-SiO₂-CO₂-O₂-H₂O. This system encompasses the major ion chemistry output parameters potentially important to downstream models used to predict corrosion, colloid stability, degradation of EBS materials, dust deliquescence, and radionuclide transport. These output parameters include pH, ionic strength, total aqueous concentrations of chemical components, aqueous concentrations of species that potentially contribute to acid-neutralizing capacity, and mineral precipitation. A full description of the model and its integration is provided in Section 6. This model can be used in the presence or absence of backfill.

8.2 DEVELOPED OUTPUTS

The outputs developed in this model report are listed in Table 27 along with references to their associated uncertainty. A more complete discussion of uncertainty is presented in Section 8.4.

Table 27. Developed Output

Output DTN	Output Description	Output Uncertainty
SN0306T0510102.007 Pitzer database spreadsheets and EQ3/6 input/output files	Spreadsheet collection of thermodynamic data for Pitzer ion-interaction parameters and related EQ3/6 input/output files. Direct output to TSPA-LA.	Output uncertainty is within model validation criteria specified in the EBS TWP (BSC 2003 [165601]) (Section 7).
SN0302T0510102.002 Pitzer thermodynamic database data0.ypf	The Pitzer thermodynamic database developed in Attachment I. Direct output to TSPA-LA.	This database is validated for the intended use of the IDPS model by the results of the validation runs. Model output predictions are within the uncertainty ranges specified in the validation objectives (Table 19).
MO0303SPAMNSUP.000 Base case mineral suppressions	A list of minerals typically suppressed in the IDPS model when using the Pitzer thermodynamic database. Direct output to TSPA-LA.	This list is validated for the intended use of the IDPS model by the results of the validation runs. Model output predictions are within the uncertainty ranges specified in the validation objectives (Table 19).
MO0303SPAMEQ36.000 IDPS model input file templates	EQ3/6 input file templates for the IDPS model. Direct output to TSPA-LA.	Not applicable.
MO0303MWDJ13RB.000 J-13 validation runs	EQ3/6 files resulting from IDPS model simulation of the synthetic J-13 evaporation experiments performed by Rosenberg et al. (1999 [125338]). Not direct output to TSPA-LA.	Predictions for all model output parameters are within the uncertainty ranges specified in the validation objectives (Table 19).
MO0303MWDJ13GD.000 100x J-13 validation runs	EQ3/6 files resulting from IDPS model simulation of the synthetic 100x J-13 starting water evaporation experiment documented in CRWMS M&O (2000 [146460] p. 6-16). Not direct output to TSPA-LA.	Predictions for all model output parameters are within the uncertainty ranges specified in the validation objectives (Table 19).
MO0303MWDTSWRB.000 TSw pore water validation runs	EQ3/6 files resulting from IDPS model simulation of the synthetic Topopah Spring Tuff pore water evaporation experiments performed by Rosenberg et al. (1999 [125339]). Not direct output to TSPA-LA.	Predictions for all model output parameters are within the uncertainty ranges specified in the validation objectives (Table 19).
MO0303MWDSEDSS.000 Simple salt validation runs	EQ3/6 files resulting from IDPS model simulations of the evaporation of dilute salt solutions at 25C and 100C. Not direct output to TSPA-LA.	Predictions for all model output parameters are within the uncertainty ranges specified in the validation objectives (Table 19).
MO0303MWDINJ13.000 Pitzer vs. data0.ymp.R2 validation runs	EQ3/6 files resulting from IDPS model simulations of the evaporation of in situ J-13 well water using different thermodynamic databases (Pitzer versus data0.ymp.R2). Not direct output to TSPA-LA.	Predictions for all model output parameters are within the uncertainty ranges specified in the validation objectives (Table 19).
MO0303MWDIOJ13.000 J-13 example abstraction runs	Example IDPS model EQ3/6 input/output files for in situ J-13 well water. Not direct output to TSPA-LA.	Uncertainty in input values are not identified and propagated in this example application. Propagation of uncertainty is performed in downstream analyses that use the model. Uncertainty due to model uncertainty is estimated and summarized in Section 7.5.

Table 27. Developed Output (Continued)

Output DTN	Output Description	Output Uncertainty
MO0304SPAJ13IS.001 J-13 example lookup tables	Example IDPS model EQ3/6 lookup tables for in situ J-13 well water. Not direct output to TSPA-LA.	Uncertainty in input values are not identified and propagated in this example application. Propagation of uncertainty is performed in downstream analyses that use the model. Uncertainty due to model uncertainty is estimated and summarized in Section 7.5.
MO0307MWDSEAEV.000 Seawater evaporation predictions using the IDPS model	EQ3/6 files and spreadsheets resulting from IDPS model simulation of the evaporation of seawater. Not direct output to TSPA-LA.	Uncertainty due to model uncertainty is estimated and summarized in Section 7.5.
MO0307MWDUNEVP.000 Uncertainties in evaporation predictions using the IDPS model	EQ3/6 files and spreadsheets resulting from IDPS model prediction of deliquescence points and "measured" ionic strength. Not direct output to TSPA-LA.	Uncertainty due to model uncertainty is estimated and summarized in Section 7.5.
MO0308SPAUCIMV.000 Uncertainty comparisons in IDPS model validation cases	Summary of the relative percent differences (RPD values) between predictions and measurements in all of the IDPS model validation runs with regard to pH, ionic strength, Cl concentration, NO ₃ concentration, Cl:NO ₃ concentration ratio, and deliquescence relative humidity. Not direct output to TSPA-LA.	There is no uncertainty in these data. The accuracy of these data can be checked by consulting the source DTNs.
MO0308SPAESMUN.000 Estimated model uncertainties in IDPS model outputs	Estimated model uncertainties in pH, ionic strength, Cl concentration, NO ₃ concentration, Cl:NO ₃ concentration ratio, and deliquescence relative humidity. Direct output to TSPA-LA.	These estimates of uncertainties are justified and supported by the results of the model validation simulations, as explained in Section 7.5.

8.3 MODEL ABSTRACTION

The IDPS model can be used to generate lookup tables for downstream modeling and uncertainty analyses. The model is primarily designed to generate lookup tables for the incoming water compositions predicted by the thermal-hydrological-chemical model and for the deliquescence of dust. The resulting lookup tables are to be documented elsewhere, such as in REV 02 of *Engineered Barrier System: Physical and Chemical Environment Model* (BSC 2003 [165601]).

IDPS model lookup tables provide model parameter outputs for a full range of equilibrium relative humidity values and steady-state relative evaporation rate values (Section 6.6.3.5). These tables are designed to define a response surface from which IDPS model outputs can be obtained or interpolated for given incoming water compositions.

8.4 UNCERTAINTY AND LIMITATIONS

The IDPS model has several uncertainties and limitations. Model uncertainties include uncertainties related to individual aspects of the IDPS model, such as the conceptual model, model equations, selected mineral suppressions, and constants in the thermodynamic database. Model limitations include simplifying assumptions and validation ranges.

The IDPS model is a simplification of the effects of evaporation and deliquescence on the chemistry and quantity of liquid water within the drift. Use of the model is limited to the system Na-K-H-Mg-Ca-Al-Cl-F-NO₃-SO₄-Br-CO₃-SiO₂-CO₂-O₂-H₂O and temperatures between 0°C and 125°C. This system implies oxidizing conditions at all times, which is defined in this report as maintaining an oxygen fugacity of at least 10⁻⁹ bars (Section 4.1.2). Two assumptions also limit the model. Water in the drift is assumed to be at standard state (Section 5.1), and chemical equilibrium conditions are assumed for all reactions except for certain minerals that are not allowed to precipitate (Section 5.2). Another exception to Assumption 5.2 is that the solution does not have to be at equilibrium with respect to relative humidity when necessary inputs are provided for steady-state predictions (Section 6.6.3.3).

There are several sources for model uncertainty. First, there is uncertainty associated with the conceptual model. To evaluate this uncertainty, a number of alternative conceptual models are considered (Section 6.5). Most are not utilized, however, because they either are not as realistic as the IDPS model, do not provide the types of outputs requested of the IDPS model, or do not cover the necessary ranges of applicability. The two conceptual models that are retained and incorporated into the IDPS model are the equilibrium model (Figure 1) and the steady-state alternative conceptual model (Figure 3). Both of these conceptual models are represented in the IDPS model output templates (Section 6.6.3.5).

Another model uncertainty is the choice of mineral suppressions. Not all minerals in the Pitzer database are expected to precipitate rapidly upon super saturation under the temperature and pressure conditions anticipated in the proposed repository. Because the IDPS model is used to produce model abstractions that are time-invariant, decisions must be made regarding which minerals are allowed and not allowed to precipitate in the proposed repository. A methodology is developed in this report to aid in making these decisions (Section 6.6.2.6). For instances in which the decision is uncertain, uncertainty analyses are recommended.

Additional model uncertainties are uncertainties in the thermodynamic constants, such as equilibrium constants and Pitzer coefficients. The values of these constants control the interactions and solubilities of dissolved components, which ultimately control the evaporative evolution of a given input water and the deliquescence of a given salt assemblage.

The IDPS model uncertainties identified above are assessed as a whole in the model validation section by comparing model predictions to independent evaporation data, solubility data, and deliquescence relative humidity data (Section 7). This assessment is summarized in Section 7.5. Specifically, the validation involved comparisons of model predictions to:

- four sets of evaporation data (synthetic average J-13 well water, synthetic average 100x J-13 well water, synthetic Topopah Spring tuff pore water, and seawater) (Section 7.1),
- solubilities of 24 simple salts at temperatures ranging from 25°C to 100°C (Section 7.2.1),
- deliquescence relative humidity (RH_d) of 11 simple salt solutions (Section 7.2.2), and
- evaporation predictions using the data0.ymp.R2 database up to an ionic strength of 1 molal (Section 7.3).

The results of the comparisons include the following:

- pH was always predicted within 0.78 pH units or less (Section 7.5.1).
- Ionic strength was always predicted within 67 percent or less (Section 7.5.2).
- Deliquescence relative humidity (RH_d) was always predicted within 5.1 percent in RH units (Section 7.5.3).
- Br, CO_3 , Cl, F, Na, NO_3 , and SO_4 concentrations were always predicted within a factor of 3 or less (Section 7.5.4).
- K concentrations were always predicted within a factor of 5 or less (Section 7.5.4).
- Ca, Mg, and Si concentrations were always predicted within a factor of approximately 100 or less (Section 7.5.5).

The observed differences between predictions and measurements are likely the result of three types of uncertainties: model uncertainties, uncertainties in analytical measurements, and errors in the reported concentration factors in two of the laboratory evaporation experiments (Section 7.5).

Uncertainties owing to model uncertainty alone are estimated for pH, ionic strength, Cl concentration, NO_3 concentration, the Cl: NO_3 ratio, and RH_d (Table 20). They are as follows:

- pH within plus or minus one pH unit,
- RH_d within plus or minus 5 percent in RH units, and
- ionic strength, Cl concentration, NO_3 concentration, and Cl: NO_3 ratio within plus or minus 30 percent.

Considering the likely magnitudes of the errors in the reported concentration factors for two of the laboratory evaporation experiments, these model uncertainties are supported and justified by the accuracy of the validation simulations.

8.5 YUCCA MOUNTAIN REVIEW PLAN CRITERIA ASSESSMENT

8.5.1 Degradation of Engineered Barriers Acceptance Criteria

The degradation of engineered barriers acceptance criteria are referenced from Section 2.2.1.3.1.3 of NRC (2003 [163274]). These criteria originate from 10 CFR 63.114(a)-(c) and (e)-(g).

8.5.1.1 Acceptance Criterion 1 – System Description and Model Integration Are Adequate

- (1) The total system performance assessment adequately incorporates important design features, physical phenomena, and couplings, and uses consistent and appropriate assumptions throughout the degradation of engineered barriers abstraction process.

Development of the process model documented in this report requires only qualitative design information and is based on physical phenomena expected within repository drifts (Section 6.4). Except for thermal-chemical effects, coupled processes are not incorporated in the model. Coupled processes are to be primarily addressed in REV 02 of *Engineered Barrier System Features, Events, and Processes* (BSC 2003 [165601]). Model assumptions are consistent and appropriate for the degradation of engineered barriers abstraction process (Section 5).

- (2) Assessment abstraction of the degradation of engineered barriers uses assumptions, technical bases, data, and models that are appropriate and consistent with other related U.S. Department of Energy abstractions. For example, the assumptions used for degradation of engineered barriers should be consistent with the abstractions of the quantity and chemistry of water contacting waste packages and waste forms (Section 2.2.1.3.3); climate and infiltration (Section 2.2.1.3.5); and mechanical disruption of waste packages (Section 2.2.1.3.2). The descriptions and technical bases provide transparent and traceable support for the abstraction of the degradation of engineered barriers.

The model developed in this report uses the same technical bases and other information as are used in other TSPA-LA supporting documents concerned with engineered barrier performance. The conceptual model that forms the basis for this report is consistent with other engineered system models and repository design. One of the primary purposes of this model to take abstracted output from the unsaturated zone thermal-hydrological-chemical model to predict in-drift water chemistry. These predictions are to be documented elsewhere, such as in REV 02 of *Engineered Barrier System: Physical and Chemical Environment Model* (BSC 2003 [165601]).

- (3) The descriptions of engineered barriers, design features, degradation processes, physical phenomena, and couplings that may affect the degradation of the engineered barriers are adequate. For example, materials and methods used to construct the engineered barriers are included, and degradation processes, such as uniform corrosion, pitting corrosion, crevice corrosion, stress corrosion cracking, inter-granular corrosion, microbially influenced corrosion, dry-air oxidation, hydrogen embrittlement, and the effects of wet and dry cycles, material aging and phase stability, welding, and initial defects on the degradation modes for the engineered barriers are considered.

This model by itself does not predict or consider the effects of corrosion. Rather, it is a model designed to predict dust deliquescence and the chemical evolution of incoming water due to evaporation, temperature, and gas fugacities. This model is to be used in a separate report, REV 02 of *Engineered Barrier System: Physical and Chemical Environment Model*, to assess the

chemical effects of corrosion and microbial activity on engineered materials (BSC 2003 [165601]).

- (4) Boundary and initial conditions used in the total system performance assessment abstractions are propagated consistently throughout the abstraction approaches. For example, the conditions and assumptions used in the degradation of engineered barriers abstraction are consistent with those used to model the quantity and chemistry of water contacting waste packages and waste forms (Section 2.2.1.3.3); climate and infiltration (Section 2.2.1.3.5); and mechanical disruption of waste packages (Section 2.2.1.3.2).

This model is designed to incorporate the initial conditions used by the thermal-hydrological-chemical model, which integrates natural system boundary conditions (BSC 2003 [165601]). These boundary conditions are common to other sub-system models supporting TSPA. This model does not address input water fluxes. Input water fluxes are addressed in *Seepage Model for PA Including Drift Collapse* (BSC 2003 [163226]).

- (5) Sufficient technical bases for the inclusion of features, events, and processes related to degradation of engineered barriers in the total system performance assessment abstractions are provided.

FEPs specific to this document are discussed with their technical bases in Section 6.2. FEPs screened out of this report are to be primarily discussed in REV 02 of *Engineered Barrier System Features, Events, and Processes* (BSC 2003 [165601]).

- (7) Guidance in NUREG-1297 (Altman et al. 1988 [103597]) and NUREG-1298 (Altman et al. 1988 [103750]), or other acceptable approaches, is followed.

Technical inputs were selected and documented according to applicable YMP procedures, which comply with NUREG-1297 and NUREG-1298 (Section 4.1).

8.5.1.2 Acceptance Criterion 2 – Data Are Sufficient for Model Justification

- (1) Parameters used to evaluate the degradation of engineered barriers in the license application are adequately justified (e.g., laboratory corrosion tests, site-specific data such as data from drift-scale tests, in-service experience in pertinent industrial applications, and test results not specifically performed for the Yucca Mountain site, etc.). The U.S. Department of Energy describes how the data were used, interpreted, and appropriately synthesized into the parameters.

Validation of this model uses data obtained in laboratory evaporation experiments in which the initial waters reflect water types observed at Yucca Mountain (Section 7.1). These experiments provide adequate data for justification of the model and its parameters.

- (2) Sufficient data have been collected on the characteristics of the engineered components, design features, and the natural system to establish initial and boundary conditions for abstraction of degradation of engineered barriers.

Data and technical information needed to develop the model documented in this report are sufficient. Natural system data are used to develop the thermal-hydrological-chemical model, which is a major input to this model in the TSPA application. The TSPA application is to be documented elsewhere, such as in REV 02 of *Engineered Barrier System: Physical and Chemical Environment Model* (BSC 2003 [165601]).

8.5.1.3 Acceptance Criterion 3 – Data Uncertainty Is Characterized and Propagated Through the Model Abstraction

- (1) Models use parameter values, assumed ranges, probability distributions, and/or bounding assumptions that are technically defensible, reasonably account for uncertainties and variabilities, and do not result in an under-representation of the risk estimate.

The parameter ranges of the model are considered representative of the system (Sections 4.1.2). Values and probability distributions for these parameters are required only in applications of the model, such as the TSPA application to be documented in REV 02 of *Engineered Barrier System: Physical and Chemical Environment Model* (BSC 2003 [165601]).

- (2) For those degradation processes that are significant to the performance of the engineered barriers, the U.S. Department of Energy provides appropriate parameters, based on techniques that may include laboratory experiments, field measurements, industrial analogs, and process-level modeling studies conducted under conditions relevant to the range of environmental conditions within the waste package emplacement drifts. The U.S. Department of Energy also demonstrates the capability to predict the degradation of the engineered barriers in laboratory and field tests.

This model does not predict or consider degradation processes. Rather, it is used to predict in-drift water chemistry, which can be used as input for engineered barrier degradation models.

- (3) For the selection of parameters used in conceptual and process-level models of engineered barrier degradation that can be expected under repository conditions, assumed range of values and probability distributions are not likely to underestimate the actual degradation and failure of engineered barriers as a result of corrosion.

This report simply develops and validates a process model for TSPA. Predictions using this model are to be documented elsewhere, such as in REV 02 of *Engineered Barrier System: Physical and Chemical Environment Model* (BSC 2003 [165601]).

8.5.1.4 Acceptance Criterion 4 – Model Uncertainty Is Characterized and Propagated Through the Model Abstraction

- (1) Alternative modeling approaches of features, events, and processes are considered and are consistent with available data and current scientific understanding, and the results and limitations are appropriately considered in the abstraction.

Alternative conceptual models are considered and are consistent with available data and current scientific understanding (Section 6.5). Limitations are appropriately considered and are summarized in Section 8.4. Abstractions are to be developed elsewhere, such as in REV 02 of *Engineered Barrier System: Physical and Chemical Environment Model* (BSC 2003 [165601]).

- (2) Consideration of conceptual model uncertainty is consistent with available site characterization data, laboratory experiments, field measurements, natural analog information and process-level modeling studies; and the treatment of conceptual model uncertainty does not result in an under-representation of the risk estimate.

Uncertainties in technical inputs and in analytical methodology are considered in the development of the conceptual model and output parameters (Section 8.4). Model validation is based on natural analogues, model comparisons, and laboratory experiments (Sections 6.3, 6.6.2.6, and 7).

- (3) The U.S. Department of Energy uses alternative modeling approaches, consistent with available data and current scientific understanding, and evaluates the model results and limitations, using tests and analyses that are sensitive to the processes modeled. For example, for processes such as uniform corrosion, localized corrosion, and stress corrosion cracking of the engineered barriers, the U.S. Department of Energy considers alternative modeling approaches, to develop its understanding of Review Plan for Safety Analysis Report environmental conditions and material factors significant to these degradation processes.

Alternative conceptual models are considered in Section 6.5. The model developed in this report does not directly address engineered barrier performance, but it does provide information useful in predicting barrier performance.

8.5.1.5 Acceptance Criterion 5 – Model Abstraction Output Is Supported by Objective Comparisons

- (1) Models implemented in this total system performance assessment abstraction provide results consistent with output from detailed process-level models and/or empirical observations (laboratory and field testings and/or natural analogs).

This report develops and validates a process model for TSPA. TSPA abstractions using this model are to be documented elsewhere, such as in REV 02 of *Engineered Barrier System: Physical and Chemical Environment Model* (BSC 2003 [165601]).

- (5) Accepted and well-documented procedures are used to construct and test the numerical models that simulate the engineered barrier chemical environment and degradation of engineered barriers.

The quality assurance program governing development of this report is discussed in Section 2. This model has been constructed and documented according to AP-SIII.10Q, *Models*. Validation complies with AP-SIII.10Q and applicable guidance. This report was generated according to the requirements of the Technical Work Plan (BSC 2003 [165601]) as directed by AP-2.27Q, *Planning for Science Activities*.

8.5.2 Quantity and Chemistry of Water Contacting Waste Packages and Waste Forms Acceptance Criteria

The acceptance criteria for the quantity and chemistry of water contacting waste packages and waste forms are referenced from Section 2.2.1.3.3.3 of NRC (2003 [163274]) and 10 CFR 63.114(a)-(c) and (e)-(g).

8.5.2.1 Acceptance Criterion 1 – System Description and Model Integration are Adequate

- (1) Total system performance assessment adequately incorporates important design features, physical phenomena, and couplings, and uses consistent and appropriate assumptions throughout the quantity and chemistry of water contacting waste packages and waste forms abstraction process.

Development of the model documented in this report requires only qualitative design information and is based on physical phenomena expected within repository drifts (Section 6.4). Except for thermal-chemical coupling, coupled processes are not incorporated in the model. Coupled processes are to be primarily addressed in REV 02 of *Engineered Barrier System Features, Events, and Processes* (BSC 2003 [165601]). Model assumptions are consistent and appropriate for the quantity and chemistry of water contacting waste packages and waste forms abstraction process (Section 5).

- (2) The abstraction of the quantity and chemistry of water contacting waste packages and waste forms uses assumptions, technical bases, data, and models, that are appropriate and consistent with other related U.S. Department of Energy abstractions. For example, the assumptions used for the quantity and chemistry of water contacting waste packages and waste forms are consistent with the abstractions of “Degradation of Engineered Barriers” (Section 2.2.1.3.1); “Mechanical Disruption of Waste Packages” (Section 2.2.1.3.2); “Radionuclide Release Rates and Solubility Limits” (Section 2.2.1.3.4); “Climate and Infiltration” (Section 2.2.1.3.5); and “Flow Paths in the Unsaturated Zone” (Section 2.2.1.3.6). The descriptions and technical bases provide transparent and traceable support for the abstraction of quantity and chemistry of water contacting waste packages and waste forms.

The model developed in this report uses the same technical bases and other information as are used in other TSPA-LA supporting documents concerned with the chemistry of water contacting waste packages and waste forms. The conceptual model that forms the basis for this report is consistent with other system models. One of the primary purposes of this model to take abstracted output from the unsaturated zone thermal-hydrological-chemical model to predict in-drift water chemistry. These predictions are to be documented elsewhere, such as in REV 02 of *Engineered Barrier System: Physical and Chemical Environment Model* (BSC 2003 [165601]). This model does not address input water fluxes. Input water fluxes are addressed in *Seepage Model for PA Including Drift Collapse* (BSC 2003 [163226]).

- (3) Important design features, such as waste package design and material selection, backfill, drip shield, ground support, thermal loading strategy, and degradation processes, are adequate to determine the initial and boundary conditions for calculations of the quantity and chemistry of water contacting waste packages and waste forms.

Initial and boundary conditions are taken from the predictions of the thermal-hydrological-chemical model. Design features of the engineered barrier systems affect the predictions of the thermal-hydrological-chemical model, which in turn adequately determine the initial and boundary conditions for the IDPS model. The IDPS model does not predict water flux nor requires a water flux as input.

- (5) Sufficient technical bases and justification are provided for total system performance assessment assumptions and approximations for modeling coupled thermal-hydrologic-mechanical-chemical effects on seepage and flow, the waste package chemical environment, and the chemical environment for radionuclide release. The effects of distribution of flow on the amount of water contacting the waste packages and waste forms are consistently addressed, in all relevant abstractions.

Except for thermal-chemical effects, coupled thermal-hydrological-mechanical-chemical effects are not specifically included in this model. They are to be primarily discussed in REV 02 of *Engineered Barrier System Features, Events, and Processes* (BSC 2003 [165601]). This model is not concerned with distribution of flow within the drift.

- (6) The expected ranges of environmental conditions within the waste package emplacement drifts, inside of breached waste packages, and contacting the waste forms and their evolution with time are identified. These ranges may be developed to include: (i) the effects of the drip shield and backfill on the quantity and chemistry of water (e.g., the potential for condensate formation and dripping from the underside of the shield); (ii) conditions that promote corrosion of engineered barriers and degradation of waste forms; (iii) irregular wet and dry cycles; (iv) gamma-radiolysis; and (v) size and distribution of penetrations of waste packages.

The model is developed for the expected ranges of environmental conditions within the drifts (Section 4.1.2). It does not consider the effect of the drip shield on the quantity and chemistry of water, but it is designed to characterize conditions that affect corrosion of engineered barriers. Wet and dry cycles, gamma radiolysis, and size and distribution of waste packages are not considered in the model.

- (7) The model abstraction for quantity and chemistry of water contacting waste packages and waste forms is consistent with the detailed information on waste package design and other engineered features. For example, consistency is demonstrated for: (i) dimensionality of the abstractions; (ii) various design features and site characteristics; and (iii) alternative conceptual approaches. Analyses are adequate to demonstrate that no deleterious effects are caused by

design or site features that the U.S. Department of Energy does not take into account in this abstraction.

This report develops and validates a process model for TSPA. TSPA abstractions using this model are to be documented elsewhere, such as in REV 02 of *Engineered Barrier System: Physical and Chemical Environment Model* (BSC 2003 [165601]).

- (12) Guidance in NUREG-1297 (Altman et al. 1988 [103597]) and NUREG-1298 (Altman et al. 1988 [103750]), or other acceptable approaches, is followed.

Technical inputs were selected and documented according to applicable BSC procedures, which comply with NUREG-1297 and 1298 (see Section 4.1).

8.5.2.2 Acceptance Criterion 2 – Data are Sufficient for Model Justification

- (1) Geological, hydrological, and geochemical values used in the license application are adequately justified. Adequate description of how the data were used, interpreted, and appropriately synthesized into the parameters is provided.

Sources of input data are contained in Section 4.1.2 and tabulated in the DIRS. The thermodynamic data used in this model are internationally accepted (Appendix I) and other geochemical data are adequately justified (Sections 6 and 7). Site specific data are used to justify and validate the model (Section 4.4 and 7.1). The data providing the basis for characterizing model uncertainty include laboratory evaporation data obtained from evaporation experiments of synthetic J-13 well water and Topopah Spring pore water and a demonstration of the IDPS model using an average J-13 well water composition (Section 6.7).

- (2) Sufficient data were collected on the characteristics of the natural system and engineered materials to establish initial and boundary conditions for conceptual models of thermal-hydrologic-mechanical-chemical coupled processes, that affect seepage and flow and the waste package chemical environment.

Data and technical information needed for this model are sufficient (Section 4.1). TSPA abstractions using this model are to be documented elsewhere, such as in REV 02 of *Engineered Barrier System: Physical and Chemical Environment Model* (BSC 2003 [165601]).

8.5.2.3 Acceptance Criterion 3 – Data Uncertainty Is Characterized and Propagated Through the Model Abstraction

- (1) Models use parameter values, assumed ranges, probability distributions, and bounding assumptions that are technically defensible, reasonably account for uncertainties and variabilities, and do not result in an under-representation of the risk estimate.

The parameter ranges of the model are considered representative of the system (Sections 4.1.2). Although the analysis is intended to show how the IDPS model is used in downstream abstractions, input parameters (Table 5) are developed to be consistent with the expected range of values for upstream and downstream modeled systems. Values and probability distributions

for these parameters are required only in applications of the model, such as the TSPA application to be documented in REV 02 of *Engineered Barrier System: Physical and Chemical Environment Model* (BSC 2003 [165601]).

- (2) Parameter values, assumed ranges, probability distributions, and bounding assumptions used in the total system performance assessment calculations of quantity and chemistry of water contacting waste packages and waste forms are technically defensible and reasonable, based on data from the Yucca Mountain region (e.g., results from large block and drift-scale heater and niche tests), and a combination of techniques that may include laboratory experiments, field measurements, natural analog research, and process-level modeling studies.

Validation of this model uses data obtained in laboratory evaporation experiments in which the initial waters reflect water types observed at Yucca Mountain (Section 7.1). These experiments provide adequate data for justification of the model and its parameters.

- (3) Input values used in the total system performance assessment calculations of quantity and chemistry of water contacting engineered barriers (e.g., drip shield and waste package) are consistent with the initial and boundary conditions and the assumptions of the conceptual models and design concepts for the Yucca Mountain site. Correlations between input values are appropriately established in the U.S. Department of Energy total system performance assessment. Parameters used to define initial conditions, boundary conditions, and computational domain in sensitivity analyses involving coupled thermal-hydrologic-mechanical-chemical effects on seepage and flow, the waste package chemical environment, and the chemical environment for radionuclide release, are consistent with available data. Reasonable or conservative ranges of parameters or functional relations are established.

The ranges of parameters developed in this report are consistent with initial and boundary conditions common to other TSPA conceptual models and are compatible with design concepts. This report uses the same technical bases and other information as are used in other LA supporting documents concerned with waste package and waste form performance, such as *General Corrosion and Localized Corrosion of Waste Package Outer Barrier* (BSC 2003 [161235]) and *In-Package Chemistry Abstraction* (BSC 2003 [161962] Section 4) and supporting documents. The conceptual model that forms the basis for this report is consistent with other engineered system models and repository design.

- (4) Adequate representation of uncertainties in the characteristics of the natural system and engineered materials is provided in parameter development for conceptual models, process-level models, and alternative conceptual models. The U.S. Department of Energy may constrain these uncertainties using sensitivity analyses or conservative limits. For example, the U.S. Department of Energy demonstrates how parameters used to describe flow through the engineered barrier system bound the effects of backfill and excavation-induced changes.

Uncertainty in the natural system is adequately characterized in parameter development for conceptual models, process-level models, and alternative conceptual models. Model uncertainties are summarized in Sections 7.5 and 8.4. Propagation of IDPS model uncertainty into the TSPA model includes the uncertainty characterized in the model validation. Uncertainties in natural system characteristics are to be further explored elsewhere, such as in REV 02 of *Engineered Barrier System: Physical and Chemical Environment Model* (BSC 2003 [165601]).

8.5.2.4 Acceptance Criterion 4 – Model Uncertainty Is Characterized and Propagated Through the Model Abstraction

- (1) Alternative modeling approaches of features, events, and processes are considered and are consistent with available data and current scientific understanding, and the results and limitations are appropriately considered in the abstraction.

FEPs and alternative conceptual models specific to this document are discussed with their technical bases in Sections 6.2 and 6.5. They are consistent with available data and current scientific understanding.

- (2) Alternative modeling approaches are considered and the selected modeling approach is consistent with available data and current scientific understanding. A description that includes a discussion of alternative modeling approaches not considered in the final analysis and the limitations and uncertainties of the chosen model is provided.

Alternative conceptual models are discussed in Sections 6.5. The selected modeling approach is consistent with available data and current scientific understanding.

- (3) Consideration of conceptual model uncertainty is consistent with available site characterization data, laboratory experiments, field measurements, natural analog information and process-level modeling studies; and the treatment of conceptual model uncertainty does not result in an under-representation of the risk estimate.

Uncertainties in the conceptual model are based on natural analogues, model comparisons, and laboratory experiments (Sections 6.3, 6.6.2.6, and 7). Model validation is consistent with these uncertainties.

- (4) Adequate consideration is given to effects of thermal-hydrologic-mechanical-chemical coupled processes in the assessment of alternative conceptual models. These effects may include: (i) thermal-hydrologic effects on gas, water, and mineral chemistry; (ii) effects of microbial processes on the waste package chemical environment and the chemical environment for radionuclide release; (iii) changes in water chemistry that may result from the release of corrosion products from the waste package and interactions between engineered materials and ground water; and (iv) changes in boundary conditions (e.g., drift shape and size) and hydrologic properties, relating to the response of the geomechanical system to thermal loading.

Thermal-chemical processes are incorporated in the IDPS model developed in this report. Additional coupling is to be addressed elsewhere, such as in REV 02 of *Engineered Barrier System: Physical and Chemical Environment Model* and in REV 02 of *Engineered Barrier System Features, Events, and Processes* (BSC 2003 [165601]).

8.5.2.5 Acceptance Criterion 5 – Model Abstraction Output is Supported by Objective Comparisons

- (1) The models implemented in this total system performance assessment abstraction provide results consistent with output from detailed process-level models and/or empirical observations (laboratory and field testings and/or natural analogs).

This report develops and validates a process model for TSPA. TSPA abstractions using this model are to be documented elsewhere, such as in REV 02 of *Engineered Barrier System: Physical and Chemical Environment Model* (BSC 2003 [165601]). This process model is supported by objective comparisons conducted as part of the model validation. In the model validation section, model results are compared to evaporation data for seawater and two synthetic Yucca Mountain waters (Section 7.1), handbook solubility values for 24 simple binary salts (Section 7.2), and two sets of predictions using the data0.ymp.R2 thermodynamic database (Section 7.3). Of the Yucca Mountain waters, one was synthetic average J-13 well water and the other was synthetic Topopah Spring tuff pore water.

- (2) Abstracted models for coupled thermal-hydrologic-mechanical-chemical effects on seepage and flow and the waste package chemical environment, as well as on the chemical environment for radionuclide release, are based on the same assumptions and approximations demonstrated to be appropriate for process-level models or closely analogous natural or experimental systems. For example, abstractions of processes, such as thermally induced changes in hydrological properties, or estimated diversion of percolation away from the drifts, are adequately justified by comparison to results of process-level modeling, that are consistent with direct observations and field studies.

This report develops and validates a process model for TSPA. TSPA abstractions using this model are to be documented elsewhere, such as in REV 02 of *Engineered Barrier System: Physical and Chemical Environment Model* (BSC 2003 [165601]).

- (3) Accepted and well-documented procedures are used to construct and test the numerical models that simulate coupled thermal-hydrologic-mechanical-chemical effects on seepage and flow, waste package chemical environment, and the chemical environment for radionuclide release. Analytical and numerical models are appropriately supported. Abstracted model results are compared with different mathematical models, to judge robustness of results.

The quality assurance program governing development of this report is discussed in Section 2. This model has been constructed and documented according to AP-SIII.10Q, *Models*. Validation complies with AP-SIII.10Q and applicable guidance. This report was generated according to the requirements of the Technical Work Plan (BSC 2003 [165601]) as directed by AP-2.27Q.

9. INPUTS AND REFERENCES

9.1 DOCUMENTS

- 156605 10 CFR 63. Energy: Disposal of High-Level Radioactive Wastes in a Geologic Repository at Yucca Mountain, Nevada. Readily available.
- 103750 Altman, W.D.; Donnelly, J.P.; and Kennedy, J.E. 1988. *Qualification of Existing Data for High-Level Nuclear Waste Repositories: Generic Technical Position*. NUREG-1298. Washington, D.C.: U.S. Nuclear Regulatory Commission. TIC: 200652.
- 103597 Altman, W.D.; Donnelly, J.P.; and Kennedy, J.E. 1988. *Peer Review for High-Level Nuclear Waste Repositories: Generic Technical Position*. NUREG-1297. Washington, D.C.: U.S. Nuclear Regulatory Commission. TIC: 200651.
- 162064 Archer, D.G. 1999. "Thermodynamic Properties of the KCl + H₂O System." *Journal of Physical and Chemical Reference Data*, 28, (1), 1-17. [New York, New York]: American Chemical Society. TIC: 253882.
- 162065 Archer, D.G. 2000. "Thermodynamic Properties of the NaNO₃+H₂O System." *Journal of Physical and Chemical Reference Data*, 29, (5), 1141-1156. [New York, New York]: American Chemical Society. TIC: 253379.
- 100699 Arthur, R.C. and Murphy, W.M. 1989. "An Analysis of Gas-Water-Rock Interactions During Boiling in Partially Saturated Tuff." *Science Geology Bulletin*, 42, (4), 313-327. Strasbourg, France: Sciences Geologiques Bulletin Publisher Strasbourg, Universite Louis Pasteur de Strasbourg. TIC: 235013.
- 157865 Barin, I. and Platzki, G. 1995. *Thermochemical Data of Pure Substances*. 3rd Edition. Two Volumes. New York, New York: VCH Publishers. TIC: 251934.
- 162334 Battey, M.H. 1986. *Mineralogy for Students*. 2nd Edition. New York, New York: Longman. TIC: 252929.
- 162270 Bethke, C.M. 1996. *Geochemical Reaction Modeling, Concepts and Applications*. New York, New York: Oxford University Press. TIC: 252884.
- 162352 Bodine, M.W., Jr. and Jones, B.F. 1986. *The Salt Norm: A Quantitative Chemical—Mineralogical Characterization of Natural Waters*. Water Resources Investigations Report 86-4086. Reston, Virginia: U.S. Geological Survey. TIC: 254009.
- 156639 Borchardt, G. 1995. "Smectites." Chapter 14 of *Minerals in Soil Environments*. 2nd Edition. Dixon J.B. and Weed, S.B., eds. SSSA Book Series, No. 1. Madison, Wisconsin: Soil Science Society of America. TIC: 237222.
- 155640 BSC (Bechtel SAIC Company) 2001. *Environment on the Surfaces of the Drip Shield*

- and Waste Package Outer Barrier.* ANL-EBS-MD-000001 REV 00 ICN 02. Las Vegas, Nevada: Bechtel SAIC Company. ACC: MOL.20010724.0082.
- 156065 BSC (Bechtel SAIC Company) 2001. *In-Drift Precipitates/Salts Analysis.* ANL-EBS-MD-000045 REV 00 ICN 03. Las Vegas, Nevada: Bechtel SAIC Company. ACC: MOL.20011212.0252.
- 158966 BSC (Bechtel SAIC Company) 2002. *The Enhanced Plan for Features, Events, and Processes (FEPs) at Yucca Mountain.* TDR-WIS-PA-000005 REV 00. Las Vegas, Nevada: Bechtel SAIC Company. ACC: MOL.20020417.0385.
- 162050 BSC (Bechtel SAIC Company) 2003. *Drift-Scale Coupled Processes (DST and THC Seepage) Models.* MDL-NBS-HS-000001 REV 02. Las Vegas, Nevada: Bechtel SAIC Company. ACC: DOC.20030804.0004.
- 161235 BSC (Bechtel SAIC Company) 2003. *General Corrosion and Localized Corrosion of Waste Package Outer Barrier.* ANL-EBS-MD-000003 REV 01. Las Vegas, Nevada: Bechtel SAIC Company. ACC: DOC.20030916.0010.
- 161962 BSC (Bechtel SAIC Company) 2003. *In-Package Chemistry Abstraction.* ANL-EBS-MD-000037 REV 02. Las Vegas, Nevada: Bechtel SAIC Company. ACC: DOC.20030723.0003.
- 165179 BSC (Bechtel SAIC Company) 2003. *Q-List.* TDR-MGR-RL-000005 REV 00. Las Vegas, Nevada: Bechtel SAIC Company. ACC: DOC.20030930.0002.
- 165601 BSC (Bechtel SAIC Company) 2003. *Technical Work Plan for: Engineered Barrier System Department Modeling and Testing FY03 Work Activities.* TWP-MGR-MD-000015 REV 04 ICN 02. Las Vegas, Nevada: Bechtel SAIC Company. ACC: DOC.20031001.0008.
- 163226 BSC (Bechtel SAIC Company) 2003. *Seepage Model for PA Including Drift Collapse.* MDL-NBS-HS-000002 REV 02. Las Vegas, Nevada: Bechtel SAIC Company. ACC: DOC.20030709.0001.
- 161900 BSC (Bechtel SAIC Corporation) 2003. *Software Code: GetEQData.* V1.0.1. PC w/Windows 2000. 10809-1.0.1-0.
- 162228 BSC 2003. *Software Code: EQ3/6.* V8.0. PC w/ Windows 95/98/2000/NT 4.0. 10813-8.0-00.
- 161770 Canori, G.F. and Leitner, M.M. 2003. *Project Requirements Document.* TER-MGR-MD-000001 REV 01. Las Vegas, Nevada: Bechtel SAIC Company. ACC: DOC.20030404.0003.
- 105213 Carlos, B.A.; Chipera, S.J.; Bish, D.L.; and Raymond, R. 1995. "Distribution and

- Chemistry of Fracture-Lining Zeolites at Yucca Mountain, Nevada." *Natural Zeolites '93: Occurrence, Properties, Use, Proceedings of the 4th International Conference on the Occurrence, Properties, and Utilization of Natural Zeolites, June 20-28, 1993, Boise, Idaho*. Ming, D.W. and Mumpton, F.A., eds. Pages 547-563. Brockport, New York: International Committee on Natural Zeolites. TIC: 243086.
- 160453 Chen, C.-T.A. and Marshall, W.L. 1982. "Amorphous Silica Solubilities IV. Behavior in Pure Water and Aqueous Sodium Chloride, Sodium Sulfate, Magnesium Chloride, and Magnesium Sulfate Solutions up to 350°C." *Geochimica et Cosmochimica Acta*, 46, 279-287. [New York, New York]: Pergamon Press. TIC: 235346.
- 162066 Clarke, E.C.W. and Glew, D.N. 1985. "Evaluation of the Thermodynamic Functions for Aqueous Sodium Chloride from Equilibrium and Calorimetric Measurements below 154°C." *Journal of Physical and Chemical Reference Data*, 14, (2), 489-610. [New York, New York]: American Chemical Society. TIC: 253934.
- 162067 Clegg, S.L. and Brimblecombe, P. 1990. "Equilibrium Partial Pressures and Mean Activity and Osmotic Coefficients of 0–100% Nitric Acid as a Function of Temperature." *Journal of Physical Chemistry*, 94, (13), 5369-5380. [Washington, D.C.]: American Chemical Society. TIC: 253935.
- 159187 Clegg, S.L. and Brimblecombe, P. 1990. "Solubility of Volatile Electrolytes in Multicomponent Solutions with Atmospheric Applications." Chapter 5 of *Chemical Modeling of Aqueous Systems II*. Melchior, D.C. and Bassett, R.L., eds. ACS Symposium Series 416. Washington, D.C.: American Chemical Society. TIC: 241139.
- 162089 Clegg, S.L. and Brimblecombe, P. 1990. "The Solubility and Activity Coefficient of Oxygen in Salt Solutions and Brines." *Geochimica et Cosmochimica Acta*, 54, (12), 3315-3328. New York, New York: Pergamon Press. TIC: 253874.
- 162068 Clegg, S.L.; Milioto, S.; and Palmer, D.A. 1996. "Osmotic and Activity Coefficients of Aqueous (NH₄)₂SO₄ as a Function of Temperature, and Aqueous (NH₄)₂SO₄–H₂SO₄ Mixtures at 298.15 K and 323.15 K." *Journal of Chemical and Engineering Data*, 41, (3), 455-467. [Washington, D.C.: American Chemical Society]. TIC: 253389.
- 152734 Clegg, S.L.; Rard, J.A.; and Pitzer, K.S. 1994. "Thermodynamic Properties of 0–6 mol kg⁻¹ Aqueous Sulfuric Acid from 273.15 to 328.15 K." *Journal of the Chemical Society Faraday Transactions*, 90, (13), 1875–1894. [Cambridge, England: Royal Society of Chemistry]. TIC: 248984.
- 100358 CRWMS M&O 1998. "Near-Field Geochemical Environment." Chapter 4 of *Total System Performance Assessment-Viability Assessment (TSPA-VA) Analyses Technical Basis Document*. B00000000-01717-4301-00004 REV 01. Las Vegas, Nevada: CRWMS M&O. ACC: MOL.19981008.0004.

- 146460 CRWMS M&O 2000. *Environment on the Surfaces of the Drip Shield and Waste Package Outer Barrier*. ANL-EBS-MD-000001 REV 00. Las Vegas, Nevada: CRWMS M&O. ACC: MOL.20000328.0590.
- 153246 CRWMS M&O 2000. *Total System Performance Assessment for the Site Recommendation*. TDR-WIS-PA-000001 REV 00 ICN 01. Las Vegas, Nevada: CRWMS M&O. ACC: MOL.20001220.0045.
- 161608 Dana, E.S. and Ford, W.E. 1922. *A Textbook of Mineralogy with an Extended Treatise on Crystallography and Physical Mineralogy*. 3rd Edition. New York, New York: John Wiley & Sons. TIC: 252975.
- 162110 de Lima, M.C.P. and Pitzer, K.S. 1983. "Thermodynamics of Saturated Electrolyte Mixtures of NaCl with Na₂SO₄ and with MgCl₂." *Journal of Solution Chemistry*, 12, (3), 187-199. [New York, New York]: Plenum Publishing Corporation. TIC: 253875.
- 100722 Dean, J.A. 1992. *Lange's Handbook of Chemistry*. 14th Edition. New York, New York: McGraw-Hill. TIC: 240690.
- 102773 Deer, W.A.; Howie, R.A.; and Zussman, J. 1966. *An Introduction to the Rock-Forming Minerals*. New York, New York: John Wiley & Sons. TIC: 245492.
- 118564 Drever, J.I. 1988. *The Geochemistry of Natural Waters*. 2nd Edition. Englewood Cliffs, New Jersey: Prentice-Hall. TIC: 242836.
- 100743 Eugster, H.P. and Hardie, L.A. [1978]. "Saline Lakes." *Lakes, Chemistry, Geology, Physics*. Lerman, A., ed. Pages 237-293. New York, New York: Springer-Verlag. TIC: 240782.
- 123175 Eugster, H.P. and Jones, B.F. 1979. "Behavior of Major Solutes During Closed-Basin Brine Evolution." *American Journal of Science*, 279, 609-631. New Haven, Connecticut: Yale University, Kline Geology Laboratory. TIC: 234258.
- 162282 Faust, G.T. 1953. "Huntite, Mg₃Ca(CO₃)₄, a New Mineral." *American Mineralogist*, 38, (1-2), 4-24. Washington, D.C.: Mineralogical Society of America. TIC: 252888.
- 162112 Felmy, A.R.; Rustad, J.R.; Mason, M.J.; and de la Bretonne, R. 1994. *A Chemical Model for the Major Electrolyte Components of the Hanford Waste Tanks: The Binary Electrolytes in the System: Na-NO₃-NO₂-SO₄-CO₃-F-PO₄-OH-Al(OH)₄-H₂O*. PNL-SA-23952. Richland, Washington: Pacific Northwest Laboratory. TIC: 253271.
- 162111 Felmy, A.R.; Schroeder, C.C.; and Mason, M.J. 1994. *A Solubility Model for Amorphous Silica in Concentrated Electrolytes*. PNL-SA-25345. Richland,

- Washington: Pacific Northwest Laboratory. TIC: 253270.
- 162312 Fleischer, M. and Efremov, N. 1954. "New Mineral Names." *American Mineralogist*, 39, (3-4), 402-408. Washington, D.C.: Mineralogical Society of America. TIC: 252897.
- 162284 Fleischer, M. and Pabst, A. 1983. "New Mineral Names." *Journal of the Mineralogical Society of America*, 68, (1-2), 281-283. Washington, D.C.: Mineralogical Society of America. TIC: 252898.
- 154365 Freeze, G.A.; Brodsky, N.S.; and Swift, P.N. 2001. *The Development of Information Catalogued in REV00 of the YMP FEP Database*. TDR-WIS-MD-000003 REV 00 ICN 01. Las Vegas, Nevada: Bechtel SAIC Company. ACC: MOL.20010301.0237.
- 161804 Frye, K. 1981. *Encyclopedia of Mineralogy*. Encyclopedia of Earth Sciences, Volume 4B. Stroudsburg, Pennsylvania: Hutchinson Ross. TIC: 252977.
- 144877 Garrels, R.M. and Christ, C.L. 1990. *Solutions, Minerals, and Equilibria*. Boston, Massachusetts: Jones and Barlett Publishers. TIC: 223483.
- 123636 Garrels, R.M. and Mackenzie, F.T. 1967. "Origin of the Chemical Compositions of Some Springs and Lakes?" *Equilibrium Concepts in Natural Water Systems*. American Chemical Society Advances in Chemistry Series 67. Pages 222-242. Washington, D.C.: American Chemical Society. TIC: 246519.
- 100742 Glassley, W. 1997. *Chemical Composition of Water Before Contact with Repository Materials*. Milestone SPLA1M4, Rev. 1. [Livermore, California]: Lawrence Livermore National Laboratory. ACC: MOL.19971210.0031.
- 100741 Glassley, W.E. 1994. *Report on Near-Field Geochemistry: Water Composition Changes Due to Evaporation*. Milestone M0L26. Draft. Livermore, California: Lawrence Livermore National Laboratory. ACC: MOL.19950406.0153.
- 152684 Greenberg, J.P. and Moller, N. 1989. "The Prediction of Mineral Solubilities in Natural Waters: A Chemical Equilibrium Model for the Na-K-Ca-Cl-SO₄-H₂O System to High Concentration from 0 to 250°C." *Geochimica et Cosmochimica Acta*, 53, 2503–2518. [New York, New York]: Pergamon Press. TIC: 249020.
- 161607 Gribble, C.D. 1988. *Rutley's Elements of Mineralogy*. 27th Edition. Boston, Massachusetts: Unwin Hyman. TIC: 252976.
- 162069 Grønvold, F. and Meisingset, K.K. 1983. "Thermodynamic Properties and Phase Transitions of Salt Hydrates between 270 and 400 K. II. Na₂CO₃•H₂O and Na₂CO₃•10H₂O." *Journal of Chemical Thermodynamics*, 15, (9), 881-889. New York, New York: Academic Press. TIC: 253936.

- 100123 Hardin, E.L. 1998. *Near-Field/Altered-Zone Models Report*. UCRL-ID-129179. Livermore, California: Lawrence Livermore National Laboratory. ACC: MOL.19980630.0560.
- 100814 Harrar, J.E.; Carley, J.F.; Isherwood, W.F.; and Raber, E. 1990. *Report of the Committee to Review the Use of J-13 Well Water in Nevada Nuclear Waste Storage Investigations*. UCID-21867. Livermore, California: Lawrence Livermore National Laboratory. ACC: NNA.19910131.0274.
- 118163 Harvie, C.E.; Moller, N.; and Weare, J.H. 1984. "The Prediction of Mineral Solubilities in Natural Waters: The Na-K-Mg-Ca-H-Cl-SO₄-OH-HCO₃-CO₃-CO₂-H₂O System to High Ionic Strengths at 25°C." *Geochimica et Cosmochimica Acta*, 48, (4), 723-751. New York, New York: Pergamon Press. TIC: 239849.
- 105965 Hay, R.L. 1966. *Zeolites and Zeolitic Reactions in Sedimentary Rocks*. Special Paper 85. Boulder, Colorado: Geological Society of America. TIC: 238294.
- 162281 Hay, R.L. and Wiggins, B. 1980. "Pellets, Ooids, Sepiolite and Silica in Three Calcretes of the Southwestern United States." *Sedimentology*, 27, 559-576. [Malden, Massachusetts: Blackwell Publishing]. TIC: 222806.
- 162090 He, S. and Morse, J.W. 1993. "The Carbonic Acid System and Calcite Solubility in Aqueous Na-K-Ca-Mg-Cl-SO₄ Solutions from 0 to 90°C." *Geochimica et Cosmochimica Acta*, 57, (15), 3533-3554. New York, New York: Pergamon Press. TIC: 253894.
- 106024 Helgeson, H.C.; Kirkham, D.H.; and Flowers, G.C. 1981. "Theoretical Prediction of the Thermodynamic Behavior of Aqueous Electrolytes at High Pressures and Temperatures: IV. Calculation of Activity Coefficients, Osmotic Coefficients, and Apparent Molal and Standard and Relative Partial Molal Properties to 600°C and 5 kb." *American Journal of Science*, 281, (10), 1249-1516. New Haven, Connecticut: Yale University, Kline Geology Laboratory. TIC: 238264.
- 162073 Holmes, H.F. and Mesmer, R.E. 1983. "Thermodynamic Properties of Aqueous Solutions of the Alkali Metal Chlorides to 250 °C." *Journal of Physical Chemistry*, 87, (7), 1242-1255. Washington, D.C.: American Chemical Society. TIC: 253375.
- 162074 Holmes, H.F. and Mesmer, R.E. 1986. "Thermodynamics of Aqueous Solutions of the Alkali Metal Sulfates." *Journal of Solution Chemistry*, 15, (6), 495-518. New York, New York: Plenum Press. TIC: 253633.
- 162076 Holmes, H.F. and Mesmer, R.E. 1992. "Isopiestic Studies of H₂SO₄(aq) at Elevated Temperatures, Thermodynamic Properties." *Journal of Chemical Thermodynamics*, 24, (3), 317-328. [New York, New York]: Academic Press. TIC: 253881.

- 162077 Holmes, H.F. and Mesmer, R.E. 1993. "Isopiestic Studies of $\text{NaHSO}_4(\text{aq})$ at Elevated Temperatures. Thermodynamic Properties." *Journal of Chemical Thermodynamics*, 25, ([1]), 99-110. [New York, New York: Academic Press]. TIC: 253937.
- 162078 Holmes, H.F. and Mesmer, R.E. 1994. "An Isopiestic Study of $\{(1 - y)\text{NaHSO}_4 + y\text{Na}_2\text{SO}_4\}(\text{aq})$ at Elevated Temperatures." *Journal of Chemical Thermodynamics*, 26, ([6]), 581-594. [New York, New York]: Academic Press. TIC: 253880.
- 162083 Holmes, H.F. and Mesmer, R.E. 1998. "An Isopiestic Study of Aqueous Solutions of the Alkali Metal Bromides at Elevated Temperatures." *Journal of Chemical Thermodynamics*, 30, ([6]), 723-741. [New York, New York]: Academic Press. TIC: 253377.
- 162082 Holmes, H.F. and Mesmer, R.E. 1998. "Isopiestic Molalities for Aqueous Solutions of the Alkali Metal Hydroxides at Elevated Temperatures." *Journal of Chemical Thermodynamics*, 30, ([3]), 311-326. [New York, New York]: Academic Press. TIC: 253939.
- 162071 Holmes, H.F.; Baes, C.F., Jr.; and Mesmer, R.E. 1979. "Isopiestic Studies of Aqueous Solutions at Elevated Temperatures. II. $\text{NaCl} + \text{KCl}$ Mixtures." *Journal of Chemical Thermodynamics*, 11, 1035-1050. [New York, New York]: Academic Press. TIC: 253876.
- 162072 Holmes, H.F.; Baes, C.F., Jr.; and Mesmer, R.E. 1981. "Isopiestic Studies of Aqueous Solutions at Elevated Temperatures. III. $\{(1 - y)\text{NaCl} + y\text{CaCl}_2\}^a$." *Journal of Chemical Thermodynamics*, 13, 101-113. [New York, New York]: Academic Press. TIC: 253877.
- 162075 Holmes, H.F.; Busey, R.H.; Simonson, J.M.; Mesmer, R.E.; Archer, D.G.; and Wood, R.H. 1987. "The Enthalpy of Dilution of $\text{HCl}(\text{aq})$ to 648 K and 40 MPa, Thermodynamic Properties." *Journal of Chemical Thermodynamics*, 19, (7), 863-890. New York, New York: Academic Press. TIC: 253390.
- 162080 Holmes, H.F.; Simonson, J.M.; and Mesmer, R.E. 1997. "Aqueous Solutions of the Alkaline Earth Metal Chlorides. Corrected Constants for the Ion-Interaction Model." *Journal of Chemical Thermodynamics*, 29, ([11]), 1363-1373. [New York, New York]: Academic Press. TIC: 253938.
- 162331 Jones, B.F. 1983. "Occurrence of Clay Minerals in Surficial Deposits of Southwestern Nevada." *Sciences Géologiques*, 2, (72), 81-92. Strasbourg, France: Université Louis Pasteur de Strasbourg, Institut de Géologie. TIC: 254010.
- 162347 Jones, B.F. and Galan, E. 1988. "Sepiolite and Palygorskite." *Hydrous Phyllosilicates*. Bailey, S.W., ed. Reviews in Mineralogy Volume 19. Pages 631-674. Washington,

- D.C.: Mineralogical Society of America. TIC: 254011.
- 123192 Jones, B.F.; Eugster, H.P.; and Rettig, S.L. 1977. "Hydrochemistry of the Lake Magadi Basin, Kenya." *Geochimica et Cosmochimica Acta*, 41, 53-72. New York, New York: Pergamon Press. TIC: 246224.
- 123170 Jones, B.F.; Rettig, S.L.; and Eugster, H.P. 1967. "Silica in Alkaline Brines." *Science*, 158, 1310-1314. Washington, D.C.: American Association for the Advancement of Science. TIC: 235387.
- 162345 Kent, D.B. and Kastner, M. 1985. "Mg²⁺ Removal in the System Mg²⁺—Amorphous SiO₂—H₂O by Adsorption and Mg-Hydroxysilicate Precipitation." *Geochimica et Cosmochimica Acta*, 49, 1123-1136. [New York, New York]: Pergamon Press. TIC: 253981.
- 161606 Kerr, P.F. 1977. *Optical Mineralogy*. 4th Edition. New York, New York: McGraw-Hill. TIC: 252886.
- 100769 Kinsman, D.J.J. 1976. "Evaporites: Relative Humidity Control of Primary Mineral Facies." *Journal of Sedimentary Petrology*, 46, 273-279. Tulsa, Oklahoma: Society of Economic Paleontologists and Mineralogists. TIC: 238672.
- 124293 Klein, C. and Hurlbut, C.S., Jr. 1999. *Manual of Mineralogy*. 21st Edition, Revised. New York, New York: John Wiley & Sons. TIC: 246258.
- 162093 Königsberger, E. 2001. "Prediction of Electrolyte Solubilities from Minimal Thermodynamic Information." *Monatshefte für Chemie*, 132, 1363-1386. [Vienna], Austria: Springer-Verlag. TIC: 253382.
- 125329 Koorevaar, P.; Menelik, G.; and Dirksen, C. 1983. *Elements of Soil Physics*. Developments in Soil Science 13. New York, New York: Elsevier. TIC: 246286.
- 105909 Krauskopf, K.B. 1979. *Introduction to Geochemistry*. 2nd Edition. New York, New York: McGraw-Hill. TIC: 242816.
- 101702 Krauskopf, K.B. and Bird, D.K. 1995. *Introduction to Geochemistry*. 3rd Edition. New York, New York: McGraw-Hill. TIC: 239316.
- 100051 Langmuir, D. 1997. *Aqueous Environmental Geochemistry*. Upper Saddle River, New Jersey: Prentice Hall. TIC: 237107.
- 153218 LBNL (Lawrence Berkeley National Laboratory) 1999. *Software Code: SUPCRT92*. V1.0. PC w/Windows OS and MAC w/MAC OS. 10058-1.0-00.
- 159034 Li, G.; Peacor, D.R.; Coombs, D.S.; and Kawachi, Y. 1997. "Solid Solution in the Celadonite Family: The New Minerals Ferroceldonite, K₂Fe³⁺

- 2 subscript 2}+Fe{superscript 3 subscript 2}+Si{subscript 8}O{subscript 20}(OH){subscript 4}, and Ferroaluminoceladonite, K{subscript 2}Fe{superscript 2 subscript 2}+Al{subscript 2}Si{subscript 8}O{subscript 20}(OH){subscript 4}." *American Mineralogist*, 82, (5-6), 503-511. Washington, D.C.: Mineralogical Society of America. TIC: 252472.
- 100771 Lichtner, P.C. and Seth, M. 1996. "Multiphase-Multicomponent Nonisothermal Reactive Transport in Partially Saturated Porous Media." *Proceedings of the 1996 International Conference on Deep Geological Disposal of Radioactive Waste, September 16-19, 1996, Winnipeg, Manitoba, Canada*. Toronto, Ontario, Canada: Canadian Nuclear Society. TIC: 233923.
- 162229 Lide, D.R., ed. 2000. *CRC Handbook of Chemistry and Physics*. 81st Edition. Boca Raton, Florida: CRC Press. TIC: 253056.
- 162114 Linke, W.F. 1965. "[Solubilities: Inorganic and Metal-Organic Compounds." *4th Edition*. Volume 2]. Pages 1228-1233. Washington, D.C.: American Chemical Society. TIC: 222176.
- 125331 Mahan, B.H. 1975. *University Chemistry*. 3rd Edition. Reading, Massachusetts: Addison-Wesley Publishing. TIC: 240721.
- 162085 Marshall, W.L. 1980. "Amorphous Silica Solubilities—I. Behavior in Aqueous Sodium Nitrate Solutions; 25–300°C, 0–6 Molal." *Geochimica et Cosmochimica Acta*, 44, (7), 907-913. New York, New York: Pergamon Press. TIC: 250701.
- 160481 Marshall, W.L. 1980. "Amorphous Silica Solubilities—III. Activity Coefficient Relations and Predictions of Solubility Behavior in Salt Solutions, 0-350°C." *Geochimica et Cosmochimica Acta*, 44, (7), 925-931. New York, New York: Pergamon Press. TIC: 250702.
- 162087 Marshall, W.L. and Chen, C-T.A. 1982. "Amorphous Silica Solubilities—V. Predictions of Solubility Behavior in Aqueous Mixed Electrolyte Solutions to 300°C." *Geochimica et Cosmochimica Acta*, 46, (2), 289-291. New York, New York: Pergamon Press. TIC: 250703.
- 162086 Marshall, W.L. and Chen, C-T.A. 1982. "Amorphous Silica Solubilities—VI. Postulated Sulfate-Silicic Acid Solution Complex." *Geochimica et Cosmochimica Acta*, 46, (3), 367-370. New York, New York: Pergamon Press. TIC: 250704.
- 160483 Marshall, W.L. and Warakowski, J.M. 1980. "Amorphous Silica Solubilities—II. Effect of Aqueous Salt Solutions at 25°C." *Geochimica et Cosmochimica Acta*, 44, (7), 915-924. New York, New York: Pergamon Press. TIC: 250705.
- 164481 McCaffrey, M.A.; Lazar, B.; and Holland, H.D. 1987. "The Evaporation Path of Seawater and the Coprecipitation of Br- and K{superscript +} with Halite." *Journal of*

- Sedimentary Petrology*, 57, (5), 928-937. [Tulsa, Oklahoma]: Society of Economic Paleontologists and Mineralogists. TIC: 254627.
- 162094 Meisingset, K.K. and Grønvold, F. 1986. "Thermodynamic Properties and Phase Transitions of Salt Hydrates between 270 and 400 K. IV. $\text{CaCl}_2 \cdot 6\text{H}_2\text{O}$, $\text{CaCl}_2 \cdot 4\text{H}_2\text{O}$, $\text{CaCl}_2 \cdot 2\text{H}_2\text{O}$, and $\text{FeCl}_3 \cdot 6\text{H}_2\text{O}$." *Journal of Chemical Thermodynamics*, 18, 159-173. [New York, New York]: Academic Press. TIC: 253388.
- 163594 Millero, F.J. and Pierrot, D. 1998. "A Chemical Equilibrium Model for Natural Waters." *Aquatic Geochemistry*, 4, ([1]), 153-199. [New York, New York]: Kluwer Academic Publishers. TIC: 254365.
- 152695 Moller, N. 1988. "The Prediction of Mineral Solubilities in Natural Waters: A Chemical Equilibrium Model for the Na-Ca-Cl-SO₄-H₂O System, to High Temperature and Concentration." *Geochimica et Cosmochimica Acta*, 52, 821-837. [New York, New York]: Pergamon Press. TIC: 248981.
- 163593 Monnin, C. 1999. "A Thermodynamic Model for the Solubility of Barite and Celestite in Electrolyte Solutions and Seawater to 200°C and to 1 kBar." *Chemical Geology*, 153, ([1-4]), 187-209. [New York, New York]: Elsevier. TIC: 254364.
- 100804 Murphy, W.M. 1993. "Geochemical Models for Gas-Water-Rock Interactions in a Proposed Nuclear Waste Repository at Yucca Mountain." *Proceedings of the Topical Meeting on Site Characterization and Model Validation, FOCUS '93, September 26-29, 1993, Las Vegas, Nevada*. Pages 115-121. La Grange Park, Illinois: American Nuclear Society. TIC: 102245.
- 100805 Murphy, W.M. and Pabalan, R.T. 1994. *Geochemical Investigations Related to the Yucca Mountain Environment and Potential Nuclear Waste Repository*. NUREG/CR-6288. San Antonio, Texas: Southwest Research Institute. TIC: 227032.
- 153965 Nordstrom, D.K. and Munoz, J.L. 1986. *Geochemical Thermodynamics*. Palo Alto, California: Blackwell Scientific Publications. TIC: 208228.
- 163274 NRC (U.S. Nuclear Regulatory Commission) 2003. *Yucca Mountain Review Plan, Final Report*. NUREG-1804, Rev. 2. Washington, D.C.: U.S. Nuclear Regulatory Commission, Office of Nuclear Material Safety and Safeguards. TIC: 254568.
- 162102 Oakes, C.S.; Felmy, A.R.; and Sterner, S.M. 2000. "Thermodynamic Properties of Aqueous Calcium Nitrate $\{\text{Ca}(\text{NO}_3)_2\}$ to the Temperature 373 K Including New Enthalpy of Dilution Data." *Journal of Chemical Thermodynamics*, 32, ([1]), 29-54. [New York, New York]: Academic Press. TIC: 253509.
- 162096 Pabalan, R.T. and Pitzer, K.S. 1987. "Thermodynamics of Concentrated Electrolyte Mixtures and the Prediction of Mineral Solubilities to High Temperatures for Mixtures

- in the System Na-K-Mg-Cl-SO₄-OH-H₂O." *Geochimica et Cosmochimica Acta*, 51, (9), 2429-2443. New York, New York: Pergamon Journals. TIC: 253508.
- 162147 Pabalan, R.T. and Pitzer, K.S. 1987. "Thermodynamics of NaOH(aq) in Hydrothermal Solutions." *Geochimica et Cosmochimica Acta*, 51, (4), 829-837. New York, New York: Pergamon Press. TIC: 253383.
- 162280 Palache, C.; Berman, H.; and Frondel, C. 1951. *Halides, Nitrates, Borates, Carbonates, Sulfates, Phosphates, Arsenates, Tungstates, Molybdates, Etc.* Volume II of *The System of Mineralogy of James Dwight Dana and Edward Salisbury Dana, Yale University 1837-1892*. 7th Edition. [New York, New York]: John Wiley & Sons. TIC: 209332.
- 162274 Papke, K.G. 1976. *Evaporites and Brines in Nevada Playas*. Nevada Bureau of Mines and Geology Bulletin 87. Reno, Nevada: University of Nevada, Reno, Mackay School of Mines. TIC: 211869.
- 161609 Parkes, G.D., ed. 1961. *Mellor's Modern Inorganic Chemistry*. New York, New York: Longmans, Green and Company. TIC: 252978.
- 162097 Peiper, J.C. and Pitzer, K.S. 1982. "Thermodynamics of Aqueous Carbonate Solutions Including Mixtures of Sodium Carbonate, Bicarbonate, and Chloride." *Journal of Chemical Thermodynamics*, 14, (7), 613-638. New York, New York: Academic Press. TIC: 240175.
- 162098 Phutela, R.C. and Pitzer, K.S. 1986. "Heat Capacity and Other Thermodynamic Properties of Aqueous Magnesium Sulfate to 473 K." *Journal of Physical Chemistry*, 90, (5), 895-901. [Washington, D.C.]: American Chemical Society. TIC: 253940.
- 152738 Pitzer, K.S. 1973. "Thermodynamics of Electrolytes. I. Theoretical Basis and General Equations." *Journal of Physical Chemistry*, 77, (2), 268-277. [Washington, D.C.: American Chemical Society]. TIC: 239503.
- 152709 Pitzer, K.S. 1991. "Ion Interaction Approach: Theory and Data Correlation." Chapter 3 of *Activity Coefficients in Electrolyte Solutions*. 2nd Edition. Pitzer, K.S., ed. Boca Raton, Florida: CRC Press. TIC: 251799.
- 123206 Pitzer, K.S. and Kim, J.J. 1974. "Thermodynamics of Electrolytes. IV. Activity and Osmotic Coefficients for Mixed Electrolytes." *Journal of the American Chemical Society*, 96, (18), 5701-5707. Washington, D.C.: American Chemical Society. TIC: 246223.
- 152742 Pitzer, K.S. and Mayorga, G. 1973. "Thermodynamics of Electrolytes. II. Activity and Osmotic Coefficients for Strong Electrolytes with One or Both Ions Univalent." *Journal of Physical Chemistry*, 77, (19), 2300-2308. [Washington, D.C.: American Chemical Society]. TIC: 249019.

- 163583 Pitzer, K.S. and Oakes, C.S. 1994. "Thermodynamics of Calcium Chloride in Concentrated Aqueous Solutions and in Crystals." *Journal of Chemical and Engineering Data*, 39, (3), 553-559. [Washington, D.C.]: American Chemical Society. TIC: 253384.
- 163582 Pitzer, K.S. and Shi, Y. 1993. "Thermodynamics of Calcium Chloride in Highly Concentrated Aqueous Solution and in Hydrated Crystals." *Journal of Solution Chemistry*, 29, (2), 99-105. New York, New York: Plenum Press. TIC: 253385.
- 162099 Pitzer, K.S.; Peiper, J.C.; and Busey, R.H. 1984. "Thermodynamic Properties of Aqueous Sodium Chloride Solutions." *Journal of Physical and Chemical Reference Data*, 13, (1), 1-102. [Washington, D.C.]: American Chemical Society. TIC: 253809.
- 101699 Pokrovskii, V.A. and Helgeson, H.C. 1995. "Thermodynamic Properties of Aqueous Species and the Solubilities of Minerals at High Pressures and Temperatures: The System Al₂O₃-H₂O-NaCl." *American Journal of Science*, 295, 1255-1342. New Haven, Connecticut: Yale University, Kline Geology Laboratory. TIC: 236803.
- 162101 Polya, D.A.; Woolley, E.M.; Simonson, J.M.; and Mesmer, R.E. 2001. "The Enthalpy of Dilution and Thermodynamics of Na₂CO₃(aq) and NaHCO₃(aq) from T = 298 K to T = 523.15 K and Pressure of 40 MPa." *Journal of Chemical Thermodynamics*, 33, ([2]), 205-243. [New York, New York]: Academic Press. TIC: 253386.
- 162104 Rard, J.A. and Archer, D.G. 1995. "Isopiestic Investigation of the Osmotic and Activity Coefficients of Aqueous NaBr and the Solubility of NaBr·2H₂O(cr) at 298.15 K: Thermodynamic Properties of the NaBr + H₂O System over Wide Ranges of Temperature and Pressure." *Journal of Chemical and Engineering Data*, 40, ([1]), 170-185. [Washington, D.C.]: American Chemical Society. TIC: 253941.
- 152759 Rard, J.A. and Clegg, S.L. 1997. "Critical Evaluation of the Thermodynamic Properties of Aqueous Calcium Chloride. 1. Osmotic and Activity Coefficients of 0–10.77 mol×kg⁽⁻¹⁾ Aqueous Calcium Chloride Solutions at 298.15 K and Correlation with Extended Pitzer Ion-Interaction Models." *Journal of Chemical & Engineering Data*, 42, (5), 819–849. [Washington, D.C.: American Chemical Society]. TIC: 249002.
- 152715 Rard, J.A. and Platford, R.F. 1991. "Experimental Methods: Isopiestic." *Activity Coefficients in Electrolyte Solutions*. 2nd Edition. Pitzer, K.S., ed. 209-277. Boca Raton, Florida: CRC Press. TIC: 251798.
- 162327 Rard, J.A. and Wijesinghe, A.M. 2003. "Conversion of Parameters Between Different Variants of Pitzer's Ion-Interaction Model, both With and Without Ionic Strength Dependent Higher-Order Terms." *Journal of Chemical Thermodynamics*, 35, (3), 439-473. [New York, New York]: Academic Press. TIC: 253943.

- 162105 Rard, J.A.; Clegg, S.L.; and Palmer, D.A. 2000. "Isopiestic Determination of the Osmotic Coefficients of Na₂SO₄(aq) at 25 and 50°C, and Representation with Ion-Interaction (Pitzer) and Mole Fraction Thermodynamic Models." *Journal of Solution Chemistry*, 29, (1), 1-49. [New York, New York]: Plenum. TIC: 253942.
- 153683 Robie, R.A. and Hemingway, B.S. 1995. *Thermodynamic Properties of Minerals and Related Substances at 298.15 K and 1 Bar (10⁵ Pascals) Pressure and at Higher Temperatures*. Bulletin 2131. Reston, Virginia: U.S. Geological Survey. TIC: 249441.
- 108567 Robinson, R.A. and Stokes, R.H. 1965. *Electrolyte Solutions, The Measurement and Interpretation of Conductance, Chemical Potential and Diffusion in Solutions of Simple Electrolytes*. 2nd Edition (Revised). Washington, D.C.: Butterworth. TIC: 242575.
- 162107 Rogers, P.S.Z. and Pitzer, K.S. 1981. "High-Temperature Thermodynamic Properties of Aqueous Sodium Sulfate Solutions." *Journal of Physical Chemistry*, 85, (20), 2886-2895. [Washington, D.C.]: American Chemical Society. TIC: 253810.
- 125338 Rosenberg, N.D.; Knauss, K.G.; and Dibley, M.J. 1999. *Evaporation of J13 Water: Laboratory Experiments and Geochemical Modeling*. UCRL-ID-134852. Livermore, California: Lawrence Livermore National Laboratory. TIC: 246322.
- 125339 Rosenberg, N.D.; Knauss, K.G.; and Dibley, M.J. 1999. *Evaporation of Topopah Spring Tuff Pore Water*. UCRL-ID-135765. [Livermore, California]: Lawrence Livermore National Laboratory. TIC: 246231.
- 127320 Saxton, B.; Austin, J.B.; Dietrich, H.G.; Fenwick, F.; Fleischer, A.; Frear, G.L.; Roberts, E.J.; Smith, R.P.; Solomon, M.; and Spurlin, H.M. 1928. "Boiling-Point Elevations, Non-Volatile Solutes." *International Critical Tables of Numerical Data, Physics, Chemistry and Technology*. Volume III. 1st Edition. Pages 324-350. New York, New York: McGraw-Hill. TIC: 243268.
- 161602 Smith, W.R. and Missen, R.W. 1991. *Chemical Reaction Equilibrium Analysis: Theory and Algorithms*. Malabar, Florida: Krieger Publishing Company. TIC: 252885.
- 162494 SNL (Sandia National Laboratories) 2003. *Software User's Manual, EQ3/6, Version 8.0*. SDN: 10813-UM-8.0-00. Albuquerque, New Mexico: Sandia National Laboratories. ACC: MOL.20030312.0084.
- 152713 Spencer, R.J.; Moller, N.; and Weare, J.H. 1990. "The Prediction of Mineral Solubilities in Natural Waters: A Chemical Equilibrium Model for the Na-K-Ca-Mg-Cl-SO₄-H₂O System at Temperatures Below 25°C." *Geochimica et Cosmochimica Acta*, 54, 575-590. [New York, New York]: Pergamon Press. TIC: 248999.

- 162116 Sterner, S.M.; Felmy, A.R.; Oakes, C.S.; and Pitzer, K.S. 1998. "Correlation of Thermodynamic Data for Aqueous Electrolyte Solutions to Very High Ionic Strength Using INSIGHT: Vapor Saturated Water Activity in the System $\text{CaCl}_2\text{-H}_2\text{O}$ to 250°C and Solid Saturation." *International Journal of Thermophysics*, 19, (3), 761-770. [New York, New York]: Plenum Publishing. TIC: 253387.
- 127964 Stoessell, R.K. 1988. "25°C and 1 Atm Dissolution Experiments of Sepiolite and Kerolite." *Geochimica et Cosmochimica Acta*, 52, 365-374. [New York, New York]: Pergamon Press. TIC: 246452.
- 125332 Stumm, W. and Morgan, J.J. 1996. *Aquatic Chemistry, Chemical Equilibria and Rates in Natural Waters*. 3rd Edition. New York, New York: John Wiley & Sons. TIC: 246296.
- 162108 Thiessen, W.E. and Simonson, J.M. 1990. "Enthalpy of Dilution and the Thermodynamics of $\text{NH}_4\text{Cl(aq)}$ to 523 K and 35 MPa." *Journal of Physical Chemistry*, 94, (20), 7794-7800. [Washington, D.C.]: American Chemical Society. TIC: 253883.
- 124334 Tsang, Y.W. 1999. *Yucca Mountain Single Heater Test Final Report*. Report 42537. Berkeley, California: Lawrence Berkeley National Laboratory. ACC: MOL.19990809.0191.
- 161603 Van Zeggeren, F. and Storey, S.H. 1970. *The Computation of Chemical Equilibria*. New York, New York: Cambridge University Press. TIC: 252891.
- 107066 Vaniman, D.T.; Ebinger, M.H.; Bish, D.L.; and Chipera, S. 1992. "Precipitation of Calcite, Dolomite, Sepiolite, and Silica from Evaporated Carbonate and Tuffaceous Waters of Southern Nevada, USA." *Proceedings of the 7th International Symposium on Water-Rock Interaction, Park City, Utah, July 13-18, 1992*. Kharaka, Y.K. and Maest, A., eds. 1, 687-691. Brookfield, Vermont: A.A. Balkema. TIC: 208527.
- 162329 Wadley, S. and Buckley, C.A. 1997. *Chemical Speciation Self-Study Work Manual*. WRC Project No. K8/208. Durban, South Africa: University of Natal, Department of Chemical Engineering, Water Research Commission. TIC: 252923.
- 162283 Walling, E.M.; Rock, P.A.; and Casey, W.H. 1995. "The Gibbs Energy of Formation of Huntite, $\text{CaMg}_3(\text{CO}_3)_4$, at 298 K and 1 Bar from Electrochemical Cell Measurements." *American Mineralogist*, 80, (3-4), 355-360. Washington, D.C.: Mineralogical Society of America. TIC: 252890.
- 127454 Walton, J.C. 1994. "Influence of Evaporation on Waste Package Environment and Radionuclide Release from a Tuff Repository." *Water Resources Research*, 30, (12), 3479-3487. Washington, D.C.: American Geophysical Union. TIC: 246921.

- 162109 Wang, P.; Pitzer, K.S.; and Simonson, J.M. 1998. "Thermodynamic Properties of Aqueous Magnesium Chloride Solutions from 250 to 600 K and to 100 MPa." *Journal of Physical and Chemical Reference Data*, 27, (5), 971-991. [Washington, D.C.]: American Chemical Society. TIC: 249693.
- 100833 Weast, R.C. and Astle, M.J., eds. 1981. *CRC Handbook of Chemistry and Physics*. 62nd Edition. Boca Raton, Florida: CRC Press. TIC: 240722.
- 162148 Wesolowski, D.J. 1992. "Aluminum Speciation and Equilibria in Aqueous Solution: I. The Solubility of Gibbsite in the System Na-K-Cl-OH-Al(OH)₄ from 1 to 100°C." *Geochimica et Cosmochimica Acta*, 56, (3), 1065-1091. New York, New York: Pergamon Press. TIC: 253946.
- 100792 Wilder, D.G., ed. 1996. *Volume II: Near-Field and Altered-Zone Environment Report*. UCRL-LR-124998. [Livermore, California]: Lawrence Livermore National Laboratory. ACC: MOL.19961212.0121; MOL.19961212.0122.
- 162340 Wollast, R.; Mackenzie, F.T.; and Bricker, O.P. 1968. "Experimental Precipitation and Genesis of Sepiolite at Earth-Surface Conditions." *American Mineralogist*, 53, 1645-1662. [Washington, D.C.: Mineralogical Society of America]. TIC: 253980.

9.2 DATA, LISTED BY TRACKING NUMBER

9.2.1 Input Data

- 144913 LL000202905924.117. Environment on the Surfaces of the Drip Shield and Waste Package Outer Barrier. Submittal date: 02/18/2000.
- 120487 LL991008004241.041. Evaporation of Topopah Spring Tuff Pore Water. Submittal date: 10/21/1999.
- 120489 LL991008104241.042. Evaporation of J13 Water: Laboratory Experiments and Geochemical Modeling. Submittal date: 10/21/1999.
- 151029 MO0006J13WTRCM.000. Recommended Mean Values of Major Constituents in J-13 Well Water. Submittal date: 06/07/2000.
- 161756 MO0302SPATHDYN.000. Thermodynamic Data Input Files - Data0.YMP.R2. Submittal date: 02/05/2003.
- 161886 MO0302SPATHDYN.001. Thermodynamic Data Supporting Spreadsheet Files - Data0.YMP.R2. Submittal date: 02/05/2003.

9.2.2 Developed Data

MO0303MWDINJ13.000. Comparison of In-Drift Precipitates/Salts Model Simulations of Evaporation of In Situ J-13 Well Water Using Different Databases (YPF Pitzer vs. YMP.R2). Submittal Date: 03/04/2003.

MO0303MWDIOJ13.000. Example EQ3/6 In-Drift Precipitates/Salts Model Input/Output Files for In Situ J-13 Well Water. Submittal Date: 03/04/2003.

MO0303MWDJ13GD.000. In-Drift Precipitates/Salts Model Simulation of Synthetic J-13 Water Evaporation Experiments Documented in ANL-EBS-MD-000001. Submittal Date: 03/04/2003.

MO0303MWDJ13RB.000. In-Drift Precipitates/Salts Model Simulation of Synthetic J-13 Water Evaporation Experiments Documented in Rosenberg et al. 1999. Submittal Date: 03/04/2003.

MO0303MWSEDSS.000. In-Drift Precipitates/Salts Model Simulations of Evaporation of Dilute Salt Solutions at 25C and 100C. Submittal Date: 03/04/2003.

MO0303MWDTSWRB.000. In-Drift Precipitates/Salts Model Simulation of Synthetic Topopah Spring Tuff Pore Water Evaporation Experiments Documented in Rosenberg et al. 1999. Submittal Date: 03/04/2003.

MO0303SPAMEQ36.000. General Formats of In-Drift Precipitates/Salts Model EQ3/6 Input Files. Submittal Date: 03/04/2003.

MO0303SPAMNSUP.000. Baseline YPF Pitzer Database MineralSuppressions for the In-Drift Precipitates/Salts Model. Submittal Date: 03/04/2003.

MO0304SPAJ13IS.001. Example EQ3/6 In-Drift Precipitates/Salts Model Lookup Tables for In Situ J-13 Well Water. Submittal Date: 04/15/2003.

MO0307MWDSEAEV.000. Seawater Evaporation Predictions Using the IDPS Model. Submittal Date: 07/31/2003.

MO0307MWDUNEVP.000. Uncertainties in Evaporation Predictions Using the IDPS Model. Submittal Date: 07/31/2003.

MO0308SPAESMUN.000. Estimated Model Uncertainties in IDPS Model Outputs. Submittal Date: 08/08/2003.

MO0308SPAUCIMV.000. Uncertainty Comparisons in IDPS Model Validation Cases. Submittal Date: 08/08/2003.

SN0302T0510102.002. Pitzer Thermodynamic Database (Data0.YPF, Revision 1). Submittal Date: 02/06/2003.

SN0306T0510102.007. Revised Pitzer Thermodynamic Database Spreadsheets and EQ3/6 Input and Output Files. Submittal Date: 06/30/2002.

9.3 CODES, STANDARDS, REGULATIONS, PROCEDURES, AND SOFTWARE

AP-2.14Q, Rev. 3, ICN 0. *Document Review*. Washington, D.C.: U.S. Department of Energy, Office of Civilian Radioactive Waste Management. ACC: DOC.20030827.0018.

AP-2.27Q, Rev. 1, ICN 1. *Planning for Science Activities*. Washington, D.C.: U.S. Department of Energy, Office of Civilian Radioactive Waste Management. ACC: DOC.20030724.0001.

AP-SI.1Q, Rev. 5, ICN 2. *Software Management*. Washington, D.C.: U.S. Department of Energy, Office of Civilian Radioactive Waste Management. ACC: DOC.20030902.0003.

AP-SIII.10Q, Rev. 2, ICN 0. *Models*. Washington, D.C.: U.S. Department of Energy, Office of Civilian Radioactive Waste Management. ACC: DOC.20030929.0003.

AP-SIII.2Q, Rev. 1, ICN 1. *Qualification of Unqualified Data*. Washington, D.C.: Office of Civilian Radioactive Waste Management. ACC: DOC.20030422.0008.

AP-SV.1Q, Rev. 1, ICN 0. *Control of the Electronic Management of Information*. Washington, D.C.: U.S. Department of Energy, Office of Civilian Radioactive Waste Management. ACC: DOC.20030929.0004.

10. ATTACHMENTS

Attachment	Title
I	Pitzer Database Development: Description of the Pitzer Geochemical Thermodynamic Database (data0.ypf)
II	MINTEQA2 Mineral Occurrence Database
III	Example IDPS Evaporation Lookup Table
IV	Example IDPS Condensation Lookup Table

INTENTIONALLY LEFT BLANK

ATTACHMENT I
PITZER DATABASE DEVELOPMENT: DESCRIPTION OF THE PITZER GEOCHEMICAL
THERMODYNAMIC DATABASE (data0.ypf)

ATTACHMENT I

Pitzer Database Development: Description of the Pitzer Geochemical Thermodynamic Database (data0.ypf)

Prepared by:

Carlos F. Jove Colon (SNL)
Russell L. Jarek (SNL)
Ananda Wijesinghe (LLNL)
Joseph A. Rard (LLNL)
Thomas J. Wolery (LLNL)

CONTENTS

	Page
I-1 SCOPE	4
I-2 INPUT DATA SELECTION	5
I-3 PITZER ION-INTERACTION MODEL	7
I-3.1 GENERAL PITZER ELECTROLYTE THEORY	7
I-3.2 Temperature Functions for Pitzer Interaction Parameters	13
I-4 EVALUATION, COMPILATION AND CONVERSION OF PITZER INTERACTION PARAMETERS FROM PUBLISHED SOURCES	21
I-4.1 FITPITZERNC METHODOLOGY	27
I-4.2 PROCEDURE FOR FITTING TEMPERATURE FUNCTIONS TO PITZER PARAMETERS	29
I-4.3 CONPITZERNC METHODOLOGY	34
I-4.4 BINARY PITZER INTERACTION PARAMETERS	39
I-4.5 TERNARY PITZER INTERACTION PARAMETERS	61
I-4.6 VARIOUS MX AND MM PARAMETERS FROM TABLE I-2 AT 25 °C THAT DO NOT REQUIRE REFITTING	71
I-5 DATA FOR SOLID PHASES, AQUEOUS SPECIES AND GASES	72
I-5.1 CaCl₂ HYDRATES (CaCl₂•NH₂O WHERE N EQUALS 2, 4, AND 6)	79
I-5.2 THERMONATRITE (Na₂CO₃:H₂O)	81
I-5.3 SODA NITER (NaNO₃)	83
I-6 REFERENCES	85

I-1 SCOPE

The Pitzer database *data0.ypf* (DTN: MO0302SPATHDYN.001 and SN0302T0510102.002) was developed to calculate concentrations of electrolyte solutions resulting from the compositional evolution of waters from the unsaturated zone that are likely to seep into the waste emplacement drifts. These calculations are performed using the computer code *EQ3/6 Version 8.0* (STN: 10813-8.0-00) for which a Pitzer parameter database has been created.

As a result of above-ambient temperature conditions within the repository, water from the unsaturated zone undergoes evaporation to evolve into a concentrated electrolyte solution. These concentrated waters may accelerate degradation processes (e.g., metal corrosion) thereby affecting the integrity of Engineered Barrier System (EBS) components, such as waste packages and drip shields. For this reason, electrolyte component concentrations under long-term evaporative conditions need to be estimated to provide input for downstream Total System Performance Assessment (TSPA) models.

Geochemical modeling using data appropriate for dilute solutions, such as those data contained in the geochemical database *data0.ymp.R2*, (DTN:MO0302SPATHDYN.000) is not accurate or valid when applied to the concentrated (high ionic strength) solutions that result from the evaporation of seepage waters within the disposal drifts. As explained in Section I-3, the Pitzer database represents a more accurate way of predicting chemical behavior in concentrated aqueous electrolyte solutions. Modeling of water compositions associated with the in-drift physical and chemical environment under long-term evaporative repository conditions therefore relies upon this Pitzer database. Development of this database involves a comprehensive compilation of Pitzer model parameters reported in the literature, focusing mostly on those functional at relatively elevated temperatures (i.e., above 25 °C). Data above 25 °C are needed since the estimated long-term conditions in the repository will be above ambient temperatures.

The steps taken to develop the Pitzer database are as follows:

- Compilation of recent Pitzer parameter data focusing on temperatures at and above 25°C for major aqueous species present in natural waters that might seep into the repository drift.
- Validation and testing of compiled Pitzer data to predict osmotic coefficients and therefore water activity when compared to source literature data.
- Estimation and fitting of solubility constants (log Ks) for selected salt solids using tabulated thermodynamic and solubility data in concert with the estimated Pitzer parameters defining the activity model for the relevant salt system. This is done to bridge consistency between the compiled Pitzer electrolyte parameter data and the reported salt phase solubility reported in the scientific literature.
- Incorporation of silicate mineral log K data from the recent thermodynamic data compilation *data0.ymp.R2* (DTN: MO0302SPATHDYN.000) that include clays, zeolites, and cement phases.

I-2 INPUT DATA SELECTION

The Pitzer database was developed in this document using primary input data selected from a variety of published sources. The status of these input data is summarized in the DIRS. One primary source for input data is the YMP-generated database *data0.ymp.R2*. Additional input data are selected from widely used handbook sources, and the remainder of the data used is selected from internationally recognized peer-reviewed journals. Data sources for Pitzer parameter are entirely restricted to peer-reviewed journals. The data sources for binary electrolyte solutions are listed in Table 1 of Section 4.1.1 of this report, and the data sources for ternary solutions are listed in Table 2 of that section. Rationale for the selection of these data is discussed in the subsections of Sections I-4.4 and I-4.5.

The most important rationale for adopting the Pitzer modeling approach and related parameter data is the wide acceptance by the scientific and international community. As documented in this paragraph, this is comparable to that for scientific and technical handbooks. Since the early publications on the subject by Professor Kenneth S. Pitzer of the Department of Chemistry, the University of California at Berkeley, (e.g., Pitzer 1973, Pitzer and Mayorga 1973, Pitzer and Kim 1974), the approach to the thermodynamics of highly concentrated aqueous electrolytes, which he formulated, has been widely accepted. This is evident not only by the large number of citations of publications by him (including co-authors) and citations of publications by other independent authors, who used the same approach, but also by the range of organizations represented. Examples of this wide acceptance are by the staff at the University of California, San Diego (Møller 1988; Spencer et al. 1990); Chemistry and Analytical Sciences Division, Oak Ridge National Laboratory (Holmes and Mesmer 1994); Lawrence Livermore National Laboratory (Rard and Wijesinghe 2003); Johns Hopkins University (Eugster and Jones 1979 (see citations list in ANL-EBS-MD-00045)); Physical and Chemical Properties Division, National Institute of Standards and Technology (Archer 2000); Pacific Northwest National Laboratory in collaboration with Fluid Inclusion Technologies (Oakes, Felmy, and Sterner 2000); Plymouth Marine Laboratory, UK, in collaboration with School of Environmental Sciences, University of East Anglia, UK (Clegg and Brimblecome 1990c); Department of Chemistry, University of Coimbra, Portugal in collaboration with the Department of Chemistry, the University of California at Berkeley (de Lima and Pitzer 1987); Department of Geology, Texas A&M University (He and Morse 1993); Department of Chemistry, Murdoch University, Australia (Königsberger 2001); Department of Chemistry and Geochemistry, Colorado School of Mines (author was one of the first members of the Nuclear Waste Technical Review Board) (Langmuir 1997, pp. 138-143 (see citations list in ANL-EBS-MD-00045)); Center for Nuclear Waste Regulatory Analyses (Pabalan and Pitzer 1987 a and b), and others. The group at Oak Ridge National Laboratory (Holmes and Mesmer, 1994) are well-known for producing high quality isopiestic data at elevated temperatures thanks to their considerable improvements on this experimental technique (see Rard and Platford, 1991, section C, p. 246-249). Isopiestic experiments on electrolytes provide osmotic coefficient data that are then used to obtain Pitzer parameter data. Papers by all these authors have been extensively cited, so much so as to indicate acceptance rather than rejection, as documented below in Sections I-4.4 through I-4.6 for individual ion doublets and triplets.

The Pitzer database *data0.ypf* is divided in four sections composed of data blocks containing thermodynamic data representing: 1) coefficient data for temperature-dependent interaction

parameters defined in the Pitzer standard formulations in accord with the 3-4 term 25 °C-centric parameter equation to describe temperature dependence (see Section I-3.2) and implemented in the code *EQ3/6 Version 8.0*; 2) selected log Ks for ion pair speciation reactions; 3) log Ks for solids obtained from existing thermodynamic data compilations except those salts for which log K values were obtained in the current effort; and 4) log K solubility data for selected gases also from existing data compilations.

A thorough evaluation of existing Pitzer parameter data is required for inclusion into the database. The criteria used for accepting data from a published source are as follows:

Criterion 1: Pitzer ion-interaction parameters for a specific electrolyte should be reproduced by the equations given by the source publication to express their temperature dependence. Failure to satisfy this criterion will result in either rejection of the data or refitting of actual parameter if tabulated in the source. Parameter data given only at 25 °C do not need to satisfy this criterion since they don't require refitting.

Criterion 2: Pitzer parameter data satisfying criterion 1 for a given range of temperatures and electrolyte concentrations will be used in the conversion (if necessary) and refitting procedures described in sections I-4.1, I-4.2, and I-4.3. Upon refitting to the temperature function embedded in *EQ3/6 Version 8.0* (see section I-3.2.1.3), the ion interaction parameters are compared to check that these closely match the input values obtained from the source. The comparison between refitted and input values of osmotic coefficients should be a close match (see comparison analyses in the attached spreadsheets). Failure to satisfy this criterion will result in rejection of parameter data. Parameter data given only at 25 °C do not need to satisfy this criterion since these doesn't need refitting.

Further tests in most of the fitted parameter data involve comparison of experimentally determined osmotic coefficients for specific electrolytes from alternate sources. Due to the limited amount of osmotic coefficient data available for many electrolytes of interest, this comparison is not done on all binary parameters considered in this attachment. Nevertheless, it represents a robust validation of the predictive capabilities of the database. This test does not apply to parameter data obtained only at 25 °C.

Most of the log K data for solids comes from one source (e.g., data0.ymp.R2). Only few log K values for salt solids are needed and these were obtained through a calibration method bound by tabulated salt solubilities and the compiled Pitzer activity model. Calibration of solubility constants or log Ks for the salt solids is achieved by fitting log K values to the salt saturation molality using the obtained Pitzer activity model. Saturation molalities for salt solids as a function of temperature are obtained from tabulated handbook data or peer-review journals. For comparison, the resulting log K values are then compared to those obtained by using tabulated standard Gibbs free energy data (e.g., Robie and Hemingway, 1995). The percent difference in log K values between those obtained through calibration and those from tabulated thermodynamic data should be less than 15%. Percent differences exceeding the latter value should be regarded as unsatisfactory and will not be considered for inclusion in the database. All log K values obtained for the salt solids through the calibration method have percent differences of less than 10% rendering the calibrated values as satisfactory within the predictive capabilities of the database.

I-3 PITZER ION-INTERACTION MODEL

The theory behind the development of Pitzer equations for describing the thermodynamic properties of electrolyte solutions is rather complex, and a detailed description goes beyond the scope needed for this thermodynamic database description. The interested reader should consult the works of Pitzer (1973; 1991 and references therein) for details on fundamental theoretical groundwork on the formalism and applications of this thermodynamic model as applied to concentrated aqueous electrolyte solutions. Basically, the Pitzer model is an extension of the Debye-Hückel model for ionic solutions. Ion interactions beyond the Debye-Hückel approximation are represented by a set of ion-interaction coefficients that form an integral feature of Pitzer semi-empirical equations. These equations are described in detail in the *EQ3/6 Version 8.0 User Manual* (SDN: 10813-UM-8.0-00). For completeness, the fundamental equations pertinent to pure aqueous electrolytes and mixtures will be briefly summarized here.

I-3.1 GENERAL PITZER ELECTROLYTE THEORY

The starting point for the formulation of Pitzer's model is the equation for the excess Gibbs free energy (G^{EX}) of the total solution:

$$G^{\text{EX}}/w_w = RT \sum_i m_i (1 - \phi + \ln \gamma_i) \quad (\text{I-1})$$

where G^{EX} is the difference or "excess" in the Gibbs free energy between a real solution and an ideal solution defined on the molality composition scale, w_w is the mass of water in the solution in kilograms, m_i is the molality of the i th type of ion, ϕ is the molality based osmotic coefficient of the solvent, and γ_i is the molality based activity coefficient of the i th type of ion. R is the universal gas constant and T is the absolute temperature. Once an expression has been assumed for the dependence of G^{EX} on the ionic composition of the solution, the osmotic coefficient of the solvent and the activity coefficient of each ionic solute may be calculated by taking the appropriate partial derivatives:

$$\ln \gamma_i = [\partial \{G^{\text{EX}}/RTw_w\} / \partial m_i]_{n_w} \quad (\text{I-2})$$

$$\phi = 1 - [\partial \{G^{\text{EX}}/RT \sum_i m_i\} / \partial w_w]_{n_i} \quad (\text{I-3})$$

where n_w and n_i are the numbers of moles of water and of ion i , respectively. The osmotic coefficient is directly related to the water activity of the solution, a_w , by the relation:

$$\ln a_w = -(\sum_i m_i) \phi / \Omega \quad (\text{I-4})$$

where the quantity $\Omega = (1\text{kg}/0.018015 \text{ kg}\cdot\text{mol}^{-1}) = 55.508 \text{ mol}\cdot\text{kg}^{-1}$ is the number of moles of water present in one kilogram of water.

Pitzer (1973) initially wrote his expression for G^{EX} in the following form (except for minor differences in notation):

$$G^{\text{EX}}/(RT) = w_w f^G(I) + (1/w_w) \sum_{ij} \lambda_{ij}(I) n_i n_j + (1/w_w^2) \sum_{ijk} \mu_{ijk} n_i n_j n_k \quad (\text{I-5})$$

where $f^G(I)$ represents the total contribution of long-range electrostatic forces between ions, $\lambda_{ij}(I)$ represents the short-range specific interactions between pairs of ions i and j , and μ_{ijk} represents the short-range specific interactions between triplets of ion i , j , and k . The $f(I)$ and $\lambda_{ij}(I)$ are assumed to be functions of the ionic strength I . The ionic strength of the solution is defined on the molality concentration scale as:

$$I = (1/2) \sum_i m_i z_i^2 \quad (\text{I-6})$$

where z_i is the valence of the i th ion. Pitzer tested two different variants of the Debye-Hückel equation for the long-range electrostatic term, and selected the Debye-Hückel “osmotic” function. For the osmotic coefficient, this function has the form:

$$f^\phi(I) = -A_\phi \sqrt{I} / (1 + b \sqrt{I}) \quad (\text{I-7})$$

where $f^\phi(I)$ depends only on the ionic strength I , and A_ϕ is the Debye-Hückel limiting law slope for the osmotic coefficient. Pitzer further selected $b = 1.2$ for all aqueous electrolytes, assumed that the λ_{ij} and μ_{ijk} functions are symmetrical in their indices, e.g. $\lambda_{ij} = \lambda_{ji}$, and noted that the ratios of moles of solute ion i to the number of kilograms of water yields the molality of that ion, i.e. $n_i/w_w = m_i$.

The corresponding equation for the Debye-Hückel “osmotic” function $f^G(I)$ for the excess Gibbs free energy is:

$$f^G(I) = -(4IA_\phi/b) \ln(1 + b \sqrt{I}) \quad (\text{I-8})$$

Similarly, Debye-Hückel “osmotic” function $f'(I)$ for the activity coefficient is:

$$f'(I) = -A_\phi \{ \sqrt{I} / (1 + b \sqrt{I}) + (2/b) \ln(1 + b \sqrt{I}) \} \quad (\text{I-9})$$

I-3.1.1 Pitzer’s Model for Aqueous Binary Electrolytes

Equation (I-5) could be used as the starting point for deriving the expressions for the thermodynamic properties of the solvent and the solute ions. However, Pitzer (1973) rewrote his equations in terms of B_{MX} and C_{MX} functions which are now more commonly used, and which will be used in the subsequent discussion. Anyone interested in the explicit equations for ϕ and $\ln \gamma_i$ written in terms of the λ_{ij} and μ_{ijk} should consult Pitzer’s (1973, 1991) publications and SNL

(2003). The equations relating these two types of functions for a single aqueous electrolyte containing a cation M and anion X are:

$$B_{MX}^{\phi}(I) = \lambda_{MX} + I\lambda_{MX}' + (v_M/2v_X)(\lambda_{MM} + I\lambda_{MM}') + (v_X/2v_M)(\lambda_{XX} + I\lambda_{XX}') \quad (I-10)$$

and

$$C_{MX}^{\phi} = 3(v_M\mu_{MMX} + v_X\mu_{MXX})/\sqrt{v_M v_X} \quad (I-11)$$

where the primes denote the derivative of a function with regard to the ionic strength (e.g., $\lambda_{MX}' = \partial\lambda_{MX}/\partial I$), v_M is the stoichiometric number of cations formed by dissociation of one molecule of the solute, and v_X is the stoichiometric number of anions formed by dissociation of one molecule of the solute.

Pitzer (1973) allowed the $B_{MX}^{\phi}(I)$ to vary with the ionic strength, but assumed that C_{MX}^{ϕ} could be approximated as a parameter that is independent of ionic strength but which may vary with temperature and pressure. After testing two possible variants for the ionic-strength dependence of $B_{MX}^{\phi}(I)$, Pitzer (1973, 1991) chose the functional form,

$$B_{MX}^{\phi}(I) = \beta_{MX}^{(0)} + \beta_{MX}^{(1)} \cdot e^{-\alpha_1 \sqrt{I}} + \beta_{MX}^{(2)} \cdot e^{-\alpha_2 \sqrt{I}} \quad (I-12)$$

The $\beta_{MX}^{(2)} \cdot e^{-\alpha_2 \sqrt{I}}$ term is normally included only when modeling the thermodynamic properties of divalent metal sulfates and other high-valence electrolytes that exhibit significant association at low ionic strengths, but it is set equal to zero for strong electrolytes. The $\beta_{MX}^{(0)}$, $\beta_{MX}^{(1)}$, $\beta_{MX}^{(2)}$, and C_{MX}^{ϕ} coefficients are usually referred to as ion-interaction or Pitzer parameters. These Pitzer parameters may vary with temperature and pressure, but they do not depend on the ionic strength. The exponential coefficient α_1 is generally fixed at $\alpha_1 = 2.0$ for strong electrolytes, but for divalent metal sulfates and other 2:2 type electrolytes its value is usually fixed at $\alpha_1 = 1.4$ (Pitzer, 1991). The value of α_2 for 2:2 type electrolytes is usually fixed at $\alpha_2 = 12.0$ at 25.0 °C (298.15 K), but α_2 is either kept at this same value all other temperatures or is assumed to vary with temperature as $\alpha_2 = k \cdot A_{\phi}$, where k is a constant (Pitzer, 1991).

In terms of these ion-interaction parameters, the Pitzer equation for a binary electrolyte solution has the familiar form:

$$\phi = 1 - |z_M z_X| A_{\phi} \sqrt{I} / (1 + b \sqrt{I}) + \{2(v_M v_X)/v\} m \{ \beta_{MX}^{(0)} + \beta_{MX}^{(1)} \cdot e^{-\alpha_1 \sqrt{I}} + \beta_{MX}^{(2)} \cdot e^{-\alpha_2 \sqrt{I}} \} + \{2(v_M v_X)^{3/2}/v\} m^2 \cdot C_{MX}^{\phi} \quad (I-13)$$

for the osmotic coefficient, where m denotes the stoichiometric molality of the solution. For the mean molal activity coefficient γ_{\pm} of the electrolyte:

$$\begin{aligned}
\ln \gamma_{\pm} = & -|z_M z_X| A_{\phi} \{ \sqrt{I} / (1 + b\sqrt{I}) + (2/b) \ln(1 + b\sqrt{I}) \} + \{ 2(v_M v_X)/v \} m [2\beta_{MX}^{(0)} \\
& + 2 \{ \beta_{MX}^{(1)} / \alpha_1^2 I \} \{ 1 - (1 + \alpha_1 \sqrt{I} - \alpha_1^2 I/2) e^{-\alpha_1 \sqrt{I}} \} \\
& + 2 \{ \beta_{MX}^{(2)} / \alpha_2^2 I \} \{ 1 - (1 + \alpha_2 \sqrt{I} - \alpha_2^2 I/2) e^{-\alpha_2 \sqrt{I}} \}] \\
& + \{ 3(v_M v_X)^{3/2} / v \} m^2 \cdot C_{MX}^{\phi}
\end{aligned} \tag{I-14}$$

The corresponding expression for the excess Gibbs free energy is:

$$\begin{aligned}
G^{EX}/(n_w RT) = & -(4IA_{\phi}/b) \ln(1 + b\sqrt{I}) + (2v_M v_X) m^2 [\beta_{MX}^{(0)} \\
& + 2 \{ \beta_{MX}^{(1)} / \alpha_1^2 I \} \{ 1 - (1 + \alpha_1 \sqrt{I}) e^{-\alpha_1 \sqrt{I}} \} \\
& + 2 \{ \beta_{MX}^{(2)} / \alpha_2^2 I \} \{ 1 - (1 + \alpha_2 \sqrt{I}) e^{-\alpha_2 \sqrt{I}} \}] \\
& + (v_M z_M) m C_{MX}
\end{aligned} \tag{I-15}$$

where

$$C_{MX} = (C_{MX}^{\phi} / 2 \sqrt{|z_M z_X|}) \tag{I-16}$$

I-3.1.2 Pitzer's Model for Aqueous Electrolyte Mixtures

The corresponding Pitzer model equations for mixed electrolyte solutions of arbitrary complexity are more complicated, in part because they include mixing terms. For a system containing anions a and cations c (anions and cations chemically distinct from a and c are denoted with primes), the excess Gibbs free energy is given:

$$\begin{aligned}
G^{EX}/(w_w RT) = & f^G(I) + 2 \sum_c \sum_a m_c m_a [B_{ca} + (\sum_c m_c z_c) C_{ca}] \\
& + \sum_{c \neq c'} \sum m_c m_{c'} [2\Phi_{cc'} + \sum_a m_a \Psi_{cc'a}] \\
& + \sum_{a \neq a'} \sum m_a m_{a'} [2\Phi_{aa'} + \sum_c m_c \Psi_{caa'}]
\end{aligned} \tag{I-17}$$

where $f^G(I)$ was defined by equation (I-8), and C_{ca} is equivalent to C_{MX} defined by equation (I-16). The B_{ca} term is a function of the ion-interaction parameters and the ionic strength as given by:

$$\begin{aligned}
B_{ca} = & \beta_{ca}^{(0)} + 2 \{ \beta_{ca}^{(1)} / \alpha_1^2 I \} \{ 1 - (1 + \alpha_1 \sqrt{I}) e^{-\alpha_1 \sqrt{I}} \} \\
& + 2 \{ \beta_{ca}^{(2)} / \alpha_2^2 I \} \{ 1 - (1 + \alpha_2 \sqrt{I}) e^{-\alpha_2 \sqrt{I}} \}
\end{aligned} \tag{I-18}$$

The $\Psi_{cc'a}$ and $\Psi_{caa'}$ are mixing parameters for interactions among three distinct ions, two of which are of the same sign and the other is of opposite sign, and the $\Phi_{cc'}$ and $\Phi_{aa'}$ are mixing functions

for two different ions of the same sign. The $\Phi_{cc'}$ and $\Phi_{aa'}$ mixing functions will be described in more detail below.

The corresponding expression for the osmotic coefficient of the mixed electrolyte solutions of arbitrary complexity is given by (Pitzer, 1991):

$$\begin{aligned} \phi = 1 - (2/\sum_i m_i)[-A_\phi I^{3/2}/(1 + b\sqrt{I}) + \sum_c \sum_a m_c m_a \{B_{ca}^\phi(I) + ZC_{ca}\} \\ + \sum_{c \neq c'} \sum m_c m_{c'} [(\Phi_{cc'} + I\Phi_{cc'}) + \sum_a m_a \psi_{cc'a}] + \sum_{a \neq a'} \sum m_a m_{a'} [(\Phi_{aa'} + I\Phi_{aa'}) + \sum_c m_c \psi_{caa'}] \end{aligned} \quad (I-19)$$

where

$$Z = \sum_i m_i |z_i| \quad (I-20)$$

is the total ionic molality. For a particular cation in this mixture, M, the ionic activity coefficient is given by:

$$\begin{aligned} \ln \gamma_M = z_M^2 F + \sum_a m_a (2B_{Ma} + ZC_{Ma}) + \sum_c m_c (2\Phi_{Mc} + \sum_a m_a \psi_{Mca}) \\ + \sum_{a \neq a'} \sum m_a m_{a'} \psi_{Maa'} + z_M \sum_c \sum_a m_c m_a C_{ca} \end{aligned} \quad (I-21)$$

and for a particular anion in this mixture, X, the ionic activity coefficient is given by:

$$\begin{aligned} \ln \gamma_X = z_X^2 F + \sum_c m_c (2B_{cX} + ZC_{cX}) + \sum_a m_a (2\Phi_{Xa} + \sum_c m_c \psi_{cXa}) \\ + \sum_{c \neq c'} \sum m_c m_{c'} \psi_{cc'X} + |z_X| \sum_c \sum_a m_c m_a C_{ca} \end{aligned} \quad (I-22)$$

The quantity F that is present in both equations (I-21) and (I-22) includes the Debye-Hückel “osmotic” function $f^\phi(I)$ along with several other terms:

$$F = f^\phi(I) + \sum_c \sum_a m_c m_a B_{ca}' + \sum_{c \neq c'} \sum m_c m_{c'} \Phi_{cc'}' + \sum_{a \neq a'} \sum m_a m_{a'} \Phi_{aa'}' \quad (I-23)$$

where $\Phi_{cc'}' = (\partial\Phi_{cc'}/\partial I)$, $\Phi_{aa'}' = (\partial\Phi_{aa'}/\partial I)$, and $B_{ca}' = (\partial B_{ca}/\partial I)$ are the ionic strength derivatives of the corresponding functions.

Equations (I-17), (I-19), and (I-21) through (I-13) contain the $\Phi_{cc'}$ and $\Phi_{aa'}$ and/or $\Phi_{cc'}'$ and $\Phi_{aa'}'$ mixing functions. For the ions i and j this function can be rewritten as

$$\Phi_{ij} = {}^S\theta_{ij} + {}^E\theta_{ij}(I) \quad (I-24)$$

The values of the high-order electrostatic function ${}^E\theta_{ij}(I)$ may be calculated from theory as described by Pitzer (1991). For ions of opposite charge, and for ions of the same sign and electrical charge, ${}^E\theta_{ij}(I) = 0$, and the mixing function Φ_{ij} becomes equal to a simple (ionic strength independent) fitting parameter θ_{ij} . However, when the ions i and j are of the same sign

but have different charges, then equation (I-24) should be used. Numerical analysis of integrals contributing to ${}^E\theta_{ij}(I)$ is discussed by Pitzer (1991). For further details see SNL (2003), equations B-134 through B-147. The code *EQ3/6* includes ${}^E\theta_{ij}(I)$ in the calculation of Φ_{ij} whenever appropriate.

According to Pitzer's model (Pitzer, 1991), the thermodynamic properties of an electrolyte solution of arbitrary complexity may be represented using only the $\beta_{MX}^{(0)}$, $\beta_{MX}^{(1)}$, $\beta_{MX}^{(2)}$ (if needed), and C_{MX}^ϕ ion-interaction parameters for binary solutions, the two-ion ${}^S\theta_{MM'}$ and ${}^S\theta_{XX'}$ and the three-ion $\psi_{MM'X}$ and $\psi_{MXX'}$ mixing parameters. Within the framework of this model, the values of the mixing parameters are independent of the possible presence of other types of ions in the solution, and once their values have been determined for a particular system, then the same values may be used for all other systems. However, *in a thermodynamically consistent database, it is essential that same values of the mixing parameters be used for all systems containing those particular combinations of anions and cations.*

I-3.1.3 Extension of Pitzer's Model to Include Dissolved Neutral Molecules

The equations given above apply to single electrolytes and to their mixtures. Neutral chemical species including dissolved gases such as $O_2(aq)$, $CO_2(aq)$, or $NH_3(aq)$, and non-electrolytes such as $SiO_2(aq)$, are often present at low concentrations in natural waters and brines. Pitzer's ion-interaction model can be modified to include the effects of neutral solutes, by adding terms arising from the interactions between different neutral species, terms for the interactions between neutral species and the cations, and terms for the interactions between neutral species and the anions. For the excess Gibbs free energy, for example, Pitzer (1991) added interaction terms of the form $m_n m_c \lambda_{nc}$, $m_n m_a \lambda_{na}$, $m_n m_n' \lambda_{nn'}$, and $m_n^2 \lambda_{nn}$ for binary interactions, and terms of the form $m_n m_n' m_c \mu_{nn'c}$, $m_n m_n' m_a \mu_{nn'a}$, $m_n m_c m_a \mu_{nca}$, etc. for ternary interactions. Pitzer also defined two additional quantities, ζ_{nca} and η_{ncc} , that are linear combinations of the μ_{ijk} . A detailed presentation of the equations for the interactions neutral species and electrolytes is beyond the scope of this document, but detailed presentations are available in Appendix F of Pitzer's review (1991), in the article by Clegg and Brimblecombe (1990c), and in SNL (2003).

I-3.1.4 Thermodynamic Data Used to Derive Parameters of Pitzer's Model

The ion-interaction parameters of Pitzer's model are empirical parameters. That is, they are obtained by fitting their values to best represent the experimental thermodynamic properties of aqueous electrolyte solutions. For most fairly soluble electrolytes, the types of thermodynamic data typically used to determine the Pitzer parameters are osmotic coefficients (generally obtained from isopiestic measurements), the emfs of reversible electrochemical cells, enthalpies of dilution, and heat capacities. Mixing parameters are frequently obtained for solutes of limited solubility by modeling the variation of solubility of that component with changes in the molalities of the other solutes. These less soluble solutes include many important salts such as gypsum and calcite, $CaSO_4 \cdot 2H_2O(cr)$ and $CaCO_3(cr)$, and dissolved atmospheric gases such as $O_2(aq)$ and $CO_2(aq)$ that affect E_h and pH of solutions.

The Debye-Hückel limiting law slope used in Pitzer's model, A_ϕ , is that for the osmotic coefficient. Other authors sometimes present their equations in terms of the Debye-Hückel limiting law slope for activity coefficient, A_γ , where $A_\phi = A_\gamma/3$. Also, some values of A_γ reported in the literature may also differ by a factor of $\ln(10) = 2.302585$, depending on whether the equations are written in terms of the decadic (natural) logarithm of the activity coefficient or in terms of the decadic (base 10) logarithm of the activity coefficient. See Pitzer (1973, 1991) for a definition of A_ϕ in terms of fundamental constants and the properties of pure water.

I-3.2 Temperature Functions for Pitzer Interaction Parameters

Extension of the Pitzer approach to temperatures above 25 °C is necessary to expand its application to concentrated electrolyte solutions in many natural systems. The works of Møller (1988), and Greenberg and Møller (1989) exemplify such efforts by generating empirical functions that fit Pitzer interaction parameters as a function of both ionic strength (I) and temperature. Their approach utilizes a formulation containing eight fitting coefficients to describe the variations in the Pitzer interaction parameter as a function of temperature:

$$\chi(T) = a_1 + a_2 T + \frac{a_3}{T} + a_4 \ln T + \frac{a_5}{(T - 263)} + a_6 T^2 + \frac{a_7}{(680 - T)} + \frac{a_8}{(T - 227)} \quad (\text{I-25})$$

where χ represents any parameter of interest within the Pitzer model [Møller (1988) and Greenberg and Møller (1989) used "P" in their notation], and T corresponds to the absolute temperature. $a_1, a_2, a_3, \dots, a_8$ are the coefficients used for fitting the temperature dependence of the parameter. Some parameters will generate relatively smooth curves with a very small number or no additional fitting coefficients. Therefore, not all seven or eight parameters will be needed. Sometimes a parameter will exhibit a different set of fitting terms between different temperature ranges, but this is rarely observed. When mixed electrolytes are modeled, then one must be cautious on how to approach the problem, checking always for internal consistency in the data being used and how it applies to the model.

Variations in Pitzer's equations have been developed to explain data for relatively simple experimental systems. These variations may include the use of non-customary values for the Pitzer alpha coefficients, addition of terms to temperature functions in order to fit data to very high temperatures, and including or excluding species such as ion pairs, complexes (along with their association constants) and partially dissociated acids. When combining results from these modified Pitzer models, these variations must be dealt with to obtain an internally consistent database.

Temperature functions have been developed to support the calculation of activity coefficients in geochemical models that are valid for the temperature ranges and chemical species considered. These will be compared with the functions used by Greenberg and Møller (1989) as well as experimental data.

I-3.2.1 Models

All of the following models are suggested by the van't Hoff equation, the most common expression of which is (e.g., Garrels and Christ, 1990, eq 9.100, p. 348):

$$\frac{\partial \ln K}{\partial T} = \frac{\Delta H_r^o}{RT^2} \quad (\text{I-26})$$

where K is an equilibrium constant, T is the absolute temperature, ΔH_r^o is the standard partial molar enthalpy of reaction, and R is the universal gas constant. This equation is often used as a basis for computing the temperature dependence of equilibrium constants. The general integrated form can be written as:

$$\ln K(T) = \ln K(T_0) + \int_{T_0}^T \frac{\Delta H_r^o}{RT^2} dT \quad (\text{I-27})$$

where T_0 is normally 298.15K (25°C). As an example, the “constant enthalpy” approximation sometimes used in low-temperature geochemical modeling is given by:

$$\ln K(T) = \ln K(T_0) - \frac{\Delta H_r^o}{R} \left[\frac{1}{T} - \frac{1}{T_0} \right] \quad (\text{I-28})$$

More generally, it is recognized that ΔH_r^o is itself a function of temperature. A key relationship is:

$$\frac{\partial \Delta H_r^o}{\partial T} = \Delta C_{p,r}^o \quad (\text{I-29})$$

where $\Delta C_{p,r}^o$ is the standard partial molar heat capacity (at constant pressure) of reaction. This in turn is given by:

$$\Delta C_{p,r}^o = \sum_i b_{ir} C_{p,i}^o \quad (\text{I-30})$$

where the b_{ir} are reaction coefficients (defined as positive for products, negative for reactants) and $C_{p,i}^o$ is the standard molal heat capacity of the i^{th} chemical species. Although the heat capacity of a species can be treated as a constant, usually it is represented by some temperature function, such as the Maier-Kelley formula (cf. Nordstrom and Munoz, 1985, p. 56) that is commonly applied to describe the heat capacities of solids:

$$C_{p,i}^o = a + bT - \frac{c}{T^2} \quad (\text{I-31})$$

The van't Hoff relation can also be written as:

$$\frac{\partial(\Delta G_r^o / RT)}{\partial T} = \frac{-\Delta H_r^o}{RT^2} \quad (\text{I-32})$$

(recall that $\Delta G_r^o = -RT \ln K$). A more general “van't Hoff” relationship is given by:

$$\frac{\partial(G / RT)}{\partial T} = \frac{-H}{RT^2} \quad (\text{I-33})$$

where G is any type of Gibbs energy (for a reaction or a species, total, standard, ideal, or excess) and H is the corresponding enthalpy. Activity coefficients have a defining relationship with the excess Gibbs energy (cf. Pitzer 1973):

$$\ln \gamma_i = \frac{G_i^{EX}}{RT} \quad (\text{I-34})$$

where γ_i is the activity coefficient of the i^{th} chemical species and G_i^{EX} is the excess partial molar Gibbs energy of the same species (note that $G_i^{EX} = \partial G^{EX} / \partial n_i$, where G^{EX} is the excess Gibbs energy, and n_i is the number of moles of the i^{th} species). The above two equations can be combined to yield:

$$\frac{\partial \ln \gamma_i}{\partial T} = \frac{-H_i^{EX}}{RT^2} \quad (\text{I-35})$$

where H_i^{EX} is the excess partial molar enthalpy of the i^{th} species. This equation can be viewed as the van't Hoff equation for activity coefficients.

In Pitzer's equations, $\ln \gamma_i$ depends on a series of terms that are linear with respect to the interaction coefficients. The dependence of the activity coefficient of an ion in solution on the second-order $\beta_{ij}^{(0)}$ parameter is expressed by:

$$\ln \gamma_i = \dots + \beta_{ij}^{(0)} m_j + \dots \quad (\text{I-36})$$

(this parameter is second-order because in the equation for the total excess Gibbs energy of the solution, it appears multiplied by $m_i m_j$). This line of thinking suggests the following van't Hoff equation for interaction parameters:

$$\frac{\partial \chi}{\partial T} = \frac{-\chi^{(H)}}{RT^2} \quad (\text{I-37})$$

where χ is any interaction parameter (either second- or third-order; $\beta_{ij}^{(0)}$, $\beta_{ij}^{(1)}$, $\beta_{ij}^{(2)}$, C_{ijk}^φ , θ_{ij} , ψ_{ijk} , ζ_{ijn} , λ_{in} , or λ_{nm}) and $\chi^{(H)}$ is the corresponding parameter appearing in the calculation of the excess partial molar enthalpy. It follows that:

$$\frac{\partial \chi^{(H)}}{\partial T} = \chi^{(C_p)} \quad (\text{I-38})$$

where $\chi^{(C_p)}$ is the corresponding parameter appearing in the calculation of the excess partial molar heat capacity.

I-3.2.1.1 Constant Enthalpy

The simplest case is for the equivalent of constant enthalpy. Letting $b_1 = \chi^{(H)}$, one can write that:

$$\frac{\partial \chi}{\partial T} = \frac{-b_1}{RT^2} \quad (\text{I-39})$$

Integration then yields:

$$\chi = b_0 + \frac{b_1}{R} \left[\frac{1}{T} - \frac{1}{T_0} \right] \quad (\text{I-40})$$

where $b_0 = \chi(T_0)$. This can also be written as:

$$\chi = a_0 + \frac{a_1}{T} \quad (\text{I-41})$$

where:

$$a_0 = b_0 - \frac{b_1}{RT_0} \quad (\text{I-42})$$

$$a_1 = \frac{b_1}{R} \quad (\text{I-43})$$

Comparison of Equation I-41 with Equation I-25 shows that the former is a subset of the latter (allowing for a different system of numbering the coefficients). What this suggests is that the constant and $1/T$ terms in Equation I-25 are likely the most important, in terms of having a physical basis.

I-3.2.1.2 Constant Heat Capacity

Here one begins by writing $b_2 = \chi^{(C_p)}$. The first integration yields:

$$\chi^{(H)} = b_1 + b_2(T - T_0) \quad (\text{I-44})$$

where $b_1 = \chi^{(H)}(T_0)$. The second integration, this time using the “van’t Hoff relation,” gives:

$$\chi = b_0 + \frac{(b_1 - b_2 T_0)}{R} \left[\frac{1}{T} - \frac{1}{T_0} \right] - \frac{b_2}{R} (\ln T - \ln T_0) \quad (\text{I-45})$$

where once more $b_0 = \chi(T_0)$. This can also be written as:

$$\chi = a_0 + \frac{a_1}{T} + a_2 \ln T \quad (\text{I-46})$$

where:

$$a_0 = b_0 + \frac{b_2}{R} - \frac{b_1}{RT_0} + \frac{b_2}{R} \ln T_0 \quad (\text{I-47})$$

$$a_1 = \frac{b_1 - b_2 T_0}{R} \quad (\text{I-48})$$

$$a_2 = -\frac{b_2}{R} \quad (\text{I-49})$$

Comparison of Equation I-46 with Equation I-25 will show that the former, like Equation I-41, is a subset of the latter (again allowing for a different system of numbering the coefficients). What this suggests is that after the constant and $1/T$ terms in Equation I-25, the term in $\ln T$ is likely the most important term in terms of having a physical basis.

I-3.2.1.3 Parabolic Heat Capacity

The standard partial molar heat capacity of aqueous electrolytes does not closely follow the Maier-Kelley form commonly exhibited by solids. Rather, it is described by temperature functions that appear parabolic, at least to a first order (cf. Helgeson et al., 1981, p. 1413–1426). Here it is assumed that $\chi^{(C_p)}$ will behave in a similar fashion. One may then write:

$$\chi^{(C_p)} = b_2 + b_3(T - T_x)^2 \quad (\text{I-50})$$

where $b_2 = \chi^{(C_p)}(T_0)$ and T_x is some temperature that may be unique for each distinct Pitzer interaction parameter. If that is so, then in effect, a five-parameter model is obtained. Differentiation gives:

$$\frac{d\chi^{(C_p)}}{dT} = 2b_3(T - T_x) \quad (\text{I-51})$$

The extremis of the parabola occurs where this derivative is zero: that is, where $T = T_x$. Another step of differentiation gives:

$$\frac{d^2\chi^{(C_p)}}{dT^2} = 2b_3 \quad (\text{I-52})$$

The parabola will be convex up (the extremis will be a maximum) if b_3 is negative. Otherwise, it will be convex down (the extremis will be a minimum). Actual examples of the standard partial molar heat capacity of aqueous electrolytes are convex up, and the maximum of curves that visually resemble parabolas occurs at various different values of T (cf. Helgeson, Kirkham, and Flowers, 1981, p. 1413–1424). Thus, b_3 is expected to be a negative number.

The first integration yields:

$$\chi^{(H)} = b_1 + b_2(T - T_0) + b_3 \left(\frac{(T^3 - T_0^3)}{3} - T_x(T^2 - T_0^2) + T_x^2(T - T_0) \right) \quad (\text{I-53})$$

where again $b_1 = \chi^{(H)}(T_0)$. Before continuing, it is convenient to rearrange this into terms organized by power of T :

$$\chi^{(H)} = \left[b_1 - b_2T_0 - b_3 \left(T_x^2T_0 - T_xT_0^2 + \frac{T_0^3}{3} \right) \right] + [b_2 + b_3T_x^2]T - [b_3T_x]T^2 + \left[\frac{b_3}{3} \right]T^3 \quad (\text{I-54})$$

More simply, this can be written as:

$$\chi^{(H)} = c_1 + c_2T + c_3T^2 + c_4T^3 \quad (\text{I-55})$$

where c_1 , c_2 , c_3 , and c_4 are given by the corresponding quantities in parentheses squared brackets in Equation I-54. The second integration, performed after substituting Equation I-55 into the “van’t Hoff relation,” gives:

$$\chi = c_0 + \frac{c_1}{R} \left(\frac{1}{T} - \frac{1}{T_0} \right) - \frac{c_2}{R} (\ln T - \ln T_0) - \frac{c_3}{R} (T - T_0) - \frac{c_4}{2R} (T^2 - T_0^2) \quad (\text{I-56})$$

where $c_0 = \chi(T_0)$; in order to complete the relationships between the b and c coefficients, one may take that $c_0 = b_0$. Rearranging Equation I-56 into terms organized by power of T gives:

$$\chi = \left[c_0 - \frac{c_1}{RT_0} + \frac{c_2}{R} \ln T_0 + \frac{c_3}{R} T_0 + \frac{c_4}{2R} T_0^2 \right] + \left[\frac{c_1}{R} \right] \frac{1}{T} + \left[\frac{-c_2}{R} \right] \ln T + \left[\frac{-c_3}{R} \right] T + \left[\frac{-c_4}{2R} \right] T^2 \quad (\text{I-57})$$

This can be written more simply as:

$$\chi = a_0 + \frac{a_1}{T} + a_2 \ln T + a_3 T + a_4 T^2 \quad (\text{I-58})$$

where a_0 , a_1 , a_2 , a_3 , and a_4 are given by the corresponding quantities in square brackets in Equation I-57. Equation I-58 as implemented in *EQ3/6 Version 8.0* only takes into account up to the a_3 coefficient term. Also, the increasing order of coefficients is shifted by one as defined in the *data0.ypf*. That is, a_0 in Equation I-58 equals a_1 in the *data.ypf* database and so on. The T^2 term in Equation I-58 is not used in the *data0.ypf*.

The additional terms in T and T^2 are also present in Equation I-25. The presence of T_x in the equation for the heat capacity interaction parameter has resulted in a five-, not a four-parameter model, though T_x itself does not appear explicitly in the final result as represented by Equation I-58.

Note that the addition of a term linear in T to the equation for $\chi^{(C_p)}$ would not result in an additional term in the equivalent of Equation I-58. Adding such a term to Equation I-50 gives:

$$\chi^{(C_p)} = b_2 + b_3(T - T_x) + b_4 T \quad (\text{I-59})$$

This would add a term in T^2 in the corresponding equation for $\chi^{(H)}$. Substitution of that result into the “van’t Hoff” relation would just add to the constant term under the integral. After integration, this would result in additional contributions to a_0 and a_3 in Equation I-58, but no new term. Similarly, adding a term in T^2 to the equation for $\chi^{(C_p)}$ would result in no new term in the equivalent of Equation I-58.

I-3.2.1.4 Other Comments on Existing Temperature Functions

Recall that Equation I-25 is:

$$\chi(T) = a_1 + a_2 T + \frac{a_3}{T} + a_4 \ln T + \frac{a_5}{(T - 263)} + a_6 T^2 + \frac{a_7}{(680 - T)} + \frac{a_8}{(T - 227)}$$

The terms not suggested by the theoretical analysis given above are the fifth, seventh, and eighth. Each of these terms has the difference between T and some constant in the denominator, and thus a singularity. These occur at -10.15 , 406.85 , and -46.15 °C, respectively. The fifth and seventh terms trace back to Rogers and Pitzer (1981). They have no theoretical origin, but were introduced as empirical devices to assist in fitting data for the system $\text{Na}_2\text{SO}_4\text{-H}_2\text{O}$ over a wide range of temperatures. The eighth term is from Pitzer et al. (1984), who used it to fit data for the system $\text{NaCl-H}_2\text{O}$ over a very wide temperature range. Again, the origin of the term was purely empirical. The singularity at 406.85 °C (680 K) is well above the critical temperature of water.

Spencer et al.(1990) developed a model for the system Na-K-Ca-Mg-Cl-SO₄-H₂O for the temperature range -60 to +25°C. They recognized the above-noted singularities (two of which were in their target range) and eliminated them by using a function of the form:

$$\chi(T) = a_1 + a_2 T + \frac{a_3}{T} + a_4 \ln T + a_6 T^2 + a_9 T^3 \quad (\text{I-60})$$

All but one of the terms in this equation carry forward from Equation I-25. The origin of the new term in T^3 is obscure. Spencer et al. (1990) do not discuss it; nor do they discuss the consequences of not including this term. They do use the new term universally in their model, applying it not only to Pitzer interaction coefficients, but also to the A^φ Debye-Hückel parameter and the dimensionless standard chemical potentials (μ^0/RT) of both aqueous species and minerals. This term would imply a term in T^2 in the equation for $\chi^{(H)}$ and one in T^3 in the equation for $\chi^{(C_p)}$.

I-4 EVALUATION, COMPILATION AND CONVERSION OF PITZER INTERACTION PARAMETERS FROM PUBLISHED SOURCES

As part of the current effort to develop an internally consistent thermodynamic Pitzer parameter database for *EQ3/6 Version 8.0* an extensive search for Pitzer interaction parameters and experimental data from the scientific literature was undertaken for ionic species of interest to the Yucca Mountain Project. Because operating temperatures in the repository are expected to rise substantially above the boiling temperature of water, the primary focus of the work was on developing the Pitzer parameter database to higher temperatures up to 250 °C. Unfortunately, high temperature Pitzer parameter data are not available in the literature for all of the required chemical species, so that the data for certain ionic species included in the database are limited to lower temperature ranges. Some parameter data only applicable at 25°C are included in the database to extend the usefulness of the database to species that do not have high temperature data but, nevertheless, are of interest to the Yucca Mountain Project. A difficulty in the compilation of Pitzer binary and ternary parameters is that some data at elevated temperatures and pressures are reported from variants and extensions of the original Pitzer formulations (Rard and Clegg 1997, Sterner et al. 1998, Archer 2000, Oakes et al. 2000, Rard et al. 2000) that are potentially more accurate than the standard Pitzer model, but which cannot be used directly with the standard Pitzer model

Different authors have used different functions of temperature for the fitting of parameters to experimental data (see Section I-3.2). These different schemes make only minor differences in the goodness of fit, as stated by some of the authors themselves, and are documented for individual binary and ternary parameters in Sections I-4.4 through I-4.6. For the purposes of this AMR these refinements of the fits are unimportant. This is true even in the case of the ternary parameters, (Section I-4.5) in which the percentage changes between one author and another are large, because the ternary interactions make only minor contributions to the calculation of the osmotic coefficients and activity coefficients. To develop an integrated database that encompasses the widest possible selection of ionic species with the smallest number of temperature coefficients, it is necessary to have a rational, thermodynamically motivated basis for selecting these temperature functions. To accomplish this, a comprehensive examination of the published Pitzer parameter data was undertaken to assess the accuracy and validity of the data and the associated temperature functions for each electrolyte of interest for a wide range of temperatures and ionic strength. On the basis of this assessment, a standard form of the temperature functions was developed. The standard Pitzer parameters for each electrolyte are either refitted in this standard form of the temperature functions, or non-standard Pitzer model parameters are first converted to standard Pitzer model parameters and are then fitted to the standard form of the temperature functions. This last step requires refitting of the source Pitzer parameters to the temperature functions represented by a 4-parameter form of Equation I-58 in Section I-3.2.1.3 that includes the constant, linear, inverse and logarithmic terms, but excludes the quadratic term.

To compile, analyze, validate, refit, and convert Pitzer parameters to a form usable by *EQ3/6 Version 8.0*, Microsoft Excel 2000 spreadsheets (see Tables I-1 and I-2) were developed. The temperature function fitting method and the conversion method documented in Rard and Wijesinghe (2003) are incorporated in most of the spreadsheets and are explained in subsequent sections. Most of the spreadsheets are used to refit standard Pitzer parameters without conversion from an extended Pitzer model. These spreadsheets are named

“FitPitzerNC_Type_IonicSpecies.xls”. A second type of spreadsheet involves the conversion of parameters from an extended Pitzer model to the parameters of the standard Pitzer model, followed by fitting new temperature functions of the standard form. These spreadsheets are given the generic name “ConPitzerNC_Type_IonicSpecies.xls” and were prepared only for the electrolytes for which source models were not available in the standard Pitzer form [CaCl₂, Ca(NO₃)₂, NaNO₃, and (NH₄)₂SO₄]. The Pitzer data defined in the ‘ConPitzerNC’ spreadsheets are for binary cation-anion parameters only. The spreadsheets named ‘FitPitzerNC_Int_Param_CFJC.xls’ do not use the ‘FitPitzerNC’ methodology but refit parameters using the regression tool in MS Excel (see Tables I-1 and I-2). In all spreadsheets, error analyses including parameter and osmotic coefficient plots, root mean square (RMS) errors, and MS Excel regression statistics are given in the ‘FitPitzer’ and ‘Result Summary’ worksheets or below the ‘SUMMARY OUTPUT’ title within each worksheet. The ‘Int_Param’ part of the spreadsheet name refers to the type of binary or ternary parameters consistent with the notation given by:

MX = Cation(M)-Anion(X) binary system parameters $\beta_{MX}^{(0)}, \beta_{MX}^{(1)}, \beta_{MX}^{(2)}, C_{MX}^{\phi}$

MM = Cation(M1)-Cation(M2) ternary system parameter θ_{M1M2}

XX = Anion(X1)-Anion(X2) ternary system parameter θ_{X1X2}

MMX = Cation(M1)-Cation(M2)-Anion(X) ternary system parameter ψ_{M1M2X}

MXX = Cation(M)-Anion(X1)-Anion(X2) ternary system parameter ψ_{MX1X2}

NM = Neutral (N)-Cation (M) ternary system parameter λ_{NM}

NX = Neutral (N)-Cation (M) ternary system parameter λ_{NX}

NMX = Neutral (N)-Cation (M) – Anion (X) ternary system parameter ζ_{NMX}

Only functions intrinsic to MS Excel were used in the calculations. The following sections describe the theoretical foundations of the Pitzer parameter fitting/conversion approaches mentioned above. Tables I-1 and I-2 summarize the types of parameters compiled for specific ions and the original sources of Pitzer parameter data.

Table I-1. Catalog of Pitzer Ion-Interaction Parameter Spreadsheets. For Details On The Valid Composition Salt Range of These Parameters, the User is Referred to The Corresponding Sources.

Ion Group	Spreadsheet File Name	Original Data Source	Type	T Range (°C)
Na_Cl	FitPitzerNC_MX_NaCl.xls	Greenberg and Møller (1989)	MX	0 – 250
K_Cl	FitPitzerNC_MX_KCl.xls	Greenberg and Møller (1989)	MX	0 – 250
Na_Br	FitPitzerNC_MX_NaBr.xls	Holmes and Mesmer(1998b)	MX	0 – 250
K_Br	FitPitzerNC_MX_KBr.xls	Holmes and Mesmer(1998b)	MX	0 – 250
Li_Cl	FitPitzerNC_MX_LiCl.xls	Holmes and Mesmer(1983)	MX	0 – 250
Li_Br	FitPitzerNC_MX_LiBr.xls	Holmes and Mesmer(1998b)	MX	0 – 250
Cs_Cl	FitPitzerNC_MX_CsCl.xls	Holmes and Mesmer(1983)	MX	0 – 250
Cs_Br	FitPitzerNC_MX_CsBr.xls	Holmes and Mesmer(1998b)	MX	0 – 250
Na_SO4	FitPitzerNC_MX_Na2SO4.xls	Greenberg and Møller (1989)	MX	0 – 250
K_SO4	FitPitzerNC_MX_K2SO4.xls	Greenberg and Møller (1989)	MX	0 – 250
Ca_SO4	FitPitzerNC_MX_CaSO4.xls	Greenberg and Møller (1989)	MX	0 – 250
Mg_SO4	FitPitzerNC_MX_MgSO4.xls	Pabalan and Pitzer (1987b)	MX	0 – 250
Na_CO3	FitPitzerNC_MX_Na2CO3.xls	He and Morse (1993)	MX	0 – 90
Ca_Cl	ConPitzerNC_MX_CaCl2.xls	Stern et al. (1998)	MX	25 – 250
Mg_Cl	FitPitzerNC_MX_MgCl2.xls	Pabalan and Pitzer (1987b)	MX	0 – 250
Na_HSO4	FitPitzerNC_MX_NaHSO4.xls	Holmes and Mesmer(1994)	MX	25 – 220
Na_HCO3	FitPitzerNC_MX_NaHCO3.xls	He and Morse (1993)	MX	0 – 90
Na_AIO2	FitPitzerNC_MX_Na_AIO2.xls ¹	Felmy et al. (1994b)	MX	0 – 250
Na_OH	FitPitzerNC_MX_NaOH.xls	Pabalan and Pitzer (1987b)	MX	0 – 250
H_SO4	FitPitzerNC_MX_H2SO4.xls	Holmes and Mesmer(1994)	MX	25 – 200
H_HSO4	FitPitzerNC_MX_HHSO4.xls	Holmes and Mesmer(1994)	MX	25 – 200
H_Cl	FitPitzerNC_MX_HCl.xls	Holmes, Busey, et al. (1987)	MX	0 – 250
Na_NO3	ConPitzerNC_MX_NaNO3.xls	Rard and Wijesinghe (2003); Archer (2000)	MX	0 – 152
H_NO3	FitPitzerNC_MX_HNO3_CFJC.xls ¹	Felmy et al. (1994a); Clegg and Brimblecombe (1990a)	MX	25 – 100
Ca_NO3	ConPitzerNC_MX_Ca(NO3)2.xls	Rard and Wijesinghe (2003); Oakes et al., (2000)	MX	25 – 100
NH4_SO4	ConPitzerNC_MX_(NH4)2SO4.xls	Clegg, Milioto, and Palmer (1996)	MX	0 – 250
NH4_Cl	FitPitzerNC_MX_NH4Cl.xls	Thiessen and Simonson (1990)	MX	25 – 250
Na_K	FitPitzerNC_MM_Na_K.xls	Greenberg and Møller (1989)	MM	0 – 250
Na_Ca	FitPitzerNC_MM_Na_Ca.xls	Greenberg and Møller (1989)	MM	0 – 250 ²
K_Ca	FitPitzerNC_MM_K_Ca.xls	Greenberg and Møller (1989)	MM	0 – 250 ²
Cl_SO4	FitPitzerNC_XX_Cl_SO4.xls	Greenberg and Møller (1989)	XX	0 – 250 ³
HSO4_SO4	FitPitzerNC_XX_HSO4_SO4.xls	Holmes and Mesmer(1994)	XX	25 – 200
Na_K_Cl	FitPitzerNC_MMX_Na_K_Cl.xls	Greenberg and Møller (1989)	MMX	0 – 250
Na_K_SO4	FitPitzerNC_MMX_Na_K_SO4.xls	Greenberg and Møller (1989)	MMX	0 – 250
Na_Ca_Cl	FitPitzerNC_MMX_Na_Ca_Cl.xls	Greenberg and Møller (1989)	MMX	0 – 250 ²
Na_Ca_SO4	FitPitzerNC_MMX_Na_Ca_SO4.xls	Greenberg and Møller (1989)	MMX	0 – 250 ²
K_Ca_Cl	FitPitzerNC_MMX_K_Ca_Cl.xls	Greenberg and Møller (1989)	MMX	0 – 250

Table I-1 (Cont.). Catalog of Pitzer Ion-Interaction Parameter Spreadsheets

Ion Group	Spreadsheet File Name	Original Data Source	Type	T Range (°C)
Na_Cl_SO4	FitPitzerNC_MXX_Na_Cl_SO4.xls	Greenberg and Møller (1989)	MXX	0 – 250 ³
K_Cl_SO4	FitPitzerNC_MXX_K_Cl_SO4.xls	Greenberg and Møller (1989)	MXX	0 – 250
Ca_Cl_SO4	FitPitzerNC_MXX_Ca_Cl_SO4.xls	Greenberg and Møller (1989)	MXX	0 – 250 ²
H_HSO4_SO4	FitPitzerNC_MXX_H_HSO4_SO4.xls	Holmes and Mesmer(1994)	MXX	25 – 200
Na_HSO4_SO4	FitPitzerNC_MXX_Na_HSO4_SO4.xls	Holmes and Mesmer(1994)	MXX	25 – 225
CO2_Ca	FitPitzerNC_NaHCO3_Na2CO3_CFJC.xls ¹	He and Morse (1993)	NM	25 – 90
CO2_K	FitPitzerNC_NaHCO3_Na2CO3_CFJC.xls ¹	He and Morse (1993)	NM	25 – 90
CO2_Mg	FitPitzerNC_NaHCO3_Na2CO3_CFJC.xls ¹	He and Morse (1993)	NM	25 – 90
CO2_Na	FitPitzerNC_NaHCO3_Na2CO3_CFJC.xls ¹	He and Morse (1993)	NM	25 – 90
CO2_H	FitPitzerNC_NaHCO3_Na2CO3_CFJC.xls ¹	He and Morse (1993)	NM	25 – 90
CO2_Cl	FitPitzerNC_NaHCO3_Na2CO3_CFJC.xls ¹	He and Morse (1993)	NX	25 – 90
CO2_HSO4	FitPitzerNC_NaHCO3_Na2CO3_CFJC.xls ¹	He and Morse (1993)	NX	25 – 90
CO2_SO4	FitPitzerNC_NaHCO3_Na2CO3_CFJC.xls ¹	He and Morse (1993)	NX	25 – 90
CO2_H_Cl	FitPitzerNC_NaHCO3_Na2CO3_CFJC.xls ¹	He and Morse (1993)	NMX	25 – 90
CO2_Na_Cl	FitPitzerNC_NaHCO3_Na2CO3_CFJC.xls ¹	He and Morse (1993)	NMX	25 – 90
CO2_K_Cl	FitPitzerNC_NaHCO3_Na2CO3_CFJC.xls ¹	He and Morse (1993)	NMX	25 – 90
CO2_Ca_Cl	FitPitzerNC_NaHCO3_Na2CO3_CFJC.xls ¹	He and Morse (1993)	NMX	25 – 90
CO2_Mg_Cl	FitPitzerNC_NaHCO3_Na2CO3_CFJC.xls ¹	He and Morse (1993)	NMX	25 – 90
CO2_H_SO4	FitPitzerNC_NaHCO3_Na2CO3_CFJC.xls ¹	He and Morse (1993)	NMX	25 – 90
CO2_Na_SO4	FitPitzerNC_NaHCO3_Na2CO3_CFJC.xls ¹	He and Morse (1993)	NMX	25 – 90
CO2_K_SO4	FitPitzerNC_NaHCO3_Na2CO3_CFJC.xls ¹	He and Morse (1993)	NMX	25 – 90
CO2_Mg_SO4	FitPitzerNC_NaHCO3_Na2CO3_CFJC.xls ¹	He and Morse (1993)	NMX	25 – 90
O2_Al	FitPitzerNC_lambdas_zetas_O2_CFJC.xls ¹	Clegg and Brimblecombe (1990b)	NM	25 – 100
O2_Ba	FitPitzerNC_lambdas_zetas_O2_CFJC.xls ¹	Clegg and Brimblecombe (1990b)	NM	25 – 100
O2_Ca	FitPitzerNC_lambdas_zetas_O2_CFJC.xls ¹	Clegg and Brimblecombe (1990b)	NM	25 – 100
O2_H	FitPitzerNC_lambdas_zetas_O2_CFJC.xls ¹	Clegg and Brimblecombe (1990b)	NM	25 – 100
O2_K	FitPitzerNC_lambdas_zetas_O2_CFJC.xls ¹	Clegg and Brimblecombe (1990b)	NM	25 – 100
O2_Li	FitPitzerNC_lambdas_zetas_O2_CFJC.xls ¹	Clegg and Brimblecombe (1990b)	NM	25 – 100
O2_Mg	FitPitzerNC_lambdas_zetas_O2_CFJC.xls ¹	Clegg and Brimblecombe (1990b)	NM	25 – 100
O2_Na	FitPitzerNC_lambdas_zetas_O2_CFJC.xls ¹	Clegg and Brimblecombe (1990b)	NM	25 – 100
O2_NH4	FitPitzerNC_lambdas_zetas_O2_CFJC.xls ¹	Clegg and Brimblecombe (1990b)	NM	25 – 100
O2_Cl	FitPitzerNC_lambdas_zetas_O2_CFJC.xls ¹	Clegg and Brimblecombe (1990b)	NX	25 – 100
O2_Br	FitPitzerNC_lambdas_zetas_O2_CFJC.xls ¹	Clegg and Brimblecombe (1990b)	NX	25 – 100
O2_CO3	FitPitzerNC_lambdas_zetas_O2_CFJC.xls ¹	Clegg and Brimblecombe (1990b)	NX	25 – 100
O2_HCO3	FitPitzerNC_lambdas_zetas_O2_CFJC.xls ¹	Clegg and Brimblecombe (1990b)	NX	25 – 100
O2_I	FitPitzerNC_lambdas_zetas_O2_CFJC.xls ¹	Clegg and Brimblecombe (1990b)	NX	25 – 100
O2_NO3	FitPitzerNC_lambdas_zetas_O2_CFJC.xls ¹	Clegg and Brimblecombe (1990b)	NX	25 – 100
O2_OH	FitPitzerNC_lambdas_zetas_O2_CFJC.xls ¹	Clegg and Brimblecombe (1990b)	NX	25 – 100
O2_SO4	FitPitzerNC_lambdas_zetas_O2_CFJC.xls ¹	Clegg and Brimblecombe (1990b)	NX	25 – 100
O2_Na_Cl	FitPitzerNC_lambdas_zetas_O2_CFJC.xls ¹	Clegg and Brimblecombe (1990b)	NMX	25 – 100
O2_Na_Br	FitPitzerNC_lambdas_zetas_O2_CFJC.xls ¹	Clegg and Brimblecombe (1990b)	NMX	25 – 100
O2_Na_NO3	FitPitzerNC_lambdas_zetas_O2_CFJC.xls ¹	Clegg and Brimblecombe (1990b)	NMX	25 – 100
O2_Na_SO4	FitPitzerNC_lambdas_zetas_O2_CFJC.xls ¹	Clegg and Brimblecombe (1990b)	NMX	25 – 100
O2_K_Cl	FitPitzerNC_lambdas_zetas_O2_CFJC.xls ¹	Clegg and Brimblecombe (1990b)	NMX	25 – 100
O2_K_Br	FitPitzerNC_lambdas_zetas_O2_CFJC.xls ¹	Clegg and Brimblecombe (1990b)	NMX	25 – 100

Table I-1 (Cont.): Catalog of Pitzer Ion-Interaction Parameter Spreadsheets

Ion Group	Spreadsheet File Name	Original Data Source	Type	T Range (°C)
O2_K_OH	FitPitzerNC_lambdas_zetas_O2_CFJC.xls ¹	Clegg and Brimblecombe (1990b)	NMX	25 – 100
O2_K_NO3	FitPitzerNC_lambdas_zetas_O2_CFJC.xls ¹	Clegg and Brimblecombe (1990b)	NMX	25 – 100
O2_K_SO4	FitPitzerNC_lambdas_zetas_O2_CFJC.xls ¹	Clegg and Brimblecombe (1990b)	NMX	25 – 100
O2_Mg_Cl	FitPitzerNC_lambdas_zetas_O2_CFJC.xls ¹	Clegg and Brimblecombe (1990b)	NMX	25 – 100
O2_Mg_SO4	FitPitzerNC_lambdas_zetas_O2_CFJC.xls ¹	Clegg and Brimblecombe (1990b)	NMX	25 – 100
O2_Ca_Cl	FitPitzerNC_lambdas_zetas_O2_CFJC.xls ¹	Clegg and Brimblecombe (1990b)	NMX	25 – 100
O2_Ca_NO3	FitPitzerNC_lambdas_zetas_O2_CFJC.xls ¹	Clegg and Brimblecombe (1990b)	NMX	25 – 100
O2_Al_Cl	FitPitzerNC_lambdas_zetas_O2_CFJC.xls ¹	Clegg and Brimblecombe (1990b)	NMX	25 – 100
O2_Al_SO4	FitPitzerNC_lambdas_zetas_O2_CFJC.xls ¹	Clegg and Brimblecombe (1990b)	NMX	25 – 100
O2_H_Cl	FitPitzerNC_lambdas_zetas_O2_CFJC.xls ¹	Clegg and Brimblecombe (1990b)	NMX	25 – 100
O2_Li_Cl	FitPitzerNC_lambdas_zetas_O2_CFJC.xls ¹	Clegg and Brimblecombe (1990b)	NMX	25 – 100
O2_Na_HCO3	FitPitzerNC_lambdas_zetas_O2_CFJC.xls ¹	Clegg and Brimblecombe (1990b)	NMX	25 – 100
O2_Na_CO3	FitPitzerNC_lambdas_zetas_O2_CFJC.xls ¹	Clegg and Brimblecombe (1990b)	NMX	25 – 100
O2_K_I	FitPitzerNC_lambdas_zetas_O2_CFJC.xls ¹	Clegg and Brimblecombe (1990b)	NMX	25 – 100
O2_NH4_SO4	FitPitzerNC_lambdas_zetas_O2_CFJC.xls ¹	Clegg and Brimblecombe (1990b)	NMX	25 – 100
O2_Ba_Cl	FitPitzerNC_lambdas_zetas_O2_CFJC.xls ¹	Clegg and Brimblecombe (1990b)	NMX	25 – 100
SiO2_H	Pitzer_NMX_SiO2.xls ¹	Felmy et al. (1994a)	NX	25 – 100
SiO2_Mg	Pitzer_NMX_SiO2.xls ¹	Felmy et al. (1994a)	NM	25 – 100
SiO2_Na	Pitzer_NMX_SiO2.xls ¹	Felmy et al. (1994a)	NM	25 – 100
SiO2_Cl	Pitzer_NMX_SiO2.xls ¹	Felmy et al. (1994a)	NX	25 – 100
SiO2_NO3	Pitzer_NMX_SiO2.xls ¹	Felmy et al. (1994a)	NX	25 – 100
SiO2_SO4	Pitzer_NMX_SiO2.xls ¹	Felmy et al. (1994a)	NX	25 – 100
K_Mg_Cl	Pabalan_icf_TJW.xls	Pabalan and Pitzer (1987b)	MMX	0 – 250
Na_Mg_Cl	Pabalan_icf_TJW.xls	Pabalan and Pitzer (1987b)	MMX	0 – 250
Mg_Cl_SO4	Pabalan_icf_TJW.xls	Pabalan and Pitzer (1987b)	MMX	0 – 250
Na_K_Cl	Pabalan_icf_TJW.xls	Pabalan and Pitzer (1987b)	MMX	0 – 250
Cl_OH_Na	Pabalan_icf_TJW.xls	Pabalan and Pitzer (1987b)	MMX	0 – 250
Na_OH_SO4	Pabalan_icf_TJW.xls	Pabalan and Pitzer (1987b)	MMX	0 – 250

DTN: SN0306T0510102.007

NOTES:

¹ Spreadsheet refitting calculations do not entail the use of the "FitPitzerNC" methodology. Refitting of Pitzer parameters was conducted using the MS Excel regression function.

² The evaluation of these mixing parameters was based on the model and parameters of Greenberg and Møller (1989). Although these authors used a constant value for this parameter (rather than a temperature-dependent function), its value was chosen to represent solubilities over a wide temperature range, and thus it can be used over the indicated temperature range.

³ The evaluation of these mixing parameters is based on the model and parameters of Greenberg and Møller (1989). These authors used a constant value for this parameter from 0 to 150 °C (rather than a temperature-dependent function), and then used a temperature-dependent function at higher temperatures. Since the constant value below 150 °C was chosen to represent solubilities over a wide temperature range, it can be used over the indicated temperature range.

Table I-2: Pitzer Ion-Interaction Parameters not Requiring Refitting (Values only valid at 25 °C)

Ion Group	Spreadsheet File Name	Original Data Source	Type
Ca_Br	Some2-1Salts25C_TJW.xls	Pitzer (1991)	MX
Ca_HCO3	Some2-1Salts25C_TJW.xls	Pitzer (1991)	MX
Ca_HSO3	Some2-1Salts25C_TJW.xls	Pitzer (1991)	MX
Ca_I	Some2-1Salts25C_TJW.xls	Pitzer (1991)	MX
Cs_I	Some1-1Salts25C_TJW.xls	Pitzer (1991)	MX
Cs_F	Some1-1Salts25C_TJW.xls	Pitzer (1991)	MX
Cs_NO3	Some2-1Salts25C_TJW.xls	Pitzer (1991)	MX
Cs_OH	Some1-1Salts25C_TJW.xls	Pitzer (1991)	MX
Cs_SO4	Some2-1Salts25C_TJW.xls	Pitzer (1991)	MX
H_Br	Some1-1Salts25C_TJW.xls	Pitzer (1991)	MX
H_I	Some1-1Salts25C_TJW.xls	Pitzer (1991)	MX
K_CO3	Some2-1Salts25C_TJW.xls	Pitzer (1991)	MX
K_HCO3	Some2-1Salts25C_TJW.xls	Pitzer (1991)	MX
K_CrO4	Some2-1Salts25C_TJW.xls	Pitzer (1991)	MX
K_F	Some2-1Salts25C_TJW.xls	Pitzer (1991)	MX
K_HPO4	Some2-1Salts25C_TJW.xls	Pitzer (1991)	MX
K_SO4	Some2-1Salts25C_TJW.xls	Pitzer (1991)	MX
K_I	Some2-1Salts25C_TJW.xls	Pitzer (1991)	MX
K_NO3	Some2-1Salts25C_TJW.xls	Pitzer (1991)	MX
K_OH	Some2-1Salts25C_TJW.xls	Pitzer (1991)	MX
Li_I	Some2-1Salts25C_TJW.xls	Pitzer (1991)	MX
Li_NO3	Some2-1Salts25C_TJW.xls	Pitzer (1991)	MX
Li_OH	Some2-1Salts25C_TJW.xls	Pitzer (1991)	MX
Li_SO4	Some2-1Salts25C_TJW.xls	Pitzer (1991)	MX
Mg_Br	Some2-1Salts25C_TJW.xls	Pitzer (1991)	MX
Mg_HCO3	Some2-1Salts25C_TJW.xls	Pitzer (1991)	MX
Mg_SO4	Some2-1Salts25C_TJW.xls	Pitzer (1991)	MX
Mg_I	Some2-1Salts25C_TJW.xls	Pitzer (1991)	MX
Mg_NO3	Some2-1Salts25C_TJW.xls	Pitzer (1991)	MX
MgOH_Cl	Some2-1Salts25C_TJW.xls	Pitzer (1991)	MX
Na_CrO4	Some2-1Salts25C_TJW.xls	Pitzer (1991)	MX
Na_F	Some2-1Salts25C_TJW.xls	Pitzer (1991)	MX
Na_HPO4	Some2-1Salts25C_TJW.xls	Pitzer (1991)	MX
Na_I	Some2-1Salts25C_TJW.xls	Pitzer (1991)	MX
NH4_Br	Some2-1Salts25C_TJW.xls	Pitzer (1991)	MX
NH4_HCO3	Some2-1Salts25C_TJW.xls	Pitzer (1991)	MX
NH4_I	Some2-1Salts25C_TJW.xls	Pitzer (1991)	MX
NH4_NO3	Some2-1Salts25C_TJW.xls	Pitzer (1991)	MX
Sr_Br	Some2-1Salts25C_TJW.xls	Pitzer (1991)	MX
Sr_Cl	Some2-1Salts25C_TJW.xls	Pitzer (1991)	MX
Sr_I	Some2-1Salts25C_TJW.xls	Pitzer (1991)	MX
Sr_NO3	Some2-1Salts25C_TJW.xls	Pitzer (1991)	MX
Ca_H	No Spreadsheet ¹	Pitzer (1991)	MM
Ca_K	No Spreadsheet ¹	Pitzer (1991)	MM

Table I-2 (Cont.): Pitzer Ion-Interaction Parameters not Requiring Refitting (Values only valid at 25 °C)

Ion Group	Spreadsheet File Name	Original Data Source	Type
Ca_Na	No Spreadsheet ¹	Pitzer (1991)	MM
Ca_Mg	No Spreadsheet ¹	Pitzer (1991)	MM
Cs_H	No Spreadsheet ¹	Pitzer (1991)	MM
Cs_K	No Spreadsheet ¹	Pitzer (1991)	MM
Cs_Li	No Spreadsheet ¹	Pitzer (1991)	MM
Cs_Na	No Spreadsheet ¹	Pitzer (1991)	MM
H_K	No Spreadsheet ¹	Pitzer (1991)	MM
H_Li	No Spreadsheet ¹	Pitzer (1991)	MM
H_Mg	No Spreadsheet ¹	Pitzer (1991)	MM
H_Na	No Spreadsheet ¹	Pitzer (1991)	MM
H_NH4	No Spreadsheet ¹	Pitzer (1991)	MM
H_Sr	No Spreadsheet ¹	Pitzer (1991)	MM
K_Li	No Spreadsheet ¹	Pitzer (1991)	MM
K_Mg	No Spreadsheet ¹	Pabalan and Pitzer (1987b)	MM
K_Na	No Spreadsheet ¹	Pitzer (1991)	MM
Li_Na	No Spreadsheet ¹	Pitzer (1991)	MM
Mg_Na	No Spreadsheet ¹	Pabalan and Pitzer (1987b)	MM

DTN: SN0306T0510102.007

NOTE:

¹ 'No Spreadsheet' means that values were taken directly from tables listed in Pitzer (1991).

I-4.1 FITPITZERNC METHODOLOGY

In the FitPitzerNC spreadsheets it is assumed that the Pitzer parameters are given as functions of the system temperature, T , and pressure, P . A new output temperature-pressure function $f(T,P)$ is fitted to each Pitzer parameter that is defined in the source document in terms of a temperature-pressure function $f^0(T,P)$. Usually, both the input and output temperature-pressure functions are given as the sum of a finite series of numeric terms, each of which is the product of a constant coefficient (a_i, a_i^0), and a temperature-pressure interpolation basis function ($g_i(T,P), g_i^0(T,P)$), as in:

$$f(T,P) = \sum_{i=1}^{i=n_f} a_i g_i(T,P) \quad (\text{I-61})$$

$$f^0(T,P) = \sum_{i=1}^{i=n_f^0} a_i^0 g_i^0(T,P) \quad (\text{I-62})$$

where, (n_f, n_f^0) are the numbers of terms in the two series. While the basis functions for the input model parameters are specified in the source document, the new basis functions of the output model parameters are selected by the user of the FitPitzerNC spreadsheets from a list of up to eight basis functions. It is important to note that the fitting coefficients a_1, \dots, a_5 specified in the 'FitPitzerNC' and 'ConPitzerNC' spreadsheets do not directly correspond to those specified for the data0.ypf database. Table I-3 provides the actual correspondence between these parameters:

Table I-3. Fitting Coefficient Definitions for the 3-4 Parameter 25°C Centric Equations Used in the FitPitzerNC/ConPitzerNC Spreadsheets and data0.ypf Database File

FitPitzerNC/ConPitzerNC	data0.ypf	Temperature Function
a ₁	a ₁	Constant
a ₂	a ₄	T
a ₃	not used	T ²
a ₄	a ₂	1/T
a ₅	a ₃	ln T

Spreadsheets not using the ‘FitPitzerNC’ or ‘ConPitzerNC’ methodology express the fitting coefficients as in the data0.ypf database file.

In the FitPitzerNC spreadsheets, it is assumed a temperature dependent standard system pressure $P(T)$ that is equal to 1 atmosphere below 100°C, and is equal to the liquid-vapor saturation vapor pressure of pure water above 100°C. The reason for making this assumption is that this is the definition of system pressure used in *Software User’s Manual, EQ3/6, Version 8.0* (SNL 2003). Consequently, the functional dependence of the output temperature-pressure functions of the Pitzer parameters can be simplified according to $g_i(T,P) = g_i(T,P(T)) = g_i(T)$, and expressed as functions of the temperature only.

On the basis of thermodynamic arguments, and parameter fitting accuracy considerations, the following set of eight functions for the output basis functions $g_i(T)$ was selected:

$$\begin{aligned}
 g_1(T) &= 1 \\
 g_2(T) &= T \\
 g_3(T) &= T^2 \\
 g_4(T) &= T^{-1} \\
 g_5(T) &= \ln(T) \\
 g_6(T) &= T^3 \\
 g_7(T) &= T^{-2} \\
 g_8(T) &= T^{-3}
 \end{aligned}
 \tag{I-63}$$

This series of basis functions not only spans the entire sequence of powers of the temperature T increasing from -3 to $+2$ (i.e., T^{-3} , T^{-2} , T^{-1} , T^k ($k < 1$), T^0 , T^k ($k < 1$), T^1 , T^2), but it also incorporates as subsets important temperature function forms for the Pitzer parameters that can be justified on the basis of fundamental thermodynamic considerations.

It is convenient for parameter data verification purposes to directly represent the coefficient a_1 of the constant basis function $g_1(T)$ as the value of the fitted parameter at some reference absolute temperature T_{ref} , usually 298.15 K. This can be achieved by redefining the basis functions $g_i(T)$ as:

$$\begin{aligned}
g_1(T) &= 1 \\
g_2(T) &= T - T_{\text{ref}} \\
g_3(T) &= T^2 - T_{\text{ref}}^2 \\
g_4(T) &= T^{-1} - T_{\text{ref}}^{-1} \\
g_5(T) &= \ln\left(\frac{T}{T_{\text{ref}}}\right) \\
g_6(T) &= T^3 - T_{\text{ref}}^3 \\
g_7(T) &= T^{-2} - T_{\text{ref}}^{-2} \\
g_8(T) &= T^{-3} - T_{\text{ref}}^{-3}
\end{aligned} \tag{I-64}$$

In the FitPitzerNC spreadsheet, this feature for centering the fitted functions at any specified absolute reference temperature T_{ref} , has been implemented and can be selected as an option.

I-4.2 PROCEDURE FOR FITTING TEMPERATURE FUNCTIONS TO PITZER PARAMETERS

A least-squares error minimization method was devised for fitting the new temperature functions to the input source functions with minimum error by first defining a measure $E^2(a_i)$ of the cumulative square error between the fitted function $f(T)$ and the input function $f^0(T, P)$ over the desired temperature range $(T_{\text{min}}, T_{\text{max}})$ by:

$$E^2(a_i) = \frac{1}{n_T} \sum_{j=1}^{j=n_T} \{f(T_j) - f^0(T_j, P_j)\}^2 \tag{I-65}$$

where, T_j are the n_T discrete temperatures at which the parameters are evaluated, $T_1 = T_{\text{min}}$, $T_2 = T_{\text{max}}$, and $P_j = P(T_j)$.

Setting the partial derivatives of E with respect to the output temperature coefficients a_i equal to zero now minimizes the error measure:

$$\frac{\partial E^2}{\partial a_i} = \frac{2}{n_T} \sum_{j=1}^{j=n_T} \frac{\partial f}{\partial a_i} \{f(T_j) - f^0(T_j, P_j)\} = 0 \tag{I-66}$$

Substituting the series representations for the temperature function given by Equations I-61 and I-62 into equation I-66, and re-arranging the terms, yields the equation:

$$\sum_{k=1}^{k=n_f} \sum_{j=1}^{j=n_T} g_i(T_j) g_k(T_j) a_k = \sum_{j=1}^{j=n_T} g_i(T_j) f^0(T_j, P_j) \tag{I-67}$$

Equation I-67 can be recast in a more compact and transparent form as the matrix equations:

$$[A_{ik}](a_k) = (b_i) \quad ; \quad i, k = 1 \dots n_f \quad (\text{I-68})$$

$$A_{ik} \equiv \sum_{j=1}^{j=n_T} g_i(T_j) g_k(T_j) \quad (\text{I-69})$$

$$b_i \equiv \sum_{j=1}^{j=n_T} g_i(T_j) f^0(T_j, P_j) \quad (\text{I-70})$$

The matrix Equations I-68 through I-70 can be solved by standard matrix equation solution methods for the unknown vector of temperature coefficients (a_k) in terms of the known right-hand-side vector (b_i), and known interpolation function matrix $[A_{ik}]$.

When the temperature coefficients a_i have been determined by solving equation I-68 in this way, the input and fitted parameters $f^0(T_j)$ and $f(T_j)$ are evaluated using the values of the determined coefficients in the temperature function representations of Equation I-62. The binary and ternary system osmotic coefficients can then be calculated by substituting the input and fitted parameter values evaluated as a function of temperature in Equations I-13 and I-14, respectively.

This mathematical procedure has been implemented in each FitPitzerNC worksheet to fit new temperature functions to the source Pitzer parameters.

I-4.2.1 FitPitzerNC Worksheet Implementation

The full set of temperature basis functions given by Equation I-63 and I-64 spans the entire sequence of powers of the temperature T increasing from -3 to $+2$ (i.e., $T^3, T^2, T^1, T^k (k < 1), T^0, T^k (k < -1), T^1, T^2$). However, when implementing the FitPitzerNC methodology, it is necessary to allow for the fact that only a sub-set of the full set of basis functions may be activated, or chosen, for a particular Pitzer parameter database. A spreadsheet, that does not treat each choice as a special case, can be developed, by solving for all temperature coefficients in a way that forces the de-activated temperature coefficients a_k to be equal to zero. In this no-code version of the FitPitzer spreadsheet, this feature is implemented using only spreadsheet macro functions in the following way.

An activation-index vector IA_i (row 22 in RunSettings Worksheet) is first set up to reflect the user's choice of temperature basis functions such that

$$IA_i \equiv 1 \quad ; \quad a_i \neq 0; \quad i = 1, 2 \dots 8 \quad (\text{I-71})$$

$$IA_i \equiv 0 \quad ; \quad a_i = 0; \quad i = 1, 2 \dots 8 \quad (\text{I-72})$$

The matrix equation that is to be solved for the unknown temperature coefficients is then given by

$$[A_{ik}](a_k^p) = (b_i^p) \quad ; \quad i, k = 1 \dots n \quad (\text{I-73})$$

$$A_{ik} \equiv A_{ik}^0 \cdot IAM_{ik}; \quad i, k = 1 \dots n_f \quad (\text{I-74})$$

$$b_i^p \equiv b_i^{0p} \cdot IA_i; \quad i = 1 \dots n_f \quad (\text{I-75})$$

where p is the parameter index. The activation-index matrix IAM_{ij} is defined in terms of the activation-index vector IA_i by

$$IAM_{ij} \equiv 1 \quad ; \quad i = j \quad (\text{I-76})$$

$$IAM_{ij} \equiv IA_i \cdot IA_j \quad i \neq j \quad (\text{I-77})$$

In this way, the correct matrix coefficients and right-hand side vector values for the set of activated temperature coefficients are retrieved, while forcing the deactivated temperature coefficients to be equal to zero. All matrix-vector and matrix-matrix multiplications are performed using the MMULT and TRANSPOSE spreadsheet functions, inversion of the matrix equation I-73 is performed using the MINVERSE spreadsheet function, and the individual elements of the vector and matrix arrays are accessed using the INDEX function. These spreadsheet functions are standard intrinsic features of MS-Excel 2000 (and above).

I-4.2.2 Example Calculation for FitPitzerNC_MX_NaCl.xls Workbook:

For the purpose of illustrating the specific manner in which these calculations are carried out, the sequence of calculations performed in the FitPitzerNC_MX_NaCl.xls workbook are presented below:

1. CoverPage worksheet: On this worksheet, software identification information and spreadsheet checker review comments are first presented. Next, spreadsheet user information on a contents roadmap, an overview of methodology and data sources, protection of data and computational integrity and manner of presentation of results, are given.
2. Directions worksheet: This worksheet gives directions for fitting different temperature functions selected by the user.
3. RunSettings worksheet: Select the desired temperature basis functions.
4. RunSettings worksheet: Select, if desired Temperature centering and Reference Temperature.
5. FitPitzerNC worksheet: Constant input (Archer) and output (Standard Pitzer) model parameters are defined in lines A13:L13 and A14:L14.
6. FitPitzerNC worksheet: The input Standard Pitzer Model temperature coefficients are set in cells B17:I20, and for the Aphi Debye-Huckel parameter in cells B21:I21.
7. FitPitzerNC worksheet: The input Standard Pitzer Model parameters and the Aphi Debye-Huckel parameter are calculated as functions of temperature in cells B31:AB35.

8. FitPitzerNC worksheet: The matrix array, $G_{ij} = g_i(T_j)$, is calculated in accordance with equations I-64 or I-78 (along with the option chosen for the Tref switch), and the results placed in the range of cells, B78:AB85. The corresponding A^0_{ik} matrix is calculated according to equation I-69 (or equation I-79 below), specifically, $MMULT(G, TRANSPOSE(G))/27$, and the results placed in the range of cells, B88:I95. Division by 27 is convenient for keeping the entry for $A^0(1,1)$ the same as that for $g-1$ at 0°C :

$$G = \$B\$78 : \$AB\$85 \quad (\text{I-78})$$

$$A^0 = MMULT(G, TRANSPOSE(G)) = \$B\$88 : \$I\$95 \quad (\text{I-79})$$

9. FitPitzerNC worksheet: The input parameter function matrix array, $F^{0p}_i = f^{0p}(T_i)$, where p stands for the parameter index and i signifies the temperature value index is calculated in accordance with equation I-62 (entered as equation I-80 below), and the results placed in the range of cells, B31:AB34. The corresponding B^{0p}_i matrix is calculated according to equation I-70 (or equation I-81 below), specifically, $MMULT(G, TRANSPOSE(F^0))/27$, and the results placed in the range of cells, B128:E135. Division by 27 is needed to keep both sides of equation I-68 compatible:

$$F^0 = \$B\$31 : \$AB\$34 \quad (\text{I-80})$$

$$B^0 = MMULT(G, TRANSPOSE(F^0)) = \$B\$128 : \$E\$135 \quad (\text{I-81})$$

10. FitPitzerNC worksheet: The temperature basis function activation vector IA_i and activation matrix IAM_{ij} are setup according to equations I-82 (or equation I-76) and I-83 (or equation I-77), respectively:

$$IA = \$B\$24 : \$I\$24 \quad (\text{I-82})$$

$$IAM = \$B\$98 : \$I\$105 \quad (\text{I-83})$$

11. FitPitzerNC worksheet: The modified coefficient matrix A_{ik} and the modified matrix of right-hand side vectors B^p_i are calculated according to equations I-84 (or equation I-74) and I-85 (or equation I-75), respectively:

$$A = \$B\$108 : \$I\$115 \quad (\text{I-84})$$

$$B = \$B\$138 : \$I\$145 \quad (\text{I-85})$$

12. FitPitzerNC worksheet: Equation I-73 is solved to obtain the desired matrix of temperature coefficient vectors $CoefFIT = a^p_i$ by inverting the coefficient matrix A to obtain its inverse $AINV$ and then multiplying the inverse matrix by the modified matrix of right-hand side vectors B^p_i :

$$AINV = MINVERSE(A) = \$B\$118 : \$I\$125 \quad (I-86)$$

$$CoefFIT = MMULT(AINV, B) = \$B\$25 : \$I\$28 \quad (I-87)$$

13. FitPitzerNC worksheet: The input Standard Pitzer Model parameters, and the fitted parameters for the same model, are calculated as functions of temperature according to equations I-88 and I-89, respectively:

$$ParamDAT = \$B\$31 : \$AB\$34 \quad (I-88)$$

$$ParamFIT = MMULT(TRANSPOSE(CoefFIT), G) = \$B\$38 : \$AB\$41 \quad (I-89)$$

14. FitPitzerNC worksheet: The ionic strength dependent factors in the Debye-Huckel and exponential Beta-parameter terms in the equation for the osmotic coefficient are calculated and stored as follows:

$$DHDAT = \$D\$148 : \$D\$153 \quad (I-90)$$

$$DHFIT = \$D\$156 : \$D\$161 \quad (I-91)$$

$$PFuncDAT = \$E\$148 : \$H\$153 \quad (I-92)$$

$$PFuncFIT = \$E\$156 : \$H\$161 \quad (I-93)$$

15. FitPitzerNC worksheet: The osmotic coefficient from the Debye-Huckel and Beta-parameter terms are calculated according to the equations:

$$APhi = \$B\$35 : \$AB\$35 \quad (I-94)$$

$$PhiM1DAT = MMULT(DHDAT, APhi) + MMULT(PFuncDAT, ParamDAT); \quad (I-95)$$

$$PhiM1FIT = MMULT(DHFIT, APhi) + MMULT(PFuncFIT, ParamFIT)$$

$$PhiDAT = 1 + PhiM1DAT = \$B\$50 : \$AB\$55 \quad (I-96)$$

$$PhiFIT = 1 + PhiM1FIT = \$B\$58 : \$AB\$63 \quad (I-97)$$

16. FitPitzerNC worksheet: This completes the fitting of new temperature functions to the input Standard Pitzer Model parameters, the calculation of the input and fitted Pitzer parameters as functions of temperature, and the computation of the osmotic coefficient as a function of ionic strength and temperature from the input and fitted Pitzer parameter values at each temperature. These are used to evaluate the accuracy of fitting the Standard Pitzer parameters.

17. FitPitzerNC worksheet: The temperature function fitting error in the osmotic coefficient is calculated as the difference between the osmotic coefficients from the input and fitted Standard Pitzer Models in cells B67:AB72 as a function of temperature and ionic strength. The RMS error (cells AC67:AC72) and the Average, Maximum and Minimum values of the osmotic coefficient are also calculated for the two models in cells AD50:AF55 and AD58:AF63, respectively.

18. FitPitzerNC worksheet: Pitzer parameters, osmotic coefficients and their errors, calculated from the input and fitted Standard Pitzer Models, are plotted in charts on the extreme right hand side of each FitPitzerNC worksheet.
19. ResultsSummary worksheet: The input and fitted temperature coefficients for the Standard Pitzer Model are summarized in cells B17:I21 and B25:I28, respectively.
20. ResultsSummary worksheet: The RMS errors, Average, Maximum and Minimum values of the Pitzer parameters (B31:E34) and osmotic coefficients (A37:E42) calculated from the input and fitted Standard Pitzer Models are summarized here. These statistics enable the errors incurred in temperature function fitting to be assessed.

I-4.3 CONPITZERNC METHODOLOGY

In the “ConPitzerNC_MX_Electrolyte.xls” type spreadsheet, the parameters given as a function of temperature for an extended Pitzer model in the data source document are converted to the parameters of the standard Pitzer model. Temperature coefficients for a user specified temperature function are then fit to these standard parameters in the “FitPitzerNC” worksheet of the spreadsheet as described in Section I-4.1 above. Currently, only spreadsheets for converting binary system parameters have been developed.

This section summarizes the procedure developed by Rard and Wijesinghe (2003) used in the “ConPitzerNC” worksheets for converting parameters between the 4-parameter (i.e., $\beta^{(0)}_{MX}(T,P)$, $\beta^{(1)}_{MX}(T,P)$, $\beta^{(2)}_{MX}(T,P)$, $C^{\phi}_{MX}(T,P)$) standard Pitzer model presented in Section I-3, and the 6-parameter (i.e., $\beta^{(0)}_{MX}(T,P)$, $\beta^{(1)}_{MX}(T,P)$, $\beta^{(2)}_{MX}(T,P)$, $C^{(0)}_{MX}(T,P)$, $C^{(1)}_{MX}(T,P)$, $C^{(2)}_{MX}(T,P)$) extended Pitzer model developed by Archer (2000) and further extended by Oakes et al. (2000).

The expression for the osmotic coefficient in the 4-parameter standard Pitzer model, denoted by the superscript P , is given by:

$$\phi^P = 1 - \frac{|z_M z_X| A_{\phi} I^{1/2}}{(1 + bI^{1/2})} + \left(\frac{2\nu_M \nu_X m}{\nu_M + \nu_X} \right) \left\{ B_{MX}^{\phi,P} + m(\nu_M \nu_X)^{1/2} C_{MX}^{\phi,P} \right\} \quad (\text{I-98})$$

where

$$B_{MX}^{\phi,P}(I, T, P) \equiv \beta_{MX}^{(0,P)}(T, P) + \beta_{MX}^{(1,P)}(T, P)e^{-\alpha_1 \sqrt{I}} + \beta_{MX}^{(2,P)}(T, P)e^{-\alpha_2 \sqrt{I}} \quad (\text{I-99})$$

and $C_{MX}^{\phi,P}$ is a function of (T, P) only. The expression for the osmotic coefficient in the 6-parameter Extended Archer model (see Rard and Wijesinghe 2003 for more details), denoted by the superscript EA , is given by:

$$\phi^{EA} = 1 - \frac{|z_M z_X| A_{\phi} I^{1/2}}{(1 + bI^{1/2})} + \left(\frac{2\nu_M \nu_X m}{\nu_M + \nu_X} \right) \left\{ B_{MX}^{\phi,EA} + m(\nu_M \nu_X)^{1/2} C_{MX}^{EA} \right\} \quad (\text{I-100})$$

where

$$B_{MX}^{\phi,EA}(I,T,P) \equiv \beta_{MX}^{(0,EA)}(T,P) + \beta_{MX}^{(1,EA)}(T,P)e^{-\alpha_1\sqrt{I}} + \beta_{MX}^{(2,EA)}(T,P)e^{-\alpha_2\sqrt{I}} \quad (\text{I-101})$$

$$C_{MX}^{EA}(I,T,P) \equiv C_{MX}^{(0,EA)}(T,P) + C_{MX}^{(1,EA)}(T,P)e^{-\omega_1\sqrt{I}} + C_{MX}^{(2,EA)}(T,P)e^{-\omega_2\sqrt{I}} \quad (\text{I-102})$$

ω_1 and ω_2 are constant coefficients for $C_{MX}^{(1,EA)}$ and $C_{MX}^{(2,EA)}$ parameters, respectively, as defined in the Archer model (see Rard and Wijesinghe 2003). In contrast to $C_{MX}^{\phi,P}$ in the standard Pitzer model, the C_{MX}^{EA} is a function of ionic strength in addition to temperature and pressure, and is expressed as the sum of an ionic strength dependent parameter and two terms that decay exponentially with the square root of ionic strength. Equation I-101 is the analog of Equation I-99 for the standard Pitzer model with the same values assigned to exponents of the terms that decay exponentially with increasing ionic strength. It is important to note here that the coefficient of these functions in Equations I-98 and I-100 are not equal.

I-4.3.1 Procedure for Determining Standard Pitzer Model Parameters from Archer Model Parameters

A least-squares error minimization method was devised for determining with minimum error the set Standard Pitzer Model Parameters $X_i^P = \{\beta_{MX}^{(0,P)}(T,P), \beta_{MX}^{(1,P)}(T,P), \beta_{MX}^{(2,P)}(T,P), C_{MX}^{\phi,P}(T,P)\}$ from the set of Archer Model parameters $X_j^{EA} = \{\beta_{MX}^{(0,EA)}(T,P), \beta_{MX}^{(1,EA)}(T,P), \beta_{MX}^{(2,EA)}(T,P), C_{MX}^{(0,EA)}(T,P), C_{MX}^{(1,EA)}(T,P), C_{MX}^{(2,EA)}(T,P)\}$ by first defining a measure $E^2(X_i^P, X_j^{EA})$ of the cumulative square error ($\phi^P - \phi^{EA}$) between the osmotic coefficient in the two models over the desired ionic strength range ($0, I_{max}$)

$$E^2(X_i^P, X_j^{EA}) = \frac{1}{2} \int_0^{I_{max}} \{\phi^P(I, X_i^P) - \phi^{EA}(I, X_j^{EA})\}^2 dI \quad (\text{I-103})$$

The subsequent mathematical expressions can be simplified considerably, by recasting the difference between the errors in osmotic coefficient in terms of the differences in the model parameters as follows:

$$\begin{aligned} \phi^P - \phi^{EA} = & I\Delta\beta_{MX}^{(0)} + Ie^{-\alpha_1 I^{1/2}} \Delta\beta_{MX}^{(1)} + Ie^{-\alpha_2 I^{1/2}} \Delta\beta_{MX}^{(2)} \\ & + I^2 \Delta C_{MX}^{(0)} - \left(\frac{4\nu_M}{(\nu_M + \nu_X)z_M} \right) \left\{ I^2 e^{-\omega_1 I^{1/2}} C_{MX}^{(1,EA)} + I^2 e^{-\omega_2 I^{1/2}} C_{MX}^{(2,EA)} \right\} \end{aligned} \quad (\text{I-104})$$

where,

$$\Delta X_1 \equiv \Delta \beta_{MX}^{(0)} \equiv \beta_{MX}^{(0,P)} - \beta_{MX}^{(0,EA)} \quad (\text{I-105})$$

$$\Delta X_2 \equiv \Delta \beta_{MX}^{(1)} \equiv \beta_{MX}^{(1,P)} - \beta_{MX}^{(1,EA)} \quad (\text{I-106})$$

$$\Delta X_3 \equiv \Delta \beta_{MX}^{(2)} \equiv \beta_{MX}^{(2,P)} - \beta_{MX}^{(2,EA)} \quad (\text{I-107})$$

$$\Delta X_4 \equiv \Delta C_{MX}^{(0)} \equiv \left(\frac{2(v_M v_X)^{1/2}}{(v_M + v_X)|z_M z_X|} \right) C_{MX}^{(\phi,P)} - \left(\frac{4v_M}{(v_M + v_X)|z_X|} \right) C_{MX}^{(0,EA)} \quad (\text{I-108})$$

The error measure E is now minimized by setting the partial derivatives of E with respect to the unknown parameter differences ΔX_i equal to zero

$$\frac{\partial E^2}{\partial \Delta X_i} = \int_0^{I_{\max}} \frac{\partial(\phi^P - \phi^{EA})}{\partial \Delta X_i} (\phi^P - \phi^{EA}) dI = 0 \quad (\text{I-109})$$

Substituting for the osmotic coefficient error from Equation I-104 in Equation I-109, and rearranging the terms, yields the matrix equation

$$[A_{ik}](\Delta X_k) = (B_i) \quad ; \quad i, k = 1 \dots 4 \quad (\text{I-110})$$

where,

$$A_{ik} \equiv \int_0^{I_{\max}} \frac{\partial(\phi^P - \phi^{EA})}{\partial \Delta X_i} \frac{\partial(\phi^P - \phi^{EA})}{\partial \Delta X_k} dI$$

$$B_i \equiv \left(\frac{4v_M}{(v_M + v_X)|z_X|} \right) \int_0^{I_{\max}} \frac{\partial(\phi^P - \phi^{EA})}{\partial \Delta X_i} \{ I^2 \cdot e^{-\bar{\omega}_1 I^{1/2}} C_{MX}^{(1,EA)} + I^2 \cdot e^{-\bar{\omega}_2 I^{1/2}} C_{MX}^{(2,EA)} \} dI \quad (\text{I-111})$$

and,

$$\frac{\partial(\phi^P - \phi^{EA})}{\partial \Delta X_i} = \{ I, I e^{-\alpha_1 I^{1/2}}, I e^{-\alpha_2 I^{1/2}}, I^2 \} \quad (\text{I-112})$$

The integrals in the definitions I-111-112 above can be evaluated in closed form as analytical expressions and are given in the paper by Rard and Wijesinghe (2003). The matrix equation I-110 can be solved by standard matrix equation solution methods for the unknown parameter differences ΔX_i . The unknown Standard Pitzer Model parameters can then be evaluated using these parameter differences and the known Archer Model parameters from Equations I-105-108 recast as follows:

$$\beta_{MX}^{(0,P)} = \Delta X_1 + \beta_{MX}^{(0,EA)} = \Delta\beta_{MX}^{(0)} + \beta_{MX}^{(0,EA)} \quad (\text{I-114})$$

$$\beta_{MX}^{(1,P)} = \Delta X_2 + \beta_{MX}^{(1,EA)} = \Delta\beta_{MX}^{(1)} + \beta_{MX}^{(1,EA)} \quad (\text{I-115})$$

$$\beta_{MX}^{(2,P)} = \Delta X_3 + \beta_{MX}^{(2,EA)} = \Delta\beta_{MX}^{(2)} + \beta_{MX}^{(2,EA)} \quad (\text{I-116})$$

$$\begin{aligned} C_{MX}^{(\phi,P)} &= \left(\frac{(\nu_M + \nu_X) |z_M z_X|}{2(\nu_M \nu_X)^{1/2}} \right) \left(\Delta X_4 + \left(\frac{4\nu_M}{(\nu_M + \nu_X) |z_X|} \right) C_{MX}^{(0,EA)} \right) \\ &= \left(\frac{(\nu_M + \nu_X) |z_M z_X|}{2(\nu_M \nu_X)^{1/2}} \right) \left(\Delta C_{MX}^{(0)} + \left(\frac{4\nu_M}{(\nu_M + \nu_X) |z_X|} \right) C_{MX}^{(0,EA)} \right) \end{aligned} \quad (\text{I-117})$$

This mathematical procedure has been implemented in the ConPitzerNC worksheet of each ConPitzerNC workbook, to determine the Standard Pitzer Model parameters from the Archer Model Parameters at each temperature and pressure. The Pitzer parameter values at each temperature determined in this way, are then used by the FitPitzerNC worksheet in each ConPitzerNC workbook to fit new temperature functions, and determine the corresponding temperature coefficients.

I-4.3.2 ConPitzerNC Workbook Implementation

The ConPitzerNC workbooks are designed to first compute the Standard Pitzer Model parameters from Archer Model parameters in a ConPitzerNC type worksheet and then fit new temperature functions to these values using a FitPitzerNC type worksheet. The FitPitzerNC worksheet methodology and implementation are the same as that described in Section 1.3, and will not be discussed further in this Section. The only user specifiable parameters in the ConPitzerNC worksheets are the values IDmax and DImax used to specify the method of imposing the upper limit I_{max} of the range of ionic strength over which the parameter conversion between models is valid. They are used together to implement three different options, as follows:

1. IDmax=1 Maximum Ionic Strength Limit $I_{max} = \text{DImax}$, a user assigned value
2. IDmax=2 Maximum Ionic Strength Limit $I_{max} = \text{Solubility Limit}$ as a function of temperature
3. IDmax=3 Maximum Ionic Strength Limit $I_{max} = \text{Smaller of (DImax, Solubility Limit)}$

I-4.3.3 Example Calculation for ConPitzerNC_MX_CaCl2.xls Workbook:

For the purpose of illustrating the specific manner in which these calculations are carried out, the sequence of calculations performed in the ConPitzerNC_MX_CaCl2.xls workbook are presented below:

1. CoverPage worksheet: On this worksheet, software identification information and spreadsheet checker review comments are first presented. Next, spreadsheet user information on a contents roadmap, an overview of methodology and data sources, protection of data and computational integrity and manner of presentation of results, are given.

2. Directions worksheet: This worksheet gives directions for converting parameters from Archer to Standard Pitzer Models and fitting different temperature functions selected by the user to the converted parameters.
3. RunSettings worksheet: Select the desired temperature basis functions.
4. RunSettings worksheet: Select, if desired Temperature centering and Reference Temperature.
5. RunSettings worksheet: Select Maximum Ionic Strength Option and Maximum Ionic Strength Cut-off Value.
6. ConPitzerNC worksheet: Constant input (Archer) and output (Standard Pitzer) model parameters are defined in lines B13:L13 and B14:L14.
7. ConPitzerNC worksheet: The input Archer model temperature coefficients are set in cells B17:I21 and for the Aphi Debye-Huckel parameter in cells B22:I22.
8. ConPitzerNC worksheet: The input Archer parameters and the Aphi Debye-Huckel parameter are calculated as functions of temperature in cells B32:AB37.
9. ConPitzerNC worksheet: Solubilities as a function of temperature are defined on lines B37:AB37 (molality) and B38:AB38 (ionic strength).
10. ConPitzerNC worksheet: Maximum Ionic Strength is calculated as a function of temperature according to the selected option in cells B81:AB81.
11. ConPitzerNC worksheet: The least-squares coefficient matrix A is calculated at each temperature in cells B87:AB95.
12. ConPitzerNC worksheet: The right-hand side vector B is calculated at each temperature in cells B96:AB98.
13. ConPitzerNC worksheet: The matrix equation solution is carried out at each temperature in cells B99:AB105 and the final solution for parameter differences is calculated in cells B106:AB108.
14. ConPitzerNC worksheet: The Standard Pitzer Model parameters are calculated from the parameter differences obtained in Step 11, and entered in cells B42:AB45.
15. ConPitzerNC worksheet: The osmotic coefficient is calculated for the Archer Model in cells B54:AB59 as a function of temperature and ionic strength.
16. ConPitzerNC worksheet: The osmotic coefficient is calculated for the Standard Pitzer Model in cells B62:AB67 as a function of temperature and ionic strength.

17. ConPitzerNC worksheet: The model conversion error in the osmotic coefficient is calculated as the difference between the osmotic coefficients from the Standard Pitzer and Archer Models in cells B71:AB76 as a function of temperature and ionic strength.
18. The RMS error (cells AC71:AC76) and the Average, Maximum and Minimum values of the osmotic coefficient are also calculated for the two models in cells AD54:AF59 and AD62:AF67, respectively.
19. ConPitzerNC worksheet: Pitzer parameters, osmotic coefficients and their errors, calculated from the two models, are plotted in charts on the extreme right hand side of each ConPitzerNC worksheet.
20. FitPitzerNC worksheet: Standard Pitzer Model parameters are accessed from cells B42:AB45 and are used to fit the temperature coefficients displayed in cells B25:I28. The implementation is the same as previously described in Section 1.3.
21. FitPitzerNC worksheet: Pitzer parameters, osmotic coefficients and their errors, calculated from the input Standard Pitzer Model parameters and the temperature functions fitted to the same model, are plotted in charts on the extreme right hand side of the FitPitzerNC worksheet of the ConPitzerNC workbook.
22. ResultsSummary worksheet: The fitted temperature coefficients for the Standard Pitzer Model are summarized in cells B25:I28.
23. ResultsSummary worksheet: The RMS errors, Average, Maximum and Minimum values of the osmotic coefficients calculated from the output Standard Pitzer Model and the input Archer Model are summarized here separately for the model conversion and temperature function steps. These statistics enable the errors incurred in the model conversion and temperature function fitting steps to be separately assessed.

The testing and validation of the Pitzer parameters involves the comparison of computed osmotic coefficients from the binary (MX), and ternary (MMX, MXX) spreadsheets with the predictions obtained between different Pitzer models reported in the literature sources in order to examine the accuracy of the conversion. This process also includes evaluation of the accuracy of temperature functions of the refitted parameters. Pitzer parameters obtained through the refitting of reported values will be discussed individually in the following section. Parameters obtained for 25 °C only will be summarized in a single section since those did not require refitting.

I-4.4 BINARY PITZER INTERACTION PARAMETERS

In this section, the selected Pitzer ion interaction parameters for major salt constituents included in the *data0.ypf* database will be described. All these parameters and associated spreadsheets are listed in Tables I-1 and I-2 as Type MX. The discussions on the compilation of parameter data are focused on those that needed refitting due to their temperature dependence. Many parameters did not require any refitting since the gathered values are only valid at 25 °C. For these, only simple conversions were necessary.

The user is advised of the limited ranges listed in Table I-1 for several Pitzer parameters . The user must consult the original sources for more information on the permissible physico-chemical conditions for which the parameters are valid. Use of these parameters outside their respective ranges of validation is inadvisable and is not permitted for applications on the Yucca Mountain Project unless specific justification is provided.

I-4.4.1 Ions: Ca^{2+} - Cl^-

Associated Spreadsheet: ConPitzerNC_MX_CaCl2.xls

Source: Sterner et al. (1998)

Description: Input parameters and equations from Sterner et al. (1998; Model 2 in Table II and Table I) in the ConPitzerNC model parameter conversion worksheet were verified for $\beta_{MX}^{(0)}$, $\beta_{MX}^{(1)}$, $\beta_{MX}^{(2)}$, $C_{MX}^{(0)}$, $C_{MX}^{(1)}$ (termed Beta(0), Beta(1), Beta (2), C(0), and C(1), respectively, in the spreadsheets) input parameters from the approach of Archer (2000). Sterner et al. (1998) did not report tabulated values of the osmotic coefficients calculated using their 4-parameter Archer-type model. A visual comparison of the values computed using their model in the ConPitzerNC worksheet against the plotted values in Figure 2 of Sterner et al. (1998) indicates general agreement. The standard Pitzer model parameters $\beta_{MX}^{(0)}$, $\beta_{MX}^{(1)}$, and C^ϕ were determined from the Archer model parameters using the methodology presented by Rard and Wijesinghe (2003). The temperature coefficients for the standard form of Pitzer parameters $\beta_{MX}^{(0)}$, $\beta_{MX}^{(1)}$, and C^ϕ are calculated in the FitPitzerNC worksheet using the parameter values computed as a function of temperature in the ConPitzerNC worksheet. Comparison of the osmotic coefficient calculated using these temperature coefficients with the input values from the ConPitzerNC worksheet confirms the accuracy of the temperature coefficient fits. The temperature coefficient fitting errors are acceptable for this database and negligible compared to the model parameter conversion errors that result from constraining the output model to three parameters instead of the four parameters of the source model. It should be noted that Sterner et al.'s model was claimed to be valid from 25 to 250 °C. Because of the considerable range of ionic strengths being fitted here ($I = 0\text{--}45$ mol/kg), the 3-parameter standard Pitzer model is less accurate than for many other systems. However, the present converted model should yield more accurate solubility predictions than the model presented for CaCl_2 by Greenberg and Møller (1989) that had not been developed for such high ionic strengths. Table I-4 compares the current model's 3 to 4 term osmotic coefficients to experimental results from Robinson and Stokes (1965) at 25°C. There is a notable deviation (10.5%) in the mid-ionic strength range (9 mol/kg), which is acceptable given the large range being fitted as indicated previously.

Table I-4. Comparison of Osmotic Coefficients (ϕ) From the 3 to 4 Term Fit to Those Measured for CaCl_2 at 25 °C

Molality of CaCl_2	3-4 Term Fit	Measurements ^a	Difference (%)
1.0	1.052	1.046	0.6
3.0	1.964	1.779	10.5
6.0	2.847	2.891	1.5
8.0	3.114	3.151	1.2
10.0	3.123	3.169	1.5

^a Taken from Robinson and Stokes (1965), Appendix 8.5, Table 1, p. 478.

I-4.4.2 Ions: Ca^{2+} - NO_3^-

Associated Spreadsheet: ConPitzerNC_MX_Ca(NO3)2.xls

Source: Rard and Wijesinghe (2003); Oakes et al. (2000)

Description: Input parameters and equations from Oakes et al. (2000; Table 4 and Equation 49) in the ConPitzerNC model parameter conversion worksheet were verified for $\beta_{MX}^{(0)}$, $\beta_{MX}^{(1)}$, $C_{MX}^{(0)}$, $C_{MX}^{(1)}$, and $C_{MX}^{(2)}$ input parameters (termed Beta(0), Beta(1), C(0), C(1) and C(2), respectively in the spreadsheet). The osmotic coefficients from the Oakes et al. (2000) model parameters calculated at selected temperatures and molalities in the worksheet agreed exactly with the values given by Oakes et al. (2000; Table 5), except for occasional differences of 0.001 related to rounding errors. The standard Pitzer model parameters $\beta_{MX}^{(0)}$, $\beta_{MX}^{(1)}$, and C^ϕ were determined from the Oakes et al. (2000) model parameters using the methodology presented by Rard and Wijesinghe (2003). The standard Pitzer model parameters calculated in this manner from the Oakes et al. (2000) parameters were verified by comparing the standard Pitzer model parameters calculated in the in the ConPitzerNC worksheet against the values given by Rard and Wijesinghe (2003). The osmotic coefficients calculated in the ConPitzerNC worksheet also agree with the plots of osmotic coefficients given by Rard and Wijesinghe (2002). The two verification methods by Rard and Wijesinghe (2003) explained in the previous section also apply in this case.

The temperature coefficients for the standard Pitzer parameters $\beta_{MX}^{(0)}$, $\beta_{MX}^{(1)}$, and C^ϕ are calculated in the FitPitzerNC worksheet using the parameter values computed as a function of temperature in the ConPitzerNC worksheet. Comparison of the osmotic coefficient calculated using these temperature coefficients with the input values from both the ConPitzerNC worksheet and the values fitted from Oakes et al. (2000). Model values in the ConPitzerNC worksheet, confirm the accuracy of the temperature coefficient fits. On average, the temperature coefficient fitting errors are a factor of 10 smaller than the model parameter conversion errors that result from constraining the output model to three parameters instead of the five parameters in the source model. In both ConPitzerNC and FitPitzerNC worksheets, the parameters are evaluated at 5 °C intervals, whereas in the paper by Rard and Wijesinghe (2003) parameter values were given at only seven selected temperatures. The fine temperature grid in the FitPitzerNC worksheet yields sufficiently accurate fits for the temperature coefficients. It should be noted that Oakes et al.'s (2000) original model was claimed to be valid from 25 to 100 °C, so that the results presented in this spreadsheet outside this temperature range represent extrapolations beyond the confirmed range of validity. The fitting errors demonstrate the acceptability of these coefficients for this database.

I-4.4.3 Ions: Cs^+ - Cl^-

Associated Spreadsheet: FitPitzerNC_MX_CsCl.xls

Source: Holmes and Mesmer (1983); cited 114 times by 3/2003.

Description: Input parameters and equations from Holmes and Mesmer (1983; Table V and Equation 25) were verified for $\beta_{MX}^{(0)}$, $\beta_{MX}^{(1)}$, and C^ϕ . Calculated values of the osmotic coefficient from this spreadsheet were compared with those listed in a supplement to the data source paper by

Holmes and Mesmer (1983; Supplementary Material). There was nearly exact agreement with values calculated in this spreadsheet, with a maximum difference of less than 0.001 over the full range of molality and temperature given in the spreadsheet. This agreement is a confirmation of the validity of the osmotic coefficient calculations reported in this spreadsheet. Additionally, Table I-5 contains a comparison of osmotic coefficients from the 3 to 4 term fitting to experimental results (Robinson and Stokes, 1965; Appendix 8.10, Table 3, p 485), with excellent agreement achieved ($\leq 0.5\%$ difference).

Table I-5. Comparison of Osmotic Coefficients (ϕ) From the 3-4 Term Fit to Those Measured for CsCl at 25 °C

Molality of CsCl	3-4 Term Fit	Measurements ^a	Difference (%)
0.1	0.916	0.917	0.1
0.5	0.872	0.869	0.3
1.0	0.861	0.857	0.5
3.0	0.881	0.880	0.1
6.0	0.950	0.945	0.5

^a Taken from Robinson and Stokes (1965), Appendix 8.10, Table 3, p. 485.

I-4.4.4 Ions: H⁺ - Cl⁻

Associated Spreadsheet: FitPitzerNC_MX_HCl.xls

Source: Holmes et al. (1987); cited 65 times by 3/2003.

Description: Input parameters and equation from Holmes et al. (1987; Table 3 [first column] and Equation 31) were verified for $\beta_{MX}^{(0)}$, $\beta_{MX}^{(1)}$, C^ϕ , and A^ϕ . The RMS error in the osmotic coefficient over the fitted temperature range (see spreadsheet tab “Results Summary”) for the 3-4 term conversion was >0.001 . Calculated values of the osmotic coefficient from this spreadsheet were compared with those listed at 25°C in the extensive tables from Robinson and Stokes (1965, Table 1, Appendix 8.10, p. 483). There was very good agreement with the spreadsheet values at 25°C as shown in Table I-6, with a maximum difference of 0.006 at I = 3 mol/kg. Model I in Holmes et al. (1987, Table 3 and text p. 876) is stated to be valid up to an ionic strength of 7.0 mol/kg. This agreement is considered to be sufficient confirmation of the validity of the osmotic coefficient calculations reported in the spreadsheet.

Table I-6. Comparison of Osmotic Coefficients (ϕ) From the 3- to 4 Term Fit to Those Measured for HCl at 25 °C

Molality of HCl	3-4 Term Fit	Measurements ^a	Difference (%)
0.1	0.944	0.943	0.1
0.5	0.974	0.974	<0.1
1.0	1.039	1.039	<0.1
3.0	1.342	1.348	0.4
6.0	1.844	1.845	<0.1

^a Taken from Robinson and Stokes (1965), Appendix 8.10, Table 1, p. 483.

I-4.4.5 Ions: H^+ - HSO_4^- **Associated Spreadsheet:** [FitPitzerNC_MX_HHSO4.xls](#)**Source:** Holmes and Mesmer (1994)

Description: Input parameters and equation from Holmes and Mesmer (1994; Table 4 and Equation 28) were verified for $\beta_{MX}^{(0)}$, $\beta_{MX}^{(1)}$, and C^ϕ . Note that there is an error in Table 4 of the source document (Holmes and Mesmer, 1994); it gives incorrect p1 parameter values that are too large by a factor of 1000. Calculated values of the hypothetical fully dissociated binary osmotic coefficient from this spreadsheet cannot be compared with any experimental values because experimentally determined values include the effects of partial dissociation into H^+ , HSO_4^- and SO_4^{2-} ions rather than H^+ and HSO_4^- ions only. However, the values of the calculated osmotic coefficient are reasonable for a fully dissociated 1-1 electrolyte, except at the highest ionic strengths where the source parameters are not constrained by experimental measurements and are larger than expected for an electrolyte of this charge type. The binary parameters for H^+ and HSO_4^- should only be used in combination with the H^+ and SO_4^{2-} parameters and the mixing parameters (θ , $\psi = 0$) should be taken from the same source document. It should also be noted that the higher order electrostatic interactions represented by the ${}^E\theta$ and ${}^E\theta'$ third order terms of the Pitzer model were taken into account in this source document. In an earlier paper (Holmes and Mesmer, 1992) the authors did not account for these interactions. Holmes and Mesmer (1994) demonstrate that their new fits result in calculations that agree well with the experimental measurements over a range of conditions that include different degrees of dissociation of HSO_4^- . In fact they found that the earlier models also result in acceptable fits.

I-4.4.6 Ions: H^+ - SO_4^{2-} **Associated Spreadsheet:** [FitPitzerNC_MX_H2SO4.xls](#)**Source:** Holmes and Mesmer (1994)

Description: Input parameters and equation from Holmes and Mesmer (1994; Table 4 and Equation 28) were verified for $\beta_{MX}^{(0)}$, $\beta_{MX}^{(1)}$, and C^ϕ . Calculated values of the hypothetical fully dissociated binary osmotic coefficient from this spreadsheet cannot be compared with any experimental values because experimentally determined values include the effects of partial dissociation into H^+ , HSO_4^- and SO_4^{2-} ions rather than H^+ and SO_4^{2-} ions only. However, the values of the calculated osmotic coefficient are reasonable for a fully dissociated 1-2 electrolyte, except at the highest ionic strengths where the source parameters are not constrained by experimental measurements and are unrealistically large. The binary parameters for H^+ and SO_4^{2-} should only be used in combination with the H^+ and HSO_4^- parameters and the mixing parameters (θ , $\psi = 0$) should be taken from the same source document. In addition, several values of C^ϕ were independently calculated using the input source data and underlying equations, and exact agreement was obtained with the values calculated in the spreadsheet. It should also be noted that the higher order electrostatic interactions represented by the ${}^E\theta$ and ${}^E\theta'$ third order terms of the Pitzer model were taken into account in this source document. In an earlier paper (Holmes and Mesmer, 1992) the authors did not account for these interactions. Holmes and Mesmer (1994)

demonstrate that their new fits result in calculations that agree well with the experimental measurements over a range of conditions that include different degrees of dissociation of HSO_4^- . In fact they found that the earlier models also result in acceptable fits.

I-4.4.7 Ions: H^+ - NO_3^-

Associated Spreadsheet: [Pitzer_MX_HNO3_CFJC.xls](#)

Source: Felmy et al. (1994a) and Clegg and Brimblecombe (1990a; cited 47 times by 3/2003)

Description: The binary parameters $\beta_{MX}^{(0)}$, $\beta_{MX}^{(1)}$, and C^ϕ listed by Clegg and Brimblecombe (1990a; Table X) at 298.15 K were confirmed against the values generated with the coefficients reported by Felmy et al. (1994a; Table 1 with Equation 2) who used the former source for derivation of Pitzer temperature-dependent parameter data. Unlike the previous FitPitzerNC spreadsheets, the binary parameters were refitted using the standard regression function in MS Excel. The reproducibility of the refitted binary parameters when compared with those tabulated from Clegg and Brimblecombe (1990a, Table 10, p. 5378) at 298.15 K was identical. Visual comparison of mean activity and rational osmotic coefficients (Clegg and Brimblecombe, 1990a; Figures 1 and 9) calculated using these binary parameters indicate a strong agreement with those in Clegg and Brimblecombe (1990a) up to an HNO_3 concentration of ~ 6 molal. These favorable comparisons demonstrate the acceptability of these coefficients for this database. The Clegg and Brimblecombe (1990a) model is mole fraction based and these authors suggested this upper concentration value for the binary parameters they report for the Pitzer model that is molality-based.

I-4.4.8 Ions: K^+ - Br^-

Associated Spreadsheet: [FitPitzerNC_MX_KBr.xls](#)

Source: Holmes and Mesmer (1998b)

Description: Input parameters and equation from Holmes and Mesmer (1998b, Table 4 and Equation 14) were verified for $\beta_{MX}^{(0)}$, $\beta_{MX}^{(1)}$, and C^ϕ . The RMS error in the osmotic coefficient over the fitted temperature range (see spreadsheet tab "Results Summary") from the 3-4 term conversion is typically ~ 0.001 , except at higher ionic strengths where the deviation becomes 0.005 and 0.026 at $I = 3$ and 6 mol/kg, respectively. Values of the osmotic coefficient calculated using the source equation were compared with experimental values listed at 25°C in Robinson and Stokes (1965, Appendix 8.10, Table 2, p. 484) and at 200°C in the source document (Holmes and Mesmer, 1998b; Table 1, p. 728). Results of the comparison at 25 °C are shown in Table I-7; there was good agreement with the 3-4 term values calculated in this spreadsheet, with a maximum difference of 0.005 at $I = 3.0$ mol/kg. Good agreement is also obtained at 200 °C up to high ionic strengths, e.g. at $I = 6.097$ mol/kg $\phi = 1.0264$ while in Holmes and Mesmer (1998b; Table 1 p. 728) at $I = 6$ mol/kg the value of $\phi = 1.0258$. It should be noted that there are two errors in Equation 14 of Holmes and Mesmer (1998b, p. 734) in the functional form of the temperature function, and in the reference temperature T_r that was incorrectly reported as 413.15 K instead of 298.15 K. The

correct version of this equation is given in the spreadsheet cover page and it is equivalent to the equation as first derived by Holmes and Mesmer (1983, Equation 25).

Table I-7. Comparison of Osmotic Coefficients (ϕ) From the 3-4 Term Fit to Those Measured for KBr at 25°C

Molality of KBr	3-4 Term Fit	Measurements ^a	Difference (%)
0.1	0.928	0.928	0.0
0.5	0.905	0.904	0.1
1.0	0.907	0.907	<0.0
3.0	0.960	0.955	0.5

^a Taken from Robinson and Stokes (1965), Appendix 8.10, Table 2, p. 484.

I-4.4.9 Ions: K⁺ - Cl⁻

Associated Spreadsheet: FitPitzerNC_MX_KCl.xls

Source: Greenberg and Møller (1989); cited 51 times as of 3/2003.

Description: Input parameters and equation from Greenberg and Møller (1989, Table 1 and 3, and Equation 3) were verified for $\beta_{MX}^{(0)}$, $\beta_{MX}^{(1)}$, C^ϕ , and A^ϕ . The RMS error in the osmotic coefficient over the fitted temperature range (see spreadsheet tab “Results Summary”) for source to 3-4 term conversion was $\Delta\phi < 0.001$. In addition, several values of $\beta_{MX}^{(0)}$ were independently calculated using the input source data and underlying equations, and exact agreement was obtained with the values calculated in the spreadsheet. Calculated values of the osmotic coefficient from this spreadsheet were compared with those from the recent critical review of Archer (1999, Table 7). There was good agreement with values calculated in this spreadsheet, with a maximum difference of 0.006, but with much better agreement at most temperatures and molalities. Direct comparison at 25 and 100 °C is shown in Table I-8 below. These minor differences most likely arise from the differences in the underlying data sources. This agreement is considered to be sufficient confirmation of the validity of the osmotic coefficient calculations reported in this spreadsheet.

Table I-8. Comparison of Osmotic Coefficients (ϕ) Values From the 3-4 Term Fit to Those Measured for KCl at 25 and 100 °C

25 °C			
Molality of KCl	3-4 Term Fit	Measurements ^a	Difference (%)
0.1	0.926	0.9261	<0.1
0.5	0.900	0.9000	0.1
1.0	0.898	0.8992	0.1
100 °C			
0.1	0.918	0.9168	0.1
0.5	0.895	0.8939	0.1
1.0	0.899	0.8984	0.1
6.0	1.032	1.0341	0.2

^a Taken from Archer (1999), Table 7.

I-4.4.10 Ions: K⁺ - SO₄²⁻**Associated Spreadsheet:** [FitPitzerNC_MX_K2SO4.xls](#)**Source:** Greenberg and Møller (1989); cited 51 times as of 3/2003.

Description: Input parameters and equation from Greenberg and Møller (1989, Tables 1 and 3, and Equation 3) were verified for $\beta_{MX}^{(0)}$, $\beta_{MX}^{(1)}$, C^ϕ , and A^ϕ . The RMS error in the osmotic coefficient over the fitted temperature range (see spreadsheet tab “Results Summary”) for the 3-4 term fitting conversion was very negligible ($<10^{-10}$). In addition, several values of $\beta_{MX}^{(0)}$, $\beta_{MX}^{(1)}$, and C^ϕ were independently calculated using the input source data and underlying equations, and exact agreement was obtained with the values calculated in the spreadsheet. In Table I-9 below, calculated values of the osmotic coefficient from this spreadsheet were compared with those listed in Holmes and Mesmer (1986, Table V; cited 55 times as of 3/2003). There was reasonable agreement of the values reported in this paper with values calculated in the spreadsheet (differences in osmotic coefficient, $\Delta\phi \leq 0.02$) except at 200 °C where the error was relatively high ($\Delta\phi_{\max} = 0.11$). Because the available data do not extend beyond $I = 2$ mol/kg at low temperatures and $I = 7$ mol/kg at high temperatures, and due to solubility limitations, the values calculated in this spreadsheet at the higher ionic strengths are not physically relevant. The agreement at lower ionic strengths and temperatures is confirmation of the validity of the osmotic coefficient calculations reported in this spreadsheet.

Table I-9. Comparison of Osmotic Coefficients (ϕ) Values From the 3-4 Term Fit to Those Measured for K₂SO₄ at 25 and 150 °C.

25 °C			
Molality of K ₂ SO ₄	3-4 Term Fit	Measurements ^a	Difference (%)
0.1	0.784	0.779	0.6
0.5	0.686	0.690	0.6
1.0	0.631	0.651	3.1
150 °C			
0.1	0.743	0.726	2.3
0.5	0.652	0.646	1.2
1.0	0.616	0.613	0.5

^a Taken from Holmes and Mesmer (1986), Table V.

I-4.4.11 Ions: Cs⁺ - Br⁻**Associated Spreadsheet:** [FitPitzerNC_MX_CsBr.xls](#)**Source:** Holmes and Mesmer (1998b)

Description: Input parameters and equations from Holmes and Mesmer (1998b, Table 4 and Equation 14) were verified for $\beta_{MX}^{(0)}$, $\beta_{MX}^{(1)}$, and C^ϕ . The RMS fitting errors over the corresponding fitted temperatures between the Holmes and Mesmer (1998b) Equation 14 and the spreadsheets 3-4 term fit were mostly $\Delta\phi < 0.001$, with the exception at $I = 6$ mol/kg where $\Delta\phi = 0.0045$. Values of the osmotic coefficient calculated using the source equation were compared with experimental values listed in the source document at 200 °C (Holmes and Mesmer, 1998b, Table 1), and at 25 °C

against Robinson and Stokes (1965; Appendix 8.10, Table 3, p. 485). At 25°C, there was good agreement with values calculated in this spreadsheet, with a maximum difference of $\Delta\phi_{\max} = 0.003$ at $I = 0.1$ mol/kg as shown in Table I-10. At 200 °C, good agreement is also obtained with $\Delta\phi = 0.055$ at ~ 6 mol/kg. It should be noted that there are two errors in Equation (14) of Holmes and Mesmer (1998b, p. 734): 1) an error in the formula of the temperature function; and 2) an error in the reference temperature T_r which was incorrectly reported as 413.15 K instead of 298.15 K. The corrected version of this equation given on the spreadsheet cover page, it is equivalent to the correct form of this equation as first derived by Holmes and Mesmer (1983, Equation 25).

Table I-10. Comparison of Source Osmotic Coefficients (ϕ) to Measured for CsBr at 25 °C

Molality of CsBr	Source Equation	Measurements ^a	Difference (%)
0.1	0.914	0.917	0.3
0.5	0.867	0.865	0.2
1.0	0.852	0.850	0.2
3.0	0.866	0.866	0.0

^a Taken from Robinson and Stokes (1965), Appendix 8.10, Table 3, p. 485.

I-4.4.12 Ions: $\text{Li}^+ - \text{Br}^-$

Associated Spreadsheet: [FitPitzerNC_MX_LiBr.xls](#)

Source: Holmes and Mesmer (1998b)

Description: Input parameters and equations from Table 4 (p. 737) and Equation 14 (p. 734) of Holmes and Mesmer (1998b) were verified for $\beta_{MX}^{(0)}$, $\beta_{MX}^{(1)}$, and C^ϕ . The RMS error in the osmotic coefficient over the fitted temperature range (see spreadsheet tab “Results Summary”) for the 3-4 term conversion is typically ~ 0.001 , except towards higher ionic strengths, e.g. deviations approach 0.02 at $I = 6$ mol/kg. Values of the osmotic coefficient calculated using the source equation were compared with experimental values listed in Holmes and Mesmer (1998b; Table 1, p. 728) at 200 °C and at 25 °C against Robinson and Stokes (1965; Appendix 8.10, Table 3). For 25 °C the comparison is shown in Table I-11; there was good agreement with values calculated in this spreadsheet, with a maximum difference of $\Delta\phi = 0.007$ at $I = 3.0$ mol/kg, increasing to $\Delta\phi = 0.01$ at $I = 6.0$ mol/kg. Good agreement is also obtained at 200 °C, e.g. $\phi = 1.146$ at 3.07 molality (Holmes and Mesmer, 1998b; Table 1, p. 728) compared with $\phi = 1.138$ from the source equation at exactly 3.0 molality. It should be noted that there are two errors in Equation (14) of Holmes and Mesmer (1998b, p. 734) for the functional form of the temperature function, and an error in the reference temperature T_r which was incorrectly reported as 413.15 K instead of 298.15 K. The correct version of this equation is given in the spreadsheet cover page and it is equivalent to the correct form of this equation as first derived by Holmes and Mesmer (1983, Equation 25).

Table I–11. Comparison of Source Osmotic Coefficients (ϕ) to Measured for LiBr at 25 °C

Molality of LiBr	Source Equation	Measurements ^a	Difference (%)
0.1	0.942	0.943	0.1
0.5	0.972	0.970	0.2
1.0	1.038	1.035	0.3
3.0	1.373	1.364	0.7
6.0	1.999	1.989	0.5

^a Taken from Robinson and Stokes (1965), Appendix 8.10, Table 1, p. 483.

I–4.4.13 Ions: Li⁺ - Cl⁻

Associated Spreadsheet: [FitPitzerNC_MX_LiCl.xls](#)

Source: Holmes and Mesmer (1983); cited 114 times by 3/2003.

Description: Input parameters and equation from the source document were verified for $\beta_{MX}^{(0)}$, $\beta_{MX}^{(1)}$, and C^ϕ data from Holmes and Mesmer (1983; Table V and Equation 25). Fitting errors between the source and spreadsheet 3-4 term equation were negligible and resulted in osmotic coefficient differences of $<10^{-5}$. Values of the osmotic coefficient at ~ 1.0 mol/kg calculated using the source equation (Holmes and Mesmer, 1983, Equation 25) were compared with experimental values listed in the source document (Table III) at 250°C at $\phi = 0.8292$ and 0.825 , respectively. For the comparison at 25 °C against Robinson and Stokes (1965; Appendix 8.10, Table 1, p. 483) there is good agreement with values calculated in this spreadsheet, with a maximum difference of $\Delta\phi = 0.004$ at $I = 6.0$ mol/kg as shown in Table I–12 below.

Table I–12. Comparison of Source Osmotic Coefficients (ϕ) to Measured for LiCl at 25 °C

Molality of LiCl	Source Equation	Measurements ^a	Difference (%)
0.1	0.941	0.939	0.2
0.5	0.963	0.963	0.0
1.0	1.016	1.018	0.2
3.0	1.287	1.286	0.1
6.0	1.795	1.791	0.2

^a Taken from Robinson and Stokes (1965), Appendix 8.10, Table 1, p. 483.

I–4.4.14 Ions: Mg²⁺ - Cl⁻

Associated Spreadsheet: [FitPitzerNC_MX_MgCl2.xls](#)

Source: Pabalan and Pitzer (1987b); cited 104 times by 3/2003.

Description: Input parameters and equations from the source document by Pabalan and Pitzer (1987b; Appendix, p. 2442) were verified for $\beta_{MX}^{(0)}$, $\beta_{MX}^{(1)}$, and C^ϕ by independently calculating these parameters, and agreement was obtained with the values calculated in the spreadsheet. The RMS error in the osmotic coefficient over the fitted temperature range (see spreadsheet tab “Results Summary”) for the 3-4 term conversion is typically <0.001 , except at $I = 18$ mol/kg when it is 0.0015. In addition, osmotic coefficients were calculated from the source equation

(Pabalan and Pitzer, 1987b, Appendix, p. 2442) and compared with those listed in the tables from Holmes et al. (1997; Table 2), and Wang et al. (1998; Table 4). There was fair agreement with values calculated in this spreadsheet, within 0.013 at 25 °C (see Table I-13), within 0.2 at 100 °C (see Table I-14), within 0.25 at 150 °C, and within 0.2 at 200 °C. These larger differences at higher temperatures arise from the differences in the data used to calculate the values in these two papers and the generally lower accuracy in high temperature thermodynamic measurements.

Table I-13. Comparison of Source Osmotic Coefficients (ϕ) to Measured for MgCl_2 at 25 °C.

Molality of MgCl_2	Source Equation	Measurements ^a	Difference (%)
0.1	0.8618	0.8606	0.14
0.5	0.9439	0.9439	0.00
1.0	1.1088	1.1100	0.11
3.0	2.0205	2.0070	0.67

^a Taken from Holmes et al. (1997), Table 2, p. 1369.

Table I-14. Comparison of Source Osmotic Coefficients (ϕ) to Measured for MgCl_2 at 100 °C.

Molality of MgCl_2	Source Equation	Measurements ^a	Difference (%)
0.05	0.8429	0.8460	0.4
0.1	0.8324	0.8332	0.1
0.5	0.8737	0.8628	1.3
1.0	0.9856	0.9921	0.7
3.0	1.6634	1.6891	1.5
6.0	2.8450	3.0357	6.3

^a Taken from Wang et al. (1998), Table 4, p. 979.

I-4.4.15 Ions: Mg^{2+} - SO_4^{2-}

Associated Spreadsheet: [FitPitzerNC_MX_MgSO4.xls](#)

Source: Pabalan and Pitzer (1987b); cited 104 times by 3/2003.

Description: Input parameters and equations from Pabalan and Pitzer (1987b; Appendix, p. 2443) were verified for $\beta_{MX}^{(0)}$, $\beta_{MX}^{(1)}$, and C^ϕ . The RMS error in the osmotic coefficient over the fitted temperature range (see spreadsheet tab “Results Summary”) for the 3-4 term conversion is typically <0.01 , except at very high ionic strengths; e.g. at $I = 12$ and 24 mol/kg then $\Delta\phi = 0.014$ and 0.132 , respectively. Calculated values of the osmotic coefficient from this spreadsheet were compared with those listed in the Table V of Phutela and Pitzer (1986), which is the original source of the temperature coefficients used by Pabalan and Pitzer (1987b). There is good agreement with source equation values calculated in this spreadsheet, with a maximum difference of ~ 0.001 . The minor differences that exist most likely arise from differences in the Debye-Hückel $A^\phi(\phi)$ coefficient. In the original source paper by Phutela and Pitzer (1986), models with both constant and temperature dependent α_2 parameters were mentioned, but the model from which the listed osmotic coefficient results were generated was not clearly specified. However, Pabalan and Pitzer (1987b) implied the use of a constant α_2 parameter, and this was confirmed by the good agreement with the calculations in this spreadsheet. It should be noted that the highest ionic strengths, for which unrealistic osmotic coefficients are calculated in this spreadsheet, greatly

exceed the concentration range for which the model was parameterized. The model should provide reasonably accurate results at ionic strengths below the solubility limit. This is supported by a comparison with experimental measurements at 25 °C in Table I–15 below, where the 3-4 term fitted results are compared to the experiments at 25 and 100 °C with a $\Delta\phi_{\max} = 0.012$.

Table I–15. Comparison of 3-4 Term Fitting Osmotic Coefficients (ϕ) to Measured for MgSO_4 at 25 and 100 °C

25 °C			
Molality of MgSO_4	3-4 Term Fit	Measurements ^a	Difference (%)
0.1	0.597	0.596	0.2
0.5	0.530	0.527	0.6
1.0	0.531	0.527	0.8
3.0	0.915	0.925	1.1
100 °C			
0.1	0.527	0.529	0.4
0.5	0.438	0.444	1.3
1.0	0.412	0.419	1.7
3.0	0.646	0.634	1.9

^a Taken from Phutela and Pitzer (1986), Table V, p. 899.

I-4.4.16 Ions: Na^+ - Br^-

Associated Spreadsheet: [FitPitzerNC_MX_NaBr.xls](#)

Source: Holmes and Mesmer (1998b)

Description: Input parameters and equations from Table 4 (p. 737) and Equation 14 (p.734) of Holmes and Mesmer (1998b) were verified for $\beta_{MX}^{(0)}$, $\beta_{MX}^{(1)}$, and C^ϕ . The average of the RMS error in the osmotic coefficient over the fitted temperature range (see spreadsheet tab “Results Summary”) for the 3-4 term conversion was 0.0013, with a $\Delta\phi_{\max} = 0.0023$. Values of the osmotic coefficient calculated using the source equation were compared with experimental values listed in Holmes and Mesmer (1998b; Table 1, p. 728) at 200 °C, and at 25 °C against both Robinson and Stokes (1965) and Rard and Archer (1995). Comparison at 25 °C is shown in Table I–16, where there was good agreement with values calculated in this spreadsheet, with a maximum difference of 0.008 at $I = 6.0$ mol/kg. At 200 °C, good agreement is obtained over this range of molalities as seen in Table I–17. It should be noted that there are two errors in Equation (14) of Holmes and Mesmer, (1998b, p. 734) for the functional form of the temperature function, and an error in the reference temperature T_r which was incorrectly reported as 413.15 K instead of 298.15 K. The correct version of this equation is given in the spreadsheet cover page and it is equivalent to the correct form of this equation as first derived by Holmes and Mesmer (1983, Equation 25).

Table I-16. Comparison of Source Osmotic Coefficients (ϕ) to Measured for NaBr at 25 °C

Molality of NaBr	Source Equation	Measurements	Difference (%)
0.1	0.935	0.934 ^a	0.1
0.5	0.933	0.933 ^a	0.0
1.0	0.959	0.958 ^a	0.1
3.0	1.109	1.107 ^a	0.2
6.0	1.381	1.389 ^b	0.6

^a Taken from Robinson and Stokes (1965), Appendix 8.10, Table 1, p. 483.

^b Taken from Rard and Archer (1995), Table 3; ϕ at 6.0 mol/kg was linearly interpolated from 5.9151 and 6.1073 mol/kg values.

Table I-17. Comparison of Source Osmotic Coefficients (ϕ) to Measured for NaBr at 200 °C

Spreadsheet Calculated Values		Experimental Values ^a	
Molality of NaBr	Source Equation	Molality of NaBr	Measured
1.0	0.921	0.9814	0.9225
3.0	1.049	2.8264	1.0431
6.0	1.234	6.1392	1.2401

^a Taken from Holmes and Mesmer (1998b), Table1, p.728.

I-4.4.17 Ions: Na⁺ - NO₃⁻

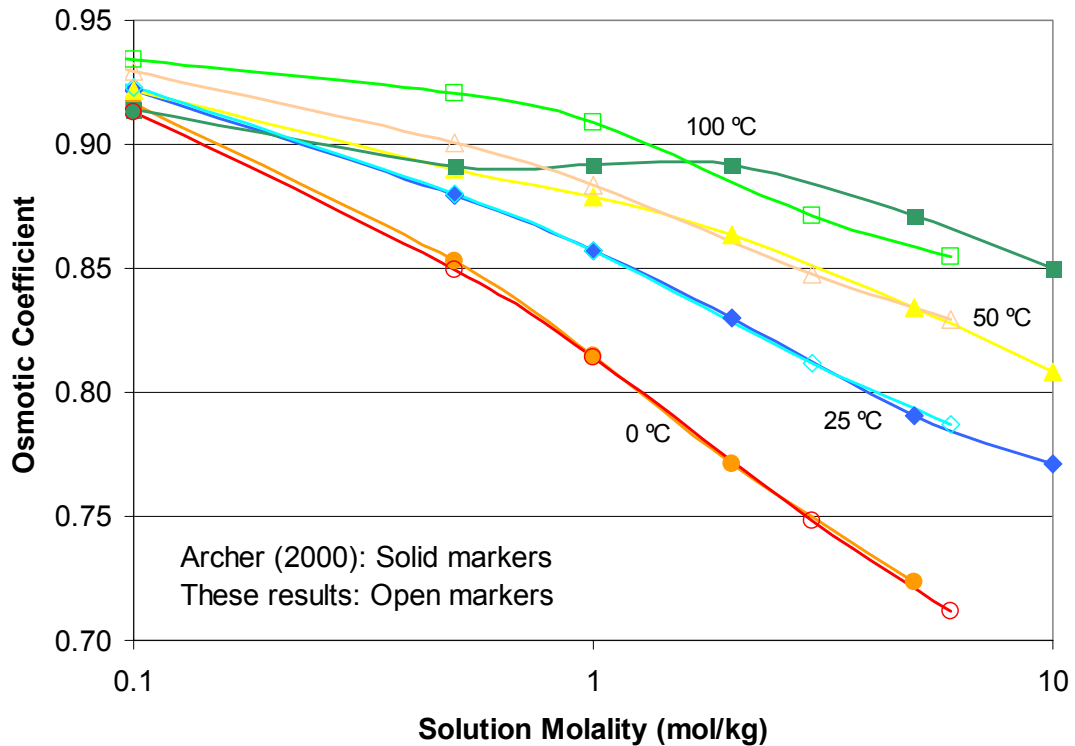
Associated Spreadsheet: ConPitzerNC_MX_NaNO3.xls

Source: Archer (2000)

Description: Input parameters and equations from Archer (2000; Table 4 and Equations 19 through 23) in the ConPitzerNC model parameter conversion worksheet were verified for $\beta_{MX}^{(0)}$, $\beta_{MX}^{(1)}$, $C_{MX}^{(1)}$, and $C_{MX}^{(1)}$ input parameters. The osmotic coefficient and Archer model parameters calculated at selected temperatures and molalities in the worksheet agreed exactly with the values given by Archer (2000; Tables 5 and 7). Note that there is a mistake in Archer's (2000) Table 5 column header for the $C_{MX}^{(1)}$ parameter and that it was not multiplied by 10^3 as indicated. The standard Pitzer model parameters $\beta_{MX}^{(0)}$, $\beta_{MX}^{(1)}$, and C^ϕ were determined from Archer's model parameters using the method presented by Rard and Wijesinghe (2003). The standard Pitzer model parameters calculated in this manner from the Archer parameters were verified by comparing the standard Pitzer model parameters calculated in the ConPitzerNC worksheet against those presented by Rard and Wijesinghe (2003). The osmotic coefficients calculated in the ConPitzerNC worksheet also agree with the plots of osmotic coefficient given by Rard and Wijesinghe (2003). The two verification methods used by Rard and Wijesinghe (2003) explained in Section I-4.4.1 also apply to this case. Both methods generated almost identical results. In the ConPitzerNC worksheet method (1) based on exact analytical matrix coefficient integration, which is more accurate than the approximate method (2), was used. The temperature coefficients for the standard Pitzer parameters $\beta_{MX}^{(0)}$, $\beta_{MX}^{(1)}$, and C^ϕ are calculated in the FitPitzerNC worksheet using the parameter values computed as a function of temperature in the ConPitzerNC worksheet. Comparison of the osmotic coefficient calculated using these temperature coefficients against the input values from both the ConPitzerNC worksheet and the verified values calculated using the Archer model in the ConPitzerNC worksheet, confirm the accuracy of the temperature

coefficient fits. On average, the temperature coefficient fitting errors are a factor of 100 smaller than the model parameter conversion errors that result from constraining the output model to three parameters instead of the four parameters in the source model. The final fitted parameters were compared with the calculated osmotic coefficients in Archer (2000; Table 7) calculated osmotic coefficients. This is shown in Figure I-1 at 4 temperatures (0, 25, 50 and 100 °C) for $I = 0.1$ to 10 mol/kg, where the Archer results have solid symbols and the spreadsheet fitted results have open symbols, and the symbol colors are based on the temperature. The results fit Archer's osmotic coefficients well in the molality range of ~1 to 10.

In both ConPitzerNC and FitPitzerNC worksheets, the parameters are evaluated at 5 °C intervals, whereas in the paper by Rard and Wijesinghe (2003) parameter values were given at only seven selected temperatures. The fine temperature grid in the FitPitzerNC worksheet yields sufficiently accurate fits for the temperature coefficients. It should be noted that Archer's original model was claimed to be valid from -37 to 152 °C, so that the results presented in this spreadsheet at higher temperatures represent an extrapolation beyond the confirmed range of validity of the source model.



DTN: SN0306T0510102.007

Figure I-1. Archer's (2000) Calculated Osmotic Coefficients Compared to Fitted Spreadsheet Results.

I-4.4.18 Ions: Na⁺ - SO₄²⁻**Associated Spreadsheet:** [FitPitzerNC_MX_Na2SO4.xls](#)**Source:** Greenberg and Møller (1989); cited 51 times as of 3/2003.

Description: Input parameters and equation from Greenberg and Møller (1989; Tables 1 and 3 and Equation 3) were verified for $\beta_{MX}^{(0)}$, $\beta_{MX}^{(1)}$, C^ϕ , and A^ϕ . The average of the RMS errors in the osmotic coefficient over the fitted temperature range (see spreadsheet tab “Results Summary”) for the 34 term conversion was 0.012, with $\Delta\phi_{\max} = 0.0436$ at $I = 18$ mol/kg, which is well above the solubility limit and not physically relevant. Calculated values of the osmotic coefficient from this spreadsheet were also compared with those listed in (1) Holmes and Mesmer (1986; Table IV) and (2) Rard et al. (2000; Table XI). There was reasonable agreement of the values reported in these two papers with values calculated in this spreadsheet, as indicated in the summary on the associated spreadsheet cover page, and specifically as shown in Table I-18 comparing the spreadsheet results to Rard et al. (2000) at 25 and 100 °C. The differences between the values in the two papers arise from differences in the underlying data sources. Also note that because the solubility does not extend to $I = 18$ mol/kg, the reported values in this spreadsheet at this high ionic are not physically relevant. This agreement is considered to be sufficient confirmation of the validity of the osmotic coefficient calculations reported in this spreadsheet. In addition, several values of $\beta_{MX}^{(0)}$, $\beta_{MX}^{(1)}$, and C^ϕ were independently calculated using the input source data and underlying equations, and exact agreement was obtained with the values calculated in the spreadsheet.

Table I-18. Comparison of Fitted Osmotic Coefficients (ϕ) to Measured for Na₂SO₄ at 25 and 100 °C

25 °C Comparison			
Molality of Na ₂ SO ₄	Fitted Equation	Measurements ^a	Difference (%)
0.05	0.8281	0.8260	0.3
0.1	0.7927	0.7902	0.3
0.5	0.6871	0.6931	0.9
1.0	0.6345	0.6451	1.6
3.0	0.6602	0.6700	1.5
100 °C Comparison			
0.05	0.8041	0.8036	0.1
0.1	0.7686	0.7682	0.1
0.5	0.6860	0.6917	0.8
1.0	0.6591	0.6595	0.1
3.0	0.6380	0.6387	0.1

^a Taken from Rard et al. (2000), Table XI.**I-4.4.19 Ions: Na⁺ - Cl⁻****Associated Spreadsheet:** [FitPitzerNC_MX_NaCl.xls](#)**Source:** Greenberg and Møller (1989); cited 51 times as of 3/2003.

Description: Input parameters and equations from Greenberg and Møller (1989; Tables 1 and 3, and Equation 3) were verified for $\beta_{MX}^{(0)}$, $\beta_{MX}^{(1)}$, C^ϕ and A^ϕ . The RMS error in the osmotic coefficient

over the fitted temperature range (see spreadsheet tab “Results Summary”) for the 3-4 term conversion was $\Delta\phi < 0.001$. Calculated values of the osmotic coefficient from this spreadsheet were compared with those listed in the extensive tables from Clarke and Glew (1985; Table 19 A). There was good agreement with values calculated in this spreadsheet, with a maximum difference of 0.005, but with much better agreement at most temperatures and molalities; this is shown in Table I–19. These minor differences most likely arise from the differences in the underlying data sources. This agreement is considered to be sufficient confirmation of the validity of the osmotic coefficient calculations reported in this spreadsheet. In addition, several values of $\beta_{MX}^{(1)}$ parameters were independently calculated using the input source data and underlying equations, and exact agreement was obtained with the values calculated in the spreadsheet.

Table I–19. Comparison of Fitted Osmotic Coefficients (ϕ) to Measured for NaCl at 25 and 100 °C

25 °C Comparison			
Molality of NaCl	Fitted Equation	Measurements ^a	Difference (%)
0.05	0.9435	0.9436	<0.1
0.1	0.9324	0.9325	<0.1
0.5	0.9214	0.9222	<0.1
1.0	0.9354	0.9373	0.2
3.0	1.0431	1.0485	0.5
6.0	1.2716	1.2688	0.2
100 °C Comparison			
0.05	0.9345	0.9346	<0.1
0.1	0.9222	0.9223	<0.1
0.5	0.9139	0.9142	<0.1
1.0	0.9332	0.9341	0.1
3.0	1.0439	1.0458	0.2
6.0	1.2108	1.2083	0.2

^a Taken from Clarke and Glew (1985), Table 19 A, pp. 525 and 526.

I–4.4.20 Ions: Na⁺ - OH⁻

Associated Spreadsheet: [FitPitzerNC_MX_NaOH.xls](#)

Source: Pabalan and Pitzer (1987a); cited 42 times as of 3/2003.

Description: Input parameters and equations from Pabalan and Pitzer (1987a; Table 3 and Equations 28 through 30) were verified for $\beta_{MX}^{(0)}$, $\beta_{MX}^{(1)}$, C^ϕ , and A^ϕ . The average of the RMS errors in the osmotic coefficient over the fitted temperature range (see spreadsheet tab “Results Summary”) for the 3-4 term conversion was 0.002 (~0.2%). In addition, several values of $\beta_{MX}^{(0)}$, $\beta_{MX}^{(1)}$, and C^ϕ were independently calculated using the input source data and underlying equations, and exact agreement was obtained with the values calculated in the spreadsheet. Calculated values of the osmotic coefficient from this spreadsheet are compared in Table I–20 below, against those listed for 25°C in Robinson and Stokes (1965; Appendix 8.10, Table 1, p. 483). There was good agreement with the fitted spreadsheet values at 25 °C, with a maximum difference of 1.3%. There was also good agreement over 110–170 °C with the osmotic coefficient values reported by Holmes and Mesmer (1998a). The direct comparison shown at 170 °C below in Table I–21. These comparisons are considered to be sufficient confirmation of the validity of the osmotic coefficient calculations reported in this spreadsheet.

Table I–20. Comparison of Fitted 3-4 Term Osmotic Coefficients (ϕ) to Those Measured for NaOH at 25 °C

Molality of NaOH	3-4 Term Fit	Measurements ^a	Difference (%)
0.1	0.932	0.925	0.8
0.5	0.925	0.937	1.3
1.0	0.947	0.958	1.1
3.0	1.104	1.094	0.9
6.0	1.442	1.434	0.6

^a Taken from Robinson and Stokes (1965), Appendix 8.10, Table 1, p. 483.

Table I–21. Comparison of Fitted 3-4 Term Osmotic Coefficients (ϕ) to Measured for NaOH at 170 °C

Spreadsheet Calculated Values		Experimental Values ^a	
Molality of NaOH	Fitted 3-4 Term ϕ	Molality of NaOH	Measured ϕ
1.0	0.875	1.0495	0.8547
3.0	0.906	3.0341	0.8922
6.0	1.001	6.0 ^b	1.0126

^a Taken from Holmes and Mesmer (1998a), Table 1, p.315.

^b Linearly interpolated from the average results between 5.6 and 6.4 molality.

I-4.4.21 Ions: $\text{NH}_4^+ - \text{SO}_4^{2-}$

Associated Spreadsheet: [ConPitzerNC_MX_\(NH4\)2SO4.xls](#)

Source: Clegg et al. (1996); cited 13 times by 3/2003.

Description: Input temperature coefficients and equation from Clegg et al. (1996; Table 5, equation therein) in the ConPitzerNC model parameter conversion worksheet were verified for $\beta_{MX}^{(0)}$, $\beta_{MX}^{(1)}$, $C_{MX}^{(0)}$, and $C_{MX}^{(1)}$ input parameters. The model used by Clegg et al. (1996) is an Archer-type extended Pitzer model with four parameters, for which conversion of model data to the standard Pitzer model was presented by Rard and Wijesinghe (2003). The osmotic coefficient calculated at selected molalities using the input model in the worksheet agreed exactly with the values given by Clegg et al. (1996; Table 7) at 25 °C. The 3-4 term fitting results differed from those osmotic coefficient values by less than 0.0009 over the 0–100 °C range. Values presented in the worksheet above 100 °C also agree well with the those calculated using the input model, but these extrapolations are beyond the range of validity claimed for the input model. The 3-4 term calculated values of the osmotic coefficient from this spreadsheet are compared with those listed at 25 and 100 °C in Clegg et al. (1996; Table 7) in Table I–22. There was very good agreement with the spreadsheet values at 25 °C with a maximum difference of 0.9%, and reasonable agreement over the 100 °C range with an RMS difference of 2.3%. The model conversion errors for the osmotic coefficient, in going from a 4-parameter Archer-type input model to the 3-parameter standard Pitzer model, as a function of temperature ranged from 0.0010 to 0.0256 from 0 to 100 °C, respectively (see spreadsheet cover page). The model conversion error can be as large as 0.06 at higher temperatures, but this is beyond the range of validity of the input model. Generally, the model conversion errors are much larger than the temperature coefficient fitting errors.

Table I–22. Comparison of Fitted 3-4 Term Osmotic Coefficients (ϕ) to Those Measured for $(\text{NH}_4)_2\text{SO}_4$ at 25 and 100 °C

25 °C			
Molality of $(\text{NH}_4)_2\text{SO}_4$	3-4 Term Fit	Measurements ^a	Difference (%)
0.05	0.8160	0.8127	0.4
0.1	0.7760	0.7723	0.5
0.5	0.6756	0.6774	0.2
1.0	0.6379	0.6420	0.9
3.0	0.6398	0.6382	0.3
6.0	0.7177	0.7138	0.6
100 °C			
0.05	0.7902	0.7687	2.8
0.1	0.7466	0.7198	3.7
0.5	0.6358	0.6316	0.7
1.0	0.5923	0.6027	1.7
3.0	0.5832	0.5810	0.4
6.0	0.6036	0.6202	2.7

^a Taken from Clegg et al. (1996), Table 7.

I–4.4.22 Ions: NH_4^+ - Cl^-

Associated Spreadsheet: [FitPitzerNC_MX_NH4Cl.xls](#)

Source: Thiessen and Simonson (1990); cited 12 times by 3/2003.

Description: Input parameters and equations from Thiessen and Simonson (1990; Table IV and Equation 24) were verified for $\beta_{MX}^{(0)}$, $\beta_{MX}^{(1)}$, and C^ϕ . Calculated values of the parameter term coefficients in the spreadsheet agreed very well with the values reported by the authors, with near exact agreement in most cases but with an occasional difference 0.001–0.002. Each osmotic coefficient RMS error over the fitted temperature range (as shown on “Results Summary” spreadsheet) was below 0.0004, with a maximum individual difference of 0.0007. This is considered to be excellent agreement, with the minor differences attributable to the A^ϕ parameter and the water saturation vapor pressure equation used to establish the system pressure. Calculated values of the osmotic coefficient from this spreadsheet were compared with those listed for 25 °C in the extensive tables from Robinson and Stokes (1965; Appendix 8.10, Table 3, p. 485). There was good agreement with the final fitted spreadsheet values at 25 °C, with $\Delta\phi_{\text{max}} = 0.002$ (Table I–23).

Table I–23. Comparison of 3-4 Term Fitted Osmotic Coefficients (ϕ) to Measured for NH_4Cl at 25 °C

Molality of NH_4Cl	3-4 Term Fitting	Measurements ^a	Difference (%)
0.1	0.925	0.927	0.2
0.5	0.899	0.899	<0.1
1.0	0.897	0.897	<0.1
3.0	0.927	0.926	0.1
6.0	0.969	0.969	<0.1

^a Taken from Robinson and Stokes (1965), Appendix 8.10, Table 3, p. 485.

I-4.4.23 Ions: Na⁺ - HCO₃⁻**Associated Spreadsheet:** [FitPitzerNC_MX_NaHCO3.xls](#)**Source:** He and Morse (1993); cited 21 times by 3/2003.

Description: Input parameters and equation from He and Morse (1993; Table 7 and the Equation on page 3548) were verified for $\beta_{MX}^{(0)}$, $\beta_{MX}^{(1)}$, and C^ϕ . The RMS error in the osmotic coefficient over the fitted temperature range (see spreadsheet tab “Results Summary”) for source to 3-4 term conversion is zero (to within calculation precision) as both use the same functional form. Calculated values of these coefficients at 25 °C from this spreadsheet agreed with the values reported by Peiper and Pitzer (1982; Table 1). The source document used Pitzer parameter values at 25 °C from this paper to determine the temperature coefficients. The osmotic coefficients calculated from the input parameters were compared with those listed in tables from Peiper and Pitzer (1982; Table 6, pp 631 through 636). There was good agreement with values calculated in this spreadsheet, with a maximum difference ranging from 0.001 to 0.002 over 0 to 1.0 mol/kg ionic strength at 25 and 45 °C as seen in Table I-24. This agreement is considered to be sufficient for the validity of the osmotic coefficient calculations reported in this spreadsheet. Pitzer parameter values over a wider temperature range than 0–90 °C have been reported in the literature, but these are limited to smaller ranges of concentration. For example, the Pitzer data given by Polya et al. (2001) are limited to an ionic strength range of 0–4.5 mol/kg for Na₂CO₃, and 0–1.0 mol/kg for NaHCO₃. Furthermore, reproduction of the results of Polya et al. (2001), which were calibrated against the 25 °C parameter values of Peiper and Pitzer (1982), using the equations given by Polya et al. (2001) was unsuccessful. Communication with these authors did not resolve the uncertainties. The model of He and Morse (1993), although it is limited to 0–90 °C, was parameterized to very high ionic strengths, and is, therefore, suitable for calculation of Na₂CO₃ solubility.

Table I-24. Comparison of Fitted 3-4 Term Osmotic Coefficients (ϕ) to Measured for NaHCO₃ at 25 and 45 °C

25 °C			
Molality of NaHCO ₃	3-4 Term Fit	Measurements ^a	Difference (%)
0.05	0.934	0.933	0.1
0.1	0.915	0.914	0.1
1.0	0.856	0.854	0.2
45 °C			
0.05	0.932 ^b	0.931	0.1
0.1	0.914 ^b	0.913	0.1
1.0	0.865 ^b	0.864	0.1

^a Taken from Peiper and Pitzer (1982), Table 6, pp 631–636.^b Linearly interpolated by hand from spreadsheet data between 40 and 50 °C.**I-4.4.24 Ions: Na⁺ - CO₃²⁻****Associated Spreadsheet:** [FitPitzerNC_MX_Na2CO3.xls](#)**Source:** He and Morse (1993); cited 21 times by 3/2003.

Description: Input parameters and equations from He and Morse (1993; Table 7 and the Equation on page 3548) were verified for $\beta_{MX}^{(0)}$, $\beta_{MX}^{(1)}$, and C^ϕ . The RMS error in the osmotic coefficient over the fitted temperature range (see spreadsheet tab “Results Summary”) for the 3-4 term conversion is zero (to within calculation precision) as both use the same functional form. Calculated values of these coefficients at 25°C from this spreadsheet agreed with the values reported by Peiper and Pitzer (1982; Table 1). The source document used the Pitzer parameter values at 25 °C from this paper to determine the temperature coefficients. The osmotic coefficients calculated from the input parameters were compared with those listed in Peiper and Pitzer (1982; Table 6) and shown in Table I–25 at 25 and 45 °C. There was good agreement with values calculated in this spreadsheet, with a maximum difference ranging from 0.002 to 0.01 over 0 to 9 mol/kg ionic strength. This agreement is considered to be sufficient confirmation of the validity of the osmotic coefficient calculations reported in this spreadsheet. Just like the NaHCO₃, Pitzer parameter values over a wider temperature range than 0 to 90 °C have been reported for Na₂CO₃ in the literature but these are limited to smaller ranges of concentration. For example, the Pitzer data given by Polya et al. (2001) are limited to an ionic strength range of 0 to 4.5 mol/kg for Na₂CO₃, and 0 to 1.0 mol/kg for NaHCO₃. Furthermore, reproduction of the results of Polya et al. (2001), which were adjusted using the 25 °C parameter values of Peiper and Pitzer (1992), using the equations given by them was not possible. The uncertainties could not be resolved.. The solubility of Na₂CO₃ above 25 °C exceeds the ionic strength range of the model at high temperatures, and as was shown by Königsberger (2001), does not yield reliable solubility predictions above about 50 °C. The model of He and Morse (1993), although limited to 0–90 °C, was parameterized to very high ionic strengths and is suitable for calculation of solubility.

Table I–25. Comparison of Fitted 3-4 Term Osmotic Coefficients (ϕ) to Measured for Na₂CO₃ at 25 and 45 °C

25 °C			
Molality of Na ₂ CO ₃	3-4 Term Fit	Measurements ^a	Difference (%)
0.05	0.842	0.847	0.6
0.1	0.814	0.817	0.4
1.0	0.681	0.683	0.3
3.0	0.737	0.739	0.3
45 °C			
0.05	0.835 ^b	0.845	1.2
0.1	0.806 ^b	0.815	1.1
1.0	0.698 ^b	0.704	0.9

^a Taken from Peiper and Pitzer (1982), Table 6, pp 631–636.

^b Linearly interpolated by hand from spreadsheet data between 40 and 50 °C.

I–4.4.25 Ions: Na⁺ - HSO₄⁻

Associated Spreadsheet: [FitPitzerNC_MX_NaHSO4.xls](#)

Source: Holmes and Mesmer (1994)

Description: Input parameters and equations from Holmes and Mesmer (1994; Table 4 and Equation 28) were verified for $\beta_{MX}^{(0)}$, $\beta_{MX}^{(1)}$, and C^ϕ , and A^ϕ . Calculated values of the osmotic

coefficient for the fully dissociated binary electrolyte from this spreadsheet cannot be compared with any experimental values because experimentally determined values include the effects of partial dissociation into Na^+ , H^+ , HSO_4^- and SO_4^{2-} ions rather than Na^+ and HSO_4^- ions only. However, the values of the calculated osmotic coefficient are reasonable for a fully dissociated 1-1 electrolyte. The binary parameters for Na^+ and HSO_4^- should only be used in combination with the mixing parameters (θ and ψ) from the same document. Furthermore, to be consistent, these parameters should only be used in combination with the binary and mixing parameters for HSO_4^- and SO_4^{2-} ions given in the source document and for Na_2SO_4 in Holmes and Mesmer (1986). Of the two models given in the latter paper, Model I with $\alpha_1 = 1.4$ instead of 2, should be used for Na_2SO_4 . Note that there is an error in Table 4 of the source document (Holmes and Mesmer, 1994); it gives incorrect p_1 parameter values that are too large by a factor of 1000. It should also be noted that the higher order electrostatic interactions represented by the ${}^E\theta$ and ${}^E\theta'$ third order terms of the Pitzer model were taken into account in this source document. In an earlier paper by Holmes and Mesmer (1993), the authors did not account for these interactions. Note that there is an error in Table 2 of this document for isothermal fits; it gives incorrect C^ϕ values that are too large by a factor of 1000.

I-4.4.26 Ions: Na^+ - AlO_2^- (equivalent to Na^+ - $\text{Al}(\text{OH})_4^-$)

Associated Spreadsheet: FitPitzerNC_MX_Na_AlO2.xls

Source: Felmy et al. (1994b)

Description: The binary parameters $\beta_{MX}^{(0)}$, $\beta_{MX}^{(1)}$, and C^ϕ generated with the coefficients and equations reported by Felmy et al. (1994b; Table 1 and Equation 1) were examined and compared with the data reported by Wesolowski (1992; Table 13) based on gibbsite solubility at alkaline conditions. Unlike previous FitPitzerNC spreadsheets, the binary parameters were refitted using the regression function intrinsic to MS Excel. The conventions used for representing aqueous aluminate ion as AlO_2^- instead of $\text{Al}(\text{OH})_4^-$ are different from those reported by Felmy et al. (1994b) and Wesolowski (1992). The convention used to denote the aluminate ion AlO_2^- is equivalent to $\text{Al}(\text{OH})_4^-$ in the two latter studies and thermodynamically consistent with the chemical reactions for aqueous and solid species in the current data0.ypf or Pitzer database and those obtained from the data0.ymp.R2 database (see Pokrovski and Helgeson, 1995 for more details on the adopted convention).

The binary parameter values obtained after refitting agree with those generated by Felmy et al. (1994b), depending on temperature. Comparison of generated parameter values with those reported by Wesolowski (1992; table 13, p.1087) for a temperature range of 25 to 100 °C are also in good agreement. Somewhat larger differences are observed for the $\beta_{MX}^{(1)}$ values but in general these are considered reasonable when all parametric differences are taken as a whole. An error in table 1 of Felmy et al. (1994b) was detected for the $\beta_{MX}^{(0)}$ parameter where the listed a_3 coefficient is actually a_4 in the fitting equation used by the authors. When the fitting coefficient is corrected, the $\beta_{MX}^{(0)}$ values obtained are nearly identical to those reported by Wesolowski (1992; Table 13).

Felmy et al. (1994b) conducted a gibbsite solubility study at ambient temperature and noticed that in order to model the effect of NaNO₃ concentration in NaOH solutions, two additional ternary parameters (θ and ψ ; see Felmy et al., 1994b) were needed. These were modified by Felmy et al. (1994b) to fit their solubility data for a mixed Na-OH-NO₃-H₂O electrolyte. A further test of these parameters was the prediction of the equilibrium solubility for gibbsite in a concentrated NaOH solution at 70 °C with the code *EQ3/6 Version 8.0* for a total Na concentration of 3.045 molal. The log K value for gibbsite was taken from the data0.ymp.R2 database. The calculated total Al (equivalent to AlO₂⁻ or Al(OH)₄⁻) was nearly identical to that in Wesolowski (1992; Table 4) for the same Na⁺ concentration (See EQ3NR output file, gibbs_weso_sol.3o in the accompanying CD).

I-4.4.27 Ions: Ca⁺⁺ - SO₄²⁻

Associated Spreadsheet: No Spreadsheet

Source: Møller (1988); Greenberg and Møller (1989)

Description: Binary parameters from Greenberg and Møller (1989) were verified for $\beta_{MX}^{(0)}$, $\beta_{MX}^{(1)}$, and C^ϕ given without any temperature dependence. The refit based on these authors work given in the spreadsheet 'FitPitzerNC_MX_CaSO4.xls' is not used here. It appears from the work of Greenberg and Møller (1989) that an explicit CaSO₄(aq) ion pair constant was used to fit a temperature range above 50 °C. The explicit use of this ion pair is what actually brings the temperature dependence to the model. As incorporated in the data0.ypf, the $\beta_{MX}^{(0)}$ term is set to zero and the CaSO₄(aq) ion pair represented in the log K data block for aqueous species is used all throughout the valid temperature range. It is suspected that the ion pair was not actually used in Greenberg and Møller (1989) at temperatures less than 50°C and extrapolation to this lower temperature range might add some additional error. Even though the ion pair is used and $\beta_{MX}^{(2)}$ is not, it appears that an α_1 value of 1.4 was retained. A corrected value of 'a1' for $\beta_{MX}^{(0)}$ was used after noticing that it differs from the original source of Møller (1988). Møller (1988) reports a value of 0.15 for the 'a1' coefficient instead of 0.015 as reported by Greenberg and Møller (1989). Millero and Pierrot (1998) and Monnin (1999) adopted a value of 0.15 for this coefficient in their Pitzer models. Monnin (1999) states in his study that the value of 0.015 reported by Greenberg and Møller (1989) appears to be incorrect since it yields significant discrepancies. Therefore, a corrected value of 0.15 is adopted in his study (Monnin 1999, Table 3, footnote f). The solubility of gypsum in water (Figure I-2) was calculated using the Pitzer parameters and compared to the curve given by Møller (1988; Figure 3, p. 827). The computed solubility by the code underestimates the saturation molalities by ~18% to ~60% for the temperature range of 25 to 100 °C, respectively. These differences are relatively large but not grossly unreasonable. No attempt was done to improve the predictions of gypsum solubility other than to adopt the parameter values and ion pair constant in the manner described above.

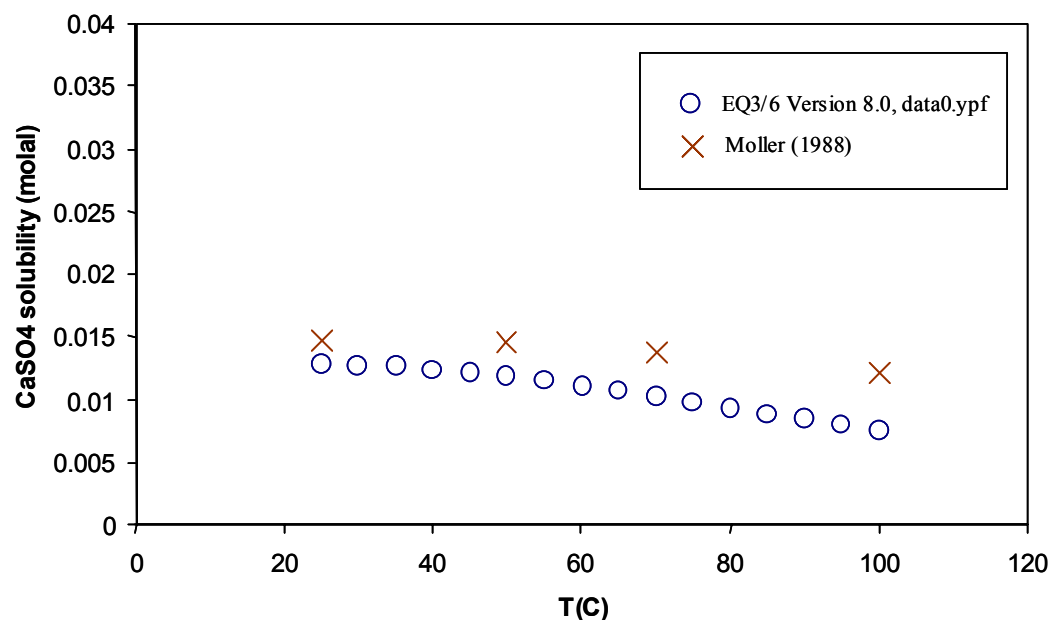


Figure I-2. Comparison saturation molalities for Gypsum. Predicted m_{sat} values (DTN: SN0303T0510102.003) were computed using data0.ypf and *EQ3/6 Version 8.0*. The Saturation Molalities for Gypsum Were Obtained From Figure 3 in Møller (1988).

I-4.5 TERNARY PITZER INTERACTION PARAMETERS

In this section, the selected ternary Pitzer ion interaction parameters for major salt constituents included in the developed *data0.ypf* database for *EQ3/6 Version 8.0* will be described. All these parameters and associated spreadsheets are listed in Tables I-1 and I-2 as “Types other than MX”. Remarks on the refitting and reproducibility of gathered Pitzer parameter data will be discussed here and on the associated spreadsheet cover pages. Discussions of parameter data are focused on the parameters that needed refitting due to their temperature dependence. Many parameters did not require any refitting since the gathered values are only valid at 25 °C and were obtained directly from tabulated data. For these, only simple conversions were necessary. The reader is reminded that ternary interaction parameters make relatively small contributions to the calculation of osmotic coefficients and activity coefficients. Thus, even large percentage differences in the values used by different authors make only small differences in the final results. For details see the individual papers cited which generally evaluate the magnitude of these differences.

Significant limitations exist for the application of the parameters discussed in the following subsections. Most have been determined only at 25°C and many only for relatively simple systems. For more complex systems, such as for most groundwater and other temperatures, refitting of the parameters to the changed conditions may be necessary to obtain accurate results. Failure to make such adjustments can lead to significant errors in some applications, e.g., modeling of evaporation of a water to near dryness, because of the accumulation of small deviations of the model from the actual chemistry. To mitigate this problem, data were taken from consistent or single sources to the extent possible. For example, many parameters were taken from Greenberg and Møller (1989), who studied the rather complex Na-K-Ca-Cl-SO₄-H₂O system. Still, this study lacked some important constituents, notably Mg and carbonate, present in most natural waters, and

did not fit the Ca poor portion of the system well. For some applications Al and Si need to be included, and, less often, other elements that are generally present in groundwater in minor to trace amounts. Thus, in spite of qualification of these data from the point of view that they generally suffice to reproduce individual details of the experimental results well, they need to be viewed with caution in respect to modeling chemical processes that change the composition of the solution.

I-4.5.1 Ions: Ca^{++} - K^+

Associated Spreadsheet: [FitPitzerNC_MM_K_Ca.xls](#)

Source: Greenberg and Møller (1989)

Description: Input parameters and equations from Greenberg and Møller (1989) were verified for θ and A^ϕ . The authors used a constant value of θ for all temperatures. At 25 °C, Pitzer and Kim (1974) reported values of $\theta = -0.040$ and $\psi = -0.015$ for K-Ca-Cl system compared to $\theta = 0.1156$ and $\psi = -0.04319$ from the spreadsheet, and $\theta = 0.032$ and $\psi = -0.025$ by Pitzer (1991). Unlike the calculations of both Pitzer and this spreadsheet, Pitzer and Kim (1974) did not account for the higher order electrostatic terms ${}^E\theta$ and ${}^E\theta'$ in their model. Therefore, the evaluation of θ is dominated by the differences in the models used by different authors. In particular, Pitzer and Kim (1974) based their parameter evaluations using isopiestic data. Although Greenberg and Møller (1989) also considered this isopiestic data they adjusted the mixing parameters to better represent solubility of sylvite (KCl) in mixed KCl-CaCl₂ solutions.

I-4.5.2 Ions: Ca^{++} - Na^+

Associated Spreadsheet: [FitPitzerNC_MM_Na_Ca.xls](#)

Source: Greenberg and Møller (1989)

Description: Input parameters and equations from Greenberg and Møller (1989) were verified for θ and A^ϕ . The authors used a constant value of θ for all temperatures. There are no independent studies of this θ parameter reported in the literature that would enable a meaningful comparison. In Holmes et al. (1981), the authors represent θ from isopiestic data by the equation $\theta = (10.7/T) - 0.0316$. Holmes et al. (1981) state that the osmotic coefficients could be reproduced to 0.5% or better even without mixing parameters, which indicates that mixing effects are small. The equation given by Holmes et al. (1981) yields values that vary from 0.0043 to -0.0090 kg/mol over 25 to 201 °C. Because θ has only a very small influence on the osmotic coefficient of the system, the evaluation of this parameter is dominated by differences in the models used by different authors. These differences include neglect of the higher order electrostatic terms ${}^E\theta$ and ${}^E\theta'$. Greenberg and Møller (1989), for example, included these terms while Holmes, Baes and Mesmer (1981) did not include them. Therefore, the adequacy of this θ parameter estimate should be assessed in combination with other binary and ternary parameters by examining the accuracy of the osmotic coefficients calculated in the MMX-type ternary parameter spreadsheets for the Na-Ca ion combination.

I-4.5.3 Ions: K^+ - Na^+

Associated Spreadsheet: [FitPitzerNC_MM_Na_K.xls](#)

Source: Greenberg and Møller (1989)

Description: Input parameters and equations from Greenberg and Møller (1989) were verified for θ and A^ϕ . There are no independent studies of this θ parameter reported in the literature that would enable a meaningful comparison. In Holmes et al. (1979, Page 1044), the authors represent θ from isopiestic data by the equation $\theta = -(6.726/T) + 0.0039$ whereas Greenberg and Møller (1989) give the expression $\theta = (14.021314/T) - 0.0502312$ for 0 to 250 °C. Greenberg and Møller (1989) used the same basic model and experimental data as Holmes et al. (1979), but adjusted the mixing parameter θ to better represent solubility data for the NaCl-KCl-H₂O system at temperatures above 150°C. Holmes et al. (1979) state that the osmotic coefficients could be reproduced to within 1% or better even without mixing parameters, which indicates that mixing effects are small. The equation given by Holmes et al. (1979) yields values that vary from -0.01866 to -0.01032 kg/mol over 25 to 200 °C. whereas the corresponding values from Greenberg and Møller (1989) vary from -0.00320 to -0.02060 mol/kg. Because θ has only a very small influence on the osmotic coefficient of the system, its evaluation is sensitive to differences in the models used by the different authors. Therefore, the adequacy of this estimate of the θ parameter should be assessed in combination with other binary and ternary parameters by examining the accuracy of the osmotic coefficients calculated in the MMX-type ternary parameter spreadsheets for the Na-K ion combination.

I-4.5.4 Ions: Cl^- - SO_4^{2-}

Associated Spreadsheet: [FitPitzerNC_XX_Cl_SO4.xls](#)

Source: Greenberg and Møller (1989)

Description: Input parameters and equations from Greenberg and Møller (1989) were verified for θ and A^ϕ . The temperature function given in the source document for θ has a discontinuity in slope at 150 °C. This discontinuity is not accurately accommodated by the fitted continuous temperature function causing the largest error in θ (about 10%) to occur in the immediate vicinity of 150 °C. De Lima and Pitzer (1987) fitted the Na-Cl-SO₄ system solubilities from 25 to 100 °C with $\theta = -0.02$ and $\psi = 0.004$ taken from an earlier evaluation by Pitzer at 25 °C. Both of these studies imply that ternary mixing contributions to the osmotic coefficient are small.

I-4.5.5 Ions: HSO_4^- - SO_4^{2-}

Associated Spreadsheet: [FitPitzerNC_XX_HSO4_SO4.xls](#)

Source: Holmes and Mesmer (1994)

Description: Input parameters and equations from Holmes and Mesmer (1994) were verified for the parameter θ . These authors regressed the model parameters simultaneously for the H-HSO₄-SO₄ and Na-HSO₄-SO₄ systems, including the ${}^E\theta$ and ${}^E\theta'$ higher order electrostatic

interactions. Clegg et al. (1994) were able to fit the thermodynamic properties of sulfuric acid without including either θ or ψ Pitzer mixing parameters, but with an additional C(1) extended binary parameter and the ${}^E\theta$ and ${}^E\theta'$ higher order electrostatic interaction parameters. It was found by Clegg et al. (1994) that these model enhancements were significant in improving the accuracy of the fit at concentrations much lower than those considered by Holmes and Mesmer (1994). Both of these studies imply that the contributions of the ternary mixing parameters are negligible in the H-HSO₄-SO₄ system, but not always negligible in the Na-HSO₄-SO₄ system. In an earlier paper by Holmes and Mesmer (1992), the authors did not account for these interactions.

I-4.5.6 Ions: K⁺ - Ca⁺⁺ - Cl⁻

Associated Spreadsheet: [FitPitzerNC_MMX_K_Ca_Cl.xls](#)

Source: Greenberg and Møller (1989)

Description: Input parameters and equations from Greenberg and Møller (1989) were verified for the θ ternary Pitzer parameter and A^ϕ . At 25 °C, Pitzer and Kim (1974) reported values of $\theta = -0.040$ and $\psi = -0.015$ for K-Ca-Cl system compared to $\theta = 0.1156$ and $\psi = -0.04319$ from the spreadsheet, and $\theta = 0.032$ and $\psi = -0.025$ by Pitzer (1991). Unlike the calculations by Pitzer and those presented in this spreadsheet, Pitzer and Kim (1974) did not account for the higher order electrostatic terms ${}^E\theta$ and ${}^E\theta'$ in their model. Therefore, the evaluation of θ is dominated by the differences in the models used by different authors. In particular, Pitzer and Kim (1974) based their parameter evaluations using these isopiestic data. Although Greenberg and Møller (1989) also considered this isopiestic data they adjusted the mixing parameters to better represent solubility of sylvite (KCl) in mixed KCl-CaCl₂ solutions. It should be noted, that the osmotic coefficient values presented in the spreadsheet for an ionic strength of $I = 18$ mol/kg are not realistic because they fall outside the range of validity of the model parameters, especially for potassium-rich solutions at low temperatures. Exact agreement was obtained between the osmotic coefficients for the limiting binary solutions, KCl(aq) and CaCl₂(aq), calculated by the ternary and the binary spreadsheets, for both input and fitted Pitzer parameters.

I-4.5.7 Ions: Na⁺ - Ca⁺⁺ - Cl⁻

Associated Spreadsheet: [FitPitzerNC_MMX_Na_Ca_Cl.xls](#)

Source: Greenberg and Møller (1989)

Description: Input parameters and equations from Greenberg and Møller (1989) were verified for ψ and A^ϕ . Holmes et al. (1981) found that the osmotic coefficients could be reproduced to within 0.5% or better even without mixing parameters, which indicates that mixing effects are small. Holmes et al. (1981) found that while using the θ mixing parameter improved the standard deviation for isothermal fits by a factor of 2, including both θ and ψ did not yield a significant improvement over using θ alone. θ varied between 0.0056 and -0.0081 over 25 to 201 °C. Because ψ has only a very small influence on the osmotic coefficient of the system, its value is dominated by differences in the models used by the different authors. These differences include

the neglect of the higher order electrostatic terms ${}^E\theta$ and ${}^E\theta'$. Greenberg and Møller (1989), for example, included these terms while Holmes et al. (1981) did not include them. Therefore, the adequacy of this estimate of the ψ parameter should be assessed in combination with other binary and ternary parameters by examining the accuracy of the osmotic coefficients calculated in the MMX-type ternary parameter spreadsheets for the Na-Ca ion combination. Exact agreement was obtained between the osmotic coefficients for the limiting binary solutions, NaCl(aq) and CaCl₂(aq), calculated by the ternary and the binary spreadsheets, for both input and fitted Pitzer parameters.

I-4.5.8 Ions: Na⁺ - Ca⁺⁺ - SO₄²⁻

Associated Spreadsheet: [FitPitzerNC_MMX_Na_Ca_SO4.xls](#)

Source: Greenberg and Møller (1989)

Description: Input parameters and equations from Greenberg and Møller (1989) were verified for the θ ternary Pitzer parameter and A^ϕ . The authors used constant values of θ and ψ for all temperatures. At 25°C, Pitzer (1991), used the values $\theta = 0.07$ and $\psi = -0.055$ compared to $\theta = 0.05$ and $\psi = -0.012$ calculated from the correlation of Greenberg and Møller (1989). Both sets of values account for the higher order terms θ and ${}^E\theta'$. At low temperatures, the calculated values of the osmotic coefficient from this spreadsheet are plausible, but, for CaSO₄-rich solutions, they become unrealistic in magnitude at temperatures beyond 100–150 °C. Because of the relatively low solubility of CaSO₄, the high concentrations cannot be achieved experimentally. The parameters were designed to represent solubility in mixed electrolyte solutions and are inadequate for representing the properties of the hypothetical pure-CaSO₄(aq) solutions. Exact agreement was obtained between the osmotic coefficients for the limiting binary solutions, Na₂SO₄(aq) and CaSO₄(aq), calculated by the ternary and the binary spreadsheets, for both input and fitted Pitzer parameters.

I-4.5.9 Ions: Na⁺ - K⁺ - Cl⁻

Associated Spreadsheet: [FitPitzerNC_MMX_Na_K_Cl.xls](#)

Source: Greenberg and Møller (1989)

Description: Input parameters and equations from Greenberg and Møller (1989) were verified for ψ and A^ϕ . In Holmes et al. (1979), the authors state that the osmotic coefficients could be reproduced to within 1% or better even without mixing parameters, which indicates that mixing effects are small. However, Holmes et al. (1979) found that including the θ mixing parameter caused a significant improvement in the accuracy of representing the data with the standard deviation for isothermal fits decreasing by a factor of 2 to 4. Including both θ and ψ , resulted in no further improvement, and they recommended using θ only in the Pitzer model. Greenberg and Møller (1989) used the same basic model and experimental data as Holmes et al. (1979) but adjusted the mixing parameter θ to better represent the solubility data for the NaCl-KCl-H₂O system at temperatures above 150 °C. Because ψ has only a very small influence on the osmotic coefficient of the system, its evaluation is sensitive to differences in the models used by the

different authors. Therefore, the adequacy of the ψ parameter estimation should be assessed in combination with other binary and ternary parameters by examining the accuracy of the osmotic coefficients calculated in the MMX-type ternary parameter spreadsheets for the Na-K ion combination. Exact agreement was obtained between the osmotic coefficients for the limiting binary solutions, NaCl(aq) and KCl(aq), calculated by the ternary and the binary spreadsheets, for both input and fitted Pitzer parameters.

I-4.5.10 Ions: Na⁺ - K⁺ - SO₄²⁻

Associated Spreadsheet: [FitPitzerNC_MMX_Na_K_SO4.xls](#)

Source: Greenberg and Møller (1989)

Description: Input parameters and equations from Greenberg and Møller (1989) were verified for the ψ ternary Pitzer parameter and A^ϕ . Greenberg and Møller (1989) used a 2-term temperature function for ψ with different sets of parameters from 0 to 150 °C and 150 to 250 °C. The value of ψ was optimized using both osmotic coefficient and solubility data. Table 18 of Pitzer (1991), includes the values of $\theta = -0.012$ and $\psi = -0.010$ at 25 °C taken from the original paper by Pitzer and Kim (1974). This should be compared with the values of $\theta = -0.0032$ and $\psi = 0.0073$ at 25 °C calculated from Greenberg and Møller (1989) correlations. Both of these studies imply that ternary mixing contributions to the osmotic coefficient are small, but that the mixing parameter values should always be evaluated in combination with the binary and other ternary parameters for the electrolyte system. It should be noted here, that the osmotic coefficient values presented in the spreadsheet for an ionic strength of $I = 18$ mol/kg are not realistic because they fall outside the range of validity of the model parameters. Exact agreement was obtained between the osmotic coefficients for the limiting binary solutions, Na₂SO₄(aq) and K₂SO₄(aq), calculated by the ternary and the binary spreadsheets, for both input and fitted Pitzer parameters.

I-4.5.11 Ions: Ca⁺⁺ - Cl⁻ - SO₄²⁻

Associated Spreadsheet: [FitPitzerNC_MXX_Ca_Cl_SO4.xls](#)

Source: Greenberg and Møller (1989)

Description: Input parameters and equations from Greenberg and Møller (1989) were verified for the ψ ternary Pitzer parameter and A^ϕ . The authors used a constant value of ψ for all temperatures. At 25 °C, Pitzer (1991) used the values of $\theta = 0.030$ and $\psi = -0.002$ compared to $\theta = 0.070$ and $\psi = -0.018$ calculated from the correlation of Greenberg and Møller (1989). Both sets of values account for the higher order terms θ and ${}^E\theta'$. At low temperatures, the calculated values of the osmotic coefficient from this spreadsheet are plausible, but, for CaSO₄-rich solutions, they become unrealistic in magnitude at temperatures beyond 100–150 °C. Because of the low solubility of CaSO₄, the high concentrations cannot be achieved experimentally. The parameters were designed to represent solubility in mixed electrolyte solutions and are inadequate for representing the properties of the hypothetical pure-CaSO₄(aq) solutions. Exact agreement was obtained between the osmotic coefficients for the limiting binary solutions,

CaCl₂(aq) and CaSO₄(aq), calculated by the ternary and the binary spreadsheets, for both input and fitted Pitzer parameters.

I-4.5.12 Ions: K⁺ - Cl⁻ - SO₄²⁻

Associated Spreadsheet: [FitPitzerNC_MXX_K_Cl_SO4.xls](#)

Source: Greenberg and Møller (1989)

Description: Input parameters and equations from Greenberg and Møller (1989) were verified for ψ and A^ϕ . At 25 °C, Pitzer and Kim (1974) reported values of $\theta = -0.035$ and $\psi = 0$ compared to $\theta = 0.07$ and $\psi = -0.0016152$ from the spreadsheet. In Pitzer (1991), the higher order interaction terms were included with $\theta = 0.030$ and $\psi = -0.005$ at 25°C. These differences arise from differences in the binary parameters as well as model differences such as inclusion of the higher order electrostatic parameters ${}^E\theta$ and ${}^E\theta'$ in the spreadsheet. Therefore, the adequacy of this estimate of the ψ parameter should be assessed in combination with other binary and ternary parameters by examining the accuracy of the osmotic coefficients calculated in the MXX-type ternary parameter spreadsheets for the Cl-SO₄ ion combination. Because of the limited solubility of potassium sulfate, the calculated osmotic coefficients in the spreadsheet at certain high ionic strengths will exceed the range of validity of the model and may not be realistic. Exact agreement was obtained between the osmotic coefficients for the limiting binary solutions, KCl(aq) and K₂SO₄(aq), calculated by the ternary and the binary spreadsheets, for both input and fitted Pitzer parameters.

I-4.5.13 Ions: H⁺ - HSO₄⁻ - SO₄²⁻

Associated Spreadsheet: [FitPitzerNC_MXX_H_HSO4_SO4.xls](#)

Source: Holmes and Mesmer (1994)

Description: Input parameters and equations from Holmes and Mesmer (1994) were verified for ψ , which were set equal to zero. They regressed the model parameters simultaneously for the H-HSO₄-SO₄ and Na-HSO₄-SO₄ systems, including the ${}^E\theta$ and ${}^E\theta'$ higher order electrostatic interactions (The subscript *MBS* on ψ in Table 4 refers to Na⁺ - HSO₄⁻ - SO₄²⁻, not H⁺ - HSO₄⁻ - SO₄²⁻. See p. 582 in Holmes and Mesmer 1994). Clegg et al. (1994), were able to fit the thermodynamic properties of sulfuric acid without including both θ and ψ Pitzer mixing parameters, but with an additional C(1) extended binary ion-interaction parameter and the ${}^E\theta$ and ${}^E\theta'$ higher order electrostatic interaction parameters. It was found by Clegg et al. (1994) that these model enhancements were significant in improving the accuracy of the fit at concentrations much lower than those considered by Holmes and Mesmer (1994). Both of these studies imply that the contributions of the ternary mixing parameters are negligible in the H-HSO₄-SO₄ system, but are not always negligible in the Na-HSO₄-SO₄ system. In an earlier paper Holmes and Mesmer (1992) the authors did not account for these interactions. Exact agreement was obtained between the osmotic coefficients for the limiting binary solutions, H-HSO₄ and H₂SO₄, calculated by the ternary and the binary spreadsheets, for both input and fitted Pitzer parameters. The osmotic coefficients were calculated for arbitrary speciations that range from one pure

component to the other, but under real conditions, the equilibrium ionic concentrations would be determined by iterative speciation calculations. The H-HSO₄-SO₄ ternary system ionic strength differs from stoichiometric value because of incomplete disassociation of hydrogen ions from the bisulfate ions. The dependence of the actual ionic strength of the solution on the degree of dissociation of the sulfuric acid leads to a strong dependence of the ionic strength on the molality and temperature of the solution. For example, using the degree of dissociation given in Figure 3 of Holmes and Mesmer (1992) the degree of sulfuric acid dissociation in Table I-26 can be estimated.

Table I-26. Comparison of the Degree of Sulfuric Acid Dissociation as a Function Of Temperature and Ionic Strength

Temperature (°C)	Disassociation % SO ₄ ²⁻	Stoichiometric Molality (mol/kg)	Stoichiometric Ionic Strength (mol/kg)	Actual Ionic Strength (mol/kg)
25	17	4	12	5.4
100	4	4	12	4.3
175	1.5	4	12	4.1

The ionic strengths given in the last column of the above table was calculated from the values given in the 2nd and 3rd columns using the equation:

$$\text{Actual Ionic Strength} = [1 + 2 * (\text{Fractional Disassociation})] * (\text{Stoichiometric Molality})$$

Because the data reported in this paper were based on stoichiometric molalities that only ranged from 0.5 to 5.6 mol/kg (depending on temperature), the osmotic coefficients calculated at certain high ionic strengths fall outside the valid range of ionic strengths for their model.

I-4.5.14 Ions: Na⁺ - Cl⁻ - SO₄²⁻

Associated Spreadsheet: [FitPitzerNC_MXX_Na_Cl_SO4.xls](#)

Source: Greenberg and Møller (1989)

Description: Input parameters and equations from Greenberg and Møller (1989) were verified for ψ and A^ϕ . Greenberg and Møller (1989) use $\theta = 0.07$ for 0 to 150 °C and $\psi = -0.009$ for 0 to 250 °C. De Lima and Pitzer (1987) fitted the Na-Cl-SO₄ system solubilities from from 25 to 100 °C with $\theta = -0.02$ and $\psi = 0.004$ taken from an earlier evaluation by Pitzer at 25 °C (Pitzer, 1979). In the latter model higher order electrostatic interaction terms ${}^E\theta$ and ${}^E\theta'$ were not included. In Pitzer (1991), the higher order interaction terms were included with $\theta = 0.030$ and $\psi = 0.0$ at 25 °C. Both of these studies imply that ternary mixing contributions to the osmotic coefficient are small, but that the mixing parameter values should always be evaluated in combination with the binary and other ternary parameters for the electrolyte system. It should be noted here, that the osmotic coefficient values presented in the spreadsheet for an ionic strength of $I = 18$ mol/kg may not be realistic because they fall outside the range of validity of the model parameters. The input temperature function given by Greenberg and Møller (1989) for the ψ parameter is discontinuous with a constant value assigned from 0 to 150 °C and with varying values over the temperature range of 150 to 250 °C. Since a single continuous output function

was adopted over the entire 0 to 250 °C range, the fitting equation loses accuracy around 150 °C resulting in a maximum error of about 20% at this temperature. Exact agreement was obtained between the osmotic coefficients for the limiting binary solutions, NaCl(aq) and Na₂SO₄(aq), calculated by the ternary and the binary spreadsheets, for both input and fitted Pitzer parameters.

I-4.5.15 Ions: Na⁺ - HSO₄⁻ - SO₄²⁻

Associated Spreadsheet: FitPitzerNC_MXX_Na_HSO4_SO4.xls

Source: Holmes and Mesmer (1994)

Description: Input parameters and equations from Holmes and Mesmer (1994) were verified for ψ . They regressed the model parameters simultaneously for the H-HSO₄-SO₄ and Na-HSO₄-SO₄ systems, including the ${}^E\theta$ and ${}^E\theta'$ higher order electrostatic interactions. Clegg et al. (1994) were able to fit the properties of sulfuric acid without including both the θ and ψ Pitzer mixing parameters, but with an additional C(1) extended binary ion-interaction parameter and the ${}^E\theta$ and ${}^E\theta'$ higher order electrostatic interaction parameters. It was found by Clegg et al. (1994) that these model enhancements were significant in improving the accuracy of the fit at concentrations much lower than those considered by Holmes and Mesmer (1994). Both of these studies imply that the contributions of the ternary mixing parameters are negligible in the H-HSO₄-SO₄ system, but are not always negligible in the Na-HSO₄-SO₄ system. In an earlier paper by Holmes and Mesmer (1993), the authors did not account for these higher order electrostatic interactions. Exact agreement was obtained between the osmotic coefficients for the limiting binary solutions, NaHSO₄(aq) and Na₂SO₄(aq), calculated by the ternary and the binary spreadsheets, for both input and fitted Pitzer parameters. The osmotic coefficients were calculated for arbitrary speciations that range from one pure component to the other, but under real conditions, the equilibrium ionic concentrations would be determined by iterative speciation calculations. The Na-H-HSO₄-SO₄ system ionic strength differs from stoichiometric value because of incomplete disassociation of hydrogen ions from the bisulfate ions. The dependence of the actual ionic strength of the solution on the degree of dissociation of the bisulfate ion leads to a strong dependence of the ionic strength on the molality and temperature of the solution. The osmotic coefficients calculated at certain high ionic strengths, especially for solutions with high molality fractions of Na₂SO₄, fall outside the valid range of ionic strengths for their model. The temperature range of 0–250 °C also falls outside the range (25–225 °C) of parameterization of the model.

I-4.5.16 Neutral Species: See Table I-1 for Listing of Doublets and Triplets Parameters Among SiO₂(aq), CO₂(aq), and O₂(aq)

Associated Spreadsheet: FitPitzerNC_NaHCO3_Na2CO3_CFJC.xls, FitPitzerNC_lambdas_zetas_O2_CFJC.xls, and FitPitzerNC_lambdas_zetas_SiO2_CFJC.xls

Source: He and Morse (1993), Clegg and Brimblecombe (1990b), and Felmy et al. (1994a)

Description:

- Acid Carbonate System (data source: He and Morse, 1993): The binary, lambda (λ), and ternary, zeta (ζ), parameters for $\text{CO}_2(\text{aq})$ listed by He and Morse (1993) up to a temperature of 90 °C were refitted and verified against their reported values in Table 4 of the source. The refit resulted in an exact match given the few data points and limited temperature range from 25 to 90 °C. In validating these parameters, calcite solubility was modeled at 60 °C using *EQ3/6 (Version 8.0)* with increasing NaCl concentration at a fixed partial pressure of CO_2 of ~0.0078 bars and compared visually with that depicted in Figure 6A of He and Morse (1993) (DTN: Updated Spreadsheet/Input/Output Results). A reasonable agreement was obtained between the curves depicted in this figure and the author's model. Minor differences could be attributed to a different set of log K's representing calcite and $\text{CO}_2(\text{g})$ solubility which in this case were taken from the data0.ymp.R2 database. Visual comparison of the ion activity product calculated from these computations is very close to that depicted in Figure 8 of He and Morse (1993). Some fairly large discrepancies were found when the reported fitting coefficients and the associated equations to reproduce parameter values from the source (Table 6 of He and Morse, 1993) were used. The fitting equations in the source failed to reproduce their tabulated values as a function of temperature. For this reason, the refitting was done on the original source data listed in Table 4 of He and Morse (1993).
- O_2 solubility (data source: Clegg and Brimblecombe, 1990b): Parameters representing binary neutral-cation (NM and NX), (λ_{NM} , λ_{NX}), and ternary neutral-cation-anion (NMX) (ζ_{NMX}) interactions were obtained from the source equations and compared to data parameters reported by Clegg and Brimblecombe (1990b). The authors used O_2 solubility data from multiple sources. The generated parameters were refitted to almost the exact value reported by the authors. Visual comparison of reported activity coefficients at 298.15 K for $\text{O}_2(\text{aq})$ depicted in Clegg and Brimblecombe (1990b) in the presence of various salts such as NaNO_3 , NaCl, and MgCl_2 (DTN: Updated Spreadsheet/Input/Output Results) at relatively high concentrations indicate a strong agreement with computed values using *EQ3/6 (Version 8.0)*. Due to the manner in which the authors treated their model, i.e., selection of solubility data from different origins and, in many cases, applying density conversions, a straightforward comparison or corroboration with alternate data sources was not possible. The authors parameterized the model up to 100 °C but many of the ion parameters for some doublets and triplets don't have temperature dependence and are given only at 298.15 K.
- $\text{SiO}_2(\text{aq})$ (data source: Felmy et al., 1994a): Parameters representing binary neutral-cation (NM and NX), (λ_{NM} and λ_{NX}), and ternary neutral-cation-anion (NMX), (ζ_{NMX}) interactions were obtained from the relevant source equations and compared with those reported by Felmy et al. (1994a). The parameter fitting was based on experimental data on amorphous silica solubility at elevated temperatures as a function electrolyte type and concentration as reported by Marshall (1980a,b), Marshall and Warakowski (1980), Marshall and Chen (1982a,b), and Chen and Marshall (1982). In some cases, the authors needed to vary not only the parameter but also the standard chemical potential defining the equilibrium between solution and solid phase. According to Felmy et al. (1994a), the standard chemical potential of amorphous silica was one of the most difficult parameters to fix for the ion interaction parameter fitting. As explained by Felmy et al. (1994a) and

Marshall (1980a), the complex nature and ill-defined particle size of this phase, together with experimental difficulties, could create significant variability in solubility data under different temperatures and electrolyte concentrations. Another possible source for discrepancies is the use of different Pitzer parameters for some binary salts than those used by Felmy et al. (1994a). Further, the log K values for amorphous silica in the current data0.ypf database are taken from the data0.ymp.R2 database. Therefore, differences between calculated amorphous silica solubility and that reported by Felmy et al. (1994a) are expected. Due to the apparent variability in reported values for this phase, no attempt was made to fit amorphous silica solubility or to reproduce the values presented in Felmy et al. (1994a). Nevertheless, a validation test involving a visual comparison of the prediction of amorphous silica as a function of NaNO₃ at 25 °C (DTN: Updated Spreadsheet/Input/Output Results) with the Felmy et al. (1994a) model (Figure 3a), suggests differences that are approximately 2 to 15% of those they report. At 100°C (Felmy et al. 1994a; Figure 3b), the differences are slightly smaller at low NaNO₃ concentrations but they increase significantly at concentrations larger than 2 molal. Prediction of amorphous silica solubility in other electrolytes shows approximately the same magnitude of uncertainties. Overall, these differences appear to be reasonable given the plausible existence of uncertainties in the amorphous silica solubility data and the different log K's used in the calculations to represent the equilibrium solubility of this phase.. The parameters for SiO₂(aq) are valid only for neutral to acid conditions, in keeping with the experimental range studied.

I-4.5.17 Ions: See Table I-1 for MMX Ternary Parameters in the System Na-K-Mg-Cl-OH-SO₄

Associated Spreadsheet: [Pabalan_icf_TJW.xls](#)

Source: Pabalan and Pitzer (1987b)

Description: Some ternary parameters encompassing cation(M), cation(M), and anion (X) ($\Psi_{M_1M_2X}$) in the system Na-K-Mg-Cl-OH-SO₄ were refitted from equations and data by Pabalan and Pitzer (1987b). Some of these parameters are expressed as constants and do not need refitting.

I-4.6 VARIOUS MX AND MM PARAMETERS FROM TABLE I-2 AT 25 °C THAT DO NOT REQUIRE REFITTING

Associated Spreadsheet: [Some2-1Salts25C_TJW.xls](#) and [Some1-1Salts25C_TJW.xls](#)

Source: Pitzer (1991) (no spreadsheet in Table I-2 means that values were taken directly from the tables in this source)

Description: Binary and ternary parameters reported at 25 °C in Pitzer (1991) were also incorporated in the data0.ypf database. These parameters did not require any refitting but are expressed in the source as the product of the parameter multiplied by constant factors. The associated spreadsheets recalculate the parameter value without the multipliers so these can be incorporated in the data0.ypf database file.

I-5 DATA FOR SOLID PHASES, AQUEOUS SPECIES AND GASES

The majority of solid phases included in the data0.ypf database in the form of log K data to represent solubility are taken from the data0.ymp.R2 database (DTN: MO0302SPATHDYN.000; see Table I-27) or derived from thermodynamic data for solids reported by Barin and Platzki (1995). Log K data for most salt phases are taken from various sources such as Harvie et al. (1984), Greenberg and Møller (1989), and Pabalan and Pitzer (1987) which is in many cases given in the form of standard chemical potentials (see Table I-28 for spreadsheets Minerals_gmo.xls and Minerals_hmw.xls). For a few salts (CaCl_2 , $\text{Na}_2\text{CO}_3\cdot\text{H}_2\text{O}$, and NaNO_3), solubility data in the literature were scant and log K values for the salt dissolution reactions were estimated from combined sources of thermodynamic data such as heat capacity and standard enthalpy. For these few salts, these data were used with the code *SUPCRT92 Version 1.0* (STN: 10058-1.0-00) by addition to the *SUPCRT92* thermodynamic database. The *SUPCRT92* configuration run file (liqvap.con) and output files used for the Windows NT (suptest.tab in supcrt92test_Yueting_Chen.zip) and Windows 2000 (nano3_soda_niter.tab, thermonatrite.tab, cac12_solub.tab) runs are included in the DTN SN0306T0510102.007. Also included in this DTN is the input file 'supcrt_runs.rxn' that describes the input reactions for salt dissolution as used in all *SUPCRT92* runs. The modified *SUPCRT92* thermodynamic database (sprons96_mod2.dat and dprons96_mod2.dat) is included in the DTN: SN0306T0510102.007. In a similar fashion, MS Excel spreadsheet calculations were used to calculate the many log K's for reactions denoting salt solubility using this type of thermodynamic data as a source. Either approach allowed for the initial estimates of log K values which were then modified and fitted to the Pitzer activity model of the relevant system to predict the reported salt saturation molality values obtained from recognized sources such as Linke (1965) among others. This is done to bridge consistency between the activity model and salt solubility within the bounds of model applicability to accurately predict saturation molalities for the relevant salt. This type of fitting and optimization approach is necessary given the multiple sources of data obtained in different ways (e.g., calorimetry vs solubility). The resulting differences in log K's before and after fitting were reasonable given the associated uncertainties. Information on the fitting procedure and results is detailed in the corresponding Excel spreadsheets given in Table I-29. Only information on salt log K's that required fitting, the CaCl_2 hydrates, thermonatrite ($\text{Na}_2\text{CO}_3\cdot\text{H}_2\text{O}$), and soda niter (NaNO_3), will be summarized below. As mentioned above, log K values for other salt solids were obtained from Greenberg and Møller (1989) and Pabalan and Pitzer (1987) where no solubility constant fitting/optimization was needed due to their self-consistency with the Pitzer activity model of salt components adopted in this database development. Log K's of aqueous species were also taken from the data0.ymp.R2 database (see Tables I-30 and I-31) except for $\text{CaSO}_4(\text{aq})$ which was taken directly from Greenberg and Møller (1989) to be consistent with their activity model. Two redox related auxiliary species (NH_4^+ and NO_2^-) data were also derived from data0.ymp.R2 but were obtained through a combination of reaction log K's to generate the values incorporated in data0.ypf. The log K values for the gases were also obtained from the data0.ymp.R2 database. Table I-27 through Table I-32 below show a list of solid phases, aqueous species, and gases plus relevant spreadsheets where calculations of log K's were performed.

Table I-27. Solid Minerals Sourced from the Data0.ymp.R2 Database

Solid Mineral	Molecular Formula
Albite	NaAlSi ₃ O ₈
Alunite	KAl ₃ (OH) ₆ (SO ₄) ₂
Amesite-7A	Mg ₂ Al ₂ SiO ₅ (OH) ₄
Amesite-14A	Mg ₄ Al ₄ Si ₂ O ₁₀ (OH) ₈
Analcime	Na _{0.96} Al _{0.96} Si _{2.04} O ₆ ·H ₂ O
Analcime-dehy	Na _{0.96} Al _{0.96} Si _{2.04} O ₆
Aragonite	CaCO ₃
Artinite	Mg ₂ CO ₃ (OH) ₂ ·3H ₂ O
Beidellite-Mg	Mg _{0.165} Al _{2.33} Si _{3.67} O ₁₀ (OH) ₂
Beidellite-Ca	Ca _{0.165} Al _{2.33} Si _{3.67} O ₁₀ (OH) ₂
Beidellite-K	K _{0.33} Al _{2.33} Si _{3.67} O ₁₀ (OH) ₂
Beidellite-Na	Na _{0.33} Al _{2.33} Si _{3.67} O ₁₀ (OH) ₂
Beidellite-H	H _{0.33} Al _{2.33} Si _{3.67} O ₁₀ (OH) ₂
Boehmite	AlOOH
Brucite	Mg(OH) ₂
Calcite	CaCO ₃
Celadonite	KMgAlSi ₄ O ₁₀ (OH) ₂
Celestite	SrSO ₄
Chabazite	K _{0.6} Na _{0.2} Ca _{1.55} Al _{3.8} Si _{8.2} O ₂₄ ·10H ₂ O
Chamosite-7A	Fe ₂ Al ₂ SiO ₅ (OH) ₄
Clinoptilolite	Na _{0.954} K _{0.543} Ca _{0.761} Mg _{0.124} Sr _{0.036} Ba _{0.062} Mn _{0.002} Al _{3.45} F
Clinoptilolite-dehy	Sr _{0.036} Mg _{0.124} Ca _{0.761} Mn _{0.002} Ba _{0.062} K _{0.543} Na _{0.954} Al _{3.45} F
Clinoptilolite-Ca	Ca _{1.7335} Al _{3.45} Fe _{0.017} Si _{14.533} O ₃₆ ·10.922H ₂ O
Clinoptilolite-Cs	Ca _{3.467} Al _{3.45} Fe _{0.017} Si _{14.533} O ₃₆ ·10.922H ₂ O
Clinoptilolite-K	K _{3.467} Al _{3.45} Fe _{0.017} Si _{14.533} O ₃₆ ·10.922H ₂ O
Clinoptilolite-NH4	(NH ₄) _{3.467} Al _{3.45} Fe _{0.017} Si _{14.533} O ₃₆ ·10.922H ₂ O
Clinoptilolite-Na	Na _{3.467} Al _{3.45} Fe _{0.017} Si _{14.533} O ₃₆ ·10.922H ₂ O
Clinoptilolite-Sr	Sr _{1.7335} Al _{3.45} Fe _{0.017} Si _{14.533} O ₃₆ ·10.922H ₂ O
Corundum	Al ₂ O ₃
Cristobalite(alpha)	SiO ₂
Cronstedtite-7A	Fe ₂ Fe ₂ SiO ₅ (OH) ₄
Daphnite-14A	Fe ₅ AlAlSi ₃ O ₁₀ (OH) ₈
Daphnite-7A	Fe ₅ AlAlSi ₃ O ₁₀ (OH) ₈
Dawsonite	NaAlCO ₃ (OH) ₂
Dolomite	CaMg(CO ₃) ₂
Erionite	K _{1.5} Na _{0.9} Ca _{0.9} Al _{4.2} Si _{13.8} O ₃₆ ·13H ₂ O
Ferroaluminoceladonite	KFeAlSi ₄ O ₁₀ (OH) ₂
Ferroccladonite	KFeFeSi ₄ O ₁₀ (OH) ₂
Fe ₂ (MoO ₄) ₃	Fe ₂ (MoO ₄) ₃
FeF ₃	FeF ₃
Fe(OH) ₃	Fe(OH) ₃
Fe ₂ (SO ₄) ₃	Fe ₂ (SO ₄) ₃
Fluorapatite	Ca ₅ (PO ₄) ₃ F
Fluorite	CaF ₂
Gibbsite	Al(OH) ₃
Goethite	FeOOH
Greenalite	Fe ₃ Si ₂ O ₅ (OH) ₄
Hematite	Fe ₂ O ₃
Heulandite	Ba _{0.065} Sr _{0.175} Ca _{0.585} K _{0.132} Na _{0.383} Al _{2.165} Si _{6.835} O ₁₈ ·6H ₂ O
Huntite	CaMg ₃ (CO ₃) ₄
Hydroxylapatite	Ca ₅ (OH)(PO ₄) ₃
Hydromagnesite	Mg ₅ (CO ₃) ₄ (OH) ₂ ·4H ₂ O
Illite	K _{0.6} Mg _{0.25} Al _{1.8} Al _{0.5} Si _{3.5} O ₁₀ (OH) ₂
Jarosite	KFe ₃ (SO ₄) ₂ (OH) ₆

Solid Mineral	Molecular Formula
Jarosite-Na	$\text{NaFe}_3(\text{SO}_4)_2(\text{OH})_6$
K-Feldspar	KAlSi_3O_8
$\text{K}_2\text{CO}_3:1.5\text{H}_2\text{O}$	$\text{K}_2\text{CO}_3:1.5\text{H}_2\text{O}$
Kaolinite	$\text{Al}_2\text{Si}_2\text{O}_5(\text{OH})_4$
$\text{KMgCl}_3:2\text{H}_2\text{O}$	$\text{KMgCl}_3:2\text{H}_2\text{O}$
Lansfordite	$\text{MgCO}_3:5\text{H}_2\text{O}$
Laumontite	$\text{K}_{0.2}\text{Na}_{0.2}\text{Ca}_{1.8}\text{Al}_4\text{Si}_{8.0}\text{O}_{24}:8\text{H}_2\text{O}$
Lime	CaO
Magnesite	MgCO_3
Maximum Microcline	KAlSi_3O_8
Mesolite	$\text{Na}_{0.676}\text{Ca}_{0.657}\text{Al}_{1.99}\text{Si}_{3.01}\text{O}_{10}:2.647\text{H}_2\text{O}$
Minnesotaite	$\text{Fe}_3\text{Si}_4\text{O}_{10}(\text{OH})_2$
MoO_2Cl_2	MoO_2Cl_2
Molysite	FeCl_3
Montmorillonite-H	$\text{H}_{0.33}\text{Mg}_{0.33}\text{Al}_{1.67}\text{Si}_4\text{O}_{10}(\text{OH})_2$
Montmorillonite-Na	$\text{Na}_{0.33}\text{Mg}_{0.33}\text{Al}_{1.67}\text{Si}_4\text{O}_{10}(\text{OH})_2$
Montmorillonite-K	$\text{K}_{0.33}\text{Mg}_{0.33}\text{Al}_{1.67}\text{Si}_4\text{O}_{10}(\text{OH})_2$
Montmorillonite-Ca	$\text{K}_{0.165}\text{Mg}_{0.33}\text{Al}_{1.67}\text{Si}_4\text{O}_{10}(\text{OH})_2$
Montmorillonite-Mg	$\text{Mg}_{0.495}\text{Al}_{1.67}\text{Si}_4\text{O}_{10}(\text{OH})_2$
Mordenite	$\text{Ca}_{0.2895}\text{Na}_{0.361}\text{Al}_{0.94}\text{Si}_{5.06}\text{O}_{12}:3.468\text{H}_2\text{O}$
Natrolite	$\text{Na}_2\text{Al}_2\text{Si}_3\text{O}_{10}:2\text{H}_2\text{O}$
Nesquehonite	$\text{MgCO}_3:3\text{H}_2\text{O}$
Nontronite-Mg	$\text{Mg}_{0.165}\text{Fe}_2\text{Al}_{0.33}\text{Si}_{3.67}\text{H}_2\text{O}_{12}$
Nontronite-Ca	$\text{Ca}_{0.165}\text{Fe}_2\text{Al}_{0.33}\text{Si}_{3.67}\text{H}_2\text{O}_{12}$
Nontronite-K	$\text{K}_{0.33}\text{Fe}_2\text{Al}_{0.33}\text{Si}_{3.67}\text{H}_2\text{O}_{12}$
Nontronite-Na	$\text{Na}_{0.33}\text{Fe}_2\text{Al}_{0.33}\text{Si}_{3.67}\text{H}_2\text{O}_{12}$
Nontronite-H	$\text{H}_{0.33}\text{Fe}_2\text{Al}_{0.33}\text{Si}_{3.67}\text{H}_2\text{O}_{12}$
Phillipsite	$\text{K}_{0.7}\text{Na}_{0.7}\text{Ca}_{1.1}\text{Al}_{3.6}\text{Si}_{12.4}\text{O}_{32}:12.6\text{H}_2\text{O}$
Portlandite	$\text{Ca}(\text{OH})_2$
Pyrolusite	MnO_2
Pyrophyllite	$\text{Al}_2\text{Si}_4\text{O}_{10}(\text{OH})_2$
Quartz	SiO_2
Ripidolite-7A	$\text{Mg}_3\text{Fe}_2\text{Al}_2\text{Si}_3\text{O}_{10}(\text{OH})_8$
Ripidolite-14A	$\text{Mg}_3\text{Fe}_2\text{Al}_2\text{Si}_3\text{O}_{10}(\text{OH})_8$
Saponite-H	$\text{H}_{0.33}\text{Mg}_3\text{Al}_{0.33}\text{Si}_{3.67}\text{O}_{10}(\text{OH})_2$
Saponite-Na	$\text{Na}_{0.33}\text{Mg}_3\text{Al}_{0.33}\text{Si}_{3.67}\text{O}_{10}(\text{OH})_2$
Saponite-K	$\text{K}_{0.33}\text{Mg}_3\text{Al}_{0.33}\text{Si}_{3.67}\text{O}_{10}(\text{OH})_2$
Saponite-Ca	$\text{Ca}_{0.165}\text{Mg}_3\text{Al}_{0.33}\text{Si}_{3.67}\text{O}_{10}(\text{OH})_2$
Saponite-Mg	$\text{Mg}_{0.165}\text{Mg}_3\text{Al}_{0.33}\text{Si}_{3.67}\text{O}_{10}(\text{OH})_2$
Scolecite	$\text{CaAl}_2\text{Si}_3\text{O}_{10}:3\text{H}_2\text{O}$
Sepiolite	$\text{Mg}_4\text{Si}_6\text{O}_{15}(\text{OH})_2:6\text{H}_2\text{O}$
$\text{SiO}_2(\text{am})$	SiO_2
Smectite-high-Fe-Mg	$\text{Ca}_{0.025}\text{Na}_{0.1}\text{K}_{0.2}\text{Fe}^{++}_{0.5}\text{Fe}^{+++}_{0.2}\text{Mg}_{1.15}\text{Al}_{1.25}\text{Si}_{3.5}\text{H}_2\text{O}_{12}$
Smectite-high-Fe-Mg	$\text{Ca}_{0.02}\text{Na}_{0.15}\text{K}_{0.2}\text{Fe}^{++}_{0.29}\text{Fe}^{+++}_{0.16}\text{Mg}_{0.9}\text{Al}_{1.25}\text{Si}_{3.75}\text{H}_2\text{O}_{12}$
Stellerite	$\text{Ca}_2\text{Al}_4\text{Si}_{14}\text{O}_{36}:14\text{H}_2\text{O}$
Stilbite	$\text{Ca}_{1.019}\text{Na}_{0.136}\text{K}_{0.006}\text{Al}_{2.18}\text{Si}_{6.82}\text{O}_{18}:7.33\text{H}_2\text{O}$
Strontianite	SrCO_3
Talc	$\text{Mg}_3\text{Si}_4\text{O}_{10}(\text{OH})_2$
Whitlockite	$\text{Ca}_3(\text{PO}_4)_2$
DTN: MO0302SPATHDYN.000	

Table I-28. Cement Phases Sourced from the Data0.ymp.R2 Database

Cement Phase	Molecular Formula
Afwillite	$\text{Ca}_3\text{Si}_2\text{O}_4(\text{OH})_6$
Allite_(C3S)	$3\text{CaO}:\text{SiO}_2$

Cement Phase	Molecular Formula
Bellite_(C2S)	2CaO:SiO ₂
(C12A7)	12CaO:7Al ₂ O ₃
(C2AH8)	2CaO:Al ₂ O ₃ :8H ₂ O
(C3A)	3CaO:Al ₂ O ₃
(C4AF)	4CaO:Al ₂ O ₃ :Fe ₂ O ₃
(C4AH13)	4CaO:Al ₂ O ₃ :13H ₂ O
(C4AH19)	4CaO:Al ₂ O ₃ :19H ₂ O
(CA)	CaO:Al ₂ O ₃
(CA2)	CaO:2Al ₂ O ₃
(CAH10)	CaO:Al ₂ O ₃ :10H ₂ O
CSH:1.7	1.7Ca(OH) ₂ :SiO ₂ :0.917H ₂ O
Ettringite	3CaO:Al ₂ O ₃ :3CaSO ₄ :32H ₂ O
Ferrite-Ca	CaFe ₂ O ₄
Ferrite-Dicalcium	Ca ₂ Fe ₂ O ₅
Ferrite-Mg	MgFe ₂ O ₄
Foshagite	Ca ₄ Si ₃ O ₉ (OH) ₂ :0.5H ₂ O
Friedl_salt	CaCl ₂ (CaO) ₃ :16H ₂ O
Gehlenate_Hydrate	Ca ₂ Al ₂ SiO ₇ :8H ₂ O
Gismondine-Na	Na ₂ Al ₂ Si ₂ O ₈ :4H ₂ O
Gismondine-Ca	CaAl ₂ Si ₂ O ₈ :4H ₂ O
Gyrolite	Ca ₂ Si ₃ O ₇ (OH) ₂ :1.5H ₂ O
Hemicarboaluminate	3CaOAl ₂ O ₃ :0.5CaCO ₃ :0.5Ca(OH) ₂ :10.5H ₂ O
Hillebrandite	Ca ₂ SiO ₃ (OH) ₂ :0.17H ₂ O
Hydrogarnet	3CaO:Al ₂ O ₃ :6H ₂ O
Hydrotalcite	4MgO:Al ₂ O ₃ :10H ₂ O
Monocarboaluminate	3CaOAl ₂ O ₃ CaCO ₃ :10H ₂ O
Monosulphate	3CaO:Al ₂ O ₃ :CaSO ₄ :12H ₂ O
Okenite	CaSi ₂ O ₄ (OH) ₂ :H ₂ O
Plombierite	Ca ₅ Si ₆ H ₁₁ O _{22.5}
Riversideite	Ca ₅ H ₂ (SiO ₃) ₆ :2H ₂ O
Tobermorite	5CaO:6SiO ₂ :5.5H ₂ O
Xonotlite	Ca ₆ Si ₆ O ₁₇ (OH) ₂
DTN: MO0302SPATHDYN.000	

Table I-29. Salt Solids Sourced from Various Spreadsheets

Solid Mineral	Molecular Formula	DTN or Spreadsheet File (.xls)
Anhydrite	CaSO ₄	Minerals_gmo
Antarcticite	CaCl ₂ :6H ₂ O	cacl2_hydrates_min_cal_CFJC
Arcanite	K ₂ SO ₄	Minerals_gmo
Bischofite	MgCl ₂ :6H ₂ O	Solids_j_Pabalan_TJW_1
Bloedite	Na ₂ Mg(SO ₄) ₂ :4H ₂ O	Minerals_hmw
Brushite	CaHPO ₄ :2H ₂ O	Solids_j_Ca_TJW_1
Burkeite	Na ₆ CO ₃ (SO ₄) ₂	Minerals_hmw
CaBr ₂	CaBr ₂	Solids_j_Ca_TJW_1
Ca ₂ Cl ₂ (OH) ₂ :H ₂ O	Ca ₂ Cl ₂ (OH) ₂ :H ₂ O	Minerals_hmw
Ca ₄ Cl ₂ (OH) ₆ :13H ₂ O	Ca ₄ Cl ₂ (OH) ₆ :13H ₂ O	Minerals_hmw
CaCl ₂	CaCl ₂	cacl2_solub_tab. DTN: SN0306T0510102.007
CaCl ₂ :2H ₂ O	CaCl ₂ :2H ₂ O	cacl2_hydrates_min_cal_CFJC
CaCl ₂ :4H ₂ O	CaCl ₂ :4H ₂ O	cacl2_hydrates_min_cal_CFJC

Solid Mineral	Molecular Formula	DTN or Spreadsheet File (.xls)
CaI2	CaI ₂	Solids_j_Ca_TJW_1
Ca(NO3)2	Ca(NO ₃) ₂	Solids_j_Ca_TJW_1
Ca(NO3)2:2H2O	Ca(NO ₃) ₂ :2H ₂ O	Solids_j_Ca_TJW_1
Ca(NO3)2:3H2O	Ca(NO ₃) ₂ :3H ₂ O	Solids_j_Ca_TJW_1
Ca(NO3)2:4H2O	Ca(NO ₃) ₂ :4H ₂ O	Solids_j_Ca_TJW_1
CaOHCl	CaOHCl	Solids_j_Misc_1_TJW_1
Carnallite	KMgCl ₃ :6H ₂ O	Solids_j_Pabalan_TJW_1
Carobbite	KF	Solids_j_K_TJW_1
CaWO4	CaWO ₄	Solids_j_Ca_TJW_1
Chloromagnesite	MgCl ₂	Solids_j_Pabalan_TJW_1
Cryolite	Na ₃ AlF ₆	Solids_j_Na_TJW_1
Darapskite	Na ₃ SO ₄ NO ₃ :H ₂ O	Solids_j_Misc_1_TJW_1
Epsomite	MgSO ₄ :7H ₂ O	Minerals_hmw
Gaylussite	CaNa ₂ (CO ₃) ₂ :5H ₂ O	Minerals_hmw
Glaserite	NaK ₃ (SO ₄) ₂	Minerals_hmw
Glauberite	Na ₂ Ca(SO ₄) ₂	Minerals_gmo
Gypsum	CaSO ₄ :2H ₂ O	Minerals_gmo
Halite	NaCl	Minerals_gmo
Hemihydrate	CaSO ₄ :0.5H ₂ O	Minerals_gmo
Hexahydrate	MgSO ₄ :6H ₂ O	Solids_j_Pabalan_TJW_1
K2CO3	K ₂ CO ₃	Solids_j_K_TJW_1
K2O	K ₂ O	Solids_j_K_TJW_1
K2Si4O9	K ₂ Si ₄ O ₉	Solids_j_K_TJW_1
K3H(SO4)2	K ₃ H(SO ₄) ₂	Minerals_hmw
K8H4(CO3)6:3H2O	K ₈ H ₄ (CO ₃) ₆ :3H ₂ O	Minerals_hmw
Kainite	KmgClSO ₄ :3H ₂ O	Minerals_hmw
KAICl4	KAICl ₄	Solids_j_K_TJW_1
K2HPO4	K ₂ HPO ₄	Solids_j_K_TJW_1
K3AlCl6	K ₃ AlCl ₆	Solids_j_K_TJW_1
K3AlF6	K ₃ AlF ₆	Solids_j_K_TJW_1
K3PO4	K ₃ PO ₄	Solids_j_K_TJW_1
Kalinite	KHCO ₃	Minerals_hmw
KAl(SO4)2	KAl(SO ₄) ₂	Solids_j_K_TJW_1
KAl(SO4)2:3H2O	KAl(SO ₄) ₂ :3H ₂ O	Solids_j_K_TJW_1
KAl(SO4)2:12H2O	KAl(SO ₄) ₂ :12H ₂ O	Solids_j_K_TJW_1
KBr	KBr	Solids_j_K_TJW_1
KClO4	KClO ₄	Solids_j_K_TJW_1
KH2PO4	KH ₂ PO ₄	Solids_j_K_TJW_1
KI	KI	Solids_j_K_TJW_1
Kieserite	MgSO ₄ :H ₂ O	Solids_j_Pabalan_TJW_1
KnaCO3:6H2O	KnaCO ₃ :6H ₂ O	Minerals_hmw
KOH	KOH	Solids_j_K_TJW_1
Labile_Salt	Na ₂ Ca ₅ (SO ₄) ₆ :3H ₂ O	Minerals_gmo
Leonhardtite	MgSO ₄ :4H ₂ O	Solids_j_Pabalan_TJW_1
Leonite	K ₂ Mg(SO ₄) ₂ :4H ₂ O	Minerals_hmw
Mercallite	KHSO ₄	Minerals_hmw
MgBr2	MgBr ₂	Solids_j_Mg_TJW_1
MgCl2:H2O	MgCl ₂ :H ₂ O	Solids_j_Pabalan_TJW_1
MgCl2:2H2O	MgCl ₂ :2H ₂ O	Solids_j_Pabalan_TJW_1
MgCl2:4H2O	MgCl ₂ :4H ₂ O	Solids_j_Pabalan_TJW_1
MgI2	MgI ₂	Solids_j_Mg_TJW_1
MgMoO4	MgMoO ₄	Solids_j_Mg_TJW_1
Mg(NO3)2	Mg(NO ₃) ₂	Solids_j_Mg_TJW_1

Solid Mineral	Molecular Formula	DTN or Spreadsheet File (.xls)
MgOHCl	MgOHCl	Solids_j_Mg_TJW_1
MgSO4	MgSO ₄	Solids_j_Pabalan_TJW_1
MgWO4	MgWO ₄	Solids_j_Mg_TJW_1
Mirabilite	Na ₂ SO ₄ ·10H ₂ O	Minerals_gmo
Misenite	K ₈ H ₆ (SO ₄) ₇	Minerals_hmw
NaBr	NaBr	Solids_j_Na_TJW_1
NaClO4	NaClO ₄	Solids_j_Na_TJW_1
NaI	NaI	Solids_j_Na_TJW_1
NaNO2	NaNO ₂	Solids_j_Na_TJW_1
NaOH	NaOH	Solids_j_Na_TJW_1
Na2CO3·7H2O	Na ₂ CO ₃ ·7H ₂ O	Minerals_hmw
Na2CrO4	Na ₂ CrO ₄	Solids_j_Na_TJW_1
Na2MoO4	Na ₂ MoO ₄	Solids_j_Na_TJW_1
Na2WO4	Na ₂ WO ₄	Solids_j_Na_TJW_1
Na2O	Na ₂ O	Solids_j_Na_TJW_1
Na2SO4(Sol-3)	Na ₂ SO ₄	Solids_j_Na_TJW_1
Na3H(SO4)2	Na ₃ H(SO ₄) ₂	Minerals_hmw
Na4Ca(SO4)3·2H2O	Na ₄ Ca(SO ₄) ₃ ·2H ₂ O	Minerals_hmw
Nahcolite	NaHCO ₃	Solids_j_Na_TJW_1
Natrite	Na ₂ CO ₃	Solids_j_Na_TJW_1
Natron	Na ₂ CO ₃	Minerals_hmw
NH4Cl	NH ₄ Cl	Solids_j_NH4_TJW_1
NH4ClO4	NH ₄ ClO ₄	Solids_j_NH4_TJW_1
NH4I	NH ₄ I	Solids_j_NH4_TJW_1
(NH4)2SO4	(NH ₄) ₂ SO ₄	Solids_j_NH4_TJW_1
Niter	KNO ₃	Solids_j_K_TJW_1
Oxychloride-Mg	Mg ₂ Cl(OH) ₃ ·4H ₂ O	Minerals_hmw
Pentahydrate	MgSO ₄ ·5H ₂ O	Solids_j_Pabalan_TJW_1
Pentasalt	K ₂ Ca ₅ (SO ₄) ₆ ·H ₂ O	Minerals_gmo
Periclase	MgO	Solids_j_Mg_TJW_1
Picromerite	K ₂ Mg(SO ₄) ₂ ·6H ₂ O	Minerals_hmw
Pirssonite	Na ₂ Ca(CO ₃) ₂ ·2H ₂ O	Minerals_hmw
Polyhalite	K ₂ MgCa ₂ (SO ₄) ₄ ·2H ₂ O	Minerals_hmw
Powellite	CaMoO ₄	Solids_j_Ca_TJW_1
Sellaite	MgF ₂	Solids_j_Mg_TJW_1
Soda Niter	NaNO ₃	NaNO3_min_cal_CFJC
SrBr2	SrBr ₂	Solids_j_Sr_TJW_1
SrCl2	SrCl ₂	Solids_j_Sr_TJW_1
SrF2	SrF ₂	Solids_j_Sr_TJW_1
SrI2	SrI ₂	Solids_j_Sr_TJW_1
SrMoO4	SrMoO ₄	Solids_j_Sr_TJW_1
SrO	SrO	Solids_j_Sr_TJW_1
Sr(OH)2	Sr(OH) ₂	Solids_j_Sr_TJW_1
SrWO4	SrWO ₄	Solids_j_Sr_TJW_1
Sylvite	KCl	Minerals_gmo
Syngenite	K ₂ Ca(SO ₄) ₂ ·H ₂ O	Minerals_gmo
Tachyhydrate	Mg ₂ CaCl ₆ ·12H ₂ O	Minerals_hmw
Tarapacaite	K ₂ CrO ₄	Solids_j_K_TJW_1
Thenardite	Na ₂ SO ₄	Minerals_gmo
Thermonatrite	Na ₂ CO ₃ ·H ₂ O	thermonatrite_min_cal_CFJC
Trona	Na ₃ H(CO ₃) ₂ ·2H ₂ O	Minerals_hmw

Solid Mineral	Molecular Formula	DTN or Spreadsheet File (.xls)
Trona-K	$K_2NaH(CO_3)_2 \cdot 2H_2O$	Minerals_hmw
Villiaumite	NaF	Solids_j_Na_TJW_1
DTN: SN0306T0510102.007		

Table I–30. Auxiliary Basis Aqueous Species Data Sources

Aqueous Species	Molecular Formula	DTN or Spreadsheet
ClO4-	ClO_4^-	MO0302SPATHDYN.000
Fe+++	Fe^{3+}	MO0302SPATHDYN.000
H2(aq)	$H_2(aq)$	MO0302SPATHDYN.000
NH4+	NH_4^+	AuxBasisSpecies.xls
NO2-	NO_2^-	AuxBasisSpecies.xls
O2(aq)	$O_2(aq)$	MO0302SPATHDYN.000

Table I–31. Aqueous Species Data Sources

Aqueous Species	Molecular Formula	DTN or Spreadsheet
AlO2-	AlO_2^-	MO0302SPATHDYN.000
AlOH++	$AlOH^{2+}$	MO0302SPATHDYN.000
AlO+	AlO^+	MO0302SPATHDYN.000
CaCO3(aq)	$CaCO_3(aq)$	MO0302SPATHDYN.000
CaHCO3+	$CaHCO_3^+$	MO0302SPATHDYN.000
CaOH+	$CaOH^+$	MO0302SPATHDYN.000
CaSO4(aq)	$CaSO_4(aq)$	Minerals_gmo.xls
CO2(aq)	$CO_2(aq)$	MO0302SPATHDYN.000
CO3--	CO_3^{2-}	MO0302SPATHDYN.000
HSO4-	HSO_4^-	MO0302SPATHDYN.000
HSiO3-	$HSiO_3^-$	MO0302SPATHDYN.000
H2PO4-	$H_2PO_4^-$	MO0302SPATHDYN.000
H3PO4(aq)	$H_3PO_4(aq)$	MO0302SPATHDYN.000
MgCO3(aq)	$MgCO_3(aq)$	MO0302SPATHDYN.000
MgHCO3+	$MgHCO_3^+$	MO0302SPATHDYN.000
MgOH+	$MgOH^+$	MO0302SPATHDYN.000
NH3(aq)	$NH_3(aq)$	MO0302SPATHDYN.000
NaF(aq)	$NaF(aq)$	MO0302SPATHDYN.000
OH-	OH^-	MO0302SPATHDYN.000
PO4---	PO_4^{3-}	MO0302SPATHDYN.000

Table I–32. Gas Data Sources

Gases	Molecular Formula	DTN or Spreadsheet
CO2(g)	CO_2	MO0302SPATHDYN.000
H2(g)	H_2	MO0302SPATHDYN.000
H2O(g)	H_2O	MO0302SPATHDYN.000
HBr(g)	HBr	MO0302SPATHDYN.000
HCl(g)	HCl	MO0302SPATHDYN.000
HF(g)	HF	MO0302SPATHDYN.000

HNO3(g)	HNO ₃	MO0302SPATHDYN.000
N2O5(g)	N ₂ O ₅	MO0302SPATHDYN.000
NO3(g)	NO ₃	MO0302SPATHDYN.000
O2(g)	O ₂	Gases_j_TJW_2.xls

I-5.1 CaCl₂ HYDRATES (CaCl₂•nH₂O WHERE N EQUALS 2, 4, AND 6)

Associated Spreadsheet: cacl2_hydrates_min_cal_CFJC.xls;
Solids_j_CaCl2hydrates_TJW_1.xls; Cp_Solids_j_CaCl2hydrates_TJW_1.xls

Source: Meisingset and Grønvold (1986); Pitzer and Shi (1993); Pitzer and Oakes (1994)

Description: Solubilities of CaCl₂ hydrates (CaCl₂•nH₂O where n equals 2, 4, and 6) were estimated for a temperature range of 25 to 95 °C within the valid range of the activity model to generate bounding saturation molalities for the stable phases. Standard state thermodynamic properties were obtained from Pitzer and Shi (1993) and Pitzer and Oakes (1994) along with their reported saturation molality values of the corresponding CaCl₂ hydrate phases. Calculations of initial log K's were conducted in the 'Solids_j_CaCl2hydrates_TJW_1.xls' spreadsheet using heat capacity data from Meisingset and Grønvold (1986). Log K values for dehydrated CaCl₂ were obtained from thermodynamic data reported by Robie and Hemingway (1995) and using *SUPCRT92 Version 1.0* (See output file cacl2_solub_tab (DTN: SN0306T0510102.007) on the attached CD). Because the stability range of dehydrated CaCl₂ with respect to temperature exceeds the validity range of the activity model to predict CaCl₂•2H₂O solubility, it wasn't considered in the fitting and was added to the database for completeness. Initial log K values for the dissolution of the hydrated phases were obtained using the 'Solids_j_CaCl2hydrates_TJW_1.xls' spreadsheet and tested for prediction of solid solubility using the Pitzer parameters from Sterner et al. (1999). The log K values were then modified to fit saturation molalities of the CaCl₂ hydrates given by Pitzer and Shi (1993) and Pitzer and Oakes (1994) within their estimated temperature range of stability. The resulting log K values plus their relative differences from the initial values determined using the 'Solids_j_CaCl2hydrates_TJW_1.xls' spreadsheet are given in Table I-33 below.

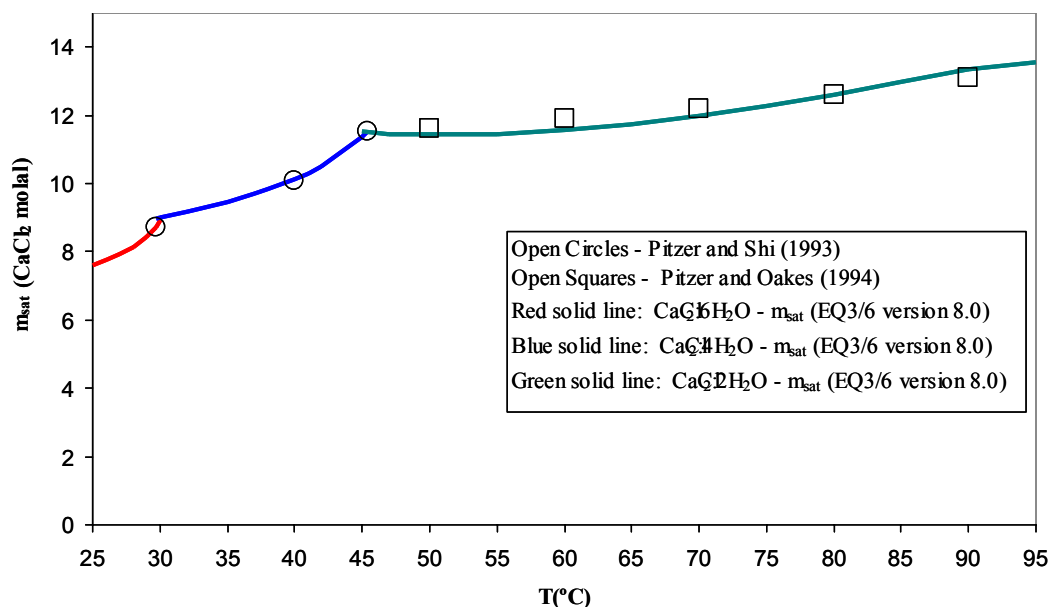
Table I-33. Comparison of Initial and Fitted log K Values for CaCl₂ Hydrates Used in the data0.ypf

T(°C)	CaCl ₂ •nH ₂ O	log K for CaCl ₂ Hydrate from Pitzer & Shi (1993) and Pitzer & Oakes (1994) data	Fitted Log K to Fit Saturation Molality	% Difference in log K
25	CaCl ₂ :6H ₂ O	3.8293	3.5993	6.39
60	CaCl ₂ :6H ₂ O	4.1076	3.9976	2.75
25	CaCl ₂ :4H ₂ O	5.3425	4.9488	7.96
60	CaCl ₂ :4H ₂ O	5.0728	4.9458	2.57
25	CaCl ₂ :2H ₂ O	7.4163	6.9891	6.11
60	CaCl ₂ :2H ₂ O	6.5028	6.2038	4.82
100	CaCl ₂ :2H ₂ O	5.4969	5.5015	-0.08
150	CaCl ₂ :H ₂ O	4.2688	4.3320	-1.46

200	CaCl ₂ :H ₂ O	3.0166	3.0196	-0.10
250	CaCl ₂ :H ₂ O	1.6525	1.8200	-9.20

As shown in the above table, the relative differences in log K computed from tabulated thermodynamic data and the fitted saturation molalities at 25, 60, and 100 °C are on the order of less than a percent up to ~9.2% depending on the temperature range. Fitting solubility data for CaCl₂•2H₂O above ~45°C was satisfactory up to a temperature of 95 °C. Above this temperature, the model begins to under-predict the solubility of this phase and log K values above 100 °C should be used with caution (see explanation later in this section and EQ6 output files cacl2_h2o_CFJC-*.60, where * stands for identifiers for different runs, on the attached CD). Overall, the differences between model predictions and reported saturation molalities for all CaCl₂ hydrates are satisfactory given the fitting approach used and combined uncertainties. It must be emphasized that these CaCl₂ hydrates undergo phase transitions to less hydrated forms with increasing temperature.

Log Ks are entered in the data0.ypf database only at specific temperatures, namely, 0, 25, 60, 100, 150, 200, 250, and 300 °C. For other temperatures EQ3/6 uses a polynomial fit, either to the log K's at the four lower temperatures, or to the five upper ones. (Thus, the fits match at 100 °C.) This means that, if a phase transition occurs between 25 and 60 °C, there will be only two points, those at 0 and 25 °C, available for fitting log K's to the phase stable below the transition temperature. In other words the fit of log K against temperature will be linear. The same situation applies to the phase stable above the transition; namely, only the points for 60 and 100 °C are available. If data for metastable equilibria, or heat capacity data, were available for these phases outside their stability ranges better fits could, of course, be obtained. Specifically, CaCl₂•6H₂O appears to be the stable phase from temperatures below 25 °C up to ~30 °C based on the reported solubility and thermodynamic data, above 30 °C CaCl₂•4H₂O becomes stable. Above ~45 °C CaCl₂•2H₂O is the dominant phase. On the basis of these considerations and the available heat capacity data, log K's calculated in spreadsheet Solids_j_CaCl2hydrates_TJW1.xls were entered into data0.ypf at 0, 25, and 60 °C for CaCl₂•6H₂O, at 25 and 60 °C for CaCl₂•4H₂O, and at all temperatures up to 250 °C for CaCl₂•2H₂O. By suppressing selected solids EQ3/6 was run at several temperatures in the range 25 to 95 °C to obtain the curves shown in Figure I-3 for these three solids. (The outputs of these runs, file names cacl2_h2o_CFJC_*.60, where * stands for identifiers for different runs, are included in attached CD.) These plots identify approximately the intersection temperatures of the calculated solubility curves. In general, m_{sat} predictions in the lower temperature range seem to fit the data acceptably, but slight deviations are apparent at temperatures above ~50 °C. Nevertheless, considering the inherent uncertainties of the CaCl₂ activity model, those associated with the parameter conversion to a standard Pitzer form, and the collective uncertainties from utilizing multiple data sources, the use of the fitted values for log K results in a fairly good level of confidence in predictions of the solubility of these highly soluble salts.



DTN: SN0306T0510102.007

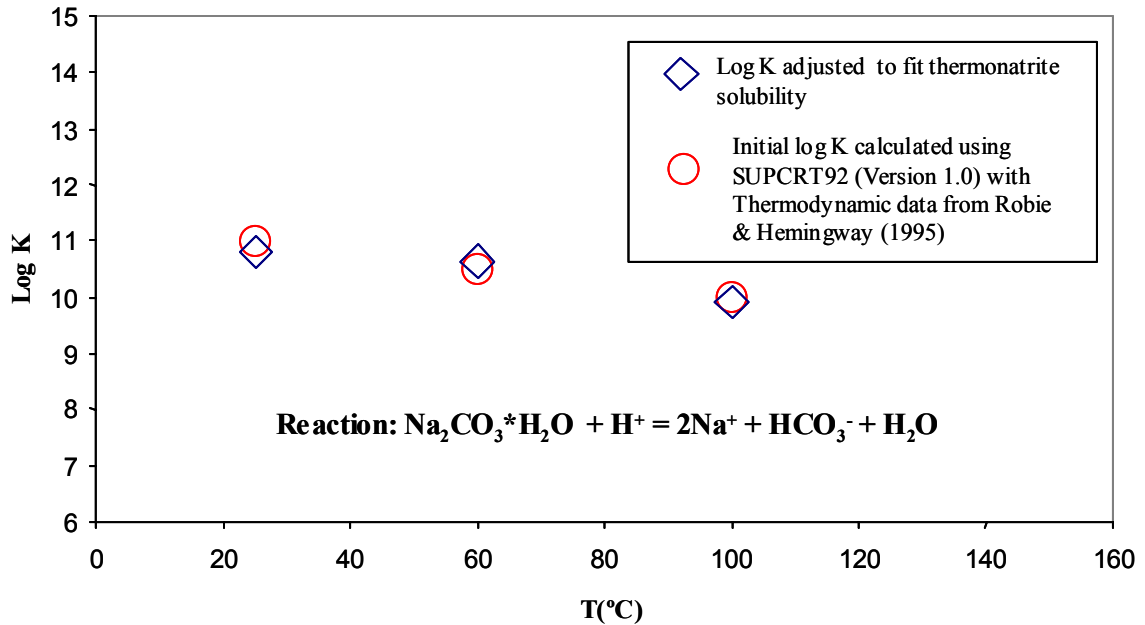
Figure I-3. Comparison predicted and compiled saturation molalities (m_{sat}) for CaCl_2 hydrates. Predicted m_{sat} values were computed using data0.ypf and EQ3/6 Version 8.0.

I-5.2 THERMONATRITE ($\text{Na}_2\text{CO}_3\cdot\text{H}_2\text{O}$)

Associated Spreadsheet: thermonatrite_min_CFJC.xls

Source: Grønbold and Mesingset (1983); Robie and Hemingway (1995); Linke (1965)

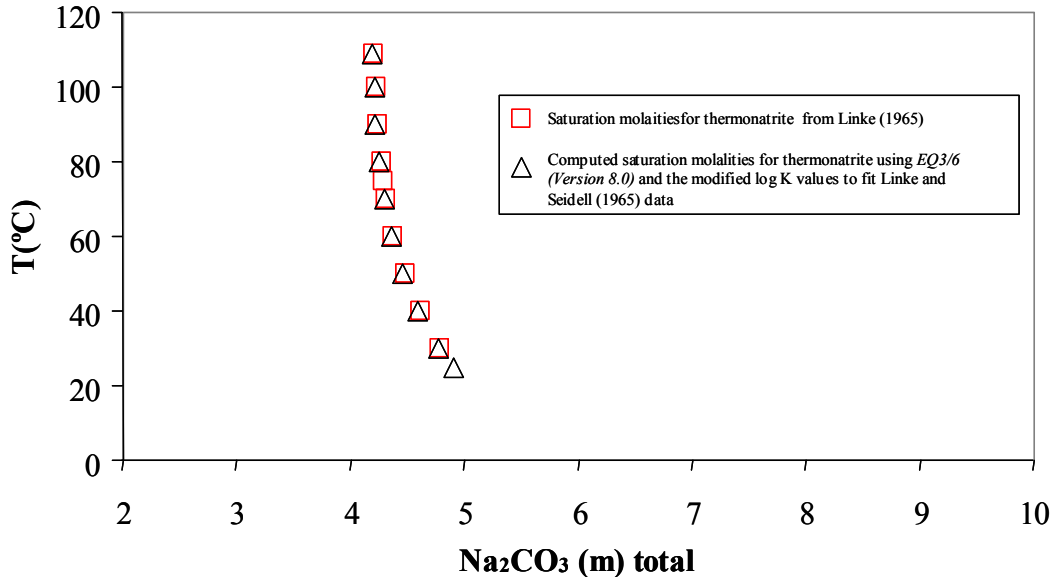
Description: Solubility of thermonatrite ($\text{Na}_2\text{CO}_3\cdot\text{H}_2\text{O}$) as predicted using the activity model of He and Morse (1993) for the carbonate system and bounded by saturation molalities reported by Linke (1965) was estimated for a temperature of 25 to 109 °C (See EQ3/6 output files input_na_cos_thermonatrite_equil_*.3o, included on the attached CD). Initial log K's were determined by SUPCRT92 Version 1.0 (DTN: SN0306T0510102.007) using thermodynamic data from Grønbold and Mesingset (1983), and Robie and Hemingway (1995). Heat capacities reported by Grønbold and Mesingset (1983) are those listed by Robie and Hemingway (1995). It should be emphasized that the log K's generated by SUPCRT92 are only use either as initial reference values or for comparison purposes only. That is, these are not used as direct data inputs. The resulting fit of these initial log K's to fit Linke (1965) saturation molalities shows that the difference between initial and fitted log K's is on the order of less than a percent to ~1.9%. Figure I-3 below shows a comparison of initial and modified log K's for the EQ3/6 temperature grid up to a temperature of 150 °C. The log K value at this latter temperature should be considered as fictive since the upper stability temperature for this phase is around 109 °C. That is, this 150 °C value was modified to fit the saturation molality at 109 °C. As shown in the figure, the fitted log K values are in good agreement with those obtained with SUPCRT92 up to a temperature of 100 °C.



DTN: SN0306T0510102.007

Figure I-4. Comparison of initial and fitted log K values for the reaction describing thermonatrite solubility as implemented in the data0.ypf database. Initial values were obtained from thermodynamic data reported by Robie and Hemingway (1995) and the code *SUPCRT92 (Version 1.0)*. Notice the relatively small difference between initial and fitted values modified in conjunction with He and Morse (1993) Pitzer parameters to fit saturation molalities for thermonatrite reported by Linke (1965).

Figure I-4 depicts the saturation molalities obtained with the use of modified log K values to fit the thermonatrite solubility in Linke (1965). Notice that the resulting saturation molalities strongly conform to the reported solubility values up to the upper stability temperature limit of 109 °C. The strong agreement in predicted saturation molalities and the relatively minimal change in log K values is viewed as a robust validation of the Pitzer activity model given the different data sources used to constrain the model.



DTN: SN0306T0510102.007

Figure I-5. Comparison of predicted saturation molalities for thermonatrite using *EQ3/6 (Version 8.0)* and *data0.ypf* to those reported by Linke (1965). The fitted log K values used in *data0.ypf* are those modified to fit Linke (1965) thermonatrite solubility data using He and Morse (1993) Pitzer parameters.

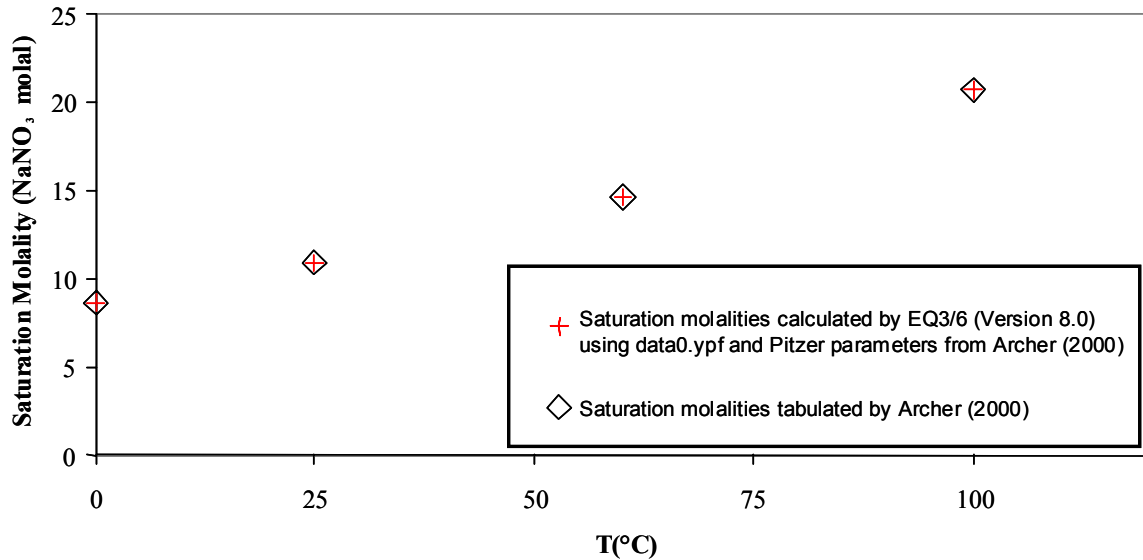
I-5.3 SODA NITER (NaNO₃)

Associated Spreadsheet: Misc_Salt_solids_CFJC

Source: Robie and Hemingway (1995); Barin and Platzki (1995); Archer (2000)

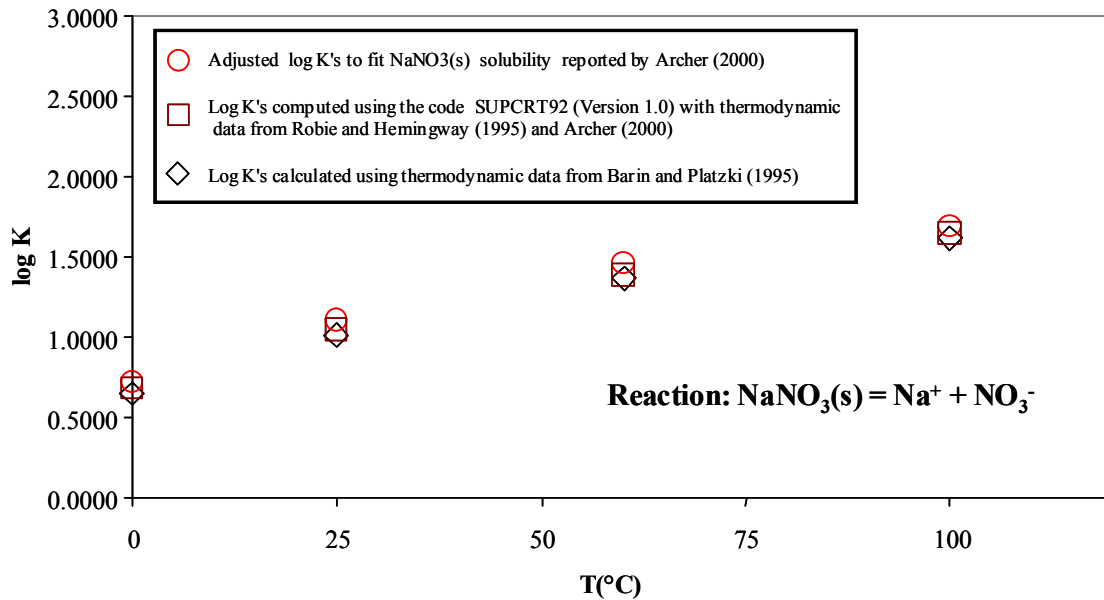
Description: The solubility of soda niter (NaNO₃) was modeled using the recent thermodynamic model and Pitzer parameters of Archer (2000) up to a temperature of 119°C. The temperature of 119°C represents the approximate maximum temperature for which solubility data are reported in Figure 10 of Archer (2000), p. 1153. Accurate log K fits were only obtained from 0 to 100 °C since saturation molality values compiled by Archer (2000) are only tabulated in this temperature range. The log K value at 150°C in the *data0.ypf* data block for this phase is suspect since it was fitted to obtain an approximate bounding saturation molality value of ~24.1 at 119°C. Figure I-6 shows a comparison between log K values obtained from 1) combined data from Robie and Hemingway (1995) and Archer (2000) incorporated into the modified database for *SUPCRT92 Version 1.0* (DTN: SN0306T0510102.007), 2) data from Barin and Platzki (1995) (see spreadsheet 'Solids_j_Na_TJW_1.xls'), and 3) log K values fitted to saturation molalities reported in Archer (2000). It should be emphasized that the log K's generated by *SUPCRT92* or the Excel spreadsheet using data from Barin and Platzki (1995) are only use as either intital reference values or for comparison purposes only. That is, these are not used as direct data inputs. As shown in the figure, the differences in log K values between different data sets are relatively minor. Figure I-7 shows the predicted saturation molalities for soda niter from 0 to 100 °C indicating nearly identical values to those reported by Archer (2000). The close agreement of log K values from multiple sources and those obtained in the fitting, together with

the prediction of saturation molalities in Archer (2000) validates the Pitzer activity model for NaNO_3 .



DTN: SN0306T0510102.007

Figure I-6. Comparison of log K values for soda niter ($\text{NaNO}_3(\text{s})$) dissolution from various sources and those obtained by fitting saturation molalities reported by Archer (2000).



DTN: SN0306T0510102.007

Figure I-7. Comparison of saturation molalities for soda niter ($\text{NaNO}_3(\text{s})$) predicted by EQ3/6 Version 8.0 using data0.ypf and fitted log K to those in Archer (2000) up to a temperature of 100 °C.

I-6 REFERENCES

Archer, D. G. 1999. "Thermodynamic Properties of the KCl + H₂O System." *Journal of Physical and Chemical Reference Data*, 28, 1–17. College Park, Maryland: American Institute of Physics. TIC: 253882

Archer, D. G. 2000. "Thermodynamic Properties of the NaNO₃ + H₂O System." *Journal of Physical and Chemical Reference Data*, 29, 1141–1156. College Park, Maryland: American Institute of Physics. TIC: 253379

Barin, I.; Platzki, G., 1995. *Thermochemical Data of Pure Substances* (3rd ed.), Weinheim, Germany; New York, NY. TIC: 251934

Chen, C.T.A. and Marshall, W.L., 1982. "Amorphous Silica Solubilities - IV. Behavior In Pure Water and Aqueous Sodium Chloride, Sodium Sulfate, Magnesium Chloride, and Magnesium Sulfate Solutions up To 350°C." *Geochimica et Cosmochimica Acta*, 46(2), p. 279-287. New York, New York: Elsevier Science. TIC: 235346

Clarke, E. C. and Glew, D.N., 1985. "Evaluation of the Thermodynamic Functions for Aqueous Sodium Chloride from Equilibrium and Calorimetric Measurements below 154°C." *Journal of Physical and Chemical Reference Data*, 14(2), pp. 489-610. College Park, Maryland: American Institute of Physics. TIC: 253934

Clegg, S.L. and Brimblecombe, P., 1990a. "Equilibrium partial pressures and mean activity and osmotic coefficients of 0-100% nitric acid as a function of temperature." *Journal of Physical Chemistry*, 94, p. 5369-5380. Columbus, Ohio: American Chemical Society. TIC: 253935

Clegg, S.L. and Brimblecombe, P., 1990b. "The solubility and activity coefficient of oxygen in salt solutions." *Geochimica Cosmochimica Acta*, 54, p. 3315-3328. New York, New York: Elsevier Science. TIC: 253874

Clegg, S. L., and Brimblecombe, P., 1990c. "Solubility of volatile electrolytes in multicomponent solutions with atmospheric applications." Editors: Melchior, D. C., and Bassett, R. L. *Chemical Modeling of Aqueous Systems II*. American Chemical Society Symposium Series 416, 58-73. Washington, D. C.: American Chemical Society. TIC: 241139.

Clegg, S. L.; Rard, J. A.; and Pitzer, K. S. 1994. "Thermodynamic Properties of 0–6 mol kg⁻¹ Aqueous Sulfuric Acid from 273.15 to 328.15 K." *Journal of the Chemical Society, Faraday Transactions*, 90, 1875–1894. Cambridge, United Kingdom: The Royal Society of Chemistry. TIC: 248984

Clegg, S. L., Milioto, S. and Palmer, D. A., 1996, "Osmotic and Activity Coefficients of Aqueous (NH₄)₂SO₄ as a Function of Temperature, and (NH₄)₂SO₄-H₂SO₄ Mixtures at 298.15 K and 323.15 K", *Journal of Chemical and Engineering Data*, 41, 455-467, Columbus, Ohio: American Chemical Society. TIC: 253389

De Lima, M.C.P. and Pitzer, K.S., 1983. "Thermodynamics of Saturated Electrolyte Mixtures of NaCl with Na₂SO₄ and with MgCl₂." *Journal of Solution Chemistry*, 12(3), pp 187-199. New York, New York: Kluwer Academic/Plenum Publishers. TIC: 2538754

Felmy, A.R., Schroeder, C.C., Mason, M.J., 1994a, *A solubility model for amorphous silica in concentrated electrolytes*. PNL-SA-25345 (Conf-940813-33), Pacific Northwest National Laboratory, Richland, Washington. TIC: 253270.

Felmy, A.R., Rustad, J.R., Mason, M.J., and de la Bretonne, R., 1994b. *A chemical model for the major electrolyte components of the Hanford waste tanks: the binary electrolytes in the systems: Na-NO₃-NO₂-SO₄-CO₃-F-PO₄-OH-Al(OH)₄-H₂O*. PNNL Technical Report TWRS-PP-94-090, Pacific Northwest National Laboratory, Richland, Washington. TIC: 253271.

Garrels, R.M., and Christ, C.L., 1965. *Solutions, Minerals, and Equilibria*. Freeman, Cooper, and Company, San Francisco, California, 450 p. TIC: 223483

Greenberg, J. P.; and Møller, N. 1989. "The Prediction of Mineral Solubilities in Natural Waters: A Chemical Equilibrium Model for the Na-K-Ca-Cl-SO₄-H₂O System to High Concentration from 0 to 250 °C." *Geochimica et Cosmochimica Acta*, 53, 2503–2518. New York, New York: Elsevier Science. TIC: 249020

Grønvold, F. and Meisingset, K.K., 1983. "Thermodynamic properties and phase transitions of salt hydrates between 270 and 400 K II. Na₂CO₃·H₂O and Na₂CO₃·10H₂O." *Journal of Chemical Thermodynamics*, 15, p. 881-889. Cambridge, United Kingdom: Elsevier Science. TIC: 253936.

He, S.; and Morse, J. W. 1993. "The Carbonic Acid System and Calcite Solubility in Aqueous Na-K-Ca-Mg-Cl-SO₄ Solutions From 0 to 90°C." *Geochimica et Cosmochimica Acta*, 57, 3533–3554. New York, New York: Elsevier Science. TIC: 253894

Helgeson, H.C.; Kirkham, D.H.; and Flowers, G.C. 1981. "Theoretical Prediction of the Thermodynamic Behavior of Aqueous Electrolytes at High Pressures and Temperatures: IV. Calculation of Activity Coefficients, Osmotic Coefficients, and Apparent Molal and Standard and Relative Partial Molal Properties to 600°C and 5 kb." *American Journal of Science*, 281(10), 1249-1516. New Haven, Connecticut: Yale University, Kline Geology Laboratory. TIC: 238264.

Harvie, C.E.; Moller, N.; and Weare, J.H. 1984. "The Prediction of Mineral Solubilities in Natural Waters: The Na-K-Mg-Ca-H-Cl-SO₄-OH-HCO₃-CO₃-CO₂-H₂O System to High Ionic Strengths at 25°C." *Geochimica et Cosmochimica Acta*, 48(4), 723-751. New York, New York: Pergamon Press. TIC: 239849.

Holmes, H. F.; Baes Jr., C. F.; and Mesmer, R. E. 1979. "Isopiestic Studies of Aqueous Solutions at Elevated Temperatures. II. NaCl + KCl Mixtures." *Journal of Chemical Thermodynamics*, 11, 1035–1050. Cambridge, United Kingdom: Elsevier Science. TIC: 253876

Holmes, H. F.; Baes Jr., C. F.; and Mesmer, R. E. 1981. "Isopiestic Studies of Aqueous Solutions at Elevated Temperatures. III. {(1 - y)NaCl + yCaCl₂}." *Journal of Chemical Thermodynamics*, 13, 101–113. Cambridge, United Kingdom: Elsevier Science. TIC: 253877

Holmes, H. F.; and Mesmer, R. E. 1983. "Thermodynamic Properties of Aqueous Solutions of the Alkali Metal Chlorides to 250 °C." *Journal of Physical Chemistry*, 87, 1242–1255. Columbus, Ohio: American Chemical Society. TIC: 253375

Holmes, H. F.; and Mesmer, R. E. 1986. "Thermodynamic of Aqueous Solutions of the Alkali Metal Sulfates." *Journal of Solution Chemistry*, 15, 495–518. New York, New York: Kluwer Academic/Plenum Publishers. TIC: 253633

Holmes, H. F.; Busey., R. H.; Simonson, J. M.; and Mesmer, R. E. 1987. "The Enthalpy of Dilution of HCl(aq) to 648 K and 40 MPa." *Journal of Chemical Thermodynamics*, 19, 863–890. Cambridge, United Kingdom: Elsevier Science. TIC: 253390

Holmes, H. F.; and Mesmer, R. E. 1992. "Isopiestic Studies of H₂SO₄(aq) at Elevated Temperatures. Thermodynamic Properties." *Journal of Chemical Thermodynamics*, 24, 317–328. Cambridge, United Kingdom: Elsevier Science. TIC: 253881

Holmes, H. F.; and Mesmer, R. E. 1993. "Isopiestic Studies of NaHSO₄(aq) at Elevated Temperatures. Thermodynamic Properties." *Journal of Chemical Thermodynamics*, 25, 99–110. Cambridge, United Kingdom: Elsevier Science. TIC: 253937

Holmes, H. F.; and Mesmer, R. E. 1994. "An Isopiestic Study of $\{(1 - y)\text{NaHSO}_4 + y\text{Na}_2\text{SO}_4\}$ (aq) at Elevated Temperatures." *Journal of Chemical Thermodynamics*, 26, 581–594. Cambridge, United Kingdom: Elsevier Science. TIC: 253880

Holmes, H.F, J.M. Simonson, and R.E Mesmer, 1997. "Aqueous solutions of the alkaline earth metal chlorides. Corrected constants for the ion-interaction model." *Journal of Chemical Thermodynamics*, 29(2), pp. 1363-1373. Cambridge, United Kingdom: Elsevier Science. TIC: 253938

Holmes, H. F.; and Mesmer, R. E. 1998a. "Isopiestic Molalities for Aqueous Solutions of the Alkali Metal Hydroxides at Elevated Temperatures." *Journal of Chemical Thermodynamics*, 30, 311–326. Cambridge, United Kingdom: Elsevier Science. TIC: 253939

Holmes, H. F.; and Mesmer, R. E. 1998b. "An Isopiestic Study of Aqueous Solutions of the Alkali Metal Bromides at Elevated Temperatures." *Journal of Chemical Thermodynamics*, 30, 723–741. Cambridge, United Kingdom: Elsevier Science. TIC: 253377

Königsberger, E. 2001. "Prediction of Electrolyte Solubilities from Minimal Thermodynamic Information." *Monatshefte für Chemie*, 132, 1363–1386. Vienna, Austria: Springer. TIC: 253382

Linke, W. F., 1965. *Solubilities: Inorganic and Metal-Organic Compounds*, 4th edition. Vol. 2. American Chemical Society: Washington, DC. TIC: 222176

Marshall, W.L., 1980a. "Amorphous Silica Solubilities-I. Behavior in Aqueous Sodium Nitrate Solutions: 25-300 °C, 0-6 molal." *Geochimica et Cosmochimica Acta*, 44(7), p. 907-913. New York, New York: Elsevier Science. TIC: 250701

Marshall, W.L., 1980b. "Amorphous Silica Solubilities--III. Activity Coefficient Relations and Predictions of Solubility Behavior in Salt Solutions, 0-350 °C." *Geochimica et Cosmochimica Acta*, 44(7), p. 925-931. New York, New York: Elsevier Science. TIC: 250702

Marshall, W.L. and Chen, C.T.A., 1982a. "Amorphous Silica Solubilities--VI. Postulated Sulfate-Silicic Acid Solution Complex." *Geochimica et Cosmochimica Acta*, 46(3), p. 367-370. New York, New York: Elsevier Science. TIC: 250704

Marshall, W.L. and Chen, C.T.A., 1982b. "Amorphous Silica Solubilities V. Predictions of Solubility Behavior in Aqueous Mixed Electrolyte Solutions to 300 °C." *Geochimica et Cosmochimica Acta*, 46(2), p. 289-291. New York, New York: Elsevier Science. TIC: 250703

Marshall, W.L. and Warakomski, J.M., 1980. "Amorphous Silica Solubilities-II. Effect of Aqueous Salt Solutions at 25°C." *Geochimica et Cosmochimica Acta*, 44(7), p. 915-924. New York, New York: Elsevier Science. TIC: 250705

Meisingset, K.K. and Grønvold, F., 1986, "Thermodynamic properties and phase transitions of salt hydrates between 270 and 400 K IV. CaCl₂:6H₂O, CaCl₂:4H₂O, CaCl₂:6H₂O, and FeCl₃:6H₂O." *Journal of Chemical Thermodynamics*, 18, p. 159-173. TIC: 253388.

Millero, F. J. and Pierrot, D. 1998. "A Chemical Equilibrium Model for Natural Waters." *Aquatic Geochemistry*, 4, 153-199. Amsterdam, Netherlands: Kluwer Academic Publishers. TIC: 254365

Møller, N. 1988. "The Prediction of Mineral Solubilities in Natural Waters: A Chemical Equilibrium Model for the Na- Ca-Cl-SO₄-H₂O System, to High Temperature and Concentration." *Geochimica et Cosmochimica Acta*, 52, 821-837. New York, New York: Elsevier Science. TIC: 248981

Monnin, C. 1999. "A thermodynamic model for the solubility of barite and celestite in electrolyte solutions and seawater to 200 degrees Celsius and to 1 kbar." *Chemical Geology*, 153, 87-209. Amsterdam, Netherlands: Elsevier Science. TIC: 254364

Nordstrom, D.K., and Munoz, J.L., 1985. *Geochemical Thermodynamics*. The Benjamin/Cummings Publishing Co., Inc., Menlo Park, California. TIC: 162115

Oakes, C.S.; Felmy, A.R.; and Sterner, S.M. 2000. "Thermodynamic Properties of Aqueous Calcium Nitrate {Ca(NO₃)₂} to the Temperature 373 K Including New Enthalpy of Dilution Data." *Journal of Chemical Thermodynamics*, 32, (1), 29-54. New York, New York: Academic Press. TIC: 253509.

Pabalan, R.T., and Pitzer, K.S., 1987a. "Thermodynamics of NaOH(aq) in hydrothermal solutions." *Geochimica et Cosmochimica Acta*, 51, p. 829-837. New York, New York: Elsevier Science. TIC: 253383.

Pabalan, R.T., and Pitzer, K.S., 1987b. "Thermodynamics of concentrated electrolyte mixtures and the prediction of mineral solubilities to high temperatures for mixtures in the system Na-K-Mg-Cl-SO₄-OH-H₂O." *Geochimica et Cosmochimica Acta*, 51, p. 2429-2443. New York, New York: Elsevier Science. TIC: 253508.

Peiper, J.C. and Pitzer, K.S., 1982. "Thermodynamics of aqueous carbonate solutions including mixtures of sodium carbonate, bicarbonate, and chloride." *Journal of Chemical Thermodynamics*, 14, pp 613-638, 1982. Cambridge, United Kingdom: Elsevier Science. TIC: 240175.

Phutela, R. C.; and Pitzer, K. S. 1986. "Heat Capacity and Other Thermodynamic Properties of Aqueous Magnesium Sulfate to 473 K." *Journal of Physical Chemistry*, 90, 895–901. Columbus, Ohio: American Chemical Society. TIC: 253940.

Pitzer, K. S. 1973. "Thermodynamics of Electrolytes. I. Theoretical Basis and General Equations." *Journal of Physical Chemistry*, 77, 268–277. Columbus, Ohio: American Chemical Society. TIC: 239503.

Pitzer, K. S.; and Mayorga, G. 1973. "Thermodynamics of Electrolytes. II: Activity and Osmotic Coefficients for Strong Electrolytes with One or Both Ions Univalent." *Journal of Physical Chemistry*, 77, 2300–2308. Columbus, Ohio: American Chemical Society. TIC: 249019.

Pitzer, K.S. and Kim, J.J., 1974. "Thermodynamics of Electrolytes. IV. Activity and Osmotic Coefficients for Mixed Electrolytes." *Journal of the American Chemical Society*, 96 (18), 5701-5707. Columbus, Ohio: American Chemical Society. TIC: 246223.

Pitzer, K.S., Peiper, J.C., and Busey, R.H., 1984, "Thermodynamic properties of aqueous sodium chloride solutions." *Journal of Physical and Chemical Reference Data*, 13, p. 1-102. TIC: 253809.

Pitzer, K. S. 1991. "Ion Interaction Approach: Theory and Data Correlation." Pages 75–153 of *Activity Coefficients in Electrolyte Solutions*. 2nd Edition. Pitzer, K. S., ed. Boca Raton, Florida: CRC Press. TIC: 251799.

Pitzer, K.S. and Shi, Y., 1993. "Thermodynamics of calcium chloride in highly concentrated aqueous solutions and in hydrated crystals", *Journal of Solution Chemistry*, 29, 1–49. New York, New York: Kluwer Academic/Plenum Publishers. TIC: 253385.

Pitzer, K.S. and Oakes, C.S., 1994. "Thermodynamics of calcium chloride in concentrated solutions and in crystal", *Journal of Chemical and Engineering Data*, 39, 553–559. Columbus, Ohio: American Chemical Society. TIC: 253384.

Pokrovskii, V.A. and Helgeson, H.C. 1995. "Thermodynamic Properties of Aqueous Species and the Solubilities of Minerals at High Pressures and Temperatures: The System Al₂O₃-H₂O-NaCl." *American Journal of Science*, 295, 1255-1342. New Haven, Connecticut: Yale University, Kline Geology Laboratory. TIC: 236803.

Polya, D. A.; Woolley, E. M.; Simonson, J. M.; and Mesmer, R. E. 2001. "The Enthalpy of Dilution and Thermodynamics of $\text{Na}_2\text{CO}_3(\text{aq})$ and $\text{NaHCO}_3(\text{aq})$ from $T = 298 \text{ K}$ to $T = 523.15 \text{ K}$ and Pressure of 40 MPa ." *Journal of Chemical Thermodynamics*, 33, 205–243. Cambridge, United Kingdom: Elsevier Science. TIC: 253386.

Oakes, C. S.; Felmy, A. R. and Sterner, S. M. 2000. "Thermodynamic Properties of Aqueous Calcium Nitrate $\{\text{Ca}(\text{NO}_3)_2\}$ to the Temperature 373 K Including New Enthalpy of Dilution Data." *Journal of Chemical Thermodynamics*, 32, 29–54. Cambridge, United Kingdom: Elsevier Science. TIC: 253509

Rard, J. A. and Archer, D. G. 1995. "Isopiestic Investigation of the Osmotic and Activity Coefficients of Aqueous NaBr and the Solubility of $\text{NaBr}\cdot 2\text{H}_2\text{O}(\text{cr})$ at 298.15 K : Thermodynamic Properties of the $\text{NaBr} + \text{H}_2\text{O}$ System Over Wide Ranges of Temperature and Pressure." *Journal of Chemical and Engineering Data*, 40, 170–185. Columbus, Ohio: American Chemical Society. TIC: 253941.

Rard J. A. and Clegg S. L. 1997. "Critical Evaluation of the Thermodynamic Properties of Aqueous Calcium Chloride. 1. Osmotic and Activity Coefficients of $0\text{--}10.77 \text{ mol}\cdot\text{kg}^{-1}$ Aqueous Calcium Chloride Solutions at 298.15 K and Correlation with Extended Pitzer Ion-Interaction Models." *Journal of Chemical and Engineering Data*, 42, 819–849. Columbus, Ohio: American Chemical Society. TIC: 249002.

Rard J. A., Clegg S. L. and Palmer, D. A. 2000. "Isopiestic Determination of the Osmotic Coefficients of $\text{Na}_2\text{SO}_4(\text{aq})$ at 25 and 50°C , and Representation with Ion-interaction (Pitzer) and Mole Fraction Thermodynamic Models." *Journal of Solution Chemistry*, 29, 1–49. New York, New York: Kluwer Academic/Plenum Publishers. TIC: 253942.

Rard J. A. and Wijesinghe, A. M. 2003. "Conversion of Parameters Between Different Variants of Pitzer's Ion-Interaction Model, Both With and Without Ionic Strength Dependent Higher-Order Terms." *Journal of Chemical Thermodynamics*, 35, 439–473. Cambridge, United Kingdom: Elsevier Science. TIC: 253386.

Robie, R.A. and Hemingway, B.S. 1995. "Thermodynamic Properties of Minerals and Related Substances at 298.15 K and 1 Bar (10^5 Pascals) Pressure and at Higher Temperatures." *U.S. Geological Survey Bulletin 2131*, Reston, Virginia. TIC: 249441.

Robinson, R. A.; Stokes, R. H. 1965. "Electrolyte Solutions," 2nd ed. (Revised); London, England: Butterworths. TIC: 242575.

Rogers, P.S.Z., and Pitzer, K.S., 1981. "High temperature thermodynamic properties of sodium sulfate solutions." *Journal of Physical Chemistry*, 85, p. 2886-2895. Columbus, Ohio: American Chemical Society. TIC: 253810.

SNL (Sandia National Laboratories) 2003. *Software User's Manual, EQ3/6 Version 8.0*. SDN: 10813-UM-8.0-00. Albuquerque, New Mexico: Sandia National Laboratories. ACC: MOL.20030312.0084.

Spencer, R.J., Møller, N., and Weare, J.H., 1990. "The prediction of mineral solubilities in natural waters: A chemical equilibrium model for the Na-K-Ca-Mg-Cl-SO₄-H₂O system at temperatures below 25°C." *Geochimica et Cosmochimica Acta*, 54, 575–590. New York, New York: Elsevier Science. TIC: 248999.

Sterner, S.M., Felmy, A.R., Oakes, C.S., and K.S. Pitzer, 1998. "Correlation of Thermodynamic Data for Aqueous Electrolyte Solutions to Very High Ionic Strength Using INSIGHT: Vapor Saturated Water Activity in the System CaCl₂-H₂O to 250 °C and Solid Saturation." *International Journal of Thermophysics*, 19(3), 761–770. TIC: 253387.

Thiessen, W.E. and Simonson, J.M., 1990. "Enthalpy of Dilution and the Thermodynamics of NH₄Cl(aq) to 523 K and 35 Mpa." *Journal of Physical Chemistry*, 94, 7794-7800, Columbus, Ohio: American Chemical Society. TIC: 253883.

Wang, P., and Pitzer, K.S., and Simonson, J.M., 1998. "Thermodynamic properties of aqueous magnesium chloride solutions from 250 to 600 K and to 100MPa." *Journal of Physical and Chemical Reference Data*, 27(5), pp. 1363-1373. College Park, Maryland: American Institute of Physics. TIC: 249693.

Wesolowski, D.J., 1992. "Aluminum speciation and equilibria in aqueous solutions: I. The solubility of gibbsite in the system Na-K-Cl-OH-Al(OH)₄ from 0 to 100°C" *Geochimica et Cosmochimica Acta*, 56, p. 1065-1091. New York, New York: Elsevier Science. TIC: 253946.

ATTACHMENT II
MINTEQA2 MINERAL OCCURRENCE DATABASE

ATTACHMENT II

Table II can be used as a first order approximation for whether a mineral can precipitate under ambient temperatures and pressures. Minor changes have been made to some mineral names to match those in the current EQ3/6 databases. Minerals marked with an asterisk (*) are not included in either the data0.ymp.R2 or Pitzer databases.

Table II. A Modified Listing of Mineral Occurrences from the MINTEQA2 Online Handbook (Wadley and Buckley 1997 [162329])

Mineral	Chemical Formula	Precipitates from 0-100°C and at 1 ATM	Comments on Occurrence or Formation	Source
Alum-K	$KAl(SO_4)_2 \cdot 12H_2O$	yes	When hot solutions of equimolecular quantities of aluminium sulphate + K-sulphate are mixed, and the solution cooled, octahedral crystals of a double sulphate of aluminium and potassium separate	5
Alunite	$KAl_3(OH)_6(SO_4)_2$	no	Small, imperfect, rare crystals, found in altered or mineralized organic rocks. Crystallized by heating a solution of alum and aluminium sulphate in a sealed tube at 230°C.	7
Anhydrite	$CaSO_4$	yes	Ppt under conditions of very high supersaturation (high Ca^{2+}/SO_4^{2-}). It forms at temperatures > 40°C	1, 8
Albite Low	$NaAlSi_3O_8$	yes	Occurs in igneous, sedimentary and metamorphic rocks. Can be formed by heating gelatinous silica, alumina, and caustic soda in a sealed tube.	3, 6
Analbite*	$NaAlSi_3O_8$	no	It is disordered albite.	6
Akermanite	$Ca_2MgSi_2O_7$	no	It melts congruently at 1454 and forms a solid solution series with a minimum melting temperature of 1385. Crystallization proceeds from akermanite-rich compositions.	4
Analcime	$NaAlSi_2O_6 \cdot H_2O$	no	It may occur as a primary mineral in some alkaline basic igneous rocks. It occurs as a late-stage hydrothermal mineral, crystalline in vesicles and occurs with zeolites, thomsonites, and stillbite.	5
Annite	$KFe_3Al_3Si_3O_{10}(OH)_2$	no	Part of the biotite series. It forms from chlorite in metamorphosed pelitic rocks. It is the primary mineral in acid intermediate plutonic igneous rocks and some basic plutonic rocks.	1

Mineral	Chemical Formula	Precipitates from 0-100°C and at 1 ATM	Comments on Occurrence or Formation	Source
Barite	BaSO ₄	yes	Frequently found associated with fluorite, calcite, dolomite, and quartz. Produced by slow inter-diffusion of dilute solutions of barium chloride and sulphates.	7
Bianchite*	(Zn,Fe)SO ₄ ·6H ₂ O	no	(no comments presented)	5
Boehmite	AlO(OH)	no	Widely distributed in bauxite. Produced as an intermediate product in the dehydration of gibbsite and by heating precipitated hydrous aluminium oxide or gibbsite under pressure.	7
Brucite	Mg(OH) ₂	yes	Found associated with minerals such as calcite, aragonite, hydromagnesite, and artinite. Precipitates with alkalis from solutions of magnesium salts or by hydration of magnesium oxide and reaction of water with magnesium amalgams.	5, 7, 8
Chalcedony	SiO ₂	no	Chalcedony includes a number of substances, e.g., Carnelian, sard, prase, bloodstone, agate, flint, jasper.	5
Chrysotile	Mg ₃ Si ₂ O ₅ (OH) ₄	no	It is a fibrous serpentine. It is an important variety of commercial asbestos.	5
Enstatite	MgSiO ₃	no	It is part of the pyroxene group and is found in some meteorites.	6
Cristobalite	SiO ₂	no	2 varieties viz. alpha and beta. These are SiO ₂ polymorphs and alpha cristobalite - can exist at atmospheric temperatures up to 200-275°C. Beta variety exists above 200-275°C, stable from 1470°C to its melting point 1713°C.	4
Corundum	Al ₂ O ₃	yes	How: Prepared in a crystalline condition by strongly heating a mixture of aluminium fluoride and boric acid	6
Diopside	CaMgSi ₂ O ₆	no	Diopside occurs in many metamorphic rocks especially metamorphosed dolomitic limestones and calcareous sedimentary rocks.	5
Dolomite	CaMg(CO ₃) ₂	yes	Precipitated from a solution of MgCl ₂ , CaCl ₂ and area at highly elevated pressure (higher than 2/3 atm.) at 228°C.	
Diaspore	α-AlO(OH)	no	It results from the alteration of corundum and emery. It is a basic constituent of bauxite deposits.	5
Epsomite	MgSO ₄ ·7H ₂ O	yes	MgSO ₄ occurs as kieserite, MgSO ₄ :H ₂ O. When it is digested with water and the solution, purified by re-crystallization, colorless, rhombic, prisms separate from the cold solution.	6

Mineral	Chemical Formula	Precipitates from 0-100°C and at 1 ATM	Comments on Occurrence or Formation	Source
FCO ₃ apatite*	[Ca _{9.496} Na _{0.36} Mg _{0.144} (PO ₄) _{4.8} (CO ₃) _{1.2} F _{2.48}]	no	(no comments presented)	(none)
Fluorite	CaF ₂	yes	Most fluorite is 99% CaF ₂ , with small amounts of Si, Al, and Mg due to impurities and inclusions. It can be prepared by the evaporation of a solution of CaF ₂ in HCl.	4
Forsterite	Mg ₂ SiO ₄	no	It is part of the olivene group. Occurs in crystalline limestones or ultramatic igneous rocks.	5
Gehlenite	Ca ₂ Al ₂ SiO ₇	no	It occurs in basic lava flows that are silica undersaturated.	5
Gibbsite	Al(OH) ₃	yes	It is obtained as a colloidal precipitate when ammonia or an alkaline carbonate is added to a solution of an aluminium salt	5
Goslarite (ZnSO ₄ •7H ₂ O)	ZnSO ₄ •7H ₂ O	yes	By acting upon zinc or zinc oxide with dilute sulphuric acid. The concentrated solution deposits transparent crystals of the composition ZnSO ₄ •7H ₂ O.	(none)
Gypsum	CaSO ₄ •2H ₂ O	yes	Prepared by mixing solutions of sulphates with solutions of calcium salts. Some forms by hydration of anhydrite.	5
Halite	NaCl	yes	Formed by evaporation of a highly saturated saline solution.	6
Halloysite*	Al ₄ (Si ₄ O ₁₀)(OH) ₈ •8H ₂ O	no	Similar to kaolinite, but contains interlayered water molecules.	5
Hematite	Fe ₂ O ₃	yes	Prepared by decomposing ferric chloride by steam at high temperature.	3
Hercynite*	FeAl ₂ O ₄	no	It is an iron aluminium oxide of the spinel group.	5
Huntite	Ca Mg ₃ (CO ₃) ₄	no	It occurs as an alteration of dolomite or magnesite-bearing rocks.	4
Hydroxylapatite	Ca ₅ (OH)(PO ₄) ₃	yes	Prepared by precipitation from solutions of calcium salts with the addition of ammoniacal phosphate solutions.	4
Kaolinite	Al ₂ Si ₂ O ₅ (OH) ₄	no	It forms on alteration of feldspars in granites. The alteration can be caused by weathering or by pneumatolytic action of gases on feldspars.	5
Larnite	Ca ₂ SiO ₄	no	It occurs at dolerite - limestone contacts.	5
Lime	CaO	yes	Obtained by igniting calcium carbonate or calcium oxalate at about 800	5
Leonhardite*	Ca(Al ₂ Si ₄ O ₁₂)•3H ₂ O	no	Forms when laumontite (hydrated calcium alumino-silicate) loses its water.	4

Mineral	Chemical Formula	Precipitates from 0-100°C and at 1 ATM	Comments on Occurrence or Formation	Source
Leucite*	KAlSi_2O_6	no	Occurs in K-rich basic extrusive lavas that may be silica deficient.	5
Laumonite*	$\text{Ca}(\text{Al}_2\text{Si}_4\text{O}_{12}) \bullet 4\text{H}_2\text{O}$	no	Occurs in cavities in igneous rocks, from basalts to granites. It originates from mild metamorphic alteration of volcanic glass and feldspars.	4
Merwinite	$\text{MgCa}_3(\text{SiO}_4)_2$	no	Occurs at gabbro - limestone contacts.	5
Muscovite	$\text{KAl}_3\text{Si}_3\text{O}_{10}(\text{OH})_2$	no	Common in the mica group. Found in regionally metamorphosed sediments. It can crystallize from a liquid of granite composition at pressures > 1500 atmospheres.	6
Mirabilite	$\text{Na}_2\text{SO}_4 \bullet 10\text{H}_2\text{O}$	no	Mirabilite or glaubersalt occurs in the residues of alkali lakes.	4
Melanterite	$\text{FeSO}_4 \bullet 7\text{H}_2\text{O}$	no	Results from the decomposition of pyrite in the zone of oxidation.	4
Manganous chloride ($\text{MnCl}_2 \bullet 4\text{H}_2\text{O}$)	$\text{MnCl}_2 \bullet 4\text{H}_2\text{O}$	yes	Manganous chloride is prepared by dissolving the oxide or carbonate in hydrochloric acid and evaporating the solution, the heating being continued long enough to drive off all the free chlorine.	7
Monticellite	CaMgSiO_4	no	It occurs in metamorphic and metsomatized siliceous dolomitic limestones at contacts with both basic and acid igneous rocks.	(none)
Maximum_ Microcline	KAlSi_3O_8	no	It is a constituent of alkali acid igneous rocks. It is abundant in granites and syenites and is cooled slowly at depth.	4
Nepheline	NaAlSiO_4	no	Nepheline is a characteristic primary crystallizing mineral of alkaline igneous rocks.	6
Natron	$\text{Na}_2\text{CO}_3 \bullet 10\text{H}_2\text{O}$	no	It is found in solution in soda-lakes.	1
Periclase	MgO	yes	It is made by heating MgCO_3 or the hydroxide obtained from sea- H_2O .	1
Pyrophyllite	$\text{Al}_2\text{Si}_4\text{O}_{10}(\text{OH})$	no	It occurs as a secondary product from hydrothermal alteration of feldspar. It occurs as foliated masses in crystalline schists.	5
Phlogopite	$\text{KAlMg}_3\text{Si}_3\text{O}_{10}(\text{OH})_2$	no	It occurs in metamorphosed limestones and ultrabasic rocks. It is a product of regional metamorphism of impure magnesium limestones. It is derived from the reaction between dolomite and potassium feldspar.	5

Mineral	Chemical Formula	Precipitates from 0-100°C and at 1 ATM	Comments on Occurrence or Formation	Source
Pyrochroite*	Mn(OH) ₂	no	It is a hydrothermal mineral.	(none)
Quartz	SiO ₂	no	Essential constituent of acid igneous plutonic rocks; e.g., granites. Also present in extrusive and hypabyssal rocks. Also found in conglomerates, arenities, siltstones and mudstones	1
Rhodochrosite	MnCO ₃	yes	Made by adding sodium carbonate solution to a solution of manganous salt.	(none)
Siderite	FeCO ₃	yes	By heating (NH ₄) ₂ CO ₃ with FeCl ₂	4
Sepiolite	Mg ₄ Si ₆ O ₁₅ (OH) ₂ •6H ₂ O	no	Found in beds of irregular masses in alluvial deposits derived from serpentine masses.	1, 6
Sanidine_high	KAlSi ₃ O ₈	no	High temperature K-Feldspar, which has been quickly cooled as in extrusive igneous rocks, has a tabular form and is called sanidine.	5
Spinel	MgAl ₂ O ₄	yes	It is a common high temperature mineral in metamorphic rocks and aluminium xenoliths. Occurs in contact metamorphosed limestones. It may be synthesized by fusing MgO and Al ₂ O ₃ with or without a mineralizer such as boric acid or water vapor.	(none)
Talc	Mg ₃ Si ₄ O ₁₀ (OH) ₂	no	It is formed during low-grade metamorphism of siliceous dolomites. Also by hydrothermal alteration of ultrabasic rocks.	1
Thendardite	Na ₂ SO ₄	no	Occurs in playa-lake evaporites as in the alkali lakes.	(none)
Tremolite	Ca ₂ Mg ₅ Si ₈ O ₂₂ (OH) ₂	no	In thermally metamorphosed impure dolomites, tremolite forms early by reaction between dolomite and quartz.	1
Wollastonite	CaSiO ₃	no	It is a product of high-grade thermal metamorphism of impure limestones and is found in some alkaline igneous rocks.	5
Vivianite*	Fe ₃ (PO ₄) ₂ •8H ₂ O	no	It is found with iron, copper and tin ones. It may occur in clay, and especially in bog iron-ore.	5
Wairakite	CaAl ₂ Si ₄ O ₁₂ •2H ₂ O	no	It is found in sandstones and breccias.	5
Wustite	FeO	yes	Ferrous oxide is formed when ferric oxide is heated in hydrogen at 300. It also forms when ferrous oxalate is heated out of contact with the air.	7
Zn(OH) ₂	Zn(OH) ₂	yes	It is precipitated when an equivalent quantity of an alkaline hydroxide is added to solution of a zinc salt.	7

Mineral	Chemical Formula	Precipitates from 0-100°C and at 1 ATM	Comments on Occurrence or Formation	Source
Zincite	ZnO	yes	It is formed by heating zinc in air and passing the fumes into condensing chambers where the powdered oxide collects.	7

Source: 1. Battey (1986 [162334])
 3. Dana and Ford (1922 [161608])
 4. Deer et al. (1966 [162338])
 5. Gribble (1988 [161607])
 6. Frye (1981 [161804])
 7. Palache et al. (1951 [162280])
 8. Parkes (1961 [161609])

NOTE: Minerals marked with an asterisk (*) are not included in the YMP databases.

ATTACHMENT III
EXAMPLE IDPS EVAPORATION LOOKUP TABLE

ATTACHMENT III

Table III is an example IDPS model lookup table for the example evaporation of average in situ J-13 well water. For this example, the rows below RH 56 percent have been truncated. The full lookup table is documented in DTN: MO0304SPA13IS.001, file j13c3t7e.xls.

Table III. Example IDPS Model Evaporation Lookup Table for Average In Situ J-13 Well Water

Calculations				RH Calc.	Temperature and Gas Fugacities				Total Elemental Aqueous Co	
				RH rel. humid.	log Xi log react. progr.	Temp. (C)	O2(g) fug.	CO2(g) fug.	log Xi log react. progr.	pH
					2/24/2003 User: Marinerp EQ3/6, Version 8.0				2/24/2003 User: Marinerp EQ3/6, Version 8.0	
CF=1/DF	Qe/Qs	1-Qe/Qs=DF		RH	log Xi - j13c3t7e.6o	Temp (C) - j13c3t7e.6o	O2(g) Fugacity	CO2(g) Fugacity	log Xi - j13c3t7e.6o	pH - j13c3t7e.6o
1.0	0.0000	1.0000		99.991%	-99999.0000	70.0000	0.1995	0.0010	-99999	8.222
1.0	0.0066	0.9934		99.991%	-0.4347	70.0000	0.1995	0.0010	-0.43469	8.224
1.1	0.0901	0.9099		99.990%	0.6990	70.0000	0.1995	0.0010	0.69897	8.247
1.2	0.1802	0.8198		99.989%	1.0000	70.0000	0.1995	0.0010	1	8.276
1.4	0.2702	0.7298		99.988%	1.1761	70.0000	0.1995	0.0010	1.17609	8.310
1.6	0.3603	0.6397		99.986%	1.3010	70.0000	0.1995	0.0010	1.30103	8.351
1.8	0.4504	0.5496		99.984%	1.3979	70.0000	0.1995	0.0010	1.39794	8.399
2.2	0.5405	0.4595		99.981%	1.4771	70.0000	0.1995	0.0010	1.47712	8.457
2.7	0.6305	0.3695		99.977%	1.5441	70.0000	0.1995	0.0010	1.54407	8.529
3.6	0.7206	0.2794		99.971%	1.6021	70.0000	0.1995	0.0010	1.60206	8.619
5.3	0.8107	0.1893		99.958%	1.6532	70.0000	0.1995	0.0010	1.65321	8.740
8.1	0.8765	0.1235		99.937%	1.6871	70.0000	0.1995	0.0010	1.68713	8.864
8.4	0.8806	0.1194		99.935%	1.6891	70.0000	0.1995	0.0010	1.68912	8.876
10.1	0.9008	0.0992		99.924%	1.6990	70.0000	0.1995	0.0010	1.69897	8.940
12.1	0.9176	0.0824		99.911%	1.7070	70.0000	0.1995	0.0010	1.707	9.002
12.6	0.9209	0.0791		99.908%	1.7086	70.0000	0.1995	0.0010	1.70857	9.015
13.2	0.9241	0.0759		99.905%	1.7101	70.0000	0.1995	0.0010	1.71006	9.029
109.0	0.9908	0.0092		99.384%	1.7404	70.0000	0.1995	0.0010	1.74036	9.551
402.6	0.9975	0.0025		98.001%	1.7433	70.0000	0.1995	0.0010	1.74328	9.724
858.0	0.9988	0.0012		95.999%	1.7439	70.0000	0.1995	0.0010	1.74386	9.772
1207.3	0.9992	0.0008		94.449%	1.7440	70.0000	0.1995	0.0010	1.74401	9.779
1307.1	0.9992	0.0008		94.001%	1.7440	70.0000	0.1995	0.0010	1.74403	9.781
1735.1	0.9994	0.0006		92.000%	1.7441	70.0000	0.1995	0.0010	1.74412	9.782
2134.5	0.9995	0.0005		90.000%	1.7442	70.0000	0.1995	0.0010	1.74416	9.781
2508.8	0.9996	0.0004		88.000%	1.7442	70.0000	0.1995	0.0010	1.74419	9.779
2862.4	0.9997	0.0003		86.000%	1.7442	70.0000	0.1995	0.0010	1.74421	9.777
3198.9	0.9997	0.0003		84.000%	1.7442	70.0000	0.1995	0.0010	1.74423	9.777
3521.4	0.9997	0.0003		82.000%	1.7442	70.0000	0.1995	0.0010	1.74424	9.777
3731.7	0.9997	0.0003		80.660%	1.7443	70.0000	0.1995	0.0010	1.74425	9.778
3731.8	0.9997	0.0003		80.660%	1.7443	70.0000	0.1995	0.0010	1.74425	9.778
4321.4	0.9998	0.0002		80.000%	1.7443	70.0000	0.1995	0.0010	1.74427	9.757
5228.4	0.9998	0.0002		78.968%	1.7443	70.0000	0.1995	0.0010	1.74428	9.725
5228.5	0.9998	0.0002		78.968%	1.7443	70.0000	0.1995	0.0010	1.74428	9.725
5628.4	0.9998	0.0002		78.676%	1.7443	70.0000	0.1995	0.0010	1.74429	9.719
6555.3	0.9998	0.0002		78.000%	1.7443	70.0000	0.1995	0.0010	1.7443	9.704
9289.0	0.9999	0.0001		76.000%	1.7443	70.0000	0.1995	0.0010	1.74432	9.660
12000.4	0.9999	0.0001		74.001%	1.7443	70.0000	0.1995	0.0010	1.74433	9.615
14682.1	0.9999	0.0001		72.000%	1.7443	70.0000	0.1995	0.0010	1.74434	9.568
17325.7	0.9999	0.0001		70.000%	1.7443	70.0000	0.1995	0.0010	1.74434	9.521
19932.5	0.9999	0.0001		68.000%	1.7443	70.0000	0.1995	0.0010	1.74434	9.473
22499.7	1.0000	0.0000		66.000%	1.7444	70.0000	0.1995	0.0010	1.74435	9.425
22746.8	1.0000	0.0000		65.813%	1.7444	70.0000	0.1995	0.0010	1.74435	9.421
25461.5	1.0000	0.0000		65.336%	1.7444	70.0000	0.1995	0.0010	1.74435	9.415
34019.8	1.0000	0.0000		64.000%	1.7444	70.0000	0.1995	0.0010	1.74435	9.396
48219.0	1.0000	0.0000		61.999%	1.7444	70.0000	0.1995	0.0010	1.74436	9.362
61040.9	1.0000	0.0000		60.000%	1.7444	70.0000	0.1995	0.0010	1.74436	9.332
71518.2	1.0000	0.0000		58.000%	1.7444	70.0000	0.1995	0.0010	1.74436	9.309
80564.9	1.0000	0.0000		56.000%	1.7444	70.0000	0.1995	0.0010	1.74436	9.293

Table III. Example IDPS Model Evaporation Lookup Table for Average In Situ J-13 Well Water
(Continued)

Composition											
RH	IS	H2O (kg)	Al	C	Ca	Cl	F	K	Mg	N	
rel. humid.	ionic strength (m)		aluminum	carbon	calcium	chlorine	fluorine	potassium	magnesium	nitrogen	
a(w) -	(l) -	Mass Solvent	Al	C	Ca	Cl	F	K	Mg	N	
j13c3t7e.6o	j13c3t7e.6o	(kg) -	Moles/kg.								
		j13c3t7e.6o	H2O								
1.000	2.644E-03	1.000E+00	1.096E-09	1.368E-03	1.070E-04	2.014E-04	1.147E-04	1.289E-04	7.979E-06	1.416E-04	
1.000	2.657E-03	9.934E-01	1.078E-09	1.374E-03	1.063E-04	2.027E-04	1.155E-04	1.298E-04	7.854E-06	1.425E-04	
1.000	2.842E-03	9.099E-01	8.676E-10	1.452E-03	9.725E-05	2.213E-04	1.261E-04	1.417E-04	6.360E-06	1.556E-04	
1.000	3.091E-03	8.199E-01	6.721E-10	1.558E-03	8.705E-05	2.456E-04	1.400E-04	1.572E-04	4.922E-06	1.727E-04	
1.000	3.409E-03	7.298E-01	5.079E-10	1.691E-03	7.657E-05	2.760E-04	1.572E-04	1.766E-04	3.676E-06	1.940E-04	
1.000	3.829E-03	6.397E-01	3.723E-10	1.866E-03	6.599E-05	3.148E-04	1.794E-04	2.015E-04	2.632E-06	2.214E-04	
1.000	4.399E-03	5.496E-01	2.627E-10	2.098E-03	5.554E-05	3.664E-04	2.088E-04	2.345E-04	1.788E-06	2.576E-04	
1.000	5.210E-03	4.596E-01	1.761E-10	2.421E-03	4.548E-05	4.382E-04	2.497E-04	2.805E-04	1.137E-06	3.081E-04	
1.000	6.438E-03	3.695E-01	1.100E-10	2.891E-03	3.607E-05	5.451E-04	3.106E-04	3.489E-04	6.627E-07	3.833E-04	
1.000	8.489E-03	2.794E-01	6.153E-11	3.635E-03	2.757E-05	7.208E-04	4.107E-04	4.614E-04	3.419E-07	5.068E-04	
1.000	1.254E-02	1.893E-01	2.843E-11	4.983E-03	2.020E-05	1.064E-03	6.061E-04	6.809E-04	1.458E-07	7.480E-04	
0.999	1.933E-02	1.235E-01	1.273E-11	6.990E-03	1.562E-05	1.631E-03	9.294E-04	1.044E-03	6.337E-08	1.147E-03	
0.999	2.000E-02	1.194E-01	1.311E-11	7.218E-03	1.528E-05	1.686E-03	9.608E-04	1.079E-03	6.134E-08	1.186E-03	
0.999	2.419E-02	9.924E-02	1.539E-11	8.626E-03	1.366E-05	2.029E-03	1.156E-03	1.299E-03	5.173E-08	1.427E-03	
0.999	2.929E-02	8.243E-02	1.800E-11	1.031E-02	1.243E-05	2.443E-03	1.392E-03	1.562E-03	4.448E-08	1.718E-03	
0.999	3.056E-02	7.910E-02	1.751E-11	1.071E-02	1.220E-05	2.546E-03	1.451E-03	1.617E-03	4.315E-08	1.790E-03	
0.999	3.187E-02	7.594E-02	1.692E-11	1.114E-02	1.199E-05	2.652E-03	1.511E-03	1.684E-03	4.188E-08	1.865E-03	
0.994	2.908E-01	9.171E-03	3.253E-12	8.132E-02	8.655E-06	2.196E-02	1.251E-02	1.394E-02	2.239E-08	1.544E-02	
0.980	1.126E+00	2.484E-03	1.280E-12	2.790E-01	9.063E-06	8.109E-02	4.620E-02	5.148E-02	2.598E-08	5.701E-02	
0.960	2.442E+00	1.166E-03	7.376E-13	5.762E-01	1.005E-05	1.728E-01	9.845E-02	1.097E-01	3.313E-08	1.215E-01	
0.944	3.456E+00	8.283E-04	5.595E-13	8.016E-01	1.068E-05	2.432E-01	1.385E-01	1.544E-01	3.743E-08	1.710E-01	
0.940	3.749E+00	7.651E-04	5.226E-13	8.688E-01	1.083E-05	2.632E-01	1.440E-01	1.671E-01	3.836E-08	1.851E-01	
0.920	5.007E+00	5.763E-04	4.013E-13	1.156E+00	1.125E-05	3.494E-01	1.670E-01	2.219E-01	4.108E-08	2.457E-01	
0.900	6.182E+00	4.685E-04	3.219E-13	1.424E+00	1.138E-05	4.299E-01	1.882E-01	2.729E-01	4.199E-08	3.022E-01	
0.880	7.282E+00	3.986E-04	2.655E-13	1.674E+00	1.133E-05	5.053E-01	2.087E-01	3.208E-01	4.181E-08	3.552E-01	
0.860	8.319E+00	3.494E-04	2.233E-13	1.909E+00	1.115E-05	5.765E-01	2.293E-01	3.660E-01	4.104E-08	4.053E-01	
0.840	9.305E+00	3.126E-04	1.904E-13	2.131E+00	1.091E-05	6.442E-01	2.504E-01	4.090E-01	4.002E-08	4.530E-01	
0.820	1.025E+01	2.840E-04	1.642E-13	2.343E+00	1.064E-05	7.092E-01	2.722E-01	4.503E-01	3.895E-08	4.986E-01	
0.807	1.086E+01	2.680E-04	1.494E-13	2.479E+00	1.045E-05	7.515E-01	2.874E-01	4.772E-01	3.827E-08	5.284E-01	
0.807	1.086E+01	2.680E-04	1.494E-13	2.479E+00	1.045E-05	7.516E-01	2.874E-01	4.772E-01	3.827E-08	5.284E-01	
0.800	1.105E+01	2.314E-04	1.301E-13	2.362E+00	1.009E-05	8.703E-01	2.789E-01	5.526E-01	3.576E-08	6.119E-01	
0.790	1.137E+01	1.913E-04	1.088E-13	2.188E+00	9.653E-06	1.053E+00	2.664E-01	6.685E-01	3.294E-08	7.404E-01	
0.790	1.137E+01	1.913E-04	1.088E-13	2.188E+00	9.653E-06	1.053E+00	2.664E-01	6.686E-01	3.294E-08	7.404E-01	
0.787	1.139E+01	1.777E-04	1.014E-13	2.160E+00	9.515E-06	1.134E+00	2.624E-01	7.197E-01	3.240E-08	7.970E-01	
0.780	1.142E+01	1.526E-04	8.759E-14	2.093E+00	9.234E-06	1.320E+00	2.532E-01	8.382E-01	3.134E-08	9.282E-01	
0.760	1.155E+01	1.077E-04	6.276E-14	1.901E+00	8.643E-06	1.871E+00	2.282E-01	1.188E+00	2.941E-08	1.315E+00	
0.740	1.172E+01	8.333E-05	4.912E-14	1.717E+00	8.290E-06	2.417E+00	2.061E-01	1.534E+00	2.878E-08	1.699E+00	
0.720	1.194E+01	6.811E-05	4.041E-14	1.542E+00	8.076E-06	2.957E+00	1.867E-01	1.877E+00	2.898E-08	2.079E+00	
0.700	1.220E+01	5.772E-05	3.432E-14	1.378E+00	7.944E-06	3.489E+00	1.698E-01	2.215E+00	2.976E-08	2.453E+00	
0.680	1.251E+01	5.017E-05	2.975E-14	1.225E+00	7.864E-06	4.014E+00	1.550E-01	2.549E+00	3.096E-08	2.822E+00	
0.660	1.286E+01	4.445E-05	2.618E-14	1.084E+00	7.814E-06	4.531E+00	1.422E-01	2.877E+00	3.251E-08	3.186E+00	
0.658	1.289E+01	4.396E-05	2.588E-14	1.072E+00	7.811E-06	4.578E+00	1.411E-01	2.909E+00	3.267E-08	3.221E+00	
0.653	1.327E+01	3.928E-05	2.390E-14	1.057E+00	7.782E-06	4.508E+00	1.380E-01	3.256E+00	3.291E-08	3.605E+00	
0.640	1.447E+01	2.939E-05	1.944E-14	9.990E-01	7.716E-06	4.290E+00	1.285E-01	4.350E+00	3.372E-08	4.817E+00	
0.620	1.657E+01	2.074E-05	1.466E-14	8.687E-01	7.656E-06	3.939E+00	1.139E-01	6.166E+00	3.525E-08	6.828E+00	
0.600	1.873E+01	1.638E-05	1.140E-14	7.166E-01	7.630E-06	3.636E+00	1.018E-01	7.805E+00	3.716E-08	8.643E+00	
0.580	2.090E+01	1.398E-05	9.097E-15	5.658E-01	7.622E-06	3.405E+00	9.250E-02	9.145E+00	3.943E-08	1.013E+01	
0.560	2.377E+01	1.241E-05	7.356E-15	3.962E-01	7.628E-06	3.250E+00	8.424E-02	1.030E+01	4.221E-08	1.141E+01	

Table III. Example IDPS Model Evaporation Lookup Table for Average In Situ J-13 Well Water
(Continued)

			ANC species concentrations									
Na	S	Si	log Xi	H2O (kg)	HCO3-	CO3--	HSiO3-	CaHCO3+	OH-	MgHCO3+		
sodium	sulfur	silicon	log react. progr.									
			2/24/2003									
			User: Marinerp									
			EQ3/6,									
			Version 8.0									
Na		Si	Mass Solvent									
Moles/kg.	S Moles/kg.	Moles/kg.	log Xi -	(kg) -	HCO3-	CO3--	HSiO3-	CaHCO3+	OH-	MgHCO3+		
H2O	H2O	H2O	j13c3t7e.6o	j13c3t7e.6o	Molality	Molality	Molality	Molality	Molality	Molality		
1.992E-03	1.915E-04	8.995E-04	-1.000E+05	1.000E+00	1.324E-03	2.092E-05	1.001E-04	1.622E-06	2.757E-05	1.280E-07		
2.005E-03	1.928E-04	9.053E-04	-4.347E-01	9.934E-01	1.329E-03	2.110E-05	1.011E-04	1.616E-06	2.768E-05	1.264E-07		
2.189E-03	2.105E-04	9.850E-04	6.990E-01	9.099E-01	1.405E-03	2.367E-05	1.155E-04	1.535E-06	2.926E-05	1.068E-07		
2.430E-03	2.336E-04	1.090E-03	1.000E+00	8.199E-01	1.507E-03	2.735E-05	1.359E-04	1.439E-06	3.136E-05	8.712E-08		
2.730E-03	2.625E-04	1.222E-03	1.176E+00	7.298E-01	1.636E-03	3.243E-05	1.636E-04	1.335E-06	3.404E-05	6.918E-08		
3.114E-03	2.994E-04	1.391E-03	1.301E+00	6.397E-01	1.803E-03	3.969E-05	2.026E-04	1.221E-06	3.750E-05	5.314E-08		
3.625E-03	3.485E-04	1.618E-03	1.398E+00	5.496E-01	2.025E-03	5.055E-05	2.599E-04	1.099E-06	4.210E-05	3.918E-08		
4.335E-03	4.168E-04	1.933E-03	1.477E+00	4.596E-01	2.330E-03	6.780E-05	3.490E-04	9.675E-07	4.843E-05	2.738E-08		
5.392E-03	5.184E-04	2.403E-03	1.544E+00	3.695E-01	2.771E-03	9.753E-05	4.989E-04	8.287E-07	5.755E-05	1.780E-08		
7.130E-03	6.856E-04	3.177E-03	1.602E+00	2.794E-01	3.457E-03	1.555E-04	7.827E-04	6.824E-07	7.172E-05	1.040E-08		
1.052E-02	1.012E-03	4.688E-03	1.653E+00	1.893E-01	4.667E-03	2.946E-04	1.436E-03	5.282E-07	9.660E-05	5.087E-09		
1.614E-02	1.551E-03	7.182E-03	1.687E+00	1.235E-01	6.388E-03	5.802E-04	2.706E-03	4.087E-07	1.318E-04	2.441E-09		
1.668E-02	1.604E-03	7.263E-03	1.689E+00	1.194E-01	6.578E-03	6.177E-04	2.786E-03	3.989E-07	1.357E-04	2.383E-09		
2.007E-02	1.930E-03	7.754E-03	1.699E+00	9.924E-02	7.730E-03	8.736E-04	3.276E-03	3.495E-07	1.591E-04	2.088E-09		
2.417E-02	2.324E-03	8.320E-03	1.707E+00	8.243E-02	9.055E-03	1.229E-03	3.840E-03	3.080E-07	1.860E-04	1.841E-09		
2.519E-02	2.421E-03	8.454E-03	1.709E+00	7.910E-02	9.369E-03	1.323E-03	3.974E-03	2.999E-07	1.923E-04	1.792E-09		
2.623E-02	2.522E-03	8.593E-03	1.710E+00	7.594E-02	9.694E-03	1.425E-03	4.113E-03	2.920E-07	1.989E-04	1.745E-09		
2.172E-01	2.089E-02	2.298E-02	1.740E+00	9.171E-03	4.234E-02	3.896E-02	1.843E-02	1.227E-07	8.008E-04	7.399E-10		
8.021E-01	7.712E-02	4.269E-02	1.743E+00	2.484E-03	8.216E-02	1.969E-01	3.790E-02	1.185E-07	1.320E-03	7.323E-10		
1.709E+00	1.643E-01	6.092E-02	1.744E+00	1.166E-03	1.120E-01	4.642E-01	5.573E-02	1.328E-07	1.487E-03	8.507E-10		
2.405E+00	2.313E-01	7.218E-02	1.744E+00	8.283E-04	1.268E-01	6.748E-01	6.666E-02	1.409E-07	1.478E-03	9.287E-10		
2.604E+00	2.504E-01	7.539E-02	1.744E+00	7.651E-04	1.307E-01	7.381E-01	6.977E-02	1.424E-07	1.469E-03	9.469E-10		
3.457E+00	3.323E-01	8.883E-02	1.744E+00	5.763E-04	1.454E-01	1.011E+00	8.276E-02	1.466E-07	1.399E-03	1.012E-09		
4.252E+00	4.088E-01	1.015E-01	1.744E+00	4.685E-04	1.571E-01	1.267E+00	9.492E-02	1.473E-07	1.313E-03	1.057E-09		
4.998E+00	4.805E-01	1.137E-01	1.744E+00	3.986E-04	1.671E-01	1.507E+00	1.067E-01	1.456E-07	1.226E-03	1.087E-09		
5.702E+00	5.483E-01	1.260E-01	1.744E+00	3.494E-04	1.760E-01	1.733E+00	1.185E-01	1.424E-07	1.143E-03	1.106E-09		
6.373E+00	6.127E-01	1.383E-01	1.744E+00	3.126E-04	1.842E-01	1.947E+00	1.303E-01	1.382E-07	1.066E-03	1.119E-09		
7.015E+00	6.745E-01	1.508E-01	1.744E+00	2.840E-04	1.919E-01	2.151E+00	1.423E-01	1.334E-07	9.955E-04	1.126E-09		
7.432E+00	7.148E-01	1.594E-01	1.744E+00	2.680E-04	1.968E-01	2.282E+00	1.505E-01	1.299E-07	9.514E-04	1.129E-09		
7.432E+00	7.148E-01	1.594E-01	1.744E+00	2.680E-04	1.968E-01	2.282E+00	1.505E-01	1.299E-07	9.514E-04	1.129E-09		
7.548E+00	8.277E-01	1.557E-01	1.744E+00	2.314E-04	1.872E-01	2.175E+00	1.472E-01	1.329E-07	9.312E-04	1.172E-09		
7.739E+00	1.001E+00	1.502E-01	1.744E+00	1.913E-04	1.734E-01	2.015E+00	1.423E-01	1.378E-07	8.986E-04	1.243E-09		
7.739E+00	1.001E+00	1.502E-01	1.744E+00	1.913E-04	1.734E-01	2.015E+00	1.423E-01	1.378E-07	8.986E-04	1.243E-09		
7.739E+00	9.878E-01	1.484E-01	1.744E+00	1.777E-04	1.704E-01	1.989E+00	1.407E-01	1.384E-07	8.873E-04	1.256E-09		
7.742E+00	9.591E-01	1.442E-01	1.744E+00	1.526E-04	1.636E-01	1.930E+00	1.369E-01	1.400E-07	8.613E-04	1.290E-09		
7.773E+00	8.810E-01	1.325E-01	1.744E+00	1.077E-04	1.447E-01	1.756E+00	1.263E-01	1.451E-07	7.851E-04	1.400E-09		
7.836E+00	8.127E-01	1.217E-01	1.744E+00	8.333E-05	1.277E-01	1.589E+00	1.165E-01	1.511E-07	7.109E-04	1.527E-09		
7.931E+00	7.531E-01	1.119E-01	1.744E+00	6.811E-05	1.124E-01	1.429E+00	1.074E-01	1.579E-07	6.397E-04	1.674E-09		
8.057E+00	7.017E-01	1.030E-01	1.744E+00	5.772E-05	9.878E-02	1.279E+00	9.910E-02	1.655E-07	5.724E-04	1.844E-09		
8.214E+00	6.576E-01	9.489E-02	1.744E+00	5.017E-05	8.672E-02	1.138E+00	9.149E-02	1.740E-07	5.093E-04	2.038E-09		
8.400E+00	6.200E-01	8.753E-02	1.744E+00	4.445E-05	7.607E-02	1.008E+00	8.454E-02	1.832E-07	4.508E-04	2.262E-09		
8.418E+00	6.170E-01	8.689E-02	1.744E+00	4.396E-05	7.516E-02	9.964E-01	8.393E-02	1.841E-07	4.455E-04	2.284E-09		
8.428E+00	6.549E-01	8.840E-02	1.744E+00	3.928E-05	7.735E-02	9.795E-01	8.564E-02	1.822E-07	4.119E-04	2.290E-09		
8.467E+00	7.882E-01	9.325E-02	1.744E+00	2.939E-05	8.427E-02	9.147E-01	9.101E-02	1.766E-07	3.204E-04	2.300E-09		
8.606E+00	1.074E+00	1.012E-01	1.744E+00	2.074E-05	9.502E-02	7.737E-01	9.963E-02	1.686E-07	2.069E-04	2.322E-09		
8.908E+00	1.447E+00	1.075E-01	1.744E+00	1.638E-05	1.020E-01	6.147E-01	1.064E-01	1.643E-07	1.339E-04	2.397E-09		
9.435E+00	1.908E+00	1.113E-01	1.744E+00	1.398E-05	1.029E-01	4.629E-01	1.104E-01	1.648E-07	8.904E-05	2.550E-09		
1.056E+01	2.655E+00	1.128E-01	1.744E+00	1.241E-05	9.453E-02	3.017E-01	1.120E-01	1.739E-07	5.710E-05	2.861E-09		

Table III. Example IDPS Model Evaporation Lookup Table for Average In Situ J-13 Well Water
(Continued)

H+ MgOH+ CaOH+ HSO4- Ca++ Mg++						Mineral Precipitation				
						H2O (kg)	Calcite	Celadonite	Fluorite	log react. progr.
						2/24/2003 User: Marinerp EQ3/6, Version 8.0				
						Mass Solvent				
H+	MgOH+	CaOH+	HSO4-	Ca++	Mg++	log Xi -	Calcite	Celadonite	Fluorite	
						j13c3t7e.6o	(kg) -	Moles	Moles	Moles
						j13c3t7e.6o				
6.392E-09	6.462E-08	1.131E-07	3.551E-10	9.591E-05	7.609E-06	-99999	1	0.0002168		
6.368E-09	6.381E-08	1.127E-07	3.559E-10	9.521E-05	7.488E-06	-0.43469	0.99338	0.00021821		
6.049E-09	5.392E-08	1.071E-07	3.665E-10	8.626E-05	6.043E-06	0.69897	0.90993	0.00023536		
5.671E-09	4.398E-08	1.004E-07	3.779E-10	7.624E-05	4.654E-06	1	0.81985	0.00025248		
5.258E-09	3.492E-08	9.308E-08	3.891E-10	6.597E-05	3.455E-06	1.17609	0.72977	0.00026797		
4.810E-09	2.682E-08	8.516E-08	4.002E-10	5.563E-05	2.454E-06	1.30103	0.6397	0.00028163		
4.327E-09	1.977E-08	7.661E-08	4.111E-10	4.546E-05	1.648E-06	1.39794	0.54962	0.00029332		
3.811E-09	1.382E-08	6.748E-08	4.222E-10	3.571E-05	1.032E-06	1.47712	0.45955	0.00030295		
3.263E-09	8.978E-09	5.780E-08	4.343E-10	2.663E-05	5.875E-07	1.54407	0.36947	0.00031052		
2.686E-09	5.242E-09	4.759E-08	4.492E-10	1.849E-05	2.919E-07	1.60206	0.27939	0.00031615		
2.077E-09	2.562E-09	3.684E-08	4.719E-10	1.151E-05	1.164E-07	1.65321	0.18932	0.00032003		
1.605E-09	1.228E-09	2.850E-08	5.018E-10	7.234E-06	4.622E-08	1.68713	0.12346	0.00032192		
1.567E-09	1.198E-09	2.782E-08	5.016E-10	6.919E-06	4.428E-08	1.68912	0.11943	0.00032202		
1.372E-09	1.049E-09	2.438E-08	5.007E-10	5.434E-06	3.512E-08	1.69897	0.099242	0.00032249		
1.208E-09	9.242E-10	2.148E-08	5.008E-10	4.325E-06	2.823E-08	1.707	0.082431	0.00032229	1.5085E-07	
1.176E-09	8.997E-10	2.092E-08	5.013E-10	4.123E-06	2.697E-08	1.70857	0.0791	0.00032334	1.0377E-06	
1.145E-09	8.759E-10	2.037E-08	5.016E-10	3.931E-06	2.578E-08	1.71006	0.075938	0.00032346	1.0377E-06	
4.641E-10	3.619E-10	8.556E-09	6.222E-10	1.057E-06	7.683E-09	1.74036	0.0091707	0.00032429	1.0377E-06	
4.094E-10	3.489E-10	8.263E-09	8.064E-10	1.501E-06	1.096E-08	1.74328	0.0024836	0.00032434	1.0377E-06	
4.036E-10	4.041E-10	9.259E-09	9.256E-10	2.480E-06	1.742E-08	1.74386	0.0011655	0.00032436	1.0377E-06	
3.893E-10	4.442E-10	9.824E-09	9.715E-10	3.108E-06	2.118E-08	1.74401	0.00082827	0.00032433	1.0377E-06	2.6299E-08
3.832E-10	4.541E-10	9.933E-09	9.791E-10	3.248E-06	2.196E-08	1.74403	0.00076505	0.00032209	1.0377E-06	2.2742E-06
3.515E-10	4.920E-10	1.023E-08	9.974E-10	3.669E-06	2.400E-08	1.74412	0.00057634	0.0003151	1.0377E-06	9.2572E-06
3.171E-10	5.209E-10	1.027E-08	9.974E-10	3.808E-06	2.423E-08	1.74416	0.0004685	0.00031106	1.0377E-06	1.3297E-05
2.835E-10	5.431E-10	1.016E-08	9.848E-10	3.756E-06	2.334E-08	1.74419	0.0003986	0.00030859	1.0377E-06	1.5775E-05
2.521E-10	5.605E-10	9.933E-09	9.633E-10	3.588E-06	2.184E-08	1.74421	0.00034936	0.00030705	1.0377E-06	1.7316E-05
2.234E-10	5.743E-10	9.640E-09	9.353E-10	3.353E-06	2.006E-08	1.74423	0.00031261	0.00030613	1.0377E-06	1.8239E-05
1.976E-10	5.854E-10	9.303E-09	9.027E-10	3.087E-06	1.819E-08	1.74424	0.00028398	0.00030564	1.0377E-06	1.8723E-05
1.819E-10	5.917E-10	9.061E-09	8.792E-10	2.902E-06	1.695E-08	1.74425	0.00026797	0.0003055	1.0377E-06	1.8868E-05
1.819E-10	5.917E-10	9.061E-09	8.792E-10	2.902E-06	1.695E-08	1.74425	0.00026797	0.0003055	1.0377E-06	1.8869E-05
1.701E-10	6.192E-10	9.272E-09	1.013E-09	2.530E-06	1.408E-08	1.74427	0.00023141	0.00029926	1.0377E-06	2.5104E-05
1.533E-10	6.655E-10	9.608E-09	1.212E-09	2.074E-06	1.068E-08	1.74428	0.00019126	0.00029247	1.0377E-06	3.1895E-05
1.533E-10	6.655E-10	9.608E-09	1.212E-09	2.074E-06	1.068E-08	1.74428	0.00019126	0.00029247	1.0377E-06	3.1895E-05
1.477E-10	6.761E-10	9.653E-09	1.198E-09	1.935E-06	9.987E-09	1.74429	0.00017767	0.0002903	1.0377E-06	3.4066E-05
1.356E-10	7.017E-10	9.762E-09	1.165E-09	1.652E-06	8.552E-09	1.7443	0.00015255	0.00028631	1.0377E-06	0.00003806
1.055E-10	7.876E-10	1.012E-08	1.069E-09	1.055E-06	5.463E-09	1.74432	0.00010765	0.00027928	1.0377E-06	4.5091E-05
8.243E-11	8.911E-10	1.054E-08	9.785E-10	6.957E-07	3.559E-09	1.74433	8.33308E-05	0.00027558	1.0377E-06	4.8786E-05
6.476E-11	1.017E-09	1.101E-08	8.928E-10	4.744E-07	2.372E-09	1.74434	6.81103E-05	0.00027335	1.0377E-06	5.1015E-05
5.119E-11	1.169E-09	1.155E-08	8.127E-10	3.352E-07	1.620E-09	1.74434	5.77179E-05	0.00027189	1.0377E-06	5.2473E-05
4.069E-11	1.355E-09	1.213E-08	7.382E-10	2.453E-07	1.134E-09	1.74434	5.01695E-05	0.00027088	1.0377E-06	5.3485E-05
3.253E-11	1.582E-09	1.278E-08	6.694E-10	1.859E-07	8.141E-10	1.74435	4.44452E-05	0.00027015	1.0377E-06	5.4214E-05
3.186E-11	1.606E-09	1.284E-08	6.634E-10	1.814E-07	7.898E-10	1.74435	4.39623E-05	0.00027009	1.0377E-06	5.4273E-05
2.921E-11	1.628E-09	1.271E-08	6.787E-10	1.553E-07	6.487E-10	1.74435	3.92752E-05	0.0002697	1.0377E-06	5.4664E-05
2.229E-11	1.680E-09	1.232E-08	7.268E-10	9.529E-08	3.445E-10	1.74435	2.93947E-05	0.00026888	1.0377E-06	5.5484E-05
1.432E-11	1.741E-09	1.176E-08	8.008E-10	4.293E-08	1.179E-10	1.74436	2.07388E-05	0.00026818	1.0377E-06	5.6192E-05
9.586E-12	1.817E-09	1.146E-08	8.483E-10	2.172E-08	4.444E-11	1.74436	1.63825E-05	0.00026783	1.0377E-06	5.6539E-05
6.755E-12	1.943E-09	1.149E-08	8.559E-10	1.327E-08	1.973E-11	1.74436	1.39825E-05	0.00026764	1.0377E-06	5.6727E-05
4.557E-12	2.207E-09	1.213E-08	8.069E-10	1.003E-08	8.885E-12	1.74436	1.24124E-05	0.00026752	1.0377E-06	0.00005685

Table III. Example IDPS Model Evaporation Lookup Table for Average In Situ J-13 Well Water
(Continued)

Halite	Natrite	Sepiolite	SiO2(am)	Stellerite	Thenardite	#VALUE!	#VALUE!	#VALUE!	#VALUE!	#VALUE!
Halite	Natrite	Sepiolite	SiO2(am)	Stellerite	Thenardite					
Moles	Moles	Moles	Moles	Moles	Moles					
		0.00001868		2.5916E-07						
		1.8724E-05		2.5917E-07						
		1.9228E-05		2.5924E-07						
		1.9666E-05		2.593E-07						
		2.0004E-05		2.5934E-07						
		2.0254E-05		2.5938E-07						
		2.0429E-05		2.594E-07						
		2.0544E-05		2.5942E-07						
		2.0614E-05		2.5943E-07						
		2.0651E-05		2.5943E-07						
		2.0668E-05		2.5944E-07						
		2.0673E-05	8.8945E-07	2.5944E-07						
		2.0673E-05	2.0169E-05	2.5944E-07						
		2.0673E-05	0.00011804	2.5944E-07						
		2.0636E-05	0.00020192	2.2172E-07						
		2.0414E-05	0.0002199							
		2.0415E-05	0.00023608							
		2.0415E-05	0.00067782							
		2.0415E-05	0.00078257							
		2.0415E-05	0.00081759							
		2.0415E-05	0.00082881							
		2.0415E-05	0.00083092							
		2.0415E-05	0.0008374							
		2.0415E-05	0.00084106							
		2.0415E-05	0.00084326							
		2.0415E-05	0.00084459							
		2.0415E-05	0.00084537							
		2.0415E-05	0.00084577							
	2.5601E-07	2.0415E-05	0.00084589							
	2.7273E-07	2.0415E-05	0.00084589							
	0.00012272	2.0415E-05	0.00085257							
	0.00025585	2.0415E-05	0.00085986		1.6162E-07					
	0.00025586	2.0415E-05	0.00085986		1.6668E-07					
	0.00029255	2.0415E-05	0.00086223		1.6028E-05					
	0.00036034	2.0415E-05	0.0008666		4.5228E-05					
	0.00048102	2.0415E-05	0.00087434		9.6694E-05					
	0.0005458	2.0415E-05	0.00087845		0.00012382					
	0.00058577	2.0415E-05	0.00088097		0.00014024					
	0.00061254	2.0415E-05	0.00088265		0.00015104					
	0.00063151	2.0415E-05	0.00088384		0.00015855					
	0.00064545	2.0415E-05	0.00088471		0.00016398					
	1.1477E-07	0.00064658	2.0415E-05	0.00088478	0.00016441					
	2.4346E-05	0.0006526	2.0415E-05	0.00088513	0.00016582					
	7.5306E-05	0.00066563	2.0415E-05	0.00088586	0.00016837					
	0.0001197	0.00067774	2.0415E-05	0.0008865	0.00016926					
	0.00014183	0.00068438	2.0415E-05	0.00088684	0.00016783					
	0.00015379	0.00068838	2.0415E-05	0.00088704	0.00016486					
	0.00016105	0.00069144	2.0415E-05	0.0008872	0.00015859					

ATTACHMENT IV
EXAMPLE IDPS CONDENSATION LOOKUP TABLE

ATTACHMENT IV

Table IV is an example IDPS model lookup table for the example dilution of average in situ J-13 well water by condensation of water vapor. This lookup table is documented in DTN: MO0304SPAJ13IS.001, file j13c3t7c.xls.

Table IV. Example IDPS Model Condensation Lookup Table for Average In Situ J-13 Well Water

Calculations				RH Calc.	Temperature and Gas Fugacities				Total Elemental Aqueous Co	
CF=1/DF	Qe/Qs	1-Qe/Qs=DF		RH	log Xi - j13c3t7c.6o	Temp (C) - j13c3t7c.6o	O2(g) Fugacity	CO2(g) Fugacity	log Xi - j13c3t7c.6o	pH - j13c3t7c.6o
1.000	0.0000	1.0000		99.9906%	0.0000	70.0000	0.1995	0.0010	0	8.222
0.631	-0.5853	1.5853		99.9933%	0.2000	70.0000	0.1995	0.0010	0.2	8.124
0.537	-0.8632	1.8632		99.9940%	0.2701	70.0000	0.1995	0.0010	0.27012	8.099
0.469	-1.1300	2.1300		99.9946%	0.3282	70.0000	0.1995	0.0010	0.32821	8.057
0.398	-1.5130	2.5130		99.9953%	0.4000	70.0000	0.1995	0.0010	0.4	7.992
0.365	-1.7406	2.7406		99.9957%	0.4376	70.0000	0.1995	0.0010	0.43764	7.958
0.364	-1.7444	2.7444		99.9957%	0.4382	70.0000	0.1995	0.0010	0.43824	7.957
0.251	-2.9833	3.9833		99.9969%	0.6000	70.0000	0.1995	0.0010	0.6	7.806
0.158	-5.3135	6.3135		99.9979%	0.8000	70.0000	0.1995	0.0010	0.8	7.616
0.148	-5.7359	6.7359		99.9980%	0.8281	70.0000	0.1995	0.0010	0.82812	7.589
0.100	-9.0067	10.0067		99.9986%	1.0000	70.0000	0.1995	0.0010	1	7.422
0.063	-14.8600	15.8600		99.9990%	1.2000	70.0000	0.1995	0.0010	1.2	7.227
0.040	-24.1368	25.1368		99.9992%	1.4000	70.0000	0.1995	0.0010	1.4	7.030
0.025	-38.8396	39.8396		99.9994%	1.6000	70.0000	0.1995	0.0010	1.6	6.833
0.016	-62.1420	63.1420		99.9995%	1.8000	70.0000	0.1995	0.0010	1.8	6.637
0.010	-99.0738	100.0738		99.9996%	2.0000	70.0000	0.1995	0.0010	2	6.443
0.010	-99.0738	100.0738		99.9996%	2.0000	70.0000	0.1995	0.0010	2	6.443

Table IV. Example IDPS Model Condensation Lookup Table for Average In Situ J-13 Well Water
(Continued)

Composition											
RH	IS	H2O (kg)	Al	C	Ca	Cl	F	K	Mg	N	
rel. humid.	ionic strength (m)		aluminum	carbon	calcium	chlorine	fluorine	potassium	magnesium	nitrogen	
a(w) -	(l) -	Mass Solvent	Al	C	Ca	Cl	F	K	Mg	N	
j13c3t7c.6o	j13c3t7c.6o	(kg) -	Moles/kg.								
		H2O	H2O	H2O	H2O	H2O	H2O	H2O	H2O	H2O	H2O
1.000	2.644E-03	1.000E+00	1.096E-09	1.368E-03	1.070E-04	2.014E-04	1.147E-04	1.289E-04	7.979E-06	1.416E-04	
1.000	1.972E-03	1.585E+00	3.450E-09	1.084E-03	1.574E-04	1.270E-04	7.238E-05	8.131E-05	2.155E-05	8.932E-05	
1.000	1.824E-03	1.863E+00	5.046E-09	1.022E-03	1.738E-04	1.081E-04	6.158E-05	6.918E-05	2.881E-05	7.600E-05	
1.000	1.639E-03	2.130E+00	7.095E-09	9.260E-04	1.520E-04	9.455E-05	5.387E-05	6.052E-05	3.883E-05	6.648E-05	
1.000	1.393E-03	2.513E+00	1.299E-08	7.934E-04	1.289E-04	8.014E-05	4.566E-05	5.130E-05	3.291E-05	5.635E-05	
1.000	1.278E-03	2.741E+00	1.787E-08	7.314E-04	1.182E-04	7.349E-05	4.187E-05	4.703E-05	3.018E-05	5.167E-05	
1.000	1.277E-03	2.744E+00	1.789E-08	7.304E-04	1.180E-04	7.338E-05	4.181E-05	4.695E-05	3.013E-05	5.160E-05	
1.000	8.827E-04	3.983E+00	4.327E-08	5.142E-04	8.133E-05	5.056E-05	2.881E-05	3.235E-05	2.076E-05	3.555E-05	
1.000	5.584E-04	6.314E+00	1.316E-07	3.332E-04	5.136E-05	3.190E-05	1.817E-05	2.042E-05	1.310E-05	2.243E-05	
1.000	5.235E-04	6.736E+00	1.541E-07	3.136E-04	4.816E-05	2.990E-05	1.704E-05	1.914E-05	1.228E-05	2.102E-05	
1.000	3.527E-04	1.001E+01	1.037E-07	2.169E-04	3.241E-05	2.013E-05	1.147E-05	1.288E-05	8.264E-06	1.415E-05	
1.000	2.227E-04	1.586E+01	6.543E-08	1.428E-04	2.045E-05	1.270E-05	7.235E-06	8.128E-06	5.214E-06	8.928E-06	
1.000	1.406E-04	2.514E+01	4.128E-08	9.566E-05	1.290E-05	8.012E-06	4.565E-06	5.128E-06	3.290E-06	5.633E-06	
1.000	8.883E-05	3.984E+01	2.605E-08	6.583E-05	8.142E-06	5.055E-06	2.880E-06	3.236E-06	2.076E-06	3.554E-06	
1.000	5.619E-05	6.314E+01	1.644E-08	4.701E-05	5.137E-06	3.190E-06	1.817E-06	2.042E-06	1.310E-06	2.243E-06	
1.000	3.567E-05	1.001E+02	1.037E-08	3.519E-05	3.241E-06	2.012E-06	1.147E-06	1.288E-06	8.264E-07	1.415E-06	
1.000	3.567E-05	1.001E+02	1.037E-08	3.519E-05	3.241E-06	2.012E-06	1.147E-06	1.288E-06	8.264E-07	1.415E-06	

Table IV. Example IDPS Model Condensation Lookup Table for Average In Situ J-13 Well Water
(Continued)

			ANC species concentrations								
Na sodium	S sulfur	Si silicon	log Xi log react. progr.	H2O (kg)	HCO3-	CO3--	HSiO3-	CaHCO3+	OH-	MgHCO3+	
			2/24/2003								
			User: Marinerp								
			EQ3/6,								
			Version 8.0								
Na Moles/kg. H2O	S Moles/kg. H2O	Si Moles/kg. H2O	log Xi - j13c3t7c.6o	Mass Solvent (kg) - j13c3t7c.6o	HCO3- Molality	CO3-- Molality	HSiO3- Molality	CaHCO3+ Molality	OH- Molality	MgHCO3+ Molality	
1.992E-03	1.915E-04	8.995E-04	0.000E+00	1.000E+00	1.324E-03	2.092E-05	1.001E-04	1.622E-06	2.757E-05	1.280E-07	
1.257E-03	1.208E-04	5.922E-04	2.000E-01	1.585E+00	1.047E-03	1.288E-05	5.334E-05	2.017E-06	2.181E-05	2.876E-07	
1.069E-03	1.028E-04	5.196E-04	2.701E-01	1.863E+00	9.864E-04	1.140E-05	4.434E-05	2.132E-06	2.056E-05	3.670E-07	
9.353E-04	8.992E-05	4.750E-04	3.282E-01	2.130E+00	8.943E-04	9.315E-06	3.704E-05	1.724E-06	1.864E-05	4.552E-07	
7.927E-04	7.622E-05	4.026E-04	4.000E-01	2.513E+00	7.668E-04	6.795E-06	2.722E-05	1.287E-06	1.598E-05	3.379E-07	
7.269E-04	6.989E-05	3.693E-04	4.376E-01	2.741E+00	7.069E-04	5.752E-06	2.313E-05	1.101E-06	1.473E-05	2.885E-07	
7.259E-04	6.979E-05	3.692E-04	4.382E-01	2.744E+00	7.059E-04	5.736E-06	2.310E-05	1.099E-06	1.471E-05	2.878E-07	
5.001E-04	4.809E-05	2.544E-04	6.000E-01	3.983E+00	4.953E-04	2.781E-06	1.138E-05	5.554E-07	1.032E-05	1.445E-07	
3.155E-04	3.034E-05	1.607E-04	8.000E-01	6.314E+00	3.171E-04	1.122E-06	4.677E-06	2.339E-07	6.609E-06	6.056E-08	
2.958E-04	2.844E-05	1.507E-04	8.281E-01	6.736E+00	2.977E-04	9.871E-07	4.124E-06	2.068E-07	6.204E-06	5.353E-08	
1.991E-04	1.914E-05	1.015E-04	1.000E+00	1.001E+01	2.019E-04	4.493E-07	1.900E-06	9.682E-08	4.208E-06	2.503E-08	
1.256E-04	1.208E-05	6.401E-05	1.200E+00	1.586E+01	1.282E-04	1.792E-07	7.658E-07	3.965E-08	2.671E-06	1.024E-08	
7.925E-05	7.620E-06	4.039E-05	1.400E+00	2.514E+01	8.120E-05	7.135E-08	3.075E-07	1.612E-08	1.692E-06	4.165E-09	
5.001E-05	4.808E-06	2.548E-05	1.600E+00	3.984E+01	5.143E-05	2.844E-08	1.232E-07	6.530E-09	1.072E-06	1.687E-09	
3.155E-05	3.033E-06	1.608E-05	1.800E+00	6.314E+01	3.263E-05	1.139E-08	4.941E-08	2.641E-09	6.799E-07	6.824E-10	
1.991E-05	1.914E-06	1.014E-05	2.000E+00	1.001E+02	2.082E-05	4.619E-09	1.991E-08	1.072E-09	4.338E-07	2.769E-10	
1.991E-05	1.914E-06	1.014E-05	2.000E+00	1.001E+02	2.082E-05	4.619E-09	1.991E-08	1.072E-09	4.338E-07	2.769E-10	

Table IV. Example IDPS Model Condensation Lookup Table for Average In Situ J-13 Well Water
(Continued)

H+ MgOH+ CaOH+ HSO4- Ca++ Mg++						
H+	MgOH+	CaOH+	HSO4-	Ca++	Mg++	
H+ Molality	MgOH+ Molality	CaOH+ Molality	HSO4- Molality	Ca++ Molality	Mg++ Molality	
6.392E-09	6.462E-08	1.131E-07	3.551E-10	9.591E-05	7.609E-06	
7.951E-09	1.452E-07	1.407E-07	2.857E-10	1.458E-04	2.079E-05	
8.403E-09	1.853E-07	1.487E-07	2.582E-10	1.622E-04	2.787E-05	
9.220E-09	2.299E-07	1.203E-07	2.508E-10	1.432E-04	3.770E-05	
1.067E-08	1.706E-07	8.973E-08	2.505E-10	1.228E-04	3.212E-05	
1.153E-08	1.457E-07	7.680E-08	2.504E-10	1.132E-04	2.952E-05	
1.155E-08	1.453E-07	7.662E-08	2.504E-10	1.131E-04	2.948E-05	
1.622E-08	7.299E-08	3.874E-08	2.508E-10	7.922E-05	2.047E-05	
2.496E-08	3.059E-08	1.631E-08	2.520E-10	5.062E-05	1.299E-05	
2.654E-08	2.704E-08	1.442E-08	2.522E-10	4.751E-05	1.218E-05	
3.873E-08	1.264E-08	6.752E-09	2.535E-10	3.214E-05	8.221E-06	
6.045E-08	5.174E-09	2.765E-09	2.551E-10	2.035E-05	5.197E-06	
9.467E-08	2.104E-09	1.125E-09	2.564E-10	1.287E-05	3.283E-06	
1.486E-07	8.522E-10	4.554E-10	2.572E-10	8.127E-06	2.073E-06	
2.330E-07	3.447E-10	1.842E-10	2.572E-10	5.131E-06	1.309E-06	
3.638E-07	1.399E-10	7.476E-11	2.555E-10	3.239E-06	8.260E-07	
3.638E-07	1.399E-10	7.476E-11	2.555E-10	3.239E-06	8.260E-07	